THE UNIVERSITY OF
SYDNEY

Biomechanics and Remodelling for Design and Optimisation in Oral Prosthesis and Therapeutical Procedure

JUNNING CHEN, B.E. (Hon)

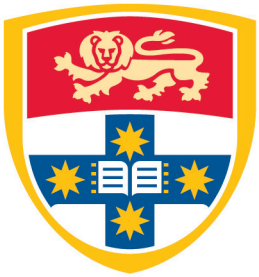

THE UNIVERSITY OF SYDNEY

A thesis submitted in fulfilment of the requirements for the degree

of Doctor of Philosophy

School of Aerospace, Mechanical and Mechatronic Engineering

The University of Sydney, Australia

August, 2014

Declaration

I hereby declare that the work presented in this thesis is solely my own work, and that to the best of my knowledge, the work is original except where otherwise indicated by reference to other authors or works. No part of this work has been submitted for a degree or diploma at any other university of institute.

Name: Junning CHEN

SID: 306005166

Signed: 

Date: 09-March-2015

Author

Junning Chen

Biomedical Engineering (1st Class Hons)

The University of Sydney

Email: junning.chen@sydney.edu.au

Supervisors

Prof. Qing Li

Course Coordinator of Biomedical Engineering

School of AMME, the University of Sydney

Phone: +61 2 9351 8607

Email: qing.li@sydney.edu.au

Prof. Michael V. Swain

Head of Biomaterials Research Unit

Faculty of Dentistry, the University of Sydney

Phone: +61 2 9351 8357

Email: mswain@mail.usyd.edu.au

Acknowledgement

Through this four-year PhD study, I received all kinds of help and support which I always appreciate from the heart. For the first and foremost, I would like to express my deepest appreciation to my supervisors, Prof. Qing Li, Prof. Michael Swain, and Dr. Wei Li, for their enthusiastic guidance and help in not just my research but also my life. They have continually and convincingly encourage me to explore the academic field and the Australian style of life with a spirit of adventure. Their persistent inspiration and thoughtful understanding lead to all my achievements in this dissertation through a truly enjoyable journey.

I feel grateful to be in the wonderful research team which is full of energetic and friendly members. These amazing people are Shiwei Zhou, Chaiy Rungsiyakull, Yuhang Chen, Joseph Cadman, Zhongpu Zhang, Sriram Tammareddi, Paul Wong, Phillip Tran, Andrian Sue, Zhipeng Liao, Che-Cheng Chang, Marco Zheng, Fangli Jia, Scott Townsend, Eric Li, Jianguang Fang, Guangyong Sun, and Sujuan Hou. Their loyal friendship and kind assistance through my study is always appreciated.

The majority of my work cannot be accomplished without my local and international collaborators, especially A.Prof. Rohana Ahmad from University of Tekenologi Malaysia and Dr. Hanako Suenaga from Tohoku University Japan who have been providing extensive support in the clinical studies. Dr. Matthey Foley and Dr. Dennis Dwarte from Australian Centre of Microscopy and Microanalysis has trained me for SEM and micro-CT, and helped me through my *in vitro* and *in vivo* examination. My work is also supported by all the staff at School of Aerospace, Mechanical and Mechatronic Engineering, leading by Prof. Lin Ye and Prof. Steven Armfield. The financial support from the school and faculty is gratefully acknowledged.

I also wish to thank my colleagues, Michael Hogg, Peter Lok, Alex Baume, Yujia Ma, Christine Poon, Andy Wang, Zhibin Chen, Yujie Chan, Yang Cao, and Jingli Sun, for enjoying the PhD candidature together, and hope everyone push it through in the soon future.

Finally, I would like to express my warmest gratitude to my parents, who have raised me up with all their love and sent me to Australia to give me the opportunity of exploring my life, and my dearest fiancée, Shijia Ding, who has been feeding me in the last four years and waiting for my graduation.

I hope I have made all of you proud.

Abstract

The purpose of dental prostheses is to restore the oral function for partially or completely edentulous patients; however, introducing any dental prosthesis into mouth will alter the biomechanical status of the oral environment, consequently inducing bone remodelling. Despite the advantageous benefits brought by dental prostheses, the attendant clinical complications and challenges, such as pain, discomfort, tooth root resorption, and residual ridge reduction, remain to be addressed. This thesis aims to explore several different dental prostheses, including dental implants, orthodontic appliances, partial removal dentures, conventional complete dentures and implant-retained dentures, by understanding the biomechanics associated with the potential tissue responses and adaptation, and thereby applying the new knowledge gained from these studies to dental prosthetic design and optimisation.

Within its biomechanics focus, the research studies presented in this thesis are related to three major clinical areas, namely prosthodontics, orthodontics and dental implantology. The oral mucosa is the most common soft tissue covering the majority of the oral cavity, and it plays a critical role in distributing occlusal forces from either full or partial dentures to the underlying bony structure. Upon reviewing the existing literature, the mucosal response is found in a complex, dynamic and nonlinear manner subject to occlusal loading. Through critical comparison of the residual ridge remodelling over a year and subsequent numerical modelling, it is discovered that hydrostatic pressure is the most important indicator to the potential resorption induced by prosthetic denture insertion. With this discovery, a patient-specific analysis is performed to investigate the effects caused by various types of dentures and prediction of the bone remodelling activities. Further exploration on this topic revealed the biomechanical differences between these treatment types. Furthermore, the denture base shape can be optimised to minimise the stress

concentration on the mucosal surface, thereby improving the uniformity of contact pressure and preventing severe bone resorption. In orthodontic treatments, the periodontal ligament has a similar role as the oral mucosa, and the hydrostatic pressure also appears to be most relevant and able to guide the directions of orthodontic tooth movement. A dynamic algorithm is developed to analyse and predict potential bone remodelling around the target tooth during orthodontic treatment, thereby providing a numerical approach for treatment planning. Bone, as the fundamental and supportive tissue in the oral cavity, can undergo rapid adaptation to variations in biomechanical stimulus, and this activity is governed by the strain energy density along with Wolff's Law. A graded surface morphology of an implant is demonstrated to have improved osseointegration over that of a smooth uniform surface in both the short and long term. The graded surface can be optimised to achieve the best possible balance between the bone-implant contact and the peak Tresca stress for the specific clinical application need. To further enhance osseointegration and loading carrying capacity, a fully porous surface with more than 500 μm substructure in depth is also proposed by using injection moulding. This novel media can significantly reduce the property mismatch between titanium and native bone, which considerably improves contact area for cell attachment.

Throughout the nine major research projects included in this thesis and several others (not included due to the word limit, instead only the journal publication details are referred for further information), the finite element method has been demonstrated to be an effective tool for analysing tissue behaviour and its response, designing and optimising dental prostheses as well as predicting short and long term outcomes for clinical treatment planning. The methodologies established in this study provide not only dentists but also material scientists and biomedical engineers with a tissue-remodelling oriented approach for developing an optimal dental prosthesis and clinical guidance procedures in the future.

Table of Content

List of Figures

List of Tables

Chapter 1: Introduction

This chapter provides an overview to the entire thesis, including its purpose, an outline of the structure for the thesis, and the associated publications arising from the investigations conducted during the PhD candidature.

1.1 Overview

The dental needs of the modern society have evolved for as a consequence of the diverse and complex needs of individuals. The purpose of dentistry is not just to restore the oral functionality of patients, but also to maintain or improve their appearance, comfort, oral hygiene, speech ability, and even the overall health [1]. In addition, the worldwide fast growing elderly population has led to dramatically increased demands for dental treatment, especially in the edentulous group [2, 3]. Meanwhile, as the awareness of importance in oral health has been raised significantly in the last decades, the dental care for youth and children has contributed to a considerable portion of the overall expenditure on dental services [4].

There are several specialised streams in dentistry, including prosthodontics, orthodontics, and dental implantology. Prosthodontics is the dental specialty to restore oral functions by applying dental prostheses, including artificial crowns, posts and cores, fixed and removable dentures, inlay and onlay bridges, and implant-associated prostheses. This specialty also provides diagnosis and treatment planning for temporo-mandibular disorders [5]. Orthodontics is another speciality involved in the diagnosis, prevention, and treatment of problems associated with the alignment of teeth and their supporting jaws. In this type of treatment, corrective appliances, such as braces, plates, headgears, and other functional appliances, are often applied to bring teeth and jaws into desired locations and orientations [6]. Rather than being a substantive speciality, dental implantology is more like a clinical approach to achieve the desirable outcomes in several streams, including prosthodontics and orthodontics. Dental implantology is a key method, sometimes, a unique solution, to replace missing teeth, retain and support prostheses, and provide anchorages for tooth movement [7, 8].

There are several types of oral tissues that are involved in these types of treatments, including mucosa, periodontal ligament, and bone. The oral mucosa is a common soft tissue covering the majority of the oral cavity, which has a critical role in distributing occlusal forces from various types of dentures to the underlying bony tissues for fully or partially edentulous patients [9-12]. The periodontal ligament is another supportive tissue surrounding each individual tooth, and it has been found to be critical in the remodelling activities around the teeth during orthodontic treatments [13-16]. The bony tissues, including both cortical and cancellous bones, form the core load supporting structure in the oral cavity, and continuously undergo adaptation to form a structurally elegant and efficient architecture for withstanding functional loads [11, 17-21].

Introducing dental prostheses into the oral environment will certainly induce biomechanical changes on native musculoskeletal system, including soft and hard tissues. In the short term, an inappropriately designed prosthesis can cause pain and discomfort to patients [22-24], and also lead to lack of the primary stability with implants and mini screws [25-27]. In the long term, however, more severe problems can developed as a consequence of different types of treatments. Denture-induced symptoms can occur on the mucosa, including traumatic ulcers, angular cheilitis, irritation hyperplasia, and keratosis [28-30]. Tooth root resorption frequently occurs during orthodontic tooth movement [31, 32]. The worst scenario, bone resorption, can develop in several scenarios. For instance, it can be caused by lack of stimulus to maintain the bone density, such as edentulous areas under bridges or dentures [33-37], and stress-shielding around implants [38-40]. On the other hand, it can also result from mechanical overloading, such as overloading-induced apoptosis around the implants [41-44] and residual ridge resorption under a compressed mucosa [34-37, 45].

These clinical complications remain as challenges to success of the treatment outcomes, in both the short and long term. As shown in the literature, the associated tissue-prosthesis interaction is the key to treatment success; therefore, the dental prosthesis design and optimisation must be tissue-prosthesis response oriented, taking currently poorly appreciated biomechanical activities into account.

To further improve the success rate of dental treatments, substantial efforts have been devoted to clinical investigations of the dental prosthetic response, for understanding and estimating the potential effects induced by prosthetic insertion [11, 34, 46-52]. The clinical approaches often require significant sample sizes and very strict conditions to accommodate individual variances and ensure the experimental consistency, which often lead to prolonged time frames and considerable expenditures [53, 54]. In clinical practice, it can be very challenging for these traditional approaches to seek accurate and quantitative solutions to the biomechanics parameters involved, such as loading transfer and internal deformation, where highly irregular anatomy, complex tissue responses, and various biomaterials are involved [55, 56]. These sophistications prevent effective examination in the associated biomechanics and lead to substantial difficulties in predicting tissue responses.

The numerical modelling finite element (FE) method serves as an alternative to study the clinical phenomena, and it has shown compelling advantages in biomechanical analysis and surgical planning [57-67]. The most distinct advantages of FE method is to provide the possibility of numerically analysing complex biological material and structural responses [10, 57, 68, 69], the repeatability of applying different treatments and conditions to the same subject [70-74], and the feasibility of predicting time-dependent responses and outcomes [17-21, 75-77]. With the recent advance in clinical scanning technologies, such as computerized tomography (CT), sophisticated 3D FE models are capable of precisely

capturing both anatomical and biomaterial features of an individual patient, thereby faithfully reflecting the case-specific bone profile and density distribution [78]. Based on clinical observations, complex soft-tissue responses can be mimicked in a nonlinear manner to more realistically reflect biomechanical behaviours [79]. All these benefits can potentially help with an understanding of tissue biomechanics, treatment analysis and planning, and outcome predictions.

Even though most dentists and biomaterial scientists are aware that dental prostheses will certainly cause various tissue responses, thereby affecting the treatment outcomes, limited knowledge exists as to the underlying biomechanics and the associated consequence for prosthetic design and optimization, especially where the soft tissues are involved. To address these issues, this thesis aims are as follows:

1) To investigate tissue responses from clinical observations and develop biomechanical models based on empirical clinical data for various types of tissues involved in dental treatments, including the oral mucosa, the periodontal ligament and adjacent bone;

2) To examine both short-term and long-term tissue responses induced by prosthetic insertion, including tissue deformation, pain/discomfort, and remodelling activities;

3) To develop dynamic tissue remodelling algorithms for various tissue types, and validate with clinical data, for the applications of treatment planning and prosthesis design;

4) To compare various types of prostheses on their treatment outcomes in a patient-specific manner, and reveal the underpinning basic biomechanics by correlating to the clinical observations;

5) To develop integrated optimisation approaches for dental prostheses (functional graded material, implant configuration and denture-mucosa interface) involving multiple stages, including; numerical design, validation, and fabrication.

1.2 Thesis Outline

Through the PhD study, the candidate has explored a broad range of oral tissues along with associated dental prosthesis design and analysis; therefore, this thesis covers several topics across several dental disciplines including, prosthodontics (major), orthodontics and implantology. In order to present the research outcomes in a more understandable manner, this thesis is divided into three sections based on the practical applications and tissue types. Each chapter stands alone enabling a perspective of specific dental prostheses, with the knowledge gleaned during this research having commonality that can be mutually applied, such as image processing, FE model reconstruction, material property interpretation, material behaviour scripting and structural/material optimisation.

1.2.1 Prosthodontics (Oral Mucosa) – Chapters 2-7

Chapter 2 – Biomechanics of Oral mucosa

This chapter provides a systematic review of both empirical and numerical research on the biomechanics of the oral mucosa in the existing literature. In this chapter, four aspects of the mucosal responses are addressed, including static, dynamic, volumetric and interactive responses, which are interpreted by the elasticity, viscosity and permeability, apparent Poisson's ratio and friction coefficient, respectively. Both empirical studies and several numerical models are analysed and compared, and linked to observed anatomical and physiological insights. Furthermore, the clinical applications of this biomechanical knowledge on the mucosa are included to address several critical concerns, including

stimuli for tissue remodelling (interstitial hydrostatic pressure), pressure pain thresholds (PPT), tissue displaceability and residual bone resorption.

Chapter 3 – Inverse Identification of Mucosa Incompressibility and Contact Friction Coefficient by using in-vivo Measurement

As revealed through the literature review in Chapter 2, there is no existing method to directly measure apparent Poisson's ratio and friction coefficient of the oral mucosa, despite their critical importance for modelling such tissue response. This chapter aimed to inversely determine these two biomechanical parameters by utilizing *in vivo* experimental data of contact pressures developed beneath a partial denture. Firstly, a tactile electronic sensing sheet was used to measure the *in vivo* contact pressure distribution under the denture base. Secondly, a CT scan was performed on the patient and a 3D FE model was constructed based on the CT images with virtual insertion of denture. Thirdly, a range of apparent Poisson's ratios and the friction coefficients from the literature were considered for a series of nonlinear FE simulations to construct the surrogate response surface (RS) models. Finally, the deviation between computed *in silico* and measured *in vivo* results was minimized to identify the best matching Poisson's ratio and friction coefficient.

Chapter 4 – Mechanobiological Bone Reaction Induced by Removable Partial Denture (RPD) with 18F-fluoride PET Imaging

Denture insertion is likely to cause changes in the biomechanical status of the oral environment; however, to date there have been no quantitative illustration of the associated changes. This chapter utilises the instantaneous bone metabolism at various time points available from 18-fluoride positron emission tomography (PET) and correlates mechanical stimuli in the residual ridge induced by removable partial denture (RPD) insertion. The resultant mechanobiological response is analysed using a 3D finite element (FE) model derived from the CT images of a specific patient. This approach reveals the effectiveness

of applying PET to determine bone metabolic activity associated with mechanical stimuli, and the results provide us with biomechanical insights of the association of radioactive tracer uptake with bone remodeling for the first time.

Chapter 5 – Investigation of Mucosa-Induced Residual Ridge Resorption between Implant-retained Overdenture and Complete Denture

Different types of prosthodontic prostheses can lead to different tissues reactions. This chapter aimed to investigate the residual ridge resorption (RRR) induced by an implant-retained overdenture (IRO) and associative biomechanics, compared to a conventional complete denture (CD) without implants. Cone beam computerized tomography (CBCT) is applied to quantify RRR in a three dimensional (3D) manner after one year of treatment with either IROs or CDs. Twenty patients were treated with IROs and nine patients with CDs. The corresponding 3D FE model is created from a set of representative scanned images for each configuration. The numerical analysis, of the hydrostatic stresses, contact surface deformation and strain energy absorption, is well-correlated with the clinical observations.

Chapter 6 – A Comparative Study on Complete and Implant Retained Denture Treatments: A Biomechanics Perspective of Oral Mucosa

As an extension to Chapter 5, Chapter 6 further examines the potential effects induced by three different types of dentures (complete denture, 2-implant retained overdenture, and 4-implant retained overdenture) on the same patient profile. Based on CBCT scans, a 3D heterogeneous FE model is created for a typical edentulous patient, and the supportive mucosa tissue, is characterized as a hyperelastic material. Following virtual insertion of the dentures, a measured occlusal load (63 N) was applied onto these cases. Clinically, the bone resorption was measured after one year in the two implant-retained overdenture

treatments. Despite the improved stability and enhanced masticatory function, the implant-retained overdentures demonstrated the presence of higher hydrostatic stress in the mucosa at the posterior ends of the mandible due to the cantilever effect compared to the complete denture. Hydrostatic pressure in the mucosa signifies a critical indicator and can be well correlated with clinically measured bone resorption, pointing to the cantilever effect in implant-retained overdentures causing ridge resorption posteriorly. This study provides a biomechanical basis for denture treatment planning to improve long-term outcomes with minimal residual ridge resorption.

Chapter 7 – Three-Dimensional Contact Shape Optimization and Free-Form Fabrication for Removable Partial Dentures: A New Paradigm for Prosthetic CAD/CAM

To avoid pain/discomfort sensation and reduce the potential residual ridge resorption, the denture has traditionally been adjusted manually through an adaptation test, which is time consuming for both the clinician as well as patient and is without quantitative standards. This study aims to develop a fully automatic procedure for denture base contact optimization, to minimize the contact pressure on the mucosa and avoid associated clinical complications. A 3D heterogeneous FE model is constructed from scanned images, and the mucosa is modeled as a hyperelastic material from *in vivo* clinical data. A contact optimization algorithm is developed based on the bi-directional evolutionary structural optimization (BESO) technique. Both initial and optimized dentures are prototyped by 3D printers and evaluated with an *in vitro* test with fitting silicone and pressure sensitive film.

1.2.2 Orthodontics (Periodontal Ligament) – Chapter 8

Chapter 8 – A Time-Dependent Soft-Tissue Driven Bone Remodeling for Orthodontic Tooth Movement

While orthodontic tooth movement (OTM) has gained considerable popularity and clinical success, the roles played by the relevant tissues involved, particularly periodontal ligament (PDL), remain an open question in biomechanics. This chapter aims to develop a soft-tissue induced surface remodeling procedure by correlating time-dependent simulation *in-silico* with clinical data *in-vivo*, thereby providing a systematic approach for further understanding and prediction of OTM. The biomechanical stimuli, namely hydrostatic stress and displacement vectors experienced in PDL, are proposed to drive tooth movement through an iterative hyperelastic FE procedure. This algorithm is both indicative and effective to simulate OTM under different loading conditions, has considerable potential to predict therapeutical outcomes and to develop a surgical plan for sophisticated orthodontic treatment.

1.2.3 Dental Implantology (Bone) – Chapters 9-10

Chapter 9 – Multiscale design of surface morphological gradient for osseointegration

Rapid and stable osseointegration signifies a major concern for the design of implantable prostheses, which stimulates continuous development of new implant materials and structures. This chapter promotes a graded configuration of a bead/particle coated porous surface for implants by exploring how its micromechanical features determine osseointegration through a multiscale modeling technique. A typical dental implantation setting is exemplified for investigation, using the remodeling parameters determined from a systematic review of bone-implant-contact (BIC) ratio published in the literature. The global responses of a macroscale model are obtained through 48 month remodeling simulation, which form the basis for the 27 graded microscopic models created with different particle diameters of 30, 50 and 70 μm. The osseointegration responses are evaluated in terms of BIC ratio and averaged 10% peak Tresca shear stress (PTS).

Chapter 10 – Characterisation of Anisotropic Elasticity and Diffusivity in Injection-Moulded Porous Titanium for Dental and Orthopaedic Application

With the same target of enhancing osseointegration, as stated in Chapter 9, using a porous titanium implant has been shown as an alternative. This paper introduces the novel injection moulding fabrication technique and then systemically characterises the fabricated samples. Surface morphology is firstly examined using a scanning electron microscope (SEM) and then a micro-computational topology (μ-CT) scan is performed to non-invasively capture its subsurface 3D microscopic features. The porosity and the pore sizes are determined statistically based on the μ-CT image analysis. The minimum size of a representative volume element (RVE) of the scans is determined by convergence tests. Based on FE models created from these RVEs, homogenisation methods determine the microscopic heterogeneity in their anisotropic elasticity and oxygen diffusivity.

1.3 Publications

There have been a number of publications generated throughout this candidature, and future publications are in progress. This section summarises all publications in chronological order.

1.3.1 Book Chapters

1. Wei Li, **Junning Chen**, Chaiy Rungsiyakull, Zhongpu Zhang, Michael Swain, Qing Li. **Multiscale Remodelling for Topographical Optimization in Coated Porous Implants**. *Biomaterials for Implants and Scaffolds*, Springer (Accepted for publication on 28/09/2013)
2. **Junning Chen**, Liangjian Chen, Wei Li, Michael V. Swain, and Qing Li. **Porous Titanium Implant and Micro-CT Based Characterization of Sub-Surface Morphology**. *PRICM – 8.* John Wiley & Sons, Inc., 2013: p. 1579-1586.

1.3.2 Journal Publications Arising from the Thesis

1. Rohana Ahmad, **Junning Chen**, Mohamed I. Abu-Hassan, Qing Li, Michael V. Swain. **Investigation of Mucosa-Induced Residual Ridge Resorption between Implant-retained Overdenture and Complete Denture**. *The International Journal of Oral & Maxillofacial Implants*, 2014. In press (Accepted for publication on 25-Jun-2014).

2. Chaiy Rungsiyakull, **Junning Chen**, Pimduen Rungsiyakull, Wei Li, Michael V. Swain, Qing Li. **Bone's Responses to Different Designs of Implant Supported Fixed Partial Dentures**. *Biomechanics and Modeling in Mechanobiology*. In press (Accepted on 24-Aug-2014, DoI: 10.1007/s10237-014-0612-6).

3. Wei Li, Daniel Lin, **Junning Chen**, Zhongpu Zhang, Zhipeng Liao, Michael Swain, Qing Li. **Role of Mechanical Stimuli in Oral Implantation**. *Journal of Biosciences and Medicines*, 2014. 2: p. 63-68.

4. **Junning Chen**, Wei Li, Michael V. Swain, Ali M. Darendeliler, and Qing Li. **A periodontal ligament driven remodeling algorithm for orthodontic tooth movement**. *Journal of Biomechanics*, 2014. 47(7): p. 1689-1695.

5. **Junning Chen**, Rohana Ahmad, Michael V. Swain, Wei Li, Hanako Suenaga, and Qing Li. **Comparing Contact Pressure Induced by a Conventional Complete Denture and an Implant-Retained Overdenture**. *Applied Mechanics and Materials*, 2014(553): p. 384-89.

6. Hanako Suenaga, **Junning Chen**, Wei Li, Keiichiro Yamaguchi, Keiichi Sasaki, Qing Li, Michael V. Swain. **Validate Mandible Finite Element Model under Removable Partial Denture (RPD) with In Vivo Pressure Measurement**. *Applied Mechanics and Materials*, 2014. 553: p. 322-26.

7. Ke Ke Zheng, **Junning Chen**, Corey Scholes, Qing Li. **Magnetic Resonance Imaging (MRI) Based Finite Element Modeling for Analysing the Influence of Material Properties on Menisci Responses**. *Applied Mechanics and Materials*, 2014. 553: p. 305-09.

8. Caleb Christos Ioannidis, Danè Dabirrahmani, Qing Li, Zhong Pu Zhang, **Junning Chen**, Richard Appleyard. **Impaction Loads Resulting in Intraoperative Periprosthetic Femoral Fracture: A Finite Element Study**. *Applied Mechanics and Materials*, 2014. 553: p. 299-304.

9. **Junning Chen**, Chaiy Rungsiyakull, Wei Li, Yuhang Chen, Michael V. Swain, Qing Li. **Multiscale design of surface morphological gradient for osseointegration**. *Journal of the Mechanical Behavior of Biomedical Materials*, 2013. 20: p. 387-97.

10. Joseph Cadman, Che-Cheng Chang, **Junning Chen**, Yuhang Chen, Shiwei Zhou, Wei Li, Qing Li. **Bioinspired lightweight cellular materials - Understanding effects of natural variation on mechanical properties**. *Materials Science and Engineering: C*, 2013. 33(6): p. 3146-3152.

1.3.3 Journal Publications Submitted and under Review

11. **Junning Chen**, Rohana Ahmad, Wei Li, Hanako Suenaga, Michael Swain, Qing Li. **A Comparative Study on Complete and Implant Retained Denture Treatments – A Biomechanics Perspective**. Under review by *Journal Biomechanics* (13-May-2014, JBMR-B-14-0288).

12. **Junning Chen**, Hanako Suenaga, Michael Hogg, Wei Li, Michael Swain, Qing Li. **Determination of oral mucosa Poisson's ratio and friction coefficient from in-**

vivo contact pressure measurements. Submitted to *Journal of the Mechanical Behavior of Biomedical Materials* (30-Jul-2014, JMBBM-S-14-00586).

13. **Junning Chen**, Hanako Suenaga, Wei Li, Michael Swain, Qing Li. **Three-Dimensional Contact Shape Optimization and Free-Form Fabrication for Removable Partial Dentures – A New Paradigm for Prosthetic CAD/CAM**. Submitted to *the Journal of Prosthodontic Dentistry* (27-8-2014, JPD-S-14-00670).

14. Hanako Suenaga, **Junning Chen**, Keiichiro Yamaguchi, Wei Li, Keiichi Sasaki, Michael Swain, Qing Li. **Mechanobiological Bone Reaction Induced by Removable Partial Denture Quantified by PET (18F) Imaging and Finite Element Modeling**. Submitted to *Journal of Dental Research* (27-Aug-2014, JDR-14-0915).

15. **Junning Chen**, Wei Li, Michael Swain, Qing Li. **Biomechanics of Oral Mucosa**. Submitted to *Acta Biomaterialia* (28-Aug-2014, AB-14-1746)

16. Quanjun Li, Zhongpu Zhang, **Junning Chen**, G.R. Liu, Qing Li (2014) Smoothed finite element method in the analysis of multi-layered biomaterials, Submitted to *International Journal of Numerical Methods in Engineering* (29-Aug-2014).

17. **Junning Chen**, Zhongpu Zhang, Liangjian Chen, Wei Li, Michael V. Swain, Qing Li. **Injection-Moulded Porous Titanium Dental Implant and Characterization Modeling**. Submitted to *Dental Materials* (01-Sep-2014).

1.3.4 Conference Proceeding and Presentation

1. Hanako Suenaga, **Junning Chen**, Wei Li, Keiichiro Yamaguchi, Keiichi Sasaki, Michael V. Swain, and Qing Li. **Construction of a patient-specific mandible model with metallic prosthesis**. The 5th Triennial Congress of

Advanced Digital Technology in Head and Neck Reconstruction (2014). Beijing, China.

2. Zhipeng Liao, **Junning Chen**, Qing Li. **3D Heterogeneous Finite Element Modeling of Human Maxilla**. The 5th Triennial Congress of Advanced Digital Technology in Head and Neck Reconstruction (2014). Beijing, China.

3. **Junning Chen**, Hanako Suenaga, Wei Li, Michael V. Swain, and Qing Li. **Finite Element Analysis for Pressure-Induced Discomfort and Pain under a Partial Removable Denture**. The 7th World Congress of Biomechanics (2014). Boston, USA.

4. Zhipeng Liao, **Junning Chen**, Ali M Darendeliler, Michael Swain, Qing Li Biomechanical Evaluation of Optimal Orthodontic Forces on Human Maxillary Teeth. 11th. World Congress on Computational Mechanics (2014). Barcelona, Spain.

5. **Junning Chen**, Qing Li, Wei Li, and Michael Swain. **Mechanobiological Design of Functionally Graded Dental Implants to Enhance Osseointegration**. The 11th World Congress on Computational Mechanics (2014). Barcelona, Spain.

6. **Junning Chen**, Chaiy Rungsiyakull, Wei Li, Michael Swain, Qing Li. **Multi-objective Optimisation of Surface Morphology for Bone**. The 10th World Congress on Structural and Multidisciplinary Optimization (2013). Orlando, USA.

7. Keke Zheng K, Corey Scholes, Joe Lynch, **Junning Chen**, David Parker, Qing Li. **The effect of high tibial osteotomy correction angle on articular cartilage loading using finite element analysis**. 19th Australian & New Zealand Orthopaedic Research Society (2013). Sydney, Australia.

8. Keke Zheng K, Corey Scholes, Joe Lynch, **Junning Chen**, David Parker, Qing Li. **Finite element analysis of time-dependent stress and strain distribution at knee cartilage during the stance phase of gait.** The 8th Combined Meeting of Orthopaedic Research Sociality (2013). Venice, Italy.

9. **Junning Chen**, Nor Shairah Zainul Abidin, Sriram Tammareddi, Wei Li, Michael Swain, Qing Li. **Computational Modelling for Tooth Movement in Orthodontic Treatment**. The 11th International Symposium on Computer Methods in Biomechanics and Biomedical Engineering (2013). Salt Lake City, USA.

10. **Junning Chen**, Rohana Ahmad, Mohamed I. Abu-Hassan, Qing Li, Michael V. Swain. **The Effect of Mucosa Thickness on Residual Ridge Resorption with Implant-Retained Overdenture – A Combined Study with Clinical Case and FE Simulation**. The 5th Asia-Pacific Conference on Conceptual Modelling (2012). Melbourne, Australia.

11. **Junning Chen**, Liangjian Chen, Wei Li, Michael Swain, Qing Li. **Computational Tissue Differentiation Algorithm for Porous Dental Implants**. The 10th World Congress on Computational Mechanics (2012). São Paulo, Brazil.

12. **Junning Chen**, Chaiy Rungsiyakull, Qing Li, Wei Li, Michael Swain. **The Effect of Uncertainty of Dental Implant Morphology on Osseointegration**. The 11th US National Congress on Computational Mechanics (2011). Minneapolis, USA.

13. **Junning Chen**, Chaiy Rungsiyakull, Wei Li, Michael Swain, Richard Appleyard, Qing Li. **Multi-scale Modelling of Implant Surface Morphology**. The 17th Annual Conference of the Australian & New Zealand Orthopaedic Research Society (2011). Brisbane, Australia.

1.4 References

1. Macentee, M.I., R. Hole, and E. Stolar, *The significance of the mouth in old age.* Social Science & Medicine, 1997. **45**(9): p. 1449-1458.
2. Thomas-Weintraub, A., *Dental needs and dental service use patterns of an elderly edentulous population.* The Journal of Prosthetic Dentistry, 1985. **54**(4): p. 526-532.
3. Thompson, G.W. and P.S.J. Kreisel, *The impact of the demographics of aging and the edentulous condition on dental care services.* Journal of Prosthetic Dentistry, 1998. **79**(1): p. 56-59.
4. Gherunpong, S., G. Tsakos, and A. Sheiham, *A sociodental approach to assessing dental needs of children: concept and models.* International Journal of Paediatric Dentistry, 2006. **16**(2): p. 81-88.
5. Woods, W.G., *Editorial. Just what is prosthodontics.* Oral health, 1970. **60**(10): p. 5-7.
6. Dibiase, A., *What is orthodontics?* Journal of orthodontics, 2009. **36**(2): p. 71-2.
7. McKinney, R.V., Jr., et al., *The scientific basis for dental implant therapy.* Journal of dental education, 1988. **52**(12): p. 696-705.
8. Favero, L.G., A. Pisoni, and C. Paganelli, *Removal torque of osseointegrated mini-implants: an in vivo evaluation.* European Journal of Orthodontics, 2007. **29**(5): p. 443-448.
9. Kydd, W.L., C.H. Daly, and D. Nansen, *Variation in the response to mechanical stress of human soft tissues as related to age.* Journal of Prosthetic Dentistry, 1974. **32**(5): p. 493-500.
10. Sawada, A., et al., *Viscoelasticity of Human Oral Mucosa: Implications for Masticatory Biomechanics.* Journal of Dental Research, 2011. **90**(5): p. 590-595.
11. Ahmad, R., et al., *Three dimensional quantification of mandibular bone remodeling using standard tessellation language registration based superimposition.* Clin Oral Implants Res, 2013. **24**(11): p. 1273-1279.
12. Mori, S., et al., *Effect of continuous pressure on histopathological changes in denture-supporting tissues.* Journal of Oral Rehabilitation, 1997. **24**(1): p. 37-46.
13. Jones, M.L., et al., *A validated finite element method study of orthodontic tooth movement in the human subject.* Journal of orthodontics, 2001. **28**(1): p. 29-38.
14. Middleton, J., M. Jones, and A. Wilson, *The role of the periodontal ligament in bone modeling: The initial development of a time-dependent finite element model.* American Journal of Orthodontics and Dentofacial Orthopedics, 1996. **109**(2): p. 155-162.
15. Cattaneo, P.M., M. Dalstra, and B. Melsen, *The finite element method: a tool to study orthodontic tooth movement.* Journal of Dental Research, 2005. **84**(5): p. 428-433.
16. Ren, Y.J., J.C. Maltha, and A.M. Kuijpers-Jagtman, *Optimum force magnitude for orthodontic tooth movement: A systematic literature review.* Angle Orthodontist, 2003. **73**(1): p. 86-92.

17. Chen, J., et al., *Multiscale design of surface morphological gradient for osseointegration.* Journal of the Mechanical Behavior of Biomedical Materials, 2013. **20**: p. 387-97.

18. Rungsiyakull, C., et al., *Surface morphology optimization for osseointegration of coated implants.* Biomaterials, 2010. **31**(27): p. 7196-7204.

19. Lin, D., et al., *Mandibular bone remodeling induced by dental implant.* Journal of Biomechanics, 2010. **43**(2): p. 287-293.

20. Lin, D., et al., *Dental implant induced bone remodeling and associated algorithms.* Journal of the Mechanical Behavior of Biomedical Materials, 2009. **2**(5): p. 410-432.

21. Lin, D., et al., *Bone remodeling induced by dental implants of functionally graded materials.* Journal of Biomedical Materials Research Part B-Applied Biomaterials, 2010. **92B**(2): p. 430-438.

22. Suzuki, Y., et al., *Pressure pain threshold of mucosa after tooth extraction under removable denture bases.* The European journal of prosthodontics and restorative dentistry, 2011. **19**(4): p. 184-6.

23. Isobe, A., et al., *The influence of denture supporting tissue properties on pressure-pain threshold: –Measurement in dentate subjects–.* Journal of Prosthodontic Research, 2013. **57**(4): p. 275-283.

24. Ogawa, T., et al., *Pressure-pain threshold of oral mucosa and its region-specific modulation by pre-loading.* Journal of Oral Rehabilitation, 2003. **30**(11): p. 1062-1069.

25. Bischof, M., et al., *Implant stability measurement of delayed and immediately loaded implants during healing. A clinical resonance-frequency analysis study with sandblasted-and-etched ITI implants.* Clinical Oral Implants Research, 2004. **15**(5): p. 529-539.

26. Han, H.-J., S. Kim, and D.-H. Han, *Multifactorial Evaluation of Implant Failure: A 19-year Retrospective Study.* International Journal of Oral & Maxillofacial Implants, 2014. **29**(2): p. 303-310.

27. Mesa, F., et al., *Multivariate study of factors influencing primary dental implant stability.* Clinical Oral Implants Research, 2008. **19**(2): p. 196-200.

28. Jainkittivong, A., V. Aneksuk, and R.P. Langlais, *Oral mucosal lesions in denture wearers.* Gerodontology, 2010. **27**(1): p. 26-32.

29. Dorey, J.L., et al., *Oral mucosal disorders in denture wearers.* The Journal of Prosthetic Dentistry, 1985. **53**(2): p. 210-213.

30. Emami, E., et al., *Favoring trauma as an etiological factor in denture stomatitis.* Journal of Dental Research, 2008. **87**(5): p. 440-444.

31. Hohmann, A., et al., *Correspondences of hydrostatic pressure in periodontal ligament with regions of root resorption: A clinical and a finite element study of the same human teeth.* Computer Methods and Programs in Biomedicine, 2009. **93**(2): p. 155-161.

32. Hohmann, A., et al., *Periodontal ligament hydrostatic pressure with areas of root resorption after application of a continuous torque moment - A study using*

identical extracted maxillary human premolars. Angle Orthodontist, 2007. **77**(4): p. 653-659.

33. Canger, E.M. and P. Çelenk, *Radiographic evaluation of alveolar ridge heights of dentate and edentulous patients.* Gerodontology, 2012. **29**(1): p. 17-23.

34. Huumonen, S., et al., *Residual ridge resorption, lower denture stability and subjective complaints among edentulous individuals.* Journal of Oral Rehabilitation, 2012. **39**(5): p. 384-390.

35. Jahangiri, L., et al., *Current perspectives in residual ridge remodeling and its clinical implications: A review.* Journal of Prosthetic Dentistry, 1998. **80**(2): p. 224-237.

36. Klemetti, E., *A review of residual ridge resorption and bone density.* Journal of Prosthetic Dentistry, 1996. **75**(5): p. 512-514.

37. Klemetti, E., L. Lassila, and V. Lassila, *Biometric design of complete dentures related to residual ridge resorption.* Journal of Prosthetic Dentistry, 1996. **75**(3): p. 281-284.

38. Huiskes, R., et al., *Adaptive bone-remodeling theory applied to prosthetic-design analysis.* Journal of Biomechanics, 1987. **20**(11–12): p. 1135-1150.

39. Clift, S.E., J. Fisher, and C.J. Watson, *Finite element stress and strain analysis of the bone surrounding a dental implant: effect of variations in bone modulus.* Proceedings of the Institution of Mechanical Engineers. Part H, Journal of engineering in medicine, 1992. **206**(4): p. 233-41.

40. Pilliar, R.M., et al., *bone ingrowth and stress shielding with a porous surface coated fracture fixation plate.* Journal of Biomedical Materials Research, 1979. **13**(5): p. 799-810.

41. Noble, B.S. and J. Reeve, *Osteocyte function, osteocyte death and bone fracture resistance.* Molecular and Cellular Endocrinology, 2000. **159**(1-2): p. 7-13.

42. Wernig, F. and Q. Xu, *Mechanical stress-induced apoptosis in the cardiovascular system.* Progress in Biophysics and Molecular Biology, 2000. **78**(2-3): p. 105-137.

43. Xie, M., et al., *Rabbit Annulus Fibrosus Cell Apoptosis Induced by Mechanical Overload via a Mitochondrial Apoptotic Pathway.* Journal of Huazhong University of Science and Technology-Medical Sciences, 2010. **30**(3): p. 379-384.

44. Esposito, M., et al., *Biological factors contributing to failures of osseointegrated oral implants (I). Success criteria and epidemiology.* European Journal of Oral Sciences, 1998. **106**(1): p. 527-551.

45. Ozan, O., et al., *The Effect of Removable Partial Dentures on Alveolar Bone Resorption: A Retrospective Study with Cone-Beam Computed Tomography.* Journal of Prosthodontics-Implant Esthetic and Reconstructive Dentistry, 2013. **22**(1): p. 42-48.

46. Jacobs, R., et al., *Posterior jaw bone resorption in osseointegrated implant-supported overdentures.* Clinical Oral Implants Research, 1992. **3**(2): p. 63-70.

47. Romeo, E., et al., *Implant-supported fixed cantilever prosthesis in partially edentulous jaws: a cohort prospective study.* Clinical Oral Implants Research, 2009. **20**(11): p. 1278-1285.

48. Wright, P.S., et al., *The effects of fixed and removable implant-stabilised prostheses on posterior mandibular residual ridge resorption.* Clinical Oral Implants Research, 2002. **13**(2): p. 169-174.

49. Reddy, M.S., et al., *Mandibular growth following implant restoration: Does Wolff's law apply to residual ridge resorption?* International Journal of Periodontics & Restorative Dentistry, 2002. **22**(4): p. 315-322.

50. Hara, T., et al., *Effect of occlusal pressure on the histopathological changes in denture supporting tissues.* Journal of Oral Rehabilitation, 1996. **23**(6): p. 363-371.

51. Parker, R.J. and E.F. Harris, *Directions of orthodontic tooth movements associated with external apical root resorption of the maxillary central incisor.* American Journal of Orthodontics and Dentofacial Orthopedics, 1998. **114**(6): p. 677-683.

52. Fill, T.S., et al., *Experimentally determined mechanical properties of, and models for, the periodontal ligament: critical review of current literature.* Journal of dental biomechanics, 2011. **2011**: p. 312980-312980.

53. Joseph, L. and D.B. Wolfson, *Interval-based versus decision theoretic criteria for the choice of sample size.* Statistician, 1997. **46**(2): p. 145-149.

54. Strang, G. and G.J. Fix, *An analysis of the finite element method*. Vol. 212. 1973: Prentice-Hall Englewood Cliffs, NJ.

55. Kim, S.H., et al., *Hydrostatic Pressure can Control Osteogenesis and Osteoclastogenesis when Stromal Cells and Osteoclast Precursor Cells are Cocultured.* Tissue Engineering and Regenerative Medicine, 2010. **7**(4): p. 388-394.

56. Aspenberg, P. and H. van der Vis, *Fluid pressure may cause periprosthetic osteolysis - Particles are not the only thing.* Acta Orthopaedica Scandinavica, 1998. **69**(1): p. 1-4.

57. Bergomi, M., et al., *Hydro-mechanical coupling in the periodontal ligament: A porohyperelastic finite element model.* Journal of Biomechanics, 2011. **44**(1): p. 34-38.

58. Chun, H.J., et al., *Stress distributions in maxillary bone surrounding overdenture implants with different overdenture attachments.* Journal of Oral Rehabilitation, 2005. **32**(3): p. 193-205.

59. Li, W., et al., *Fibre reinforced composite dental bridge. Part II: numerical investigation.* Biomaterials, 2004. **25**(20): p. 4995-5001.

60. Mellal, A., et al., *Stimulating effect of implant loading on surrounding bone.* Clinical Oral Implants Research, 2004. **15**(2): p. 239-248.

61. Natali, A.N., et al., *Investigation of the integration process of dental implants by means of a numerical analysis.* Dental Materials, 1997. **13**(5-6): p. 325-332.

62. Reina, J.M., et al., *Numerical estimation of bone density and elastic constants distribution in a human mandible.* Journal of Biomechanics, 2007. **40**(4): p. 828-836.

63. Sturm, S., et al., *On stiffness of scaffolds for bone tissue engineering-a numerical study.* Journal of Biomechanics, 2010. **43**(9): p. 1738-1744.

64. Tomaszewski, P.K., et al., *Numerical analysis of an osseointegrated prosthesis fixation with reduced bone failure risk and periprosthetic bone loss.* Journal of Biomechanics, 2012. **45**(11): p. 1875-1880.

65. Zaw, K., et al., *Rapid identification of elastic modulus of the interface tissue on dental implants surfaces using reduced-basis method and a neural network.* Journal of Biomechanics, 2009. **42**(5): p. 634-641.

66. Middleton, J., et al., *Finite element simulation in biomechanics: bone and dental cements.* International Journal for engineering modelling, 1993. **6**: p. 1-4.

67. Hübsch, P.F., et al., *Adaptive finite-element approach for analysis of bone/prosthesis interaction* Medical and Biological Engineering and Computing, 1995. **33**(1): p. 33-37.

68. Wakabayashi, N. and T. Suzuki, *Patient-specific finite element analysis of viscoelastic masticatory mucosa.* Journal of dental biomechanics, 2013. **4**.

69. Winterroth, F., et al., *Characterizing Morphology and Nonlinear Elastic Properties of Normal and Thermally Stressed Engineered Oral Mucosal Tissues Using Scanning Acoustic Microscopy.* Tissue Engineering Part C-Methods, 2013. **19**(5): p. 345-351.

70. Barão, V.A.R., et al., *Comparison of different designs of implant-retained overdentures and fixed full-arch implant-supported prosthesis on stress distribution in edentulous mandible - A computed tomography-based three-dimensional finite element analysis.* Journal of Biomechanics, 2013. **46**(7): p. 1312-1320.

71. Liu, J., et al., *Influence of implant number on the biomechanical behaviour of mandibular implant-retained/supported overdentures: A three-dimensional finite element analysis.* Journal of Dentistry, 2013. **41**(3): p. 241-249.

72. Menicucci, G., et al., *Mandibular implant-retained overdenture: A clinical trial of two anchorage systems.* International Journal of Oral & Maxillofacial Implants, 1998. **13**(6): p. 851-856.

73. Osman, R.B., et al., *Finite Element Analysis of a Novel Implant Distribution to Support Maxillary Overdentures.* International Journal of Oral & Maxillofacial Implants, 2013. **28**(1): p. E1-E10.

74. Tanino, F., et al., *Finite element analysis of stress-breaking attachments on maxillary implant-retained overdentures.* International Journal of Prosthodontics, 2007. **20**(2): p. 193-198.

75. Rungsiyakull, C., et al., *Effects of Occlusal Inclination and Loading on Mandibular Bone Remodeling: A Finite Element Study.* International Journal of Oral & Maxillofacial Implants, 2011. **26**(3): p. 527-537.

76. Chen, J., et al., *A periodontal ligament driven remodeling algorithm for orthodontic tooth movement.* Journal of biomechanics, 2014. **47**(7): p. 1689-1695.

77. Lin, D., et al., *Design optimization of functionally graded dental implant for bone remodeling.* Composites Part B-Engineering, 2009. **40**(7): p. 668-675.

78. Field, C., et al., *Prediction of mandibular bone remodelling induced by fixed partial dentures.* Journal of Biomechanics, 2010. **43**(9): p. 1771-1779.

79. Kanbara, R., et al., *Three-dimensional finite element stress analysis: The technique and methodology of non-linear property simulation and soft tissue loading*

behavior for different partial denture designs. Dental Materials Journal, 2012. **31**(2): p. 297-308.

Chapter 2: Biomechanics of Oral Mucosa

The prevalence of prosthodontic treatment has been well recognised and the need is continuously increasing with the aging population. While the oral mucosa plays a critical role in the treatment outcome, the associated biomechanics is not yet fully understood. Using the literature available, this chapter provides a critical review on four aspects of the mucosal biomechanics, including static, dynamic, volumetric, and interactive responses, which are interpreted by its elasticity, viscosity/permeability, apparent Poisson's ratio, and friction coefficient, respectively. Both empirical studies and numerical models are analysed and compared to gain anatomical and physiological insights. Furthermore, the clinical applications of such biomechanical knowledge on the mucosa are also explored to address some critical concerns, including stimuli for tissue remodelling (interstitial hydrostatic pressure), pressure pain thresholds (PPT), tissue displaceability, and residual bone resorption. Through this review, the state-of-the-art in the mucosal biomechanics and their clinical implications are discussed for future research interests, including clinical investigation, numerical modelling, and application/design optimisation.

Associated Publications:

1. **Junning Chen**, Wei Li, Michael Swain, Qing Li. **Biomechanics of Oral Mucosa**. Submitted to *Acta Biomaterialia*.

2.1 Introduction

With an increasing worldwide elderly population, the edentulous group of patients has been continuously expanding, resulting in significantly raised needs for prosthodontic treatments [1, 2]. Complete or partial dentures have been widely used in dental clinics to restore oral function for the past century [3-5]. During mastication, the oral mucosa beneath the denture plays a critical role in distributing occlusal loads to the underlying bony ridge over a large denture-supporting tissue interface [6-9]. Within this highly vascular tissue, the functional pressure, namely interstitial fluid pressure (IFP) or hydrostatic pressure, has been identified as one of the most important etiological factors causing the accompanying clinical complications [9-14].

The mandible of aging patient is mainly supported by the periosteal plexus of blood vessels, and therefore very susceptible to diminished circulation under occlusal load induced mucosal pressure [15], which triggers nerve pain [16] and discomfortable sensation [14, 17], thus compromising patients' life quality [18, 19]. Cellular swelling, increased nuclear size, and intercellular edema will occur when the mucosa is under compression [9, 13, 20]. This inflammatory response of cells and surrounding tissue further contributes to variation in permeability of the mucosal tissue, and continues to compromise circulation [21, 22]. Once the hydrostatic pressure builds up and exceeds the capillary pressure, blood flow will be decreased and may even temporarily cease altogether as a result of the combination of active arteriolar closure and passive capillary compression [22]. Consequently, reduced nutrient supply and metabolite removal may lead to the potential residual ridge resorption [3, 9, 11, 12, 23-26], a progressive phenomenon harmful to patients' oral health [27, 28].

It is critical to understand the mucosal response to the prosthodontic prostheses for the treatment outcome, and the mucosa has been found to exhibit complex nonlinear and

time-dependent behaviours since the investigations commenced more than five decades ago [29-32]. Significant interest has arisen and extensive studies have been conducted to explore the biomechanics of the mucosa both clinically and numerically.

This chapter aims to provide a systematic review of the biomechanics of mucosal responses to mechanical loading, and it has been structured into three parts. Firstly, a brief summary of the mucosa anatomy and physiology will introduce the basic biology associated with its biomechanical responses and illustrate the insights associated with these observations. Secondly, a critical review is conducted of both experimental and numerical studies on four major aspects of the mucosal responses, namely static, dynamic, volumetric, and interactive responses. Several material models for each individual aspect are investigated and compared of 3-dimensional (3D) finite elements models of mucosa. Finally, the clinical implications of the mucosa biomechanics are discussed considering the major relevance to prosthodontic treatments, including the tissue remodelling stimulus, pressure pain threshold, tissue displaceability, and residual ridge resorption.

Understanding and adopting correct material models for the corresponding biomechanical behaviours will help identify biological determinants influencing the mucosa responses for better prosthodontic treatment planning and prediction. Furthermore, this review will demonstrate the current state-of-the-art of mucosal biomechanics research and reveals the potential research opportunities on fundamental biomechanics, clinic application and design optimisation.

2.2 Anatomy and Physiology

2.2.1 Anatomy

Oral mucosa can generally be classified into two different groups, masticatory mucosa and lining mucosa. The masticatory mucosa is firm and exhibits distinct resistance to deformation under load [21], forming more than 60% of the oral cavity surface including tongue dorsum, hard palate and attached gingiva [33]. It comprises a surface epithelial layer and a deeper connective tissue layer, namely lamina propria (Figure 2-1a). The oral epithelium is a keratinized, stratified, and squamous structure, consisting of multiple rows of cells that constitute a load-bearing layer by intercellular adhesions. Within this layer, intercellular channels exist for communication with neighbouring cells, and contain viscous material (mucopolysaccharides) providing the deformability and load resistance [21, 34]. Under the surface epithelium, there is a basal complex that forms a transient region with the underlying lamina propria.

The lamina propria is a compact fibrous structure, which comprises two sub-layers, the papillary layer connected to the basal complex and the deeper reticular layer. The superficial collagen fibres in the papillary layer are randomly oriented, and the transient regions are often irregular and non-smooth with undulating papillae ridges, providing enlarged areas for nutrient exchange [21]. The basal collagen fibres in the reticular layer gradually change to perpendicular attachments with the periosteum as shown in the middle layer of Figure 2-1a. The abundance of these fibrous attachments, known as mucoperiosteum, renders the masticatory mucosa immovable with firm connection to the bone, providing resistance to compressive and shear loads in function [33]. A capillary blood plexus lying between the papillary and deeper reticular layers provides nutrition to the mucosa, and gives rise to the blood vessels which ascend into the connective tissue

papillae. Nerve fibres penetrate the lamina propria, some ending in specialized sensory endings or cells in the papillae, whilst others extend into epithelium [35].

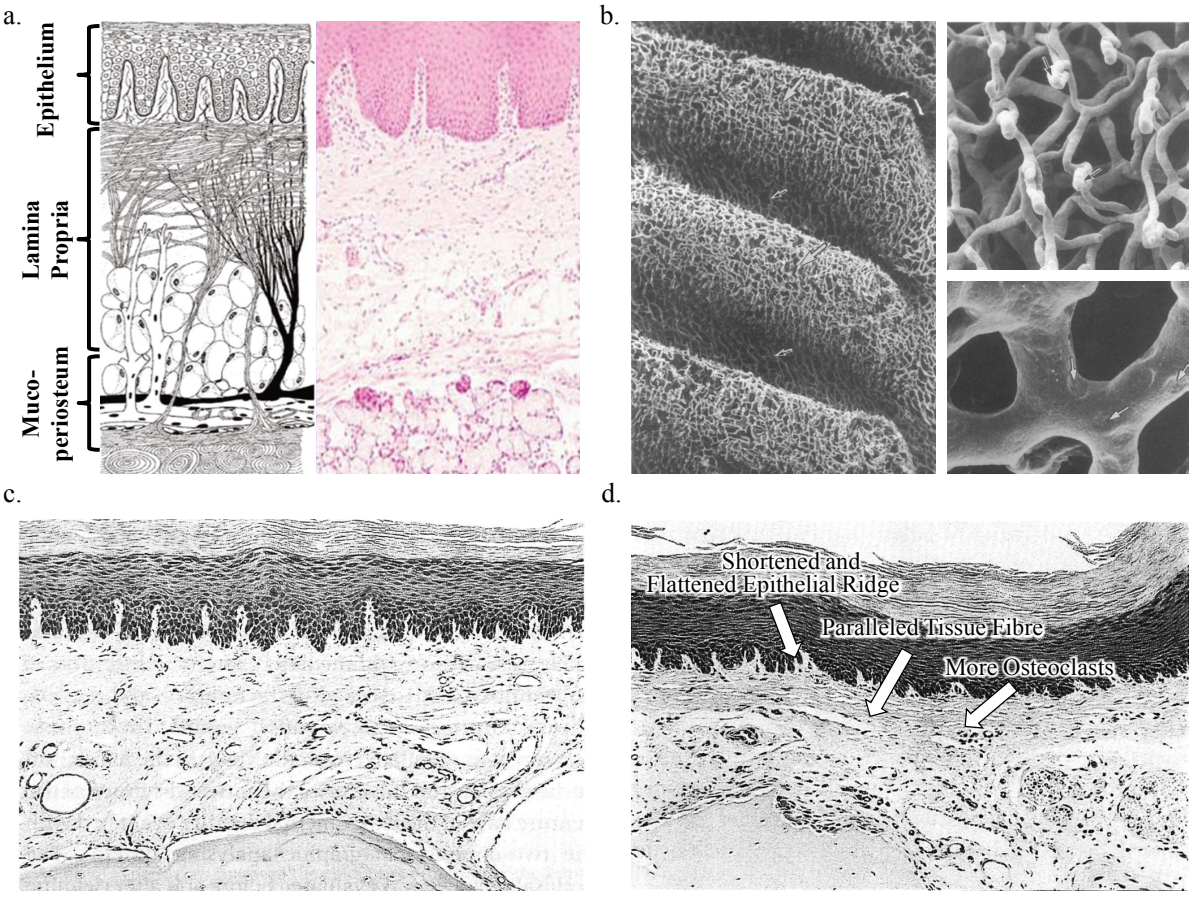

Figure 2-1 (a) Schematic diagram (left) and histological diagram of the healthy mucosa anatomy [36]; (b) SEM images of the vascular network within the rabbit palatine mucosa by corrosion casts [37]; (c) histological image of the mouse mucosa after 20 weeks underneath the denture without occlusal load [13]; (d) histological image of the mouse mucosa after 20 weeks beneath a denture with 100 µm constant deformation [13].

The second type, the lining mucosa, is highly distensible and can deform much easier than the masticatory mucosa. It is ubiquitous in the oral cavity, and covers the buccal and lingual mucosa. It has a non-keratinized stratified squamous epithelium layer with flatter and shorter ridges, and the loosely attached cells may be easily dislodged with small abrasive forces [21]. The basal complex of lining mucosa has small, cuboidal and non-polarized cells, compared to the large, columnar and polarized ones in the masticatory

mucosa [38]. The lamina propria is more compact, in which the connective tissue papillae underneath are irregular and relatively shallow, extending to the epithelium for a shorter distance, and collagen bundles appear larger and denser in the reticular layer [39]. Generally speaking, the keratinized masticatory mucosa is stiffer than the non-keratinized lining mucosa [40].

The mucosa thickness can vary over a wide range [6, 41-48], from 0.30 mm on the attached buccal mucosa in the mandibular canine to 6.7 mm in the maxillary tuberosity region. It has been determined as one of the dominant factors to affect their biomechanical responses [8], aside from its various types and locations [29, 40, 49]. Early measurements of the mucosa thickness and structure were performed by histological examination of animals [32, 33, 35, 50, 51]. X-ray photograph provided a non-invasive approach showing a range of mucosa from 2 to 3 mm [52], but the low contrast and resolution of the soft tissue limited accurate measurements with this technique. Ultrasound is now commonly used to measure the resting thickness of the oral mucosa in the maxilla and mandible of dentate and edentate individuals [41-44, 53]. Edentulous patients showed a greater variation in soft tissue thickness than dentate individuals. With recent advances in Computed Tomography (CT), the potential of using this relatively new technique as an alternative to examination of the mucosa thickness is under exploration [45-47]. Accompanying the high accuracy, the increased radiation exposure requires extra caution because of radiation dosage [45].

2.2.2 Physiology

Apart from anatomical features, the physiologic response of the oral mucosa is believed to play a critical role in distributing masticatory forces, thus protecting the underlying residual ridge from excessive loading [6-9].

Interstitial fluid

The mucosa is a highly vascularized tissue (Figure 2-1b) [37] with a considerable amount of interstitial fluid, and its protective function arises from a cushioning effect. The pressure induced by prosthetic dentures provides a pumping effect for the flow of interstitial fluid to the unloaded neighbouring tissues [21, 32]. This movement encourages collagen fibres to align along the lines of mechanical stresses, thereby providing protection to the connective tissue itself as well as the underlying bone. With increasing masticatory loads, the hydraulic interstitial fluid pressure (IFP), or hydrostatic pressure, gradually builds up, which is one of the most important factors in the mucosal physiological responses [9, 11, 12]. Once the interstitial fluid pressure exceeds the vascular pressure, blood flow will be reduced and may temporarily cease, thereby potentially leading to localized ischemia [22, 26, 54-56]. This is a time-dependent process with blood flow reduction increasing with the loading time till a plateau; and the degree of ischemia is dependent on both the loading magnitude and time. The prolonged blood flow interference will further induce local anoxia and accumulation of metabolites, leading to the destruction of the supporting bony tissues, known as residual ridge resorption [9, 10, 13, 54, 57].

Upon mechanical load release, the mucosa is capable of recovery [7, 29, 30, 49, 58]. The released surface pressure allows the interstitial fluid to flow back, and the elastic recovery of the solid matrix accelerates the backflow by forming suction [59, 60]. While the load induced impedance of blood supply is not an irreversible condition, the recovery time is somewhat proportional to the loading magnitude and duration but the extent of recovery is converse [26, 54, 56, 61]. In young subjects, the blood flow can be almost fully restored following a short duration load, and the recovery may even exceed the initial blood flow by as much as 10% [26]. Therefore, the intermittent masticatory pressure may improve circulation. In contrast, more permanent effects of the lowering of blood supply

may result from the wearing of dentures for more than six months [56]. Ischemia occurs with continuous clenching and delays the recovery of blood flow in the mucosa underlying the denture after release of compression. Continuous pressure over a prolonged duration may even alter the oral anatomy, and consequently affect the physiological responses [58]. The mucosa then becomes less resilient to withstand masticatory forces and more sensitive to pressure [62]. Clinical recommendations have been made based on these findings, that it is essential for patients to leave their dentures out at night during sleep to aid in the recovery of blood supply to palatal mucosa [63].

Mucosa Aging

Aging is one of the most important factors affecting the mucosal mechanical properties and responses [64]. Clinically, the aged mucosa often has a smoother, glossier, and dryer surface than that of a young subject. Atrophy develops in the oral mucosa and is manifested by the reduction in surface epithelial layers, consequently the overall thickness decreases [46, 48, 65]. As the epithelial ridges flatten, the interface between the epithelium and the connective tissues becomes smooth. With a decreased number of cells in the lamina propria, the collagen fibre becomes thicker and is arranged in a denser parallel pattern, similarly to the reticular layer [66, 67]. Osteoporosis is also often presented with edentulous patients, and spurs of bone project into the overlying lamina propria, breaking the integrity of the mucosa unit [66]. Functionally, there is no evidence to show that the blood flow is affected by the cardiovascular status of the subject without disease [68], but most aged alveolar and gingival arteries exhibit arteriosclerosis, with narrowing vessels, even becoming occluded in some cases [66]. Decreased vascularisation, blood vessels stiffening, and lipid deposition lead to the reduction of the effective blood flow to the oral tissues, consequently impairing tissue healing ability and tolerance to pressure [69-71]. Also the metabolic activity slows down in the aging mucosa, leading to the reduction in

tissue turnover rate [72], which makes the mucosa more vulnerable to wear and tear induced by external loads.

Histomorphological and Histochemical Change under Compression

In order to clarify the histopathological basics associated with the denture prosthetic effects on the oral mucosa, various studies have been undertaken to investigate the morphological and biochemical changes under different occlusal loads and physiological conditions. Despite the clearly unfavourable effects caused by denture insertion [10, 13, 57, 73], early studies generated contradictory findings; some reported enhanced inflammatory responses in the supporting tissues underneath the dentures [5, 74, 75], while others suggested minimal or no inflammation [28, 76, 77].

Distributed compression (e.g. flat contact) can introduce surface wrinkles to the oral mucosa, and the intercellular spaces were immediately reduced in both the epithelial and the lamina propria layers [32]. A concentrated load (e.g. convex contact) can further induce deformed epidermal and connective tissue ridges, accompanied by collapsed capillary vessels in the submucosa at the concentration point. Without an occlusal load present, the only histological change under the denture was slightly narrowed epithelial ridges in the first twelve weeks, which subsequently disappeared gradually [78] (Figure 2-1c). Neither morphological or biochemical changes were observed in the epithelium and the lamina propria after 28 weeks without pressure.

Under occlusal loading, however, inflammatory change and alveolar bone resorption occurred in the epithelium and the lamina propria, and the extent of these symptoms was proportional to the occlusal pressure [9, 13]. Within two weeks, the thickness of epithelium can be severely reduced (exceeding 30%) [55], manifested with shortened and branching epithelial ridges [9, 13]. The tissue fibres in the lamina propria become parallel to the bone surface, and osteoclasts start to appear (Figure 2-1d). For

occlusal pressures less than 5 kPa, these changes continued to develop through the first 8 weeks and then reduced after 20 weeks, and showed minimal differences to the control group. Within this range, higher pressures resulted in the earlier appearance of osteoclasts, and induced more bone turnover along the endocoritcal surface than the periosteum, as indicated by the osteoblastic activities [55, 79].

The mucosa exhibits a higher tolerance to intermittent pressure than continuous pressure, as the threshold for the alveolar ridge resorption was 19.6 kPa for the former and 6.86 kPa for the latter [10]. Larger continuous pressures induced more severe residual ridge height reductions [11]. At the other extreme, a continuous pressure less than 1.96 kPa (9.8 kPa for intermittent) led to no bone resorption [10], but new bone formation was also inhibited [11]. In the patients with systemic diseases or conditions, such as diabetes mellitus or osteoporosis, the oral mucosa and the underlying bone are more sensitive to occlusal loads, as shown by the lowered thresholds [79-82].

2.3. Biomechanical Responses

While there are many aspects of the biomechanical responses of the oral mucosa, this study will focus on the four major areas which are closely relevant to clinical applications, thereby revealing the biological insights to these mechanical models. The first one is the static response, which is often known as the short-term or instant response. It is interpreted as the elasticity of a material in a path-dependent manner. The second one is the dynamic response, or so-called long-term and delayed response. It can be induced by the viscosity or permeability of the fluid component in the soft tissue, and interpreted in a time-dependent process. The third is the volumetric response, determined by the compressibility or Poisson's ratio to indicate the capability of resisting a volumetric change while the shape is deformed. The last one is the surface interactive response, which is represented by the friction coefficients between the mucosa and prosthetic materials.

2.3.1 Elasticity

As one of the fundamental parameters to define material behaviour, the modulus of elasticity is the mathematical description of an object's tendency to be deformed proportionally to the applied force. Reflecting the stiffness of a material, this parameter is defined as the slope of its stress-strain curve in the elastic deformation region. The higher the elastic modulus, the stiffer the material is.

The oral mucosa was found to be highly deformable under compression [83], and the elastic modulus appears to vary over a broad range. Being a heterogeneous material, the mucosa's instant stiffness results from both the solid matrix structure (e.g. epithelial layer, fibrous network, blood vessel, etc.) and the fluid components (e.g. interstitial fluid, blood). Several material models have been developed to interpret such mucosal behaviours, including linear elastic, biphasic, multiphasic elastic, and hyperelastic models. Within a

short instant loading, the mass transfer, such as the fluid flow, is often disregarded in these models. In other words, this aspect of mucosa response is considered time-independent.

Linear Elastic

Linear elasticity is a simplification of the general nonlinear theory of elasticity as a branch in continuum mechanics. This constitutive model governs reversible behaviour of a material which is indicated by a straight stress-strain response curve with a constant elastic modulus. When subjected to sufficiently small stresses, nearly all solid materials can be represented by linear elastic constitutive equations (Eq. (1) for an isotropic case), which are relatively easy to solve. The linear elasticity model is thus the best known and most widely used theory in biomechanics.

$$\begin{bmatrix} \varepsilon_{xx} \\ \varepsilon_{yy} \\ \varepsilon_{zz} \\ 2\varepsilon_{yz} \\ 2\varepsilon_{zx} \\ 2\varepsilon_{xy} \end{bmatrix} = \begin{bmatrix} \frac{1}{E} & -\frac{\nu}{E} & -\frac{\nu}{E} & 0 & 0 & 0 \\ -\frac{\nu}{E} & \frac{1}{E} & -\frac{\nu}{E} & 0 & 0 & 0 \\ -\frac{\nu}{E} & -\frac{\nu}{E} & \frac{1}{E} & 0 & 0 & 0 \\ 0 & 0 & 0 & \frac{2(1+\nu)}{E} & 0 & 0 \\ 0 & 0 & 0 & 0 & \frac{2(1+\nu)}{E} & 0 \\ 0 & 0 & 0 & 0 & 0 & \frac{2(1+\nu)}{E} \end{bmatrix} \begin{bmatrix} \sigma_{xx} \\ \sigma_{yy} \\ \sigma_{zz} \\ \sigma_{yz} \\ \sigma_{zx} \\ \sigma_{xy} \end{bmatrix} \quad (1)$$

At the early stage of exploring the stress-strain relationship of the mucosa, the experimental reports showed a wide range of possible compressive elastic moduli from 0.06 MPa to 8.89 MPa when using a 'dead' weight or an instant load [29, 40, 44, 51, 84]. Meanwhile, there were several other relevant findings. Firstly, the mucosa is generally stiffer under tension than compression, showing elastic moduli from 0.91 to 11.12 MPa [51]. Secondly, it has anisotropic responses under both tension and compression [51]. Lastly, both mucosa thickness and elastic moduli can vary considerably in the same subject [40] and between individuals [84]. Compared with other oral soft tissues, such as

periodontal ligament (PDL), the oral mucosa shows lower stiffness [85] and the tendency of deforming more easily, with more than 3 times of difference in the tissue displaceability relative to PDL [86].

During modelling of the linear mucosal elasticity and the associated responses to dental prostheses (e.g. complete and partial dentures, dental posts, bridges, and implants), a broad range of elastic modulus values have been adopted in research, often by assumption. Initially, due to lack of sufficient experiment data, the skin properties (19.6 MPa) were adopted [87] for being another typical soft tissue, and this assumption was accepted in two other studies [88, 89]. Another two elastic modulus values, 10 MPa [90] and 5 MPa [91], were first reported in non-English journals. Both gained wide acceptances, such as [92-96] for the former and [97-99] for the latter. To simulate the effects of different mucosa resiliency to compression, elastic moduli of 340 MPa and 680 MPa were assumed for the hard and medium mucosa, compared to the soft one (1 MPa) [100-103]. At the other extreme, a very low elastic modulus of 0.1 MPa was also assumed [104, 105], and so was 0.68 MPa [106, 107] in literature.

There were also elastic moduli derived from experimental observations. A typical value of 1 MPa was derived from the experiment by Picton [86], and adopted in several finite element analysis (FEA) studies [108-117]. Similarly, other values between 1 and 5 MPa were determined experimentally [51, 84], and adopted for simulations [118-126].

All these linear elastic models from the literature assumed linearity with homogeneity and isotropy of the mucosa, although it has been anatomically demonstrated as a heterogeneous and anisotropic composite material [51], responding to mechanical loading in a complex non-linear manner [52]. Despite the over-simplified mechanics and limited supporting biological evidence, linear elasticity has its advantages in providing simple and direct prediction for the mucosa's instant response. A simplified elastic model

is also preferred for the sake of the computational efficiency [127]. Therefore, the linear elastic material model has been extensively adopted in a number of studies, and has achieved wide acceptance, especially in the clinical field. Nevertheless, in such a simplified material model the elastic modulus varies over an enormous range from 0.1 to 680 MPa, which consequently alters the soft tissue behaviour dramatically. Figure 2-2a summarizes the frequencies of different linear elastic moduli values appearing in the previous studies, and Figure 2-2b shows some examples of linear elastic models with the moduli of 1, 5, and 20 MPa.

Bi-phasic and Multi-phasic Linear Elasticity

Previous studies have shown that the mucosa thickness reduction was not proportional to the load increase [128], and with further increased compressive loads, the effects on the mucosa are compromised, suggesting an increasing elastic modulus with higher pressures [52]. The histological analysis indicated the nonlinearity may have resulted from the microstructural deformations, such as buckling and space close-up in the fibrous network and epithelium [32]. Consequently, the simplest linear elastic model does not adequately address the nonlinearity of the mucosal response [83, 129].

A bi-phasic linear elastic model was developed by using two moduli for approximation of the nonlinear stress-strain curve, thereby addressing change of the initial and subsequent moduli in a path-dependent manner. The switching between these two moduli is determined by mechanical stress (Eq. (2), where n is the number of phases, n = 2 for this biphasic model), strain, or strain energy at a typical conversion point. The approach captures more features of the tissue responses, without substantially increasing computational cost. The effectiveness of such a bilinear material was verified using animal studies along with the other oral soft tissue, the periodontal ligaments (PDL) [130], and it has been applied in an associated finite element analysis [131].

$$\varepsilon_{ij} = \begin{cases} C_1\sigma_{ij} & if\ \sigma_{ij} \le \sigma_1^* \\ C_2(\sigma_{ij} - \sigma_1^*) + C_1\sigma_1^* & if\ \sigma_1^* < \sigma_{ij} \le \sigma_2^* \\ \quad ... & \\ C_n(\sigma_{ij} - \sigma_n^*) + C_{n-1}(\sigma_n^* - \sigma_{n-1}^*) + ... + C_1\sigma_1^* & if\ \sigma_{ij} > \sigma_n^* \end{cases} \quad (2)$$

Despite considering the modulus rise with deformation strain, the biphasic linear elastic model still remains relatively simple and primitive, and few studies of relevance to mucosal responses have adopted this material model. Instead, a subsequent multi-phasic linear elastic material model (Eq. (2)) was developed, which was capable of capturing a more precise loading path for the mucosal deformation [132] (Figure 2-2b, dash line). The multi-phasic linear elastic material model has a series of path-dependent elastic moduli and corresponding conversion points at different loading extensions, to better imitate the nonlinear behaviour. This material model was derived based on the *in vivo* results of mucosal responses in the literature [52], by using 6 von Mises stress values as determinants of the conversion path, and the compressive response matches reasonably well with the *in vivo* measurements. This model enables a balance to be made between accuracy and computational efficiency, as the true nonlinear analysis requires a large number of loading steps with a substantial time penalty. With the increasing number of elastic phases, the stress-strain curve approaches the real nonlinear indefinitely, and the computational time rises in turn with more iterations.

Hyperelastictiy

Even with a multi-phasic linear elastic material model, the exact nonlinear elasticity cannot be entirely reproduced, as segmented straight lines do not represent the true equilibrium path. A hyperelastic material (so called “Green” elastic material) requires a constitutive model, which derives the elastic response from a strain energy density function,

providing a continuum approach to nonlinearity modelling of continuous material. It has been commonly applied in the mechanics of rubber-like materials, and the similarity to biological soft tissues has recently attracted noticeable attention [133]. These types of material models respond elastically (reversibly) under very large strains, which is exactly what a biological soft tissue does under both normal and pathological conditions [134].

Hyperelastic material modelling starts with the formulation of a potential energy function based upon scalar strain. The strain energy potential defines the strain energy stored in the material per unit of reference volume (volume as in the initial configuration) as a function of the strain at a typical point in the material. Such functions can be dependent either on strain tensors of a nonlinear deformation field, or on the invariants of these strain tensors, or even directly on the principal stretches. Simply speaking, the hyperelastic material describes the stress-strain relationship using a continuous function rather than one or a series of elastic constants, generating a true nonlinear map of behaviour.

Hyperelastic material models can be generally classified into two categories, mechanistic (micro-mechanical) and phenomenological [135]. The former is directly derived from statistical mechanical arguments of the underlying material structure or idealized network, such as cross-linked polymers. Arruda-Boyce and Neo-Hookean are the two types of models in this category [135]. The mechanistic category is intrinsically tied to higher computational costs for its homogenisation procedures, and these micro-mechanical approaches link the macroscopic mechanical behaviour by using their governing parameters. Despite this profound basis, the requirements for understanding the structural composition and associated behaviours are extremely difficult in such mechanistic models, and often remain unclear or understudied for most biological tissues.

The phenomenological category, on the other hand, aim to link the functions to the direct empirical observations of phenomena, to match with fundamental theories. The functions in this category include Fung, Mooney-Rivlin, Ogden, Polynomial, Saint Venant-Kirchhoff, Yeoh, and Marlow [135]. Ogden, being a popular type, can be expressed as in Eq. (3), in which $\bar{\lambda}_i$ are the deviatoric principal stretches obtained from the principal stretches, N is the order of the fitting equation, and μ_i, α_i, and D_i are the parameters for such a hyperelastic model.

$$U = \sum_{i=1}^{N} \frac{2\mu_i}{\alpha_i^2}(\bar{\lambda}_1^{\alpha_i} + \bar{\lambda}_2^{\alpha_i} + \bar{\lambda}_3^{\alpha_i} - 3) + \sum_{i=1}^{N} \frac{1}{D_i}(J^{el} - 1)^{2i} \quad (3)$$

Compared to the stringent conditions required for the mechanistic category, the phenomenological models present distinctive advantages. The approach of fitting hyperelastic models to experimental data has been addressed in a number of textbooks [136, 137] and studies [133, 138-140], and it has been adopted for several different types of soft tissues in the human body, such as ligaments [141, 142], meniscus [143], skin [144], oesophagus [145], and oral PDL [146, 147]. Recently, Winterroth et al. characterized the nonlinear elastic property of engineered oral mucosal tissues by using scanning acoustic microscopy and fitting data to the 1st order Ogden strain energy potential function [53] (Eq. (3), where n = 1). Recent developments in computational power and techniques, have enabled more realistic models of tissue behaviour [117, 132, 146, 148, 149]. Surprisingly, little attention has been paid as yet to this material model to simulate the native oral mucosa response, which may be due to the requirements of incorporating its high nonlinearity and anisotropy [150, 151]. Figure 2-2b includes an example of hyperelastic material model (Ogden 3rd Order) derived from the clinical data reported by Kishi [52].

Comparison

To illustrate the differences between these above mentioned elasticity models, a simple three-layer block (mucosa, cortical, and cancellous bones) is adopted herein to simulate the local mucosal response under uniformly distributed compression over an area of 10 mm in diameter (Figure 2-2c). A mucosa thickness of 2 mm is assumed here based on the average clinical measurements [8]. Periodic boundaries are prescribed to the surrounding sectional planes to simulate the tissue continuity with the neighbours, and a full constraint was assigned to the bottom of the block. The load on the top surface was ramped from 0 to 100 N.

The material properties for the bony structures are isotropic and homogeneous, following the previous literature [146] to set a baseline. All three static elastic material models (linear, multi-phasic, and hyperelastic) were considered for the mucosa. Three linear elastic moduli are adopted at 1 MPa, 5 MPa, and 20 MPa to simulate low, medium and high stiffness in the most accepted range of literature values. The multi-phasic model was adopted as developed by Kanbara et al. [132]. The hyperelastic material model (Ogden 3rd Order) is derived from the empirical data by Kishi [52]. The Poisson's ratio is set to be a constant of 0.3 for all material models to focus the differences entirely on elasticity values and models. Figure 2-2d plots the percentage of the maximum mucosa thickness changes against the increasing loads under different material models.

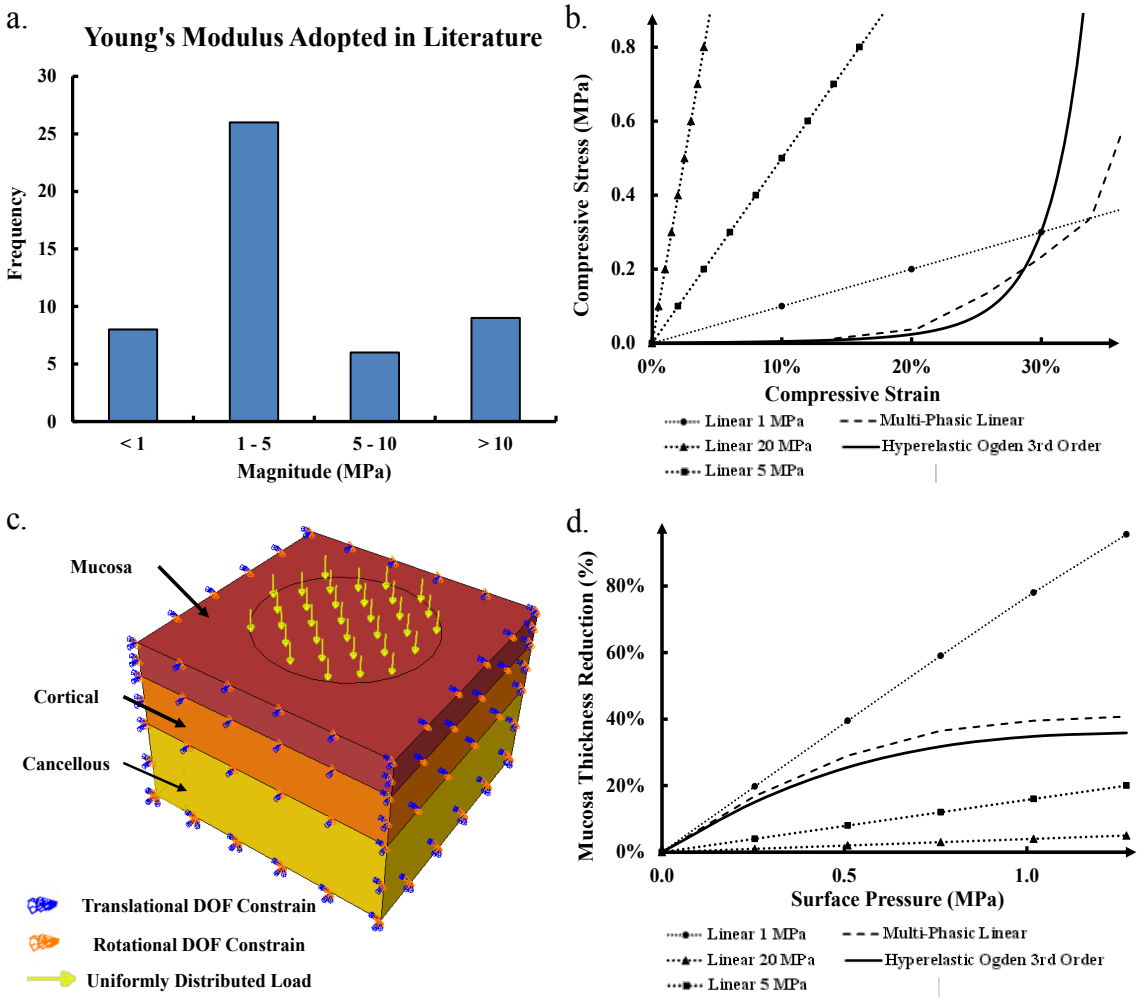

Figure 2-2 (a) The frequencies of different linear elastic moduli adopted in existing FE studies; (b) a simplified model to present a unit of mucosa-bone structure; (c) the compressive stress-strain relationships between different material models (linear elastic, multi-phasic elastic, and hyperelastic); (d) the maximum mucosa thickness changes in the different material models of mucosa under increasing loads up to 100 N in the test model.

2.3.2 Viscosity and Permeability

Accompanying the instant elastic response, the oral mucosa exhibits a dynamic response over the time under loading and upon unloading, such as creep and delayed recovery [21, 50, 85]. It is believed that, not only the interstitial fluid, but also the fluid components within the mucosa matrix contribute to this time-dependent behaviour [152]. Both the fluid viscosity and permeability contribute on the dynamic response, but the former has been better studied than the latter in the current literature. Being a complex

composite material, neither the viscosity nor the permeability alone represents the mucosal characteristics; they are concurrent with the elasticity, either linear or nonlinear. This section will focus on two material models, viscoelastic and porous elastic (poro-elastic).

Viscoelasticity

The time-dependent response was firstly quantitatively illustrated as the viscoelastic property by a histometric analysis conducted on dogs in the time domain [50], which suggested that apart from the elastic response, there was a viscous component in this fluid-rich material. The viscoelastic behaviour manifested during four stages under loading and upon unloading, namely the instant deformation, the creep, the instant recovery, and the delayed recovery.

Upon immediate loading, the instant elastic deformation (1st Stage) takes place as elucidated by its elasticity, with relatively less noticeable viscous response in such a short time. The following creep at constant load (2nd Stage) can last for more than 6 hours with the trend continuing [50], sometimes for days. The extent of the creep can vary from 4% to 30% of the total mucosa thickness [44, 52, 128], and gradually slows down after 1 minute [52]. The 'elastic' modulus after the creep stage settles usually after 1 hour, which is called the 'steady' modulus, and it can however still vary from 0.04 to 2.35 MPa [40, 44, 52, 128, 153]. Upon unloading, some proportion of the elastic deformation recovers (3rd Stage), typically from 46% to 91% of the total mucosa thickness, which is also dependent on the loading history, including magnitude and duration, in a nonlinear manner [6, 86, 128]. Similar to creep, the delayed viscous recovery (4th Stage) continues for much longer than the instant recovery, and may reach 70-90% of the initial thickness [44, 128]. Compared with the PDL [85, 86], the protracted recovery that was observed in the mucosa, which could take more than 1 hour to complete, while it was only 1 to 2 minutes for the PDL.

With increasing loads, these differences were significant, suggesting a more considerable viscous behaviour in the mucosa.

Several factors can affect the viscoelastic response [6], and are attributed to the physiology of incorporated biofluid. The mucosa in the elderly often has more significant viscous behaviour, especially the prolonged time and the less rebound with delayed recovery. It was suggested this arose because of the reduced amount of elastin and the greater capability of maintaining fluid in the mucosa with patient age [21]. Increasing contact areas generally lead to the stiffer mucosal responses [6, 52, 128], and higher loading rates also have similar effects [40, 86, 128]. Male subjects were found to exhibit stiffer mucosa response with slower recovery than female subjects [29], and it was suggested that female subjects usually have thicker mucosa than males [6].

The most fundamental material model for viscoelasticity has two components as observed in experimental studies, the elasticity and the viscosity [154], which can be modeled in series (known as Maxwell model, Figure 2-3a upper left) or in parallel (known as Kelvin-Voigt model, Figure 2-3a upper right). A materials' elasticity can be a path-dependent factor following Hooke's Law just like a spring, and the viscosity exhibits the time-dependent effect like a dashpot.

In the literature, there are only few reports on the usage of viscoelastic models for mucosa. Two of the early studies [155, 156] assumed the orthotropic mucosa properties in a simplified 2-dimensional finite element model assuming a standard linear solid of a Kelvin-Voigt and Maxwell model in series, with the elasticity E_1 = 1.1 MPa, E_2 = 1.2 MPa, and the viscosity η_1 = 18 MPa·s, η_2 = 250 MPa·s. Other researchers [7, 157] assumed an isotropic, homogeneous, and linearly elastic body under isothermal conditions, and attempted to use an exponential function (Eq. (4)) [158]. In this equation, the modulus is

dependent upon time (t) and determined by two parameters, the initial modulus (E_0) and the relaxation time (τ). By matching the numerical model with clinical data, the initial modulus was determined through a reverse-engineering approach at 0.083 ± 0.020 MPa, and the relaxation time is 503 ± 46 seconds [7, 157].

$$E_0(t) = E_0 \times e^{(-t/\tau)} \tag{4}$$

These two-component systems are the simplified version of the generalized Maxwell model (Maxwell-Wiechert model, Figure 2-3a lower), in which several Maxwell elements (spring plus dashpot) are assembled in parallel to accommodate more complex relaxation and creep behaviours.

Prony's method is often used in the interpretation of the experimental data, to derive the coefficients for the Prony's expansion of multiple exponential terms (Eq. (5), for relaxation modulus) [159, 160]. It should be noted that G in this equation represents the shear modulus, but it can also be tensile-compressive modulus E, or bulk modulus K when needed, τ is the relaxation time. Often, the relaxation coefficient (g_i) is normalized against the modulus as in Eq. (6).

$$G(t) = G_0 - \sum_{i=1}^{n} G_i \times [1 - e^{(-t/\tau_i)}] \tag{5}$$

$$G(t) = G_0 (1 - \sum_{i=1}^{n} g_i \times [1 - e^{(-t/\tau_i)}]) \tag{6}$$

Besides the time domain, another approach is to study and model the viscoelasticity in the frequency domain, by using dynamical mechanical testing (DM) and magnetic resonance elastography (MRE) [161-163], by applying a small oscillatory stress and measuring the resulting strain. This approach expresses the viscoelastic properties by using the complex modulus (Eq. (7)).

$$G^*(\omega) = G'(\omega) + iG''(\omega) \quad (7)$$

In this equation, *i* is the imaginary unit, G′ and G″ are the storage modulus (elastic) and the loss modulus (viscous), respectively. The stress and strain are in phase for the purely elastic materials, generating the immediate response of one caused by the other, so the second term comes to zero. In contrast, the purely viscous material has a 90 degree phase lag in strain response. Viscoelastic materials behave somewhere between these two extreme types of materials. The two complex modulus parameters were determined as 2.53 ± 0.31 MPa (G′) and 0.90 ± 0.22 MPa (G″) by *in vivo* MRE [164]. The impact of fluid amount in the mucosa was also verified under DM [153]. While this approach has been applied to PDL numerical modelling [165], there has not been any report on the mucosa.

Porous elasticity (Poro-elasticity)

In contrast to the viscoelastic material model assuming a homogenized material, the porous elastic model considers the mucosa as a two-phase material, consisting of the solid porous matrix (e.g. collagen) and the ground (fluidic) substance (e.g. watery solutes) [59]. The ground substance, or the interstitial fluid for the mucosa, is allowed to flow from a stressed region to the unloaded neighbour regions, and the fluidic behaviour is described by Darcy's law (Eq. (8)), in which Q is the total discharge rate (usually in mm^3/min), A is the active area, h is the specimen thickness, and ΔP is the pressure difference to drive the flow. The permeability k in Eq. (8) is porosity-dependent (Eq. (9)), and is affected by the void ratio e at a certain time instant [166]. At zero strain, k_0 is the initial permeability at the initial void ratio e_0. M is a dimensionless constant.

$$Q = k\frac{A\Delta P}{h} \quad (8)$$

$$k = k_0 \frac{e(1+e_0)}{e_0(1+e)} \exp(M(\frac{1+e}{1+e_0})) \quad (9)$$

Current research interest regarding mucosa permeability lies in drug delivery through oral tissues [167, 168], and the permeability examined in the literature was mostly for the absorption from the external space through the mucosa (perpendicular to the mucosa). Due to the structural complexity and the difficulty in preserving mucosa integrity, the permeability (parallel to the mucosa) that defines internal fluid flow has not been well studied. For other oral soft tissue, e.g. PDL, *in vivo* tests [169] have been performed to investigate the role of interstitial fluid on its mechanical response, and a porous hyperelastic (nonlinear elasticity) numerical model has been developed to match with the experimental results [170]. The initial permeability k_0 and the dimensionless constant M were found as 8.81×10^{-9} mm^2 and 14.2, respectively, which provide some insight for future studies on the mucosa.

Comparison

As some fundamental data for the mucosa is not yet available for incorporating into a porous elastic material model, this literature review focuses on the dynamic differences in the viscoelastic model, by varying the viscous terms. A Prony series is adopted as a general approach to deriving viscous response of soft tissue from clinical data by the least-square method [159]. Based on the creep data reported by Kydd et al. [6], a 1st order Prony series (one exponential term, Eq. (10)) provides sufficient fit (strain error < 1%). The linear elastic constant, E_e, is inversely determined at 0.083 MPa assuming Poisson's ratio at 0.3, similar to some early reports [7, 157]. The normalized relaxation coefficient, g_1, is found at 0.527 (or 0.044 MPa for the absolute value with the determined elastic modulus), and the time constant, τ_1 is 90.6 seconds.

$$E(t) = E_e(1 - g_1 \times [1 - e^{(-t/\tau_1)}]) \quad (10)$$

We adopted these inversely determined parameters for the same model used in Section 3.1, and tested under a constant loading of 50 kPa (equivalent to the average contact pressure under a common denture base with an occlusal load of 150 N) [7]. The volume-averaged strain under the loading area along the loading direction (ε_{33}) is plotted against time (brown solid line, Figure 2-3b), showing 10 minutes of creep and 10 minutes of recovery. The clinical data [6] is also included as shown by black rectangles for comparison.

Upon varying one of the two parameters, we can compare the variation in mucosal responses. At the constant τ_1 (90.6 seconds), the higher normalized relaxation coefficient g_1 at 0.7 (pink solid line) imply increased viscous response than the elastic component, whereas the lower g_1 at 0.3 (green dash line) is opposite. At the constant g_1 (0.527), the time constant τ_1 at 60 and 300 seconds indicate faster creep (blue dash line) and slower creep (red solid line), respectively.

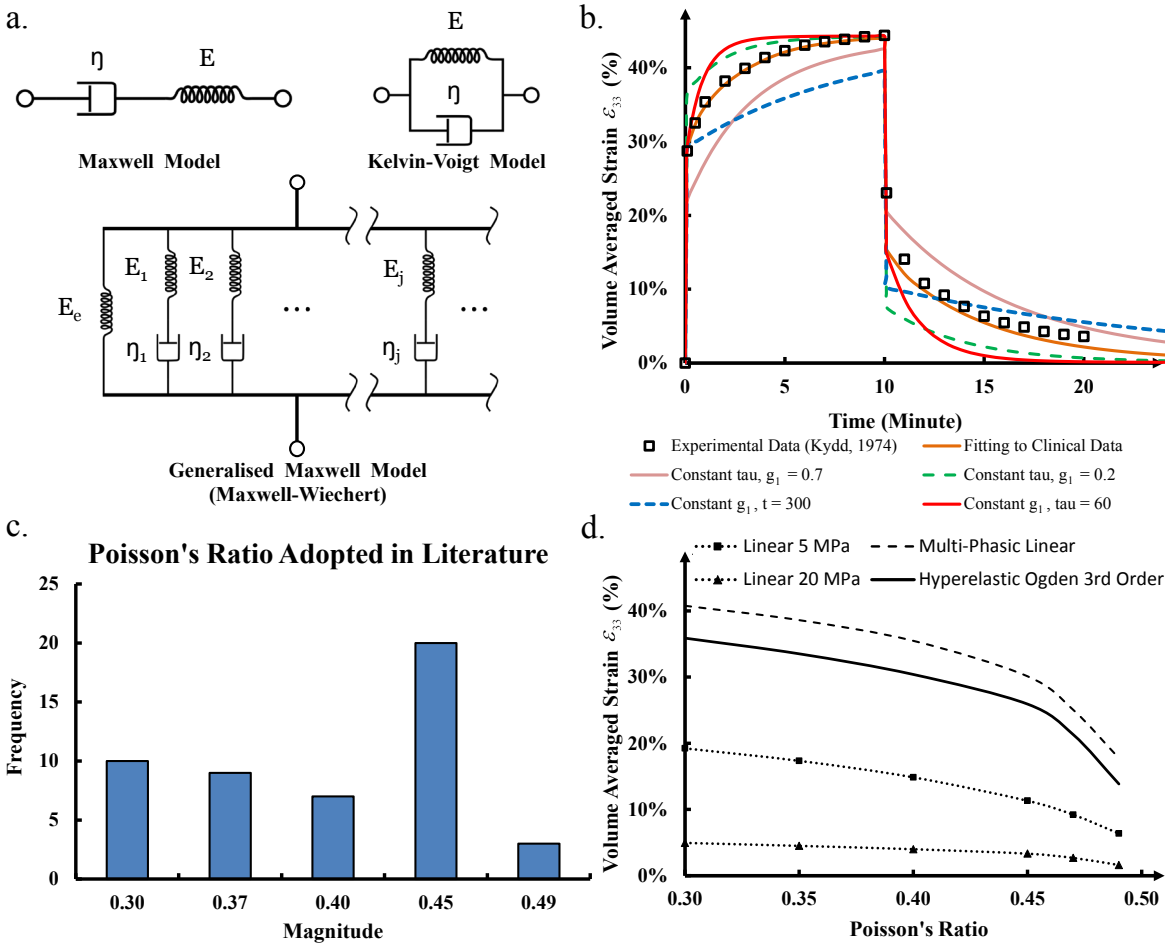

Figure 2-3 (a) The schematic diagrams of common viscoelastic material models; (b) the viscoelastic responses of different parameters in the test model, compared to the clinical data; (c) the frequencies of different Poisson's ratios adopted in existing FE studies; (d) the volume averaged strain responses by the different Poisson's ratios of mucosa under 100 N in the test model.

2.3.3 Poisson's Ratio

Poisson's ratio is the other fundamental mechanical property just like the elastic modulus, which defines the volumetric response of the mucosa to mechanical loading. It is the tendency to resist a volumetric change when the material shape is deformed, and it is often defined by the negative ratio of the transverse strain to the longitudinal strain. Under compression, material tends to expand sidewise along the perpendicular directions to the loading direction; while under tension, it then tends to shrink. As another natural property, Poisson's ratio indicates the compressibility of material, and the value of 0.5 indicates a

perfectly incompressible material. Thus, the volumetric behaviour of the oral mucosa is determined by its Poisson's ratio.

As the oral mucosa is a nonlinear and heterogeneous composite material, this volumetric response is more appropriately considered as 'the apparent Poisson's ratio' or 'the Poisson's effect', to reflect the homogenized behaviour generated by all the individual components involved. The term 'Poisson's ratio' used in this review is for brevity and common acceptance in elastic materials.

Compared to the exhaustive investigation conducted on the mucosa stress-strain relationship (elasticity), few reports are available regarding its lateral responses, or its compressibility, with surrounding neighbour tissues involved. The primary reason is the difficulty of measuring the lateral response. The highly complex and continuous anatomic morphology makes direct *in vivo* measurement difficult (if not impossible), and the mucosa acts as a unit from the surface epithelium to the sub-surface periosteum bonded to the bone, which prevents *ex vivo* loading to break its integrity. There are some non-invasive *in vivo* techniques to measure the displacement/strain responses in soft tissues but these are somewhat limited, they are termed elastography (and include ultrasound elasticity imaging, magnetic resonance elasticity imaging, and tactile imaging) [171-174]. These image-based techniques can monitor the lateral motion under a constant compression or dynamic vibration along the axial motion. In addition to the benefits of being non-invasive, the accuracy significantly relies on the image resolution and noise deduction procedures. So far, the only application of elastography to the oral mucosa was documented by Cheng et al. [164] on its elastic modulus, but no information was reported on the Poisson's ratio or lateral response. Apart from the technique issues, the other reason is perhaps the insufficient awareness of the importance of Poisson's ratio. In fact, the discrepancy of

different Poisson's ratios was claimed as a non-critical factor for its response in the literature [29].

Without sufficient experimental data, most finite element studies have made assumptions of Poisson's ratios based upon the knowledge gained from other soft tissues. One typical value of 0.3, adopted from skin [87], has been widely accepted for static linear elastic studies [88, 89, 104, 105, 112-115] and dynamic viscoelastic analysis [7, 157]. Another two values often appearing in literature are 0.37 [127] and 0.4 [92], derived from earlier experimental studies [86, 90], have gained wide acceptance [94, 96, 100-103, 108-110, 116-119].

Biological soft tissues are often considered as 'incompressible'; and being one of them, the mucosa was also assumed to have higher Poisson's ratios to simulate the low compressibility or non-compressibility (perfectly incompressible). The values of 0.45 [95, 100-103, 106, 107, 111, 121-124, 126, 175] and above [97-99], or even 0.5 [29] have been suggested for finite element study purposes. Apart from the constant Poisson's ratio, a series of multi-phasic Poisson's ratios have been adopted by Kanbara et al. [132], in which the Poisson's ratio increases with von Mises stresses at the conversion points from 0.3 to 0.49. In conclusion, a range of Poisson's ratios from 0.3 to 0.5 have been adopted in the previous studies, and the frequency in the literature is summarized in Figure 2-3c.

To illustrate the effects of Poisson's ratio on the mucosal responses, the same model used in Section 3.1 is tested with the Poisson's ratios from 0.3 to 0.49, with linear elastic (E = 5 and 20 MPa) and hyperelastic (Ogden 3rd Order) material models, under a constant load of 100 N. The volume-averaged strain is plotted in Figure 2-3d against increased Poisson's ratio values. Clearly, Poisson's ratios affect the mucosal response in a nonlinear manner, where the higher the Poisson's ratio, the less deformable the tissue.

2.3.4 Friction Coefficient

The oral mucosa being a protective layer over the residual ridge, does not just sustain the compressive loading, but also the surface shear induced by the friction beneath the dentures. The prevalence of mucosal lesions associated with denture wearing is well known. Acute or chronic reactions to the mechanical injury can be caused by both microbial denture plaque and constituents of denture materials [176]. Most of these denture-induced symptoms, such as traumatic ulcers, angular cheilitis, irritation hyperplasia and keratosis, are related to the frictional loading on the mucosa and are hard to cure [177-179].

Understanding the interactive response between denture and the supporting mucosa is critical to prevent soft tissue injuries, and the associated occlusal load transmission requires correct determination of nonlinear elastic contact. This interactive response can be related to the friction coefficient, which differs significantly among subjects, depending on their oral physiological conditions and denture materials used [180].

The variability of saliva generation alters the friction coefficient, thereby affecting the contact responses [181]. Xerostomia (known as dry mouth) is one of the most common problems in the elderly edentulous population, associated with reduction of saliva production, which has been shown to cause severe impact on denture usage, leading to membrane stomatitis [97, 180, 182, 183]. In experimental studies, high friction coefficients between 0.3 and 0.4 were reported with ‘dried’ surfaces (hydration index closes to 0, to simulate xerostomia) [181, 184], whereas a low value around 0.02 was reported for well-lubricated conditions [184].

With the same oral condition, the friction coefficient can also change between different denture materials. A material with higher wettability will be more likely to form a

superior lubricating layer between the supporting mucosa surface and the denture base, thus protecting the surface tissue by reduced friction. Seven types of common denture liner materials were tested *in silico* [185]. Under dry conditions, the friction coefficient was between 0.35 and 0.97; after being wetted in a warm water bath, the friction coefficient dropped to between 0.24 and 0.90. Acrylic resin material was found to have significantly better wettability than silicones [186], and the friction coefficient decreased drastically when wet [185].

Clinically, no effective *in vivo* approach has been reported for measuring the friction coefficient of individual patients. Meanwhile, due to the complexity of the nonlinear contact simulation, the results of such finite element studies are somewhat diverse. By comparing the linear and non-linear contacts under the denture base, a finite element study found that while the difference was less than 20% in terms of the magnitude of the von Mises stress in the mucosa and claimed to be insignificant [187]. Other studies have adopted either fully bonded, fully tied, or other linear contact mechanism between the denture and the mucosa, to simulate a linear transmission of occlusal forces [98, 103, 106, 107, 112, 119, 120, 122, 126]. On the other hand, while incorporating this nonlinear mechanism, most studies adopted different frictional coefficients from 0 (frictionless) to 0.75 (penalty contact) [96, 97, 104, 105, 108, 110, 111, 113, 117, 121, 157, 181, 183, 188].

Nevertheless, there has been no systematic study on the effects induced by different friction coefficients, and this review will test the common range reported in literature, from 0.02 to 0.8, for both linear elastic (elastic modulus at 5 and 20 MPa) and hyperelastic (Ogden 3rd Order) material models as used in Section 3.1.3. The interactive reaction is highly dependent on the surface morphology of the interface; therefore, a simple 3D jaw model is constructed from the CT images. The complete denture is made of acrylic containing $BaSO_4$, to impart radio-opacity, with an elastic modulus of 2.67 GPa and a

Poisson's ratio of 0.167 [189, 190]. A pair of bilateral occlusal loads equivalent to 60 N is assigned to the vicinity of the first molar, along the tooth root direction, and full constrains are applied to the distal condyles of the mandible (Figure 2-4a) [190]. As the primary indication for the pathological consequences, the maximum contact pressure of the mucosa surface is plotted in Figure 2-4b against the frictional coefficient. The linearly elastic material models show either marginal differences or decrease in the maximum contact pressures, with increasing friction coefficients, which obviously do not match the clinical observations [181, 184]. In this figure, the path-dependent material models, multi-phasic elastic and hyperelastic, show gradually increasing maximum contact pressures with increasing friction coefficients.

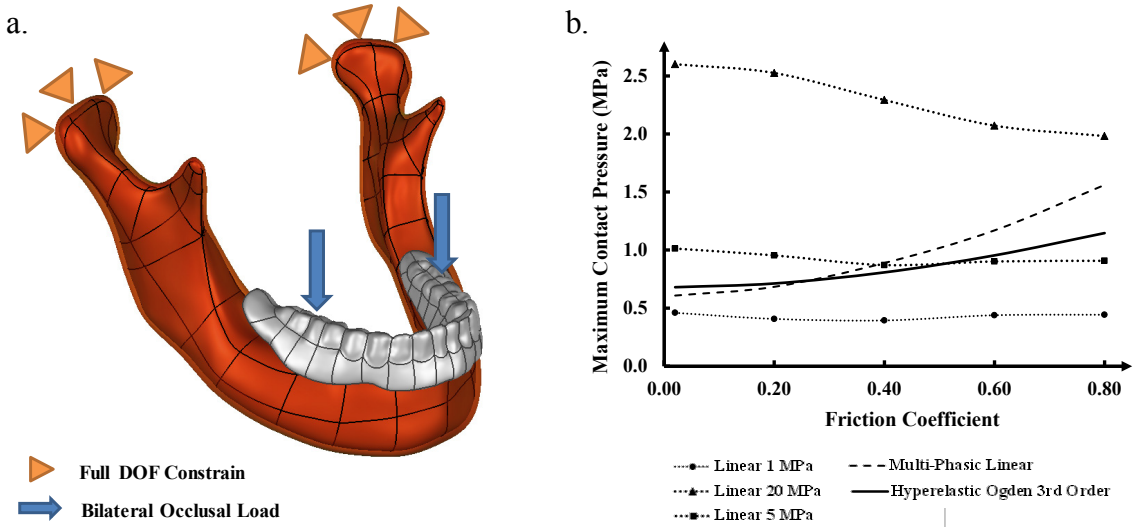

Figure 2-4 (a) The schematic diagram of the finite element model in the friction coefficient test; (b) the maximum contact pressure against increasing friction coefficients in different material models.

2.4. Clinical Implication

All biomechanical models of the mucosa serve the purpose to interpret, analyse, and predict the various biomechanical aspects of the mucosal responses to dental prostheses, for possible optimal treatment outcomes and with minimum side effects to patients. This section will illustrate some common clinical concerns and link them back to the biomechanics to identify specific insights relevant to dental prosthetic design and treatment planning.

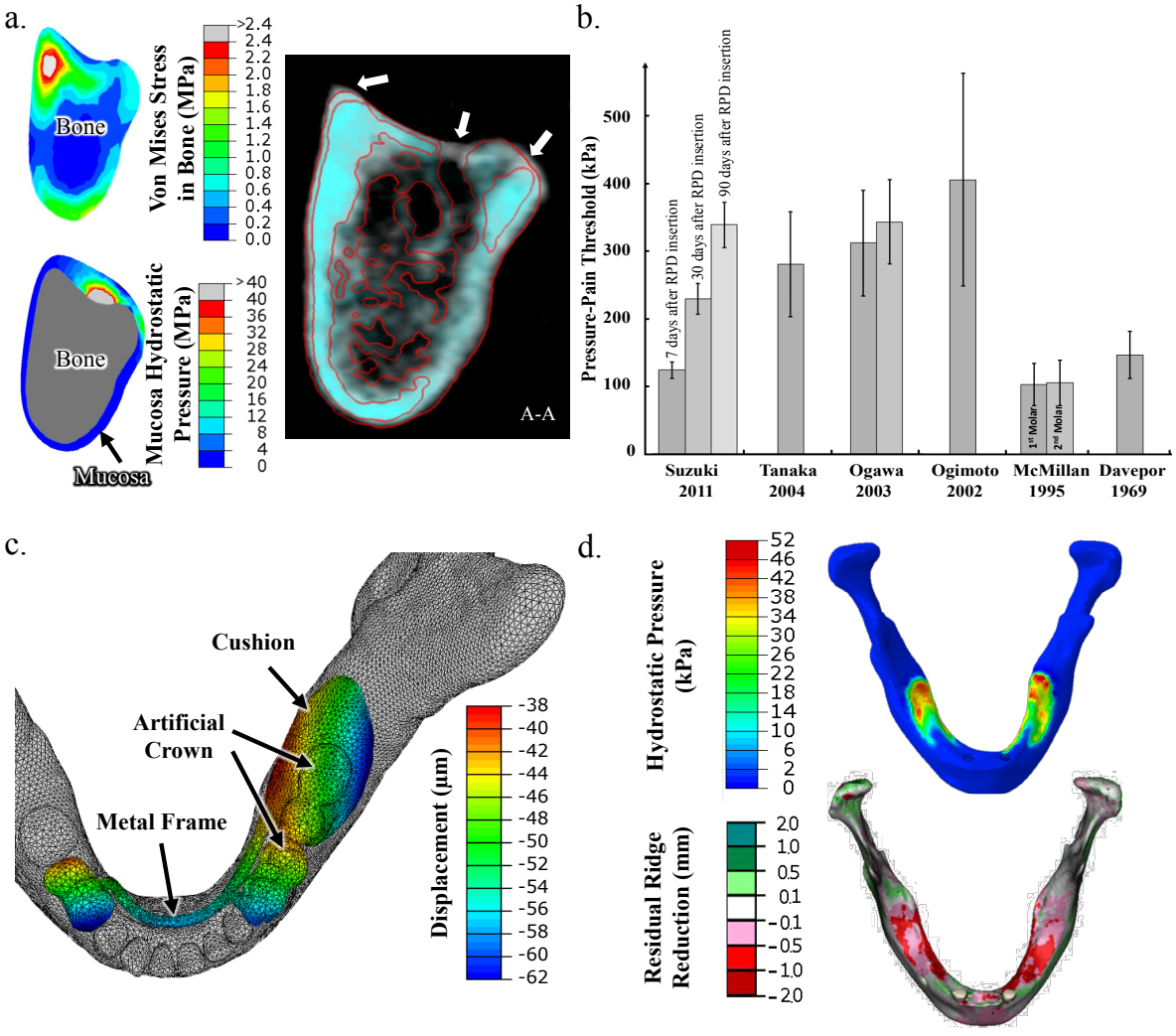

Figure 2-5 (a) The distribution patterns of the von Mises stress in bone and the hydrostatic pressure in mucosa compared to the residual ridge resorption under CT (white: before denture insertion; cyan: 1 year after denture insertion); (b) the PPT thresholds determined in the clinical data of literature; (c) the vertical displacement of a removable partial denture

under an occlusal load of 60 N on the 1st molar; (d) the mucosa hydrostatic pressure pattern vs. the residual ridge height reduction.

2.4.1 Tissue Stimulus

Often mechanical bodies experience more than one type of mechanical stresses (e.g. normal and shear) along different directions, and a general expression of these stresses can be defined by the Cauchy stress tensors (Eq. (11)). To assess the collective effect of these different components on biological variations, several scalar forms can be computed from the Cauchy stress tensor, such as the von Mises, Tresca and maximum principal stresses.

$$\begin{bmatrix} \sigma_{xx} & \sigma_{xy} & \sigma_{xz} \\ \sigma_{yx} & \sigma_{yy} & \sigma_{yz} \\ \sigma_{zx} & \sigma_{zy} & \sigma_{zz} \end{bmatrix} \tag{11}$$

Among these scalar forms, the von Mises (VM) stress (Eq. (12)) has been most prominent and widely applied in the finite element analysis for materials engineering. It is also known as the equivalent stress in biomechanics, and derived based on the von Mises yield criterion, suggesting the yielding of material occurs once the second deviatoric stress invariant reaches a critical value. In dentistry, its applications to dental implants and other metallic prostheses (such as some parts of the partial removable denture, the metallic sleeve/bar within overdentures) has been well recognized [102, 106, 107, 148, 191]. With assumptions regarding homogeneity and isotropy, the application of such an equivalent stress has been extended from metallic materials to both cortical and cancellous bones [192-195].

$$\sigma_{vm} = \sqrt{\frac{(\sigma_{xx} - \sigma_{yy})^2 + (\sigma_{yy} - \sigma_{zz})^2 + (\sigma_{xx} - \sigma_{zz})^2 + 6(\sigma_{xy}^2 + \sigma_{yz}^2 + \sigma_{xz}^2)}{2}} \tag{12}$$

A histological study on the anatomy of mucosa has revealed it as a complex structure with a large number of channels and vessels [37]. The interstitial fluid filling this

porous structure can flow to the neighbouring mucosa under compression and transmit loads through a highly vascularized network embedded inside the mucosa [21, 32]. This fluid-induced stress over any nominal internal plane is equal in magnitude and always directed perpendicular to this plane, regardless of its orientation. This isotropic stress status is known as the interstitial fluid pressure (IFP) or hydrostatic pressure (Eq. (13)) within the mucosa, and indicates the functional pressure. Different to the von Mises stress, the hydrostatic pressure is related to the first stress invariant.

$$\sigma_{\text{hydro}} = \frac{\sigma_{11} + \sigma_{22} + \sigma_{33}}{3} \tag{13}$$

The hydrostatic pressure from animal studies varies across different locations in the oral mucosa [196-198]. In rats, the highest IFP of 1.97 kPa was found at the hard palate, and the lowest ones were found at the alveolar mucosa and the free gingiva at 0.48 and 0.31 kPa, respectively. Around the attached gingiva, the pressure can vary from 1.14 to 1.23 kPa. The hydrostatic pressure can increase if there is an inflammatory response [199], which may occur following denture insertion [21, 22] and consequently compromise mucosa permeability [168, 200]. Being one of the most important etiological factors to denture-induced symptoms [9-14], excessive interstitial fluid pressure (hydrostatic pressure) can reduce blood circulation and even temporary cause localized ischemia [26, 54-56], accompanied by pain and discomfort [85]. Such prolonged excessive pressure may lead to the destruction of the supporting bony tissues, known as residual ridge resorption [8-10].

To investigate mucosal responses to external loading, such as denture insertion, the hydrostatic pressure determined from FEA provides meaningful indication to possible internal biomechanical changes [201-204]. Figure 2-5a compares the distributions of the von Mises stress in the bone and the hydrostatic pressure in the mucosa, and examines their relevance to the residual ridge resorption measured from two sets of CT scan images over

one year duration. The white mask in the CT scan is the pre-insertion status of the patient, and the cyan mask is 1-year post-insertion. The white triangles indicate the most severe locations of bone resorption, which obviously better correlated to hydrostatic pressure distribution.

While fundamental knowledge concerning hydrostatic pressure has been well studied in fluid statics problems, its application to biological tissues is gradually increasing and being recognized over a wide range of anatomical components, such as stomach, heart, liver, lung, ligament, and cartilage [204-208]. For the oral mucosa, it has been used to evaluate the possibility of tissue remodelling driven by the occlusal loads during tooth eruption under the combined stimuli of intermittent tongue, lip and cheek actions [209]. In the other oral tissue, PDL, the hydrostatic pressure has also been shown as a mechanical stimulus for remodelling in the surrounding bony structure during orthodontic treatment [146], as well as the accompanying root resorption [201, 210]. If the hydrostatic pressure in PDL exceeds the capillary blood pressure, partial or complete collapse of the capillaries may occur just like in the mucosa. The distributions of hydrostatic pressure matched well with the clinical observations of residual ridge reduction.

Hydrostatic pressure also plays a role of predicting the outcome of removable denture treatments, which is closely associated with both mechanical and physiologic functions of the soft tissues beneath denture bases. Mechanically, the mucosa acts as a buffer or cushion to distribute the mastication loading from denture to supporting bone. Physiologically, the blood vessels provide nourishment to the supporting bone of the denture foundation. A denture that mechanically abuses the subjacent soft tissues hinders the physiologic functions of these tissues. On the other hand, any systemic condition that unfavourably affects the physiologic function also influences the mechanical capabilities of the tissues, thereby jeopardizing the outcome of such denture treatments [83].

2.4.2 Pressure Pain Threshold (PPT)

The sensation of pain is the most direct indication of a maladaptive denture to the supporting mucosa, and it is the most common and critical issue affecting the denture function [17]. While the biochemical pathway of triggering the pain is not yet fully understood [211], previous research has revealed that high contact pressure can cause pain in the mucosa [212-214]. To clarify this statement, the contact pressure here refers to the load borne perpendicularly on the mucosal surface, rather than the internal hydrostatic pressure. A pressure-pain threshold (PPT) has been proposed as a measure of the lowest pressure that causes pain, which links the objective stimulus (pressure) to the subjective response (pain) in a quantitative fashion. A pressure algometer is a common technique to measure the *in vivo* PPTs, and its validity and reliability have been verified in literature, showing positive and consistent associations in clinics [211, 215].

Several studies have been carried out to investigate PPT (Figure 2-5b), and it was found to vary from 102 to 405 kPa [17, 62, 211-213, 216]. There are several factors affecting PPT, including mucosa thickness, morphology, location, age, loading rate, and loading history. Patients with thin mucosa covering sharp bony ridges are more likely to have lower PPT than thick mucosa over a flat bone surface under a denture base [14, 128]. The loading locations, such as the palatal, lingual, and buccal mucosa, have their different morphologies, thickness, and anatomical features, leading to the various PPTs observed in clinics [62, 211, 212, 216]. Aging is a critical factor in the changes of mucosa anatomy and physiology as reviewed in Section 2, and it also influences PPT. A general trend indicates that younger people have lower PPT, whereas the oral mechanosensitivity was found to decrease with age [217]. The viscous responses associated with interstitial fluid are reflected in both loading rate and loading history as discussed in Section 3.2. Slower loading rates generally result in lower thresholds, as the fluid has more time to flow into

unstressed neighbouring tissues before building up substantial resistance to internal deformation [211, 212, 215]. In contrast, a faster impact stiffens the tissue and develops higher pressures [7, 21, 157]. The pain tolerance can ramp up with increasing loading duration, and the extent of the recovery of the mucosa affects the subsequent PPT [16, 17].

All these factors above are reflected in the biomechanical responses of the mucosa [14]. Simplified mucosa material models (e.g. linear elastic) often find that the denture induced pressures [112, 218] are below the measured pain thresholds, which is contrary to the clinical observations [219]. Correctly established finite element models can provide objective diagnostic criteria of the surface contact pressure for predicting the discomforts induced by denture treatment. Furthermore, the internal hydrostatic pressure can be determined based on the transmission of contact pressure through mucosa, and allows further insights into biomechanics triggering the pain sensation.

2.4.3 Tissue Displaceability

Some dentures are not fully supported by a single type of tissue, and they more often distribute occlusal loads unevenly to multiple supporting tissues, such as tooth (including PDL), mucosa and bone around an implant [148]. The tissues have quite distinct material behaviours and alter the denture deformation in a complex manner. Removable partial dentures and implant-retained overdentures are typical examples, which are not entirely tooth/implant supported but also by mucosa and bone. These displaceability differences lead to the varying denture/tissue deformation in both directions, along and across the residual ridge. As an example, Figure 2-5c shows the displacement of a removable partial denture under occlusal loading (60 N on the 1st molar of the denture).

Compared with complete denture, the teeth supported partial denture and the implant-retained overdenture have much stiffer support sites somewhere in the dental arch

than the mucosa. The former is often supported by a complex native tooth unit, consisting enamel (or artificial crown), dentin, and PDL. Their different material properties contribute to the difference in the denture displacement [128, 148, 220, 221]. The displacement of contact surface generally increases from the supporting tooth unit towards the distal extension (often called free-end-saddle) [222], resulting in stress concentrations in the underlying mucosa [223]. It should also be noted that the oral mucosa responds differently to loads than PDL in a dynamic manner, as the mucosa is much easier to displace than PDL and takes longer to recover for the same load [86, 128]. In an implant-retained overdenture, the metallic implants provide even more rigid support [127], and enlarge the displacement difference at the distal ends of the denture with more severe stress concentrations, known as the cantilever effects [191, 192, 224, 225]. Across the residual ridge, the mucosa morphology and thickness can vary significantly [42-44, 48, 218], and the heterogeneous bone with different qualities underneath [226-228] further contributes to the varying mechanical responses. The difference of tissue displaceability is also likely to trigger denture instability [229, 230].

The tissue displaceability difference does not just cause stress-induced pain, discomfort, and bone resorption to patients through mucosa [3, 24-26], but also affects the long-term health of the remaining teeth and other surrounding soft tissues [149, 179, 231]. Several impression techniques [232-235] have been developed to minimize the effects from the displaceability differences in clinical practice. Various partial denture rests (supports) have been developed and compared to reduce potential stress concentration [95, 106, 132]. Shortening the denture arms [93, 236] or adding stiffer metal frame or wires [237] were suggested to reduce the cantilever effect. In the implant retained cases, the number, location, type of implants [102, 107, 127, 238] have been analysed for their effects on the interaction with underlying tissues. Through all these clinical and numerical

studies, understanding of the displaceability and material behaviour will contribute to enhancement of more successful treatment outcomes.

2.4.4 Residual Ridge Resorption

The residual ridge provides essential support to different kinds of dentures, and the bone quality is critical to the stability and functionality of a denture [3, 57, 239-241]. On the other hand, bone is a dynamic tissue that continuously undergoes adaptation to form a structurally elegant and efficient architecture for withstanding change of functional loads [242, 243]. This adaptive process involves bone formation (apposition) and removal (resorption), which has the capability of evolving in relation to the change of habitual loading environment [228].

As indicated in Figure 2-5a, introducing dental prostheses is likely to alter the biomechanical state in the oral structures with respect to both stimulus transfer and distribution [8, 244-246]. It is believed that the alveolar bone begins to atrophy following teeth extraction or with edentulous aging, due to lack of stimulus to maintain the local bone quality [3, 241, 247]. However, the stimulus induced by the denture basal surface may not necessarily positively stimulate bone growth, in contrast, it may cause residual ridge resorption [3, 4, 239, 241, 247] (Figure 2-5d). The established remodelling algorithms for long bones, such as Wolff's rule, are arguably inappropriate for explaining this denture-induced bone resorption [248].

From clinical observations, the residual ridge around implants often shows to various extent positive gains of mass density, or at least preservation of mass, [248, 249]; and the similar trends present in numerical studies [106, 127, 191]. On the other hand, the load-borne mucosal regions often suffer from bone loss, including the posterior arms of implant-retained overdentures and the basal areas of partial or complete dentures [25, 109,

224, 250-253], even though the stresses induced in the mucosa are much lower than the ones around the implants [10, 13, 57]. These existing studies imply that, with the soft tissue involved, the residual ridge remodelling is not just the consequence of mechanical stimuli, but also affected by the physiological conditions in the surrounding tissues of mucosa, such as nutrient supply and metabolite removal to the supporting mandibular bone [15].

Clinical investigations have been exploring the etiological pathway of denture-induced residual ridge resorption [8-12]. As pointed out in previous sections of this review, the hydrostatic pressure in the mucosa plays a critical role, especially in the aging population. An inappropriately designed dental prosthesis may cause further clinical complications rather than solving the initial problem of restoring masticatory function if the relevant biomechanics is not considered properly. In the literature, mucosal responses have gradually begun to attract considerable attention to help understand and analyse potential signs of residual ridge resorption [92, 109, 155, 224]. However, unlike Wolff's law, there is a lack of systematic studies on soft tissue driven remodelling rules to guide relevant clinical activities to date.

2.5. Conclusion

With the rapid developments in molecular and cellular biology, further information has been gradually revealed as to the physiological reactions of the oral mucosa to occlusal loading, including the histological changes and biochemical reactions. Such knowledge assists with comprehending the biomechanical responses of the mucosa, and provides valuable insights for numerical modelling of these responses from clinical observations. The limitations of these biomechanical models should certainly be recognized. Proper application of these biomechanics models does not just assist with dental prosthetic design, but also enables estimating and predicting successful treatment outcomes. Furthermore, these models can in turn contribute towards discovery of the physiological factors associated with the biomechanical responses to advance our understanding in clinical and biological research.

This chapter has reviewed four aspects of the biomechanical responses in the oral mucosa, namely the static, dynamic, volumetric, and interactive responses. The first aspect, as interpreted by the assumption of linear and/or nonlinear elasticity, has been more extensively explored than the other three, and this nonlinear finite element analysis has enabled a better match with the realistic responses of soft tissue. The dynamic response is interpreted by the viscosity component, often with assumption of homogeneity of mucosa tissue. The heterogeneity of the mucosa has not been extensively explored as yet, which from biomechanical perspective results in interstitial fluid activity and the associated dynamic response, thereby linking microscopic biomechanics to its physiology. The presented in-depth studies on the apparent Poisson's ratio effect and contact interaction between mucosa and dental prosthetic devices remains preliminary, and their relationship to either the mucosal anatomy or physiology is unclear. Future experimental research

would be appreciated in all these areas to expand the existing knowledge in the mucosal biomechanics and assist clinical treatment and surgical planning for long term success.

Acknowledgement

This work is supported by Australian Research Council (ARC) and Australian Postgraduate Award (APA).

2.6 References

1. Hill, E.E. and L.C. Breeding, *Who Is Teaching Undergraduate Prosthodontics in US Dental Schools, 2007?* Journal of Prosthodontics-Implant Esthetic and Reconstructive Dentistry, 2009. **18**(2): p. 195-198.
2. Bidra, A.S., T.D. Taylor, and J.R. Agar, *Computer-adided technology for fabricating complete dentures: systematic review of historical background, current status, and future perspectives.* Journal of Prosthetic Dentistry, 2013. **109**(6): p. 361-366.
3. Klemetti, E., *A review of residual ridge resorption and bone density.* Journal of Prosthetic Dentistry, 1996. **75**(5): p. 512-514.
4. Ozan, O., et al., *The Effect of Removable Partial Dentures on Alveolar Bone Resorption: A Retrospective Study with Cone-Beam Computed Tomography.* Journal of Prosthodontics-Implant Esthetic and Reconstructive Dentistry, 2013. **22**(1): p. 42-48.
5. Ostlund, S.G., *The effect of complete dentures on the gum tissues.* Acta Odontol Scand, 1958. **16**((1)): p. 1-41.
6. Kydd, W.L., C.H. Daly, and D. Nansen, *Variation in the response to mechanical stress of human soft tissues as related to age.* Journal of Prosthetic Dentistry, 1974. **32**(5): p. 493-500.
7. Sawada, A., et al., *Viscoelasticity of Human Oral Mucosa: Implications for Masticatory Biomechanics.* Journal of Dental Research, 2011. **90**(5): p. 590-595.
8. Ahmad, R., et al., *Three dimensional quantification of mandibular bone remodeling using standard tessellation language registration based superimposition.* Clin Oral Implants Res, 2013. **24**(11): p. 1273-1279.
9. Mori, S., et al., *Effect of continuous pressure on histopathological changes in denture-supporting tissues.* Journal of Oral Rehabilitation, 1997. **24**(1): p. 37-46.
10. Sato, T., et al., *Threshold for bone resorption induced by continuous and intermittent pressure in the rat hard palate.* Journal of Dental Research, 1998. **77**(2): p. 387-392.
11. Imai, Y., et al., *A histomorphometric analysis on bone dynamics in denture supporting tissue under continuous pressure.* J Oral Rehabil, 2002. **29**(1): p. 72-9.
12. Blum, I.R. and J.F. McCord, *A clinical investigation of the morphological changes in the posterior mandible when implant-retained overdentures are used.* Clinical Oral Implants Research, 2004. **15**(6): p. 700-8.
13. Hara, T., et al., *Effect of occlusal pressure on the histopathological changes in denture supporting tissues.* Journal of Oral Rehabilitation, 1996. **23**(6): p. 363-371.
14. Isobe, A., et al., *The influence of denture supporting tissue properties on pressure-pain threshold: –Measurement in dentate subjects–.* Journal of Prosthodontic Research, 2013. **57**(4): p. 275-283.
15. Bradley, J.C., *The clinical significance of age changes in the vascular supply to the mandible.* International Journal of Oral Surgery, 1981. **10**: p. 71-76.

16. Suzuki, Y., et al., *Pressure pain threshold of mucosa after tooth extraction under removable denture bases.* The European journal of prosthodontics and restorative dentistry, 2011. **19**(4): p. 184-6.

17. Ogawa, T., et al., *Pressure-pain threshold of oral mucosa and its region-specific modulation by pre-loading.* Journal of Oral Rehabilitation, 2003. **30**(11): p. 1062-1069.

18. Bae, K.H., et al., *A comparison of oral health related quality of life between complete and partial removable denture-wearing older adults in Korea.* Journal of Oral Rehabilitation, 2006. **33**(5): p. 317-322.

19. Celebic, A., et al., *The patient's and the therapist's evaluation of complete denture therapy.* Collegium Antropologicum, 2000. **24**: p. 71-77.

20. Kydd, W.L. and C.H. Daly, *The biologic and mechanical effects of stress on oral mucosa.* J Prosthet Dent, 1982. **47**(3): p. 317-29.

21. Kydd, W.L. and C.H. Daly, *The biologic and mechanical effects of stress on oral mucosa.* Journal of Prosthetic Dentistry, 1982. **47**(3): p. 317-29.

22. Ashton, H., *Effect of increased tissue pressure on blood flow.* Clinical Orthopaedics and Related Research, 1975(113): p. 15-26.

23. Maruo, Y., et al., *Stress distribution prevents ischaemia and bone resorption in residual ridge.* Archives of Oral Biology, 2010. **55**(11): p. 873-878.

24. Tallgren, A., *Alveolar bone loss in denture wearers as related to facial morphology.* Acta Odontol Scand, 1970. **28**(2): p. 251-70.

25. Wright, P.S., et al., *The effects of fixed and removable implant-stabilised prostheses on posterior mandibular residual ridge resorption.* Clinical Oral Implants Research, 2002. **13**(2): p. 169-174.

26. Akazawa, H. and K. Sakurai, *Changes of blood flow in the mucosa underlying a mandibular denture following pressure assumed as a result of light clenching.* Journal of Oral Rehabilitation, 2002. **29**(4): p. 336-340.

27. Atwood, D.A., *Reduction of Residual Ridges - Major Oral Disease Entity.* Journal of Prosthetic Dentistry, 1971. **26**(3): p. 266-79.

28. Tallgren, A., *The continuing reduction of the residual alveolar ridges in complete denture wearers: a mixed-longitudinal study covering 25 years.* Journal of Prosthetic Dentistry, 1972. **27**(2): p. 120-32.

29. Inoue, K., et al., *Viscoelastic properties of oral soft tissue. 1. A method of determining elastic modulus of oral soft tissue.* Dent Mater J, 1985. **4**(1): p. 47-53.

30. Yatabe, M., *Study on measurement of dynamic viscoelasticity of maxillary mucosa.* Kokubyo Gakkai zasshi. The Journal of the Stomatological Society, Japan, 1991. **58**(1): p. 74-94.

31. Al-Ani, S., G. Shklar, and A.A. Yurkstas, *The effect of dentures on the exfoliative cytology of palatal and buccal oral mucosa.* The Journal of prosthetic dentistry, 1966. **16**(3): p. 513-521.

32. Scapino, R.P., *Biomechanics of Prehensile Oral Mucosa.* Journal of Morphology, 1967. **122**(2): p. 89-&.

33. Fleisch, L. and J.C. Austin, *HISTOLOGIC STUDY OF RESPONSE OF MASTICATORY AND LINING MUCOSA TO MECHANICAL LOADING IN VERVET MONKEY.* Journal of Prosthetic Dentistry, 1978. **39**(2): p. 211-216.

34. Tucker, R., *Surface specialisations of mechanically laden epithelia.* Res Vet Sci, 1968. **9**(5): p. 381-96.

35. Sloan, P., M. Picardo, and S.L. Schor, *The structure and function of oral mucosa.* Dental Update, 1991. **18**: p. 208-216.

36. Squier, C. and K. Brogden, *Human Oral Mucosa: Development, Structure and Function*. 2011: Wiley.

37. Consentino, M., et al., *Corrosion casts of young rabbit palatine mucosa angioarchitecture.* Annals of Anatomy-Anatomischer Anzeiger, 2000. **182**(6): p. 529-531.

38. Coslet, J.G. and D.W. Cohen, *The basal cell layer of the developing oral mucosa in the human fetus.* J Period Res, 1967. **2**((4)): p. 297-316.

39. Coslet, J.G. and D.W. Cohen, *THE BASAL CELL LAYER OF THE DEVELOPING ORAL MUCOSA IN THE HUMAN FETUS.* Journal of Periodontal Research, 1968. **3**(3): p. 194-211.

40. Goktas, S., J.J. Dmytryk, and P.S. McFetridge, *Biomechanical Behavior of Oral Soft Tissues.* Journal of Periodontology, 2011. **82**(8): p. 1178-1186.

41. Schulze, R.K.W., D. Curic, and B. d'Hoedt, *B-mode versus A-mode ultrasonographic measurements of mucosal thickness in vivo.* Oral Surgery Oral Medicine Oral Pathology Oral Radiology and Endodontics, 2002. **93**(1): p. 110-117.

42. Uchida, H., K. Kobayashi, and M. Nagao, *MEASUREMENT INVIVO OF MASTICATORY MUCOSAL THICKNESS WITH 20 MHZ B-MODE ULTRASONIC DIAGNOSTIC EQUIPMENT.* Journal of Dental Research, 1989. **68**(2): p. 95-100.

43. Muller, H.P., N. Schaller, and T. Eger, *Ultrasonic determination of thickness of masticatory mucosa.* Oral Surgery Oral Medicine Oral Pathology Oral Radiology and Endodontics, 1999. **88**(2): p. 248-253.

44. Kydd, W.L., C.H. Daly, and J.B. Wheeler, *THICKNESS MEASUREMENT OF MASTICATORY MUCOSA IN-VIVO.* International Dental Journal, 1971. **21**(4): p. 430-&.

45. Ueno, D., et al., *Accuracy of Oral Mucosal Thickness Measurements Using Spiral Computed Tomography.* Journal of Periodontology, 2011. **82**(6): p. 829-836.

46. Song, J.E., et al., *Thickness of posterior palatal masticatory mucosa: The use of computerized tomography.* Journal of Periodontology, 2008. **79**(3): p. 406-412.

47. Dvorak, G., et al., *The "puffed cheek method" to evaluate mucosal thickness: case series.* Clinical Oral Implants Research, 2013. **24**(7): p. 719-724.

48. Wara-aswapati, N., et al., *Thickness of palatal masticatory mucosa associated with age.* Journal of Periodontology, 2001. **72**(10): p. 1407-1412.

49. Yatabe, M., *STUDY ON MEASUREMENT OF DYNAMIC VISCOELASTICITY OF MAXILLARY MUCOSA.* Journal of the Stomatological Society Japan, 1991. **58**(1): p. 74-94.

50. Kydd, W.L., et al., *EFFECT OF MECHANICAL STRESS ON ORAL MUCOPERIOSTEUM OF DOGS.* Archives of Oral Biology, 1969. **14**(8): p. 921-&.

51. Kydd, W.L. and J. Mandley, *STIFFNESS OF PALATAL MUCOPERIOSTEUM.* Journal of Prosthetic Dentistry, 1967. **18**(2): p. 116-&.

52. Kishi, M., *Experimental studies on the relation between area and displacement of loading surfaces in connection with displaceability in the mucosa of edentulous alveolar ridge under pressure.* Shika gakuho. Dental science reports, 1972. **72**(6).

53. Winterroth, F., et al., *Characterizing Morphology and Nonlinear Elastic Properties of Normal and Thermally Stressed Engineered Oral Mucosal Tissues Using Scanning Acoustic Microscopy.* Tissue Engineering Part C-Methods, 2013. **19**(5): p. 345-351.

54. Atasever, N.E., et al., *EFFECT OF WEARING COMPLETE DENTURES ON HUMAN PALATAL MUCOSAL BLOOD-FLOW MEASURED BY XE-133 CLEARANCE.* Archives of Oral Biology, 1991. **36**(9): p. 627-630.

55. Tsuruoka, M., et al., *Morphological and molecular changes in denture-supporting tissues under persistent mechanical stress in rats.* Journal of Oral Rehabilitation, 2008. **35**(12): p. 889-897.

56. Kocabalkan, E. and M. Turgut, *Variation in blood flow of supporting tissue during use of mandibular complete dentures with hard acrylic resin base and soft relining: A preliminary study.* International Journal of Prosthodontics, 2005. **18**(3): p. 210-213.

57. Carlsson, G.E., *Clinical morbidity and sequelae of treatment with complete dentures.* Journal of Prosthetic Dentistry, 1998. **79**(1): p. 17-23.

58. Kumakura, S., et al., *Relationship between buccal mucosa ridging and viscoelastic behaviour of oral mucosa.* Journal of Oral Rehabilitation, 2011. **38**(6): p. 429-433.

59. Leiderman, R., et al., *Coupling between elastic strain and interstitial fluid flow: ramifications for poroelastic imaging.* Physics in Medicine and Biology, 2006. **51**(24): p. 6291-6313.

60. Stokes, I.A.F., et al., *Refinement of Elastic, Poroelastic, and Osmotic Tissue Properties of Intervertebral Disks to Analyze Behavior in Compression.* Annals of Biomedical Engineering, 2011. **39**(1): p. 122-131.

61. Yoshida, N., et al., *EFFECT OF MECHANICAL PRESSURE ON THE BLOOD-FLOW IN HUMAN PALATAL MUCOSA MEASURED BY TEMPERATURE CONTROLLED THERMOELECTRICAL METHOD.* Journal of Oral Rehabilitation, 1992. **19**(5): p. 527-533.

62. Tanaka, M., et al., *Denture wearing and strong bite force reduce pressure pain threshold of edentulous oral mucosa.* Journal of Oral Rehabilitation, 2004. **31**(9): p. 873-878.

63. Tautin, F.S., *Should dentures be worn continuously?* The Journal of prosthetic dentistry, 1978. **39**(4): p. 372-4.

64. Breustedt, A., *Age-induced changes in the oral mucosa and their therapeutic consequences.* International dental journal, 1983. **33**(3): p. 272-280.

65. Pickett, H.G., R.G. Appleby, and M.O. Osborn, *CHANGES IN DENTURE SUPPORTING TISSUES ASSOCIATED WITH AGING PROCESS.* Journal of Prosthetic Dentistry, 1972. **27**(3): p. 257-&.

66. Nedelman, C.I. and S. Bernick, *SIGNIFICANCE OF AGE-CHANGES IN HUMAN ALVEOLAR MUCOSA AND BONE.* Journal of Prosthetic Dentistry, 1978. **39**(5): p. 495-501.

67. Cruchley, A.T., et al., *LANGERHANS CELL-DENSITY IN NORMAL HUMAN ORAL-MUCOSA AND SKIN - RELATIONSHIP TO AGE, SMOKING AND ALCOHOL-CONSUMPTION.* Journal of Oral Pathology & Medicine, 1994. **23**(2): p. 55-59.

68. Hill, M.W., C.A. Squier, and P. Preston, *BLOOD-FLOW IN SKIN AND MUCOSA OF YOUNG AND OLD RATS.* Journal of Dental Research, 1987. **66**: p. 238-238.

69. Bradley, J.C., *RADIOLOGICAL INVESTIGATION INTO AGE-CHANGES OF INFERIOR DENTAL ARTERY.* British Journal of Oral Surgery, 1975. **13**(1): p. 82-90.

70. Bradley, J.C., *THE CLINICAL-SIGNIFICANCE OF AGE-CHANGES IN THE VASCULAR SUPPLY TO THE MANDIBLE.* International Journal of Oral Surgery, 1981. **10**: p. 71-76.

71. Bradley, J.C., *AGE-CHANGES OF THE INFERIOR ALVEOLAR ARTERY.* British Journal of Oral & Maxillofacial Surgery, 1988. **26**(6): p. 517-519.

72. Hill, M.W., et al., *INFLUENCE OF AGE ON THE RESPONSE OF ORAL MUCOSA TO INJURY*. Effect of Aging in Oral Mucosa and Skin, ed. C.A. Squier and M.W. Hill. 1994. 129-142.

73. Campbell, R.L., *A comparative study of the resorption of the alveolar ridges in denture wearers and non-denture wearers.* Jour Amer Dental Assoc, 1960. **60**((2)): p. 143-153.

74. Razek, M.K. and N.A. Shaaban, *Histochemical and histopathologic studies of alveolar mucosa under complete dentures.* The Journal of prosthetic dentistry, 1978. **39**(1): p. 29-36.

75. Sharma, A.K. and F.D. Mirza, *Palatal mucosa under dentures: A qualitative histologic and histochemical analysis.* The Journal of Prosthetic Dentistry, 1986. **56**(5): p. 574-582.

76. Pendleton, E.C., *CHANGES IN THE DENTURE SUPPORTING TISSUES.* Journal of the American Dental Association, 1951. **42**(1): p. 1-15.

77. Carlsson, G.E., N. Ragnarson, and P. Astrand, *Changes in height of the alveolar process in edentulous segments. A longitudinal clinical and radiographic study of full upper denture cases with residual lower anteriors.* Odontologisk tidskrift, 1967. **75**(3): p. 193-208.

78. Nakashima, K., et al., *AN EXPERIMENTAL-STUDY ON HISTOPATHOLOGICAL CHANGES IN THE TISSUE COVERED WITH DENTURE BASE WITHOUT OCCLUSAL PRESSURE.* Journal of Oral Rehabilitation, 1994. **21**(3): p. 263-272.

79. Oki, K., et al., *Histopathological changes in the tissues under a denture base in experimental osteoporosis with a non-pressure covering or bearing continuous pressure.* Journal of Oral Rehabilitation, 2002. **29**(6): p. 594-603.

80. Maruo, Y., et al., *The effect of diabetes mellitus on the expression of Argyrophilic nucleolar organizer regions (AgNORs) in mucosal epithelium under experimental denture bases in rats.* Journal of Oral Pathology & Medicine, 2003. **32**(3): p. 171-175.

81. Maruo, Y., et al., *The effect of diabetes mellitus on histopathological changes in the tissues under denture base bearing masticatory pressure.* Journal of Oral Rehabilitation, 1999. **26**(4): p. 345-355.

82. Mori, S., et al., *The effect of diabetes mellitus on histopathological changes in the denture-supporting tissues under continuous mechanical pressure in rat.* Journal of Oral Rehabilitation, 1999. **26**(1): p. 80-90.

83. Lytle, R.B., *SOFT TISSUE DISPLACEMENT BENEATH REMOVABLE PARTIAL AND COMPLETE DENTURES.* Journal of Prosthetic Dentistry, 1962. **12**(1): p. 34-&.

84. Tomlin, H.R. and H.J. Wilson, *The measurement of thickness and hardness of oral soft tissues.* British dental journal, 1968. **124**(1): p. 22-7.

85. Daly, C.H., et al., *BIO MECHANICS OF THE ORAL TISSUES*. Kenedi, R.M. 1973. 181-185.

86. Picton, D.C.A. and D.J. Wills, *Viscoelastic properties of periodontal-ligament and mucosa-membrane.* Journal of Prosthetic Dentistry, 1978. **40**(3): p. 263-272.

87. Davy, D.T., G.L. Dilley, and R.F. Krejci, *DETERMINATION OF STRESS PATTERNS IN ROOT-FILLED TEETH INCORPORATING VARIOUS DOWEL DESIGNS.* Journal of Dental Research, 1981. **60**(7): p. 1301-1310.

88. Reinhardt, R.A., et al., *DENTIN STRESSES IN POST-RECONSTRUCTED TEETH WITH DIMINISHING BONE SUPPORT.* Journal of Dental Research, 1983. **62**(9): p. 1002-1008.

89. Ko, C.-C., et al., *Effects of posts on dentin stress distribution in pulpless teeth.* The Journal of Prosthetic Dentistry, 1992. **68**(3): p. 421-427.

90. Nokubi, T., et al., *Finite Element Stress Analysis of Tooth, Periodontal Membrane and Alveolar Bone.* Journal of Japanese Research Society on Dental Material Application, 1976. **33**(369-378).

91. Jozefowicz, W., *[Results of studies on elasticity moduli of the soft tissues of the denture-bearing area]*. Protet Stomatol, 1970. **20**(3): p. 171-6.

92. Maeda, Y. and W.W. Wood, *Finite Element Method Simulation of Bone Resorption Beneath a Complete Denture.* Journal of Dental Research, 1989. **68**(9): p. 1370-1373.

93. Maeda, Y., M. Sogo, and S. Tsutsumi, *Efficacy of a posterior implant support for extra shortened dental arches: a biomechanical model analysis.* Journal of Oral Rehabilitation, 2005. **32**(9): p. 656-660.

94. Geng, J.-P., K.B.C. Tan, and G.-R. Liu, *Application of finite element analysis in implant dentistry: A review of the literature.* The Journal of Prosthetic Dentistry, 2001. **85**(6): p. 585-598.

95. Gonda, T., J. Dong, and Y. Maeda, *Stress Analysis of an Overdenture Using the Finite Element Method.* International Journal of Prosthodontics, 2013. **26**(4): p. 340-342.

96. Osman, R.B., et al., *Finite Element Analysis of a Novel Implant Distribution to Support Maxillary Overdentures.* International Journal of Oral & Maxillofacial Implants, 2013. **28**(1): p. E1-E10.

97. Zmudzki, J., G. Chladek, and J. Kasperski, *The influence of a complete lower denture destabilization on the pressure of the mucous membrane foundation.* Acta of Bioengineering and Biomechanics, 2012. **14**(3): p. 67-73.

98. Kasperski, J., J. Żmudzki, and G. Chladek, *Denture foundation tissues loading criteria in evaluation of dentures wearing characteristics.* Journal of Achievements in Materials and Manufacturing Engineering, 2010. **43**(1): p. 324-32.

99. Sadr, K., J. Alipour, and F. Heidary, *Finite Element Analysis of Soft-lined Mandibular Complete Denture and its Supporting Structures.* Journal of dental research, dental clinics, dental prospects, 2012. **6**(2).

100. Barão, V.A.R., et al., *Effect of different mucosa thickness and resiliency on stress distribution of implant-retained overdentures-2D FEA.* Computer Methods and Programs in Biomedicine, 2008. **92**(2): p. 213-223.

101. Assunção, W.G., et al., *Comparison of stress distribution between complete denture and implant-retained overdenture-2D FEA.* Journal of Oral Rehabilitation, 2008. **35**(10): p. 766-774.

102. Barão, V.A.R., et al., *Comparison of different designs of implant-retained overdentures and fixed full-arch implant-supported prosthesis on stress distribution in edentulous mandible - A computed tomography-based three-dimensional finite element analysis.* Journal of Biomechanics, 2013. **46**(7): p. 1312-1320.

103. Bacchi, A., et al., *Influence of different mucosal resiliency and denture reline on stress distribution in peri-implant bone tissue during osseointegration. A three-dimensional finite element analysis.* Gerodontology, 2012. **29**(2): p. E833-E837.

104. Takayama, Y., et al., *The dynamic behaviour of a lower complete denture during unilateral loads: analysis using the finite element method.* Journal of Oral Rehabilitation, 2001. **28**(11): p. 1064-1074.

105. Kibi, M., et al., *Development of an RPD CAD system with finite element stress analysis.* Journal of Oral Rehabilitation, 2009. **36**(6): p. 442-450.

106. Verri, F.R., et al., *Evaluation of Bone Insertion Level of Support Teeth in Class I Mandibular Removable Partial Denture Associated With an Osseointegrated Implant: A Study Using Finite Element Analysis.* Implant Dentistry, 2011. **20**(3): p. 192-+.

107. Verri, F.R., et al., *Influence of length and diameter of implants associated with distal extension removable partial dentures.* Implant Dentistry, 2007. **16**(3): p. 270-276.

108. Liu, J., et al., *Influence of implant number on the biomechanical behaviour of mandibular implant-retained/supported overdentures: A three-dimensional finite element analysis.* Journal of Dentistry, 2013. **41**(3): p. 241-249.

109. H., M.L.O., et al., *Stresses in implant-supported overdentures with bone resorption: A 3-D finite element analysis.* Revista Odonto Ciencia, 2012. **27**: p. 41-6.

110. Tanino, F., et al., *Finite element analysis of stress-breaking attachments on maxillary implant-retained overdentures.* International Journal of Prosthodontics, 2007. **20**(2): p. 193-198.

111. Hussein, M.O., *Stress-strain distribution at bone-implant interface of two splinted overdenture systems using 3D finite element analysis.* Journal of Advanced Prosthodontics, 2013. **5**(3): p. 333-340.

112. Kawasaki, T., et al., *Relationship between the stress distribution and the shape of the alveolar residual ridge – three-dimensional behaviour of a lower complete denture.* Journal of Oral Rehabilitation, 2001. **28**(10): p. 950-957.

113. Takayama, Y., et al., *Finite element model based on a mandibular cast and a waxed complete denture: evaluation of the accuracy and the reproducibility of analysis.* Journal of prosthodontic research, 2009. **53**(1): p. 33-7.

114. Ates, M., et al., *The effect of occlusal contact localization on the stress distribution in complete maxillary denture.* Journal of Oral Rehabilitation, 2006. **33**(7): p. 509-513.

115. Braga, I.U., et al., *Determination of expander apparatus displacements and contact pressures on the mucosa using FEM modelling considering mandibular asymmetries.* Computer Methods in Biomechanics and Biomedical Engineering, 2013. **16**(9): p. 954-962.

116. Daas, M., et al., *A complete finite element model of a mandibular implant-retained overdenture with two implants: Comparison between rigid and resilient attachment configurations.* Medical Engineering & Physics, 2008. **30**(2): p. 218-225.

117. Wang, H.Y., et al., *Effects of rigid and nonrigid extracoronal attachments on supporting tissues in extension base partial removable dental prostheses: a nonlinear finite element study.* J Prosthet Dent, 2011. **105**(5): p. 338-46.

118. Sato, Y., et al., *Finite element analysis of stress relaxation in soft denture liner.* Journal of Oral Rehabilitation, 2000. **27**(8): p. 660-663.

119. Cheng, Y.Y., W.L. Cheung, and T.W. Chow, *STRAIN ANALYSIS OF MAXILLARY COMPLETE DENTURE WITH THREE-DIMENSIONAL FINITE ELEMENT METHOD.* Journal of Prosthetic Dentistry, 2010. **103**(5): p. 309-318.

120. Cheng, Y.Y., et al., *3D FEA of high-performance polyethylene fiber reinforced maxillary dentures.* Dental Materials, 2010. **26**(9): p. E211-E219.

121. Chun, H.J., et al., *Stress distributions in maxillary bone surrounding overdenture implants with different overdenture attachments.* Journal of Oral Rehabilitation, 2005. **32**(3): p. 193-205.

122. Lima, J.B.G., et al., *Analysis of stress on mucosa and basal bone underlying complete dentures with different reliner material thicknesses: a three-dimensional finite element study.* Journal of Oral Rehabilitation, 2013. **40**(10): p. 767-773.

123. Nishigawa, G., et al., *Finite element analysis of the effect of the bucco-lingual position of artificial posterior teeth under occlusal force on the denture supporting bone of the edentulous patient.* Journal of Oral Rehabilitation, 2003. **30**(6): p. 646-652.

124. Chowdhary, R., K. Lekha, and N.P. Patil, *Two-dimensional finite element analysis of stresses developed in the supporting tissues under complete dentures using teeth with different cusp angulations.* Gerodontology, 2008. **25**(3): p. 155-161.

125. Yamada, T., *Basic studies on Konuskronen by using the finite element method. Part 2. Stress analysis of mandibular distal-extension removable partial denture.* Nihon Hotetsu Shika Gakkai zasshi, 1987. **31**(1): p. 186-99.

126. Wada, S., et al., *Influence of abutment selection in maxillary Kennedy Class II RPD on elastic stress distribution in oral mucosa: an FEM study.* Journal of prosthodontics : official journal of the American College of Prosthodontists, 2006. **15**(2): p. 89-94.

127. Menicucci, G., et al., *Mandibular implant-retained overdenture: A clinical trial of two anchorage systems.* International Journal of Oral & Maxillofacial Implants, 1998. **13**(6): p. 851-856.

128. Wills, D.J. and R.D. Manderson, *BIOMECHANICAL ASPECTS OF SUPPORT OF PARTIAL DENTURES.* Journal of Dentistry, 1977. **5**(4): p. 310-318.

129. Wakabayashi, N., et al., *Nonlinear finite element analyses: Advances and challenges in dental applications.* Journal of Dentistry, 2008. **36**(7): p. 463-471.

130. Ziegler, A., et al., *Numerical simulation of the biomechanical behaviour of multi-rooted teeth.* European Journal of Orthodontics, 2005. **27**(4): p. 333-339.

131. Borak, L., et al., *Bilinear elastic property of the periodontal ligament for simulation using a finite element mandible model.* Dental Materials Journal, 2011. **30**(4): p. 448-454.

132. Kanbara, R., et al., *Three-dimensional finite element stress analysis: The technique and methodology of non-linear property simulation and soft tissue loading behavior for different partial denture designs.* Dental Materials Journal, 2012. **31**(2): p. 297-308.

133. Ogden, R.W., G. Saccomandi, and I. Sgura, *Fitting hyperelastic models to experimental data.* Computational Mechanics, 2004. **34**(6): p. 484-502.

134. Weiss, J.A., B.N. Maker, and S. Govindjee, *Finite element implementation of incompressible, transversely isotropic hyperelasticity.* Computer Methods in Applied Mechanics and Engineering, 1996. **135**(1-2): p. 107-128.

135. Steinmann, P., M. Hossain, and G. Possart, *Hyperelastic models for rubber-like materials: consistent tangent operators and suitability for Treloar's data.* Archive of Applied Mechanics, 2012. **82**(9): p. 1183-1217.

136. Ogden, R.W., *Non-linear Elastic Deformations*. 1997: Dover Publications.

137. Basar, Y. and D. Weichert, *Nonlinear Continuum Mechanics of Solids: Fundamental Mathematical and Physical Concepts*. 2000: Springer.

138. Ateshian, G.A., et al., *Finite deformation biphasic material properties of bovine articular cartilage from confined compression experiments.* Journal of Biomechanics, 1997. **30**(11-12): p. 1157-1164.

139. Van Loocke, M., C.G. Lyons, and C.K. Simms, *A validated model of passive muscle in compression.* Journal of Biomechanics, 2006. **39**(16): p. 2999-3009.

140. Sussman, T. and K.-J. Bathe, *A model of incompressible isotropic hyperelastic material behavior using spline interpolations of tension-compression test data.* Communications in Numerical Methods in Engineering, 2009. **25**(1): p. 53-63.

141. Cheung, J.T.M., et al., *Three-dimensional finite element analysis of the foot during standing - a material sensitivity study.* Journal of Biomechanics, 2005. **38**(5): p. 1045-1054.

142. Hirokawa, S. and R. Tsuruno, *Three-dimensional deformation and stress distribution in an analytical/computational model of the anterior cruciate ligament.* Journal of Biomechanics, 2000. **33**(9): p. 1069-1077.

143. Pena, E., et al., *A three-dimensional finite element analysis of the combined behavior of ligaments and menisci in the healthy human knee joint.* Journal of Biomechanics, 2006. **39**(9): p. 1686-1701.

144. Gambarotta, L., et al., *In vivo experimental testing and model identification of human scalp skin.* Journal of Biomechanics, 2005. **38**(11): p. 2237-2247.

145. Li, B., Y.-P. Cao, and X.-Q. Feng, *Growth and surface folding of esophageal mucosa: A biomechanical model.* Journal of Biomechanics, 2011. **44**(1): p. 182-188.

146. Chen, J., et al., *A periodontal ligament driven remodeling algorithm for orthodontic tooth movement.* Journal of biomechanics, 2014. **47**(7): p. 1689-1695.

147. Limbert, G., et al., *A transversely isotropic hyperelastic constitutive model of the PDL. Analytical and computational aspects.* Computer Methods in Biomechanics and Biomedical Engineering, 2003. **6**(5-6): p. 337-345.

148. Archangelo, C.M., et al., *Periodontal ligament influence on the stress distribution in a removable partial denture supported by implant: a finite element analysis.* Journal of Applied Oral Science, 2012. **20**(3): p. 362-368.

149. Muraki, H., et al., *Finite element contact stress analysis of the RPD abutment tooth and periodontal ligament.* Journal of Dentistry, 2004. **32**(8): p. 659-665.

150. Almeida, E.S. and R.L. Spilker, *Finite element formulations for hyperelastic transversely isotropic biphasic soft tissues.* Computer Methods in Applied Mechanics and Engineering, 1998. **151**(3-4): p. 513-538.

151. Menzel, A., *Modelling of anisotropic growth in biological tissues - A new approach and computational aspects.* Biomechanics and Modeling in Mechanobiology, 2005. **3**(3): p. 147-171.

152. Haslach, H.W. and J.D. Humphrey, *Dynamics of biological soft tissue and rubber: internally pressurized spherical membranes surrounded by a fluid.* International Journal of Non-Linear Mechanics, 2004. **39**(3): p. 399-420.

153. Lacoste-Ferre, M.H., et al., *Dynamic mechanical properties of oral mucosa: Comparison with polymeric soft denture liners.* Journal of the Mechanical Behavior of Biomedical Materials, 2011. **4**(3): p. 269-274.

154. Schmitt, C., A.H. Henni, and G. Cloutier, *Characterization of blood clot viscoelasticity by dynamic ultrasound elastography and modeling of the rheological behavior.* Journal of Biomechanics, 2011. **44**(4): p. 622-629.

155. Kawano, F., et al., *Effect of viscoelastic deformation of soft tissue on stresses in the structures under complete denture.* Dental materials journal, 1990. **9**(1).

156. Kawano, F., et al., *Effect of soft denture liner on stress distribution in supporting structures under a denture.* International Journal of Prosthodontics, 1993. **6**(1): p. 43-49.

157. Wakabayashi, N. and T. Suzuki, *Patient-specific finite element analysis of viscoelastic masticatory mucosa.* Journal of dental biomechanics, 2013. **4**.

158. Kinney, J.H., S.J. Marshall, and G.W. Marshall, *The mechanical properties of human dentin: A critical review and re-evaluation of the dental literature.* Critical Reviews in Oral Biology & Medicine, 2003. **14**(1): p. 13-29.

159. Crichton, M.L., et al., *Elastic modulus and viscoelastic properties of full thickness skin characterised at micro scales.* Biomaterials, 2013. **34**(8): p. 2087-2097.

160. Rashid, B., M. Destrade, and M.D. Gilchrist, *Mechanical characterization of brain tissue in simple shear at dynamic strain rates.* Journal of the Mechanical Behavior of Biomedical Materials, 2013. **28**: p. 71-85.

161. Taguchi, N., et al., *Effect of viscoelastic properties of resilient denture liners on pressures under dentures.* Journal of Oral Rehabilitation, 2001. **28**(11): p. 1003-1008.

162. Buch, D. and Y. Beal, *Surface conditions and viscoelastic properties of the denture liner Permaflex.* The International journal of prosthodontics, 1995. **8**(3): p. 285-91.

163. Muthupillai, R., et al., *MAGNETIC-RESONANCE ELASTOGRAPHY BY DIRECT VISUALIZATION OF PROPAGATING ACOUSTIC STRAIN WAVES.* Science, 1995. **269**(5232): p. 1854-1857.

164. Cheng, S., et al., *Viscoelastic properties of the tongue and soft palate using MR elastography.* Journal of Biomechanics, 2011. **44**(3): p. 450-454.

165. Komatsu, K., *Mechanical strength and viscoelastic response of the periodontal ligament in relation to structure.* Journal of dental biomechanics, 2010. **2010**.

166. Argoubi, M. and A. Shirazi-Adl, *Poroelastic creep response analysis of a lumbar motion segment in compression.* Journal of Biomechanics, 1996. **29**(10): p. 1331-1339.

167. Squier, C.A., *The Permeability of Oral Mucosa.* Critical Reviews in Oral Biology & Medicine, 1991. **2**(1): p. 13-32.

168. Lesch, C.A., et al., *The Permeability of Human Oral Mucosa and Skin to Water.* Journal of Dental Research, 1989. **68**(9): p. 1345-1349.

169. Bergomi, M., et al., *The role of the fluid phase in the viscous response of bovine periodontal ligament.* Journal of Biomechanics, 2010. **43**(6): p. 1146-1152.

170. Bergomi, M., et al., *Hydro-mechanical coupling in the periodontal ligament: A porohyperelastic finite element model.* Journal of Biomechanics, 2011. **44**(1): p. 34-38.

171. Glozman, T. and H. Azhari, *A Method for Characterization of Tissue Elastic Properties Combining Ultrasonic Computed Tomography With Elastography.* Journal of Ultrasound in Medicine, 2010. **29**(3): p. 387-398.

172. Righetti, R., et al., *The feasibility of using elastography for imaging the Poisson's ratio in porous media.* Ultrasound in Medicine and Biology, 2004. **30**(2): p. 215-228.

173. Ophir, J., et al., *Elastography: ultrasonic estimation and imaging of the elastic properties of tissues.* Proceedings of the Institution of Mechanical Engineers Part H-Journal of Engineering in Medicine, 1999. **213**(H3): p. 203-233.

174. Konofagou, E. and J. Ophir, *A new elastographic method for estimation and imaging of lateral displacements, lateral strains, corrected axial strains and Poisson's ratios in tissues.* Ultrasound in Medicine and Biology, 1998. **24**(8): p. 1183-1199.

175. Mankani, N., R. Chowdhary, and S. Mahoorkar, *Comparison of Stress Dissipation Pattern Underneath Complete Denture with Various Posterior Teeth form: An In Vitro Study.* Journal of Indian Prosthodontic Society, 2013. **13**(3): p. 212-9.

176. Budtzjorgensen, E., *Oral mucosal lesions associated with the wearing of removable dentures.* Journal of Oral Pathology & Medicine, 1981. **10**(2): p. 65-80.

177. Jainkittivong, A., V. Aneksuk, and R.P. Langlais, *Oral mucosal lesions in denture wearers.* Gerodontology, 2010. **27**(1): p. 26-32.

178. Dorey, J.L., et al., *Oral mucosal disorders in denture wearers.* The Journal of Prosthetic Dentistry, 1985. **53**(2): p. 210-213.

179. Emami, E., et al., *Favoring trauma as an etiological factor in denture stomatitis.* Journal of Dental Research, 2008. **87**(5): p. 440-444.

180. Turner, M., L. Jahangiri, and J.A. Ship, *Hyposalivation, xerostomia and the complete denture - A systematic review.* Journal of the American Dental Association, 2008. **139**(2): p. 146-150.

181. Ranc, H., et al., *Friction coefficient and wettability of oral mucosal tissue: Changes induced by a salivary layer.* Colloids and Surfaces a-Physicochemical and Engineering Aspects, 2006. **276**(1-3): p. 155-161.

182. Östlund, S.G., *Saliva and denture retention.* The Journal of Prosthetic Dentistry, 1960. **10**(4): p. 658-663.

183. Upadhyay, S.R., L. Kumar, and J. Rao, *Fabrication of a functional palatal saliva reservoir by using a resilient liner during processing of a complete denture.* The Journal of prosthetic dentistry, 2012. **108**(5): p. 332-5.

184. Prinz, J.F., R.A. de Wijk, and L. Huntjens, *Load dependency of the coefficient of friction of oral mucosa.* Food Hydrocolloids, 2007. **21**(3): p. 402-408.

185. Suchatlampong, C., E. Davies, and J.A. Vonfraunhofer, *FRICTIONAL CHARACTERISTICS OF RESILIENT LINING MATERIALS.* Dental Materials, 1986. **2**(3): p. 135-138.

186. Waters, M.G.J., R.G. Jagger, and G.L. Polyzois, *Wettability of silicone rubber maxillofacial prosthetic materials.* Journal of Prosthetic Dentistry, 1999. **81**(4): p. 439-443.

187. Chabanas, M., et al., *Comparison of linear and non-linear soft tissue models with post-operative CT scan in maxillofacial surgery*, in *Medical Simulation, Proceedings*, S. Cotin and D. Metaxas, Editors. 2004. p. 19-27.

188. Sajewicz, E., *Effect of saliva viscosity on tribological behaviour of tooth enamel.* Tribology International, 2009. **42**(2): p. 327-332.

189. Chen, J., et al., *Comparing Contact Pressure Induced by a Conventional Complete Denture and an Implant-Retained Overdenture.* Applied Mechanics and Materials, 2014(553): p. 384-89.

190. Ahmad, R., et al., *Investigation of mucosa-induced residual ridge resorption between implant-retained overdenture and complete denture.* The International Journal of Oral & Maxillofacial Implants, 2014.

191. Sertgoz, A. and S. Guvener, *Finite element analysis of the effect of cantilever and implant length on stress distribution in an implant-supported fixed prosthesis.* Journal of Prosthetic Dentistry, 1996. **76**(2): p. 165-169.

192. Barbier, L., et al., *Finite element analysis of non-axial versus axial loading of oral implants in the mandible of the dog.* Journal of Oral Rehabilitation, 1998. **25**(11): p. 847-858.

193. Cheng, H.-Y., et al., *Stress effect on bone remodeling and osseointegration on dental implant with novel nano/microporous surface functionalization.* Journal of Biomedical Materials Research Part A, 2013. **101A**(4): p. 1158-1164.

194. Chen, J., et al., *Mechanical simulation of the human mandible with and without an endosseous implant.* Medical Engineering & Physics, 1994. **16**(1): p. 53-61.

195. Mellal, A., et al., *Stimulating effect of implant loading on surrounding bone.* Clinical Oral Implants Research, 2004. **15**(2): p. 239-248.

196. Johannessen, A.C., M. Fjærtoft, and K.J. Heyeraas, *Tissue pressure in rat oral mucosa measured by micropuncture technique.* Journal of Periodontal Research, 1987. **22**(2): p. 139-143.

197. Johannessen, A.C., K.J. Heyeraas, and M. Fjaertoft, *MICROPUNCTURE MEASUREMENTS OF INTERSTITIAL FLUID PRESSURE IN RAT ORAL-MUCOSA.* Journal of Dental Research, 1985. **64**(4): p. 761-761.

198. Del Fabbro, M., et al., *Fluid dynamics of gingival tissues.* Journal of Periodontal Research, 1998. **33**(6): p. 328-334.

199. Berg, A., A. Kirkebo, and K.J. Heyeraas, *Micropuncture measurements of interstitial fluid pressure in rat nasal mucosa during early inflammatory reactions.* Journal of Applied Physiology, 1998. **85**(2): p. 465-470.

200. Thelin, W.R., et al., *The oral mucosa as a therapeutic target for xerostomia.* Oral Diseases, 2008. **14**(8): p. 683-689.

201. Hohmann, A., et al., *Correspondences of hydrostatic pressure in periodontal ligament with regions of root resorption: A clinical and a finite element study of the same human teeth.* Computer Methods and Programs in Biomedicine, 2009. **93**(2): p. 155-161.

202. Hohmann, A., et al., *Periodontal ligament hydrostatic pressure with areas of root resorption after application of a continuous torque moment - A study using identical extracted maxillary human premolars.* Angle Orthodontist, 2007. **77**(4): p. 653-659.

203. Kim, S.H., et al., *Hydrostatic Pressure can Control Osteogenesis and Osteoclastogenesis when Stromal Cells and Osteoclast Precursor Cells are Cocultured.* Tissue Engineering and Regenerative Medicine, 2010. **7**(4): p. 388-394.

204. Suh, J.K., Z.F. Li, and S.L.Y. Woo, *DYNAMIC BEHAVIOR OF A BIPHASIC CARTILAGE MODEL UNDER CYCLIC COMPRESSIVE LOADING.* Journal of Biomechanics, 1995. **28**(4): p. 357-364.

205. Saraf, H., et al., *Mechanical properties of soft human tissues under dynamic loading.* Journal of Biomechanics, 2007. **40**(9): p. 1960-1967.

206. Holmes, M.H., *FINITE DEFORMATION OF SOFT-TISSUE - ANALYSIS OF A MIXTURE MODEL IN UNIAXIAL COMPRESSION.* Journal of Biomechanical Engineering-Transactions of the Asme, 1986. **108**(4): p. 372-381.

207. Holmes, M.H. and V.C. Mow, *THE NONLINEAR CHARACTERISTICS OF SOFT GELS AND HYDRATED CONNECTIVE TISSUES IN ULTRAFILTRATION.* Journal of Biomechanics, 1990. **23**(11): p. 1145-1156.

208. Cowin, S.C., *Deviatoric and hydrostatic mode interaction in hard and soft tissue.* Journal of Biomechanics, 1990. **23**(1): p. 11-14.

209. Sarrafpour, B., et al., *Tooth eruption results from bone remodelling driven by bite forces sensed by soft tissue dental follicles: a finite element analysis.* PloS one, 2013. **8**(3): p. e58803-e58803.

210. Bourauel, C., D. Vollmer, and A. Jager, *Application of bone remodeling theories in the simulation of orthodontic tooth movements.* Journal of orofacial orthopedics = Fortschritte der Kieferorthopadie : Organ/official journal Deutsche Gesellschaft fur Kieferorthopadie, 2000. **61**(4): p. 266-79.

211. Ogimoto, T., et al., *Pressure-pain threshold determination in the oral mucosa: validity and reliability.* Journal of Oral Rehabilitation, 2002. **29**(7): p. 620-626.

212. McMillian, A.S., *Pain-pressure threshold in human gingivae.* Journal of Orofacial Pain, 1995. **9**(1): p. 44-50.

213. Davenpor, J.C., *Pressure-pain thresholds in oral cavity in man.* Archives of Oral Biology, 1969. **14**(11): p. 1267-&.

214. Kubo, K., et al., *Development of in vivo measuring system of the pressure distribution under the denture base of removable partial denture.* Journal of prosthodontic research, 2009. **53**(1): p. 15-21.

215. List, T., M. Helkimo, and R. Karlsson, *Influence of pressure rates on the reliability of a pressure threshold meter.* Journal of Craniomandibular Disorders, 1991. **5**(3): p. 173-178.

216. Ogawa, T., et al., *Mapping, profiling and clustering of pressure pain threshold (PPT) in edentulous oral mucosa.* Journal of Dentistry, 2004. **32**(3): p. 219-228.

217. Teranaka, S., et al., *Age-related changes in oral mechanosensitivity of symptom-free subjects.* Journal of medical and dental sciences, 2008. **55**(1): p. 61-9.

218. Takayama, Y., et al., *Morphological factors of mandibular edentulous alveolar ridges influencing the movement of dentures calculated using finite element analysis.* Journal of prosthodontic research, 2011. **55**(2): p. 98-103.

219. Geckili, O., et al., *Comparison of patient satisfaction, quality of life, and bite force between elderly edentulous patients wearing mandibular two implant-supported overdentures and conventional complete dentures after 4 years.* Special care in dentistry : official publication of the American Association of Hospital Dentists, the

Academy of Dentistry for the Handicapped, and the American Society for Geriatric Dentistry, 2012. **32**(4): p. 136-41.

220. Itoh, H., et al., *Effects of periodontal support and fixed splinting on load transfer by removable partial dentures.* The Journal of Prosthetic Dentistry, 1998. **79**(4): p. 465-471.

221. Suenaga, H., et al., *Validate Mandible Finite Element Model under Removable Partial Denture (RPD) with In Vivo Pressure Measurement.* Applied Mechanics and Materials, 2014. **553**: p. 322-26.

222. Igarashi, Y., *Analysis of the denture dynamics in R.P.D.'s. 1. Methods for analyzing the denture dynamics of free-end-saddle.* Nihon Hotetsu Shika Gakkai zasshi, 1989. **33**(2): p. 369-75.

223. Waters, N.E., *Denture foundation: a consideration of certain aspects of the displacement of and the pressure distribution within, the mucoperiosteum.* Journal of dentistry, 1975. **3**(2): p. 83-91.

224. Romeo, E., et al., *Implant-supported fixed cantilever prosthesis in partially edentulous jaws: a cohort prospective study.* Clinical Oral Implants Research, 2009. **20**(11): p. 1278-1285.

225. MericskeStern, R., *Force distribution on implants supporting overdentures: The effect of distal bar extensions.* Clinical Oral Implants Research, 1997. **8**(2): p. 142-151.

226. Field, C., et al., *Prediction of mandibular bone remodelling induced by fixed partial dentures.* Journal of Biomechanics, 2010. **43**(9): p. 1771-1779.

227. Field, C., et al., *A comparative mechanical and bone remodelling study of all-ceramic posterior inlay and onlay fixed partial dentures.* Journal of Dentistry, 2012. **40**(1): p. 48-56.

228. Huiskes, R., et al., *Adaptive bone-remodeling theory applied to prosthetic-design analysis.* Journal of Biomechanics, 1987. **20**(11–12): p. 1135-1150.

229. Compagnoni, M.A., R.F.d. Souza, and C.R. Leles, *Kinesiographic study of complete denture movement related to mucosa displacement in edentulous patients.* Pesquisa Odontológica Brasileira, 2003. **17**: p. 356-361.

230. Sonune, S.J., S. Singh, and S. Dange, *Displaceable Tissue: A Clinical Challenge treated with Palliative Approach.* International Journal of Prosthodontics & Restorative Dentistry, 2013. **2**(1): p. 34.

231. Kern, M. and B. Wagner, *Periodontal findings in patients 10 years after insertion of removable partial dentures.* Journal of Oral Rehabilitation, 2001. **28**(11): p. 991-997.

232. Leupold, R.J., R.J. Flinton, and D.L. Pfeifer, *Comparison of vertical movement occurring during loading of distal-extension removable partial denture bases made by three impression techniques.* The Journal of Prosthetic Dentistry, 1992. **68**(2): p. 290-293.

233. Lee, C.-J., et al., *Comparative adaptation accuracy of acrylic denture bases evaluated by two different methods.* Dental Materials Journal, 2010. **29**(4): p. 411-417.

234. Sajjan, C., *An altered cast procedure to improve tissue support for removable partial denture.* Contemporary clinical dentistry, 2010. **1**(2).

235. Hyde, T.P., et al., *A cross-over Randomised Controlled Trial of selective pressure impressions for lower complete dentures.* Journal of Dentistry, 2010. **38**(11): p. 853-858.

236. Bergendal, T. and B. Engquist, *Implant-supported overdentures: A longitudinal prospective study.* International Journal of Oral & Maxillofacial Implants, 1998. **13**(2): p. 253-262.

237. Drago, C. and K. Howell, *Concepts for Designing and Fabricating Metal Implant Frameworks for Hybrid Implant Prostheses.* Journal of Prosthodontics-Implant Esthetic and Reconstructive Dentistry, 2012. **21**(5): p. 413-424.

238. Meijer, H.J.A., F.J.M. Starmans, and W.H.A. Steen, *Location of Implants in the Interforaminal Region of the Mandible and the Consequences for the Design of the Supersutrcture.* Journal of Oral Rehabilitation, 1994. **21**(1): p. 47-56.

239. Klemetti, E., L. Lassila, and V. Lassila, *Biometric design of complete dentures related to residual ridge resorption.* Journal of Prosthetic Dentistry, 1996. **75**(3): p. 281-284.

240. Knezovic-Zlataric, D. and A. Celebic, *Mandibular bone mineral density changes in complete and removable partial denture wearers: A 6-month follow-up study.* International Journal of Prosthodontics, 2003. **16**(6): p. 661-665.

241. Huumonen, S., et al., *Residual ridge resorption, lower denture stability and subjective complaints among edentulous individuals.* Journal of Oral Rehabilitation, 2012. **39**(5): p. 384-390.

242. Chen, J., et al., *Multiscale design of surface morphological gradient for osseointegration.* Journal of the Mechanical Behavior of Biomedical Materials, 2013. **20**: p. 387-97.

243. Rungsiyakull, C., et al., *Surface morphology optimization for osseointegration of coated implants.* Biomaterials, 2010. **31**(27): p. 7196-7204.

244. Jacobs, R., et al., *Perceptual changes in the anterior maxilla after placement of endosseous implants.* Clinical implant dentistry and related research, 2001. **3**(3): p. 148-55.

245. Suenaga, H., et al., *Time course of bone metabolism at the residual ridge beneath dentures observed using 18F-fluoride positron emission computerized-tomography/computed tomography (PET/CT).* Annals of Nuclear Medicine, 2012. **26**(10): p. 817-822.

246. Suenaga, H., et al., *Bone metabolism of residual ridge beneath the denture base of an RPD observed using NaF-PET/CT.* Journal of prosthodontic research, 2012. **56**(1): p. 42-6.

247. Jahangiri, L., et al., *Current perspectives in residual ridge remodeling and its clinical implications: A review.* Journal of Prosthetic Dentistry, 1998. **80**(2): p. 224-237.

248. Reddy, M.S., et al., *Mandibular growth following implant restoration: Does Wolff's law apply to residual ridge resorption?* International Journal of Periodontics & Restorative Dentistry, 2002. **22**(4): p. 315-322.

249. Assad Ahmed, S., M.A. Abd El-Dayem, and M. Badawy Magdy, *Comparison between mainly mucosa-supported and combined mucosa-implant-supported mandibular overdentures* Implant Dentistry 2004. **13**(4): p. 386-94

250. Elsyad, M.A. and A.A. Habib, *Implant-Supported Versus Implant-Retained Distal Extension Mandibular Partial Overdentures and Residual Ridge Resorption: A 5-Year Retrospective Radiographic Study in Men.* International Journal of Prosthodontics, 2011. **24**(4): p. 306-313.

251. Lopez-Roldan, A., et al., *Bone resorption processes in patients wearing overdentures. A 6-years retrospective study.* Medicina Oral Patologia Oral Y Cirugia Bucal, 2009. **14**(4): p. E203-E209.

252. Kreisler, M., et al., *Residual ridge resorption in the edentulous maxilla in patients with implant-supported mandibular overdentures: An 8-year retrospective study.* International Journal of Prosthodontics, 2003. **16**(3): p. 295-300.

253. Kordatzis, K., P.S. Wright, and H.J.A. Meijer, *Posterior mandibular residual ridge resorption in patients with conventional dentures and implant overdentures.* International Journal of Oral & Maxillofacial Implants, 2003. **18**(3): p. 447-452.

Chapter 3: Mucosa Incompressibility and Contact Friction Properties using Inverse Analysis of in-vivo Measurements

Despite their critical importance, there are no existing methods available to directly measure apparent Poisson's ratio and friction coefficient of oral mucosa tissue. This Chapter aims to determine these two biomechanical parameters of oral mucosa by utilizing the *in vivo* experimental data of contact pressure developed beneath a partial denture. An inverse procedure is established based on nonlinear finite element analysis (FEA) and surrogate modelling technique. The established non-invasive methodology is demonstrated to effectively identify such biomechanical parameters of oral mucosa and it can be potentially used for determining biomaterial properties of other soft biological tissues.

Associated Publications:

1. Hanako Suenaga, Junning Chen, Wei Li, Keiichiro Yamaguchi, Keiichi Sasaki, Qing Li, Michael V. Swain. **Validate Mandible Finite Element Model under Removable Partial Denture (RPD) with In Vivo Pressure Measurement**. *Applied Mechanics and Materials*, 2014. 553: p. 322-26.
2. Junning Chen, Hanako Suenaga, Michael Hogg, Wei Li, Michael Swain, Qing Li. **Determination of oral mucosa Poisson's ratio and friction coefficient from in-vivo contact pressure measurements**. Submitted to *Journal of the Mechanical Behavior of Biomedical Materials*.

3.1 Introduction

Complete or partial dentures are widely used in the edentulous population to restore oral function [1, 2]. In this context, the oral mucosa plays a critical role in distributing masticatory force from the denture to the underlying bony ridge [3-5]. Some associative clinical complications often cause pain and patient discomfort mainly due to excessive contact pressures [6, 7]. The differential displacements (displaceability) of the mucosa across the residual ridge also triggers denture instability [8, 9], thus compromising the mastication ability and associated quality of patient's life [10, 11]. In the worst scenario, this may lead to bone resorption along the residual ridge [1, 12-14].

For the above reasons, significant interest has arisen and extensive studies have been undertaken regarding the biomechanical response of the mucosa under denture compression. Both the nonlinear elastic (instant or short term) response [15-18] and viscoelastic [3, 19-25] (time-dependent or long term) response of the mucosa have been examined via both experimental and computational approaches. The mucosa is a highly vascularized tissue with considerable volume fraction of interstitial fluids, and the substantial fluidic exchange occurs with surrounding tissues under compression [18, 24]. The mucosa's protective function arises from its cushioning effect and the extent to which it may be characterized by its deformation and compressibility. While exhaustive examination has been conducted on the mucosa stress-strain relationship (apparent moduli), little attention has been paid to its lateral responses (more relevant to compressibility) with surrounding neighbour tissues. In fact, the apparent Poisson's ratio (ν) of mucosa has not been considered as a critical factor in literature [21]. Previous FE modelling studies have assumed a rather broad range of possible values, from 0.30 to 0.49 [3, 16, 19, 20, 26]. From a biomechanics perspective, the effect of the apparent Poisson's ratio has not been adequately addressed thus far.

The contact between a denture and the supporting mucosa involves nonlinear mechanics, and the frictional behaviour can also vary over a considerable range, depending on the amount of saliva in oral environment. The prevalence of xerostomia (known as dry mouth) in the elderly edentulous population has been reported to have severe impact on denture usage, often resulting in pain and ulceration [27-30]. The variability of saliva generation alters the friction coefficient (f_c), thereby affecting the contact responses [31]. Clinically, no effective *in vivo* approach has been reported for measuring the friction coefficient of individual patients, and as a consequence, the use of friction coefficients in finite element in mucosa contact analysis is somewhat arbitrary.

Knowing a set of appropriate parameters including the boundary conditions, FE models have compelling features in mimicking biomechanical responses to clinical scenarios yielding considerable detail [32, 33]. In contrast, if some parameters are not precisely known, FEA can still be run over a given range of them. Following these FE trials, the most appropriate set of parameters can be determined in an inverse manner.

This chapter aims to first examine the influence of the apparent Poisson's ratio of the oral mucosa and friction coefficient on the contact pressure between the mucosa and denture base using a 3D patient-specific FE model. These two biomechanical parameters will then be determined from the *in vivo* measurement of contact pressure by minimizing its deviation to the modelling results. The study thus establishes an inverse procedure to determine oral biomechanical properties, which enables more realistic FE modelling for denture design and assists treatment planning for patients who have specific mucosa and lubrication conditions (e.g. xerstomia [30]).

3.2 Materials and Methods

3.2.1 CT Scan and in vivo Contact Pressure Measurement

The subject involved in this study was a 66-year-old woman, who was prescribed a distal extension removable partial denture (RPD) to replace the missing mandibular left molars (Figure 3-1a). The research protocols for this study were approved by the research ethics committee at both the Tohoku University Graduate School of Dentistry (Japan) and Sendai Kousei Hospital. The RPD treatment was performed in the prosthodontic clinic of Tohoku University Hospital. The CT scan of the mandible was taken using a Discovery ST Elite instrument (GE Healthcare Japan Co., Tokyo, Japan).

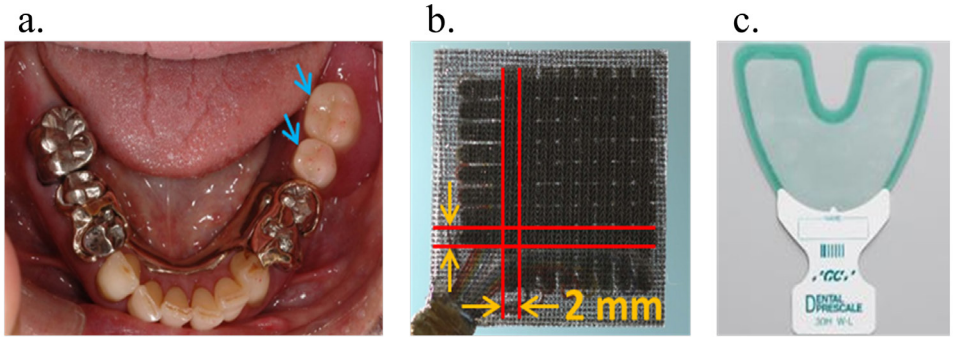

Figure 3-1 (a) Occlusal view of mandible with RPD; (b) tactile sensor sheet; (c) pressure sensitive film.

For the *in vivo* measurement of contact pressure, a duplicate RPD was fabricated using the same materials, namely platinum-gold alloy (PGA-2, Ishifuku Metal Industry co., Ltd, Tokyo, Japan) for the metal frame, resin (Acron MC, GC Co., Tokyo, Japan), and artificial teeth (Surpass Posterior Teeth, GC Co., Tokyo, Japan). A 1.0 mm thick tactile sensor sheet was used to measure the contact pressure under the denture base, with a measuring range of 0-2 MPa (Conformable TactArray SensorTM, Pressure Profile Systems Inc., CA, USA) (Figure 3-1b) [34]. The sensor was constructed from a flexible and conductive cloth that can be molded into shapes with multiple curvatures. Electrode strips, 2 mm in width, were regularly arranged in an orthogonal fashion, and the 30 overlapping

areas functioned as sensing points to measure pressure distribution in the regions of interest (ROI). The sensor sheet was bonded to the RPD basal surface using an adhesive (PPX set, Cemedine Co., Ltd., Tokyo, Japan). Following this, a fitting test was performed to check the adaptation between the sensor sheet and residual ridge. Occlusal adjustment was performed before the measurements, ensuring that the occlusal contact points were distributed evenly in the dental arch. Pressure distribution was acquired at the maximum voluntary clenching force, and five trials were conducted for the experiment. Occlusal forces on the dental arches were measured simultaneously with pressure sensor films (Dental PrescaleTM, Fuji Photo Film Co., Tokyo, Japan, Figure 3-1c) for each trial to ensure the correlation of contact pressure to force application.

3.2.2 Finite Element Modelling

Another duplicated denture was made specifically for scanning from the same cast, consisting of pure titanium for the metal frame (to reduce metal Xray scattering artefacts associated with the denser Pt-Au alloy), radiopaque resin (Scanning resin, Yamahachi Dental MFG. CO, Aichi, Japan) for denture base and radiopaque teeth (SR Ortho TAC, Ivoclar Vivadent Pty. Ltd., Municipality, Principality of Liechtenstein). The CT scan (NewTom 3G 9000, QR S.r.l., Verona, Italy) was taken with exposure parameters of 110 kV, and tube current of 6.0 mA.

The CT scan stacks for both subject and denture were segmented in ScanIP Ver. 4.3 (Simpleware Ltd, Exeter, UK). Based on Hounsfield unit (HU) values, 11 masks were created to represent the individual teeth, cortical and cancellous bone; another 3 masks were generated for the metal frame, denture base, and artificial teeth in the other stack (Figure 3-2a). Due to substantially low contrast, the mucosa was modeled by offsetting the outer layer of the cortical bone with 4 pixels to provide an average thickness of approximately 1.2 mm, as indicated in an earlier study [4]. All the masks were further

processed in 3D parametric modelling software Rhinoceros 3.0 (Robert McNeel & Associates, Seattle USA) to create geometric models by using the non-uniform rational B-splines (NURBS) (Figure 3-2b). The insertion of the RPD was performed virtually onto the patient mandible model for the final assembly, and in the mandible model, the corresponding regions of interest (ROI) were assigned by the same CT image coordinates, corresponding to the *in vivo* measurement.

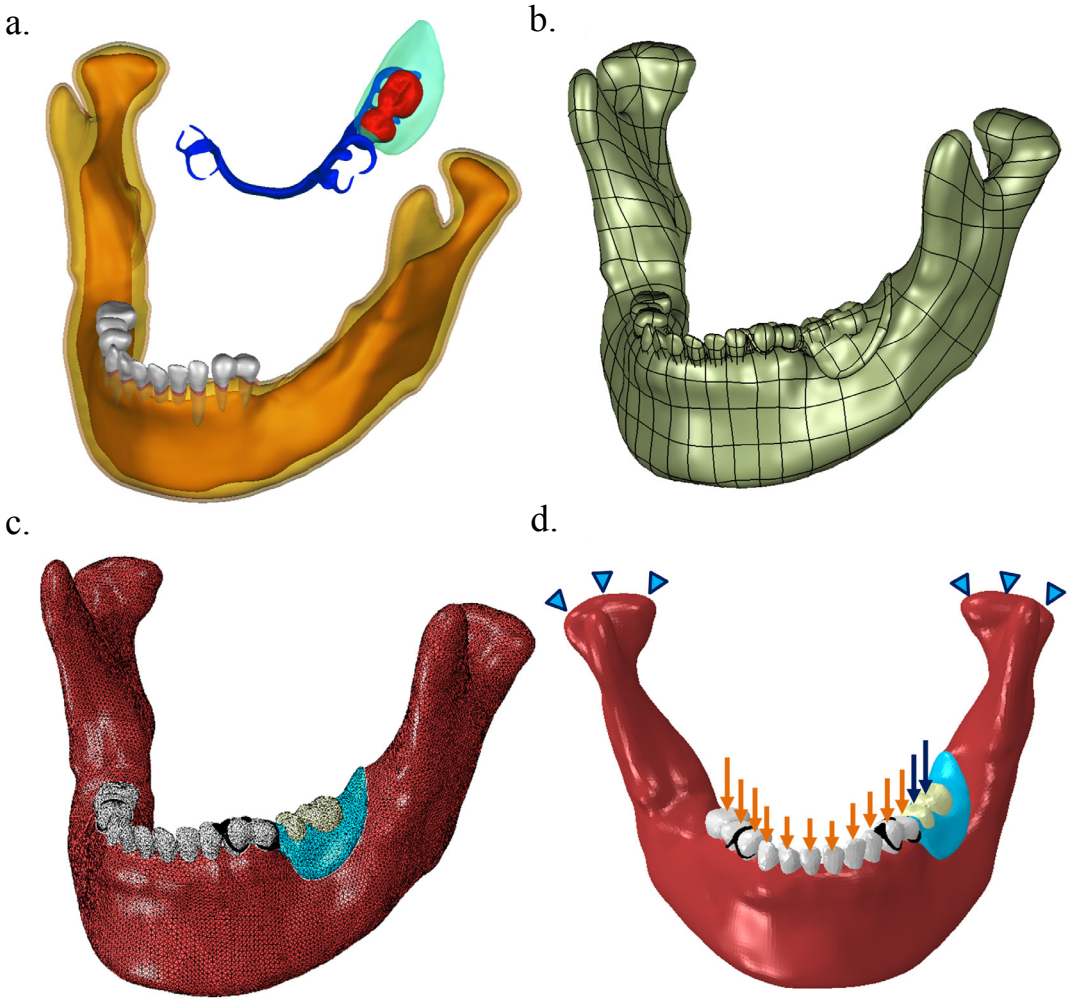

Figure 3-2 (a) Masks segmented for individual components from two individual CT scans, patient jaw and denture, mucosa (transparent maroon), cortical bone (transparent yellow), cancellous bone (opaque orange), teeth (opaque grey), denture base (transparent cyan), frame (opaque blue), and artificial crowns (opaque red); (b) solidified model with NURBS representation after visual insertion of the removable partial denture; (c) finite element models meshed in ABAQUS 6.9.2; (d) loading conditions (orange: native teeth; blue: artificial crowns) and boundary conditions (cyan triangles) assigned to the model.

The exported IGS models were meshed in ABAQUS 6.9.2 (Dassault Systèmes, Waltham USA). The adaptive mesh control was set to have a maximum elemental size of 1 mm (Figure 3-2c). For this sophisticated 3D model, hybrid formulated tetrahedral elements (C3D4H) were used to capture the complex curvature and preserved the continuity of the contact surface. The model comprises 699,411 degrees of freedom (D.O.F.) with 1,319,320 tetrahedral elements. To ensure numerical accuracy, a mesh convergence test was performed similar to our previous studies [35, 36].

The mucosa was defined as a hyperelastic material because of its nonlinear responses [3, 17, 24]. Driven by the unit volume strain energy, a third order Ogden strain energy constitutive equation [37] was derived from the *in vivo* data documented by Kishi [17] *via* a least-square fitting, which is a function of the instantaneous strain. The mechanical properties of other materials were taken from those used in the previous FE studies [33, 38-41].

The clasp of the denture frame was locked by a pressure-fit onto the crowns, and their contact was achieved by assigning a tie constraint in ABAQUS. A surface-to-surface contact was defined between the denture base and the mucosa, with a friction coefficient to be identified in Section 2.3. Occlusal loads were assigned onto each corresponding tooth as measured clinically (Table 1). The boundary conditions were prescribed to the distal ends of the condyles (Figure 3-1d) [42, 43].

Table 3-1 *In vivo* occlusal loads measured clinically on the subject

Left Side		Right Side	
Tooth	**Magnitude (N)**	**Tooth**	**Magnitude (N)**
Central Incisor	6.3 (1.8)	Central Incisor	7.9 (1.7)
Lateral Incisor	5.8 (1.3)	Lateral Incisor	7.2 (1.3)
Canine	55.4 (8.1)	Canine	71.8 (14.7)
First Premolar	48.7 (11.2)	First Premolar	42.4 (16.6)
Second Premolar	66.5 (11.3)	Second Premolar	42.5 (10.1)
First Molar (Denture)	28.7 (9.8)	First Molar	42.1 (10.9)
Second Molar (Denture)	29.4 (10.4)		

3.2.3 Response Surface Method (RSM)

In this study, the two undetermined variables were the apparent Poisson's ratio (ν) and friction coefficient (f_c). A wide range of ν has been assumed in the previous FE models reported in the literature, ranging from 0.30 to 0.49 [3, 16, 19, 20, 26]. Soft tissue is often considered as nearly incompressible, and this behaviour can be modeled with a very high Poisson's ratio ν of 0.499.

Friction coefficient f_c can also differ significantly among subjects, depending on their physiological conditions, denture materials and treatment outcomes [28]. The variability as to the amount of saliva considerably influences the friction between the denture base and the mucosa [31]. High friction coefficients between 0.3 and 0.4 were reported with 'dried' surfaces (hydration index closes to 0, to simulate xerostomia) in experimental studies [31, 44], whereas a low value around 0.02 were reported for well-lubricated conditions [44]. Previous FE studies have used values between these two extremes [26, 29, 30].

Based on the literature data available, the possible ranges of ν and f_c can be defined in Eqs. (1) and (2), respectively. Seven apparent Poisson's ratios (0.3, 0.35, 0.4, 0.45, 0.47, 0.49, and 0.499) and five friction coefficients (0.01, 0.1, 0.2, 0.3, and 0.4) were selected for sampling tests, resulting in 35 different combinations for the FE simulations. The objective function (i.e. overall deviation between FE modelling and the *in vivo* measurements over the 30 ROIs) was defined in Eq. (3), where N (=30) is the number of ROIs, and σ_i^* and σ_i (i=1, 2, …, N) are the corresponding *in vivo* and simulated contact pressures, respectively. To best match the *in vivo* results, the simulation is expected to achieve the minimum deviation with respect to a set of unknown parameters (ν, f_c).

$$0.3 \le \nu \le 0.499 \tag{1}$$

$$0.02 \le f_c \le 0.4 \tag{2}$$

$$\begin{aligned} \min J(\nu, f_c) &= \sqrt{\frac{1}{N}\sum_{i=0}^{N}(\sigma_i - \sigma_i^*)^2} \\ &= \sqrt{\frac{1}{N}[(\sigma_1 - \sigma_1^*)^2 + \ldots + (\sigma_N - \sigma_N^*)^2]} \end{aligned} \tag{3}$$

It is difficult to formulate an explicit cost function, $J(\nu, f_c)$, in Eq. (3) for such a highly nonlinear problem. Response surface method (RSM) is one of the surrogate modelling techniques that were considered an effective, and sometimes unique alternative in engineering and biomedical design [32, 40, 45, 46]. Since the knowledge of the objective functions is lacking; we attempted several different polynomial models in order to capture complex mutual effects from these two variables [47]. Using this method, the most suitable response surface (RS) function was determined based on the best fit and the least error.

3.3 Results

3.3.1 In vivo Occlusal Force and Contact Pressure

The occlusal forces measured are summarized in Table 1. These *in vivo* forces were assigned onto each corresponding tooth in the patient-specific model. Total occlusal force on the entire dental arch was 438.7 N, and total force on the artificial teeth was 84.6 N.

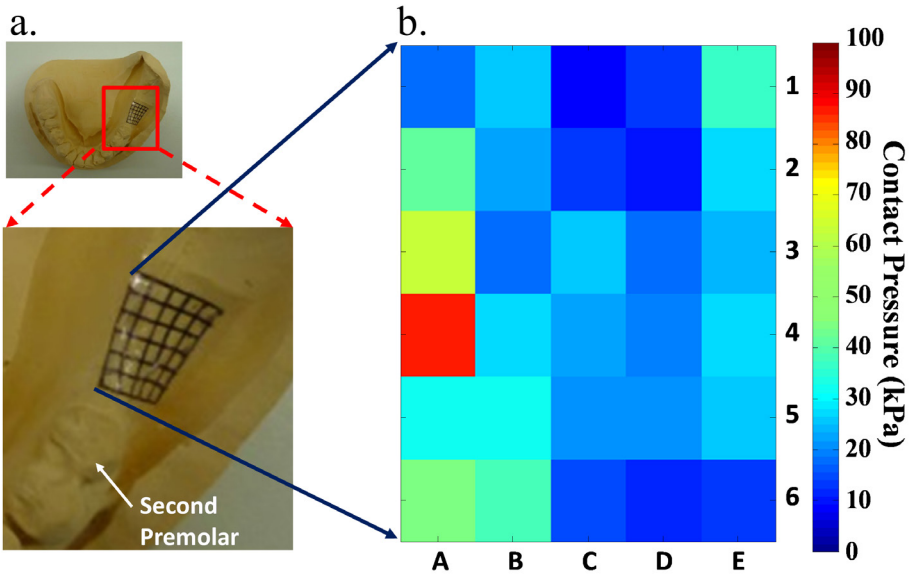

Figure 3-3 In vivo measurement of contact pressure underneath the RPD: (a) 30 sensor locations (5×6) over the residual ridge indicated on a pressed mould from the subject; (b) averaged contact pressure reading (from 5 repeat tests) of individual sensor positions.

Figure 3-3a shows the *in vivo* contact pressure measurement on the same subject, over the sensing points as specified in Figure 3-3b (5×6 matrix, lingual-buccal: A-E, distal-mesial: 1-6). The average contact pressure contour (5 measurements for all the 30 sensors) on the residual ridge beneath the denture base is presented in Figure 3-3b. The pressure range over the contact surface varied from 0.09 to 0.87 MPa, where the maximum occurs on the lingual side of the residual ridge crest (Sensing Point A4); and the minimum occurs on the mesial and distal ends of the buccal side (Sensing Points C1 and D6).

3.3.2 Numerical Contact Pressure and Mucosa Displaceability (Displacement)

The contact pressure beneath the denture base and the tissue displacement difference (relative displacement) are major concerns in denture design [8, 9]. Figure 3-4a specifies the mandibular region under the RPD. Figure 3-4b shows the reference point on the first premolar for measuring the displacement difference over the entire denture and crown.

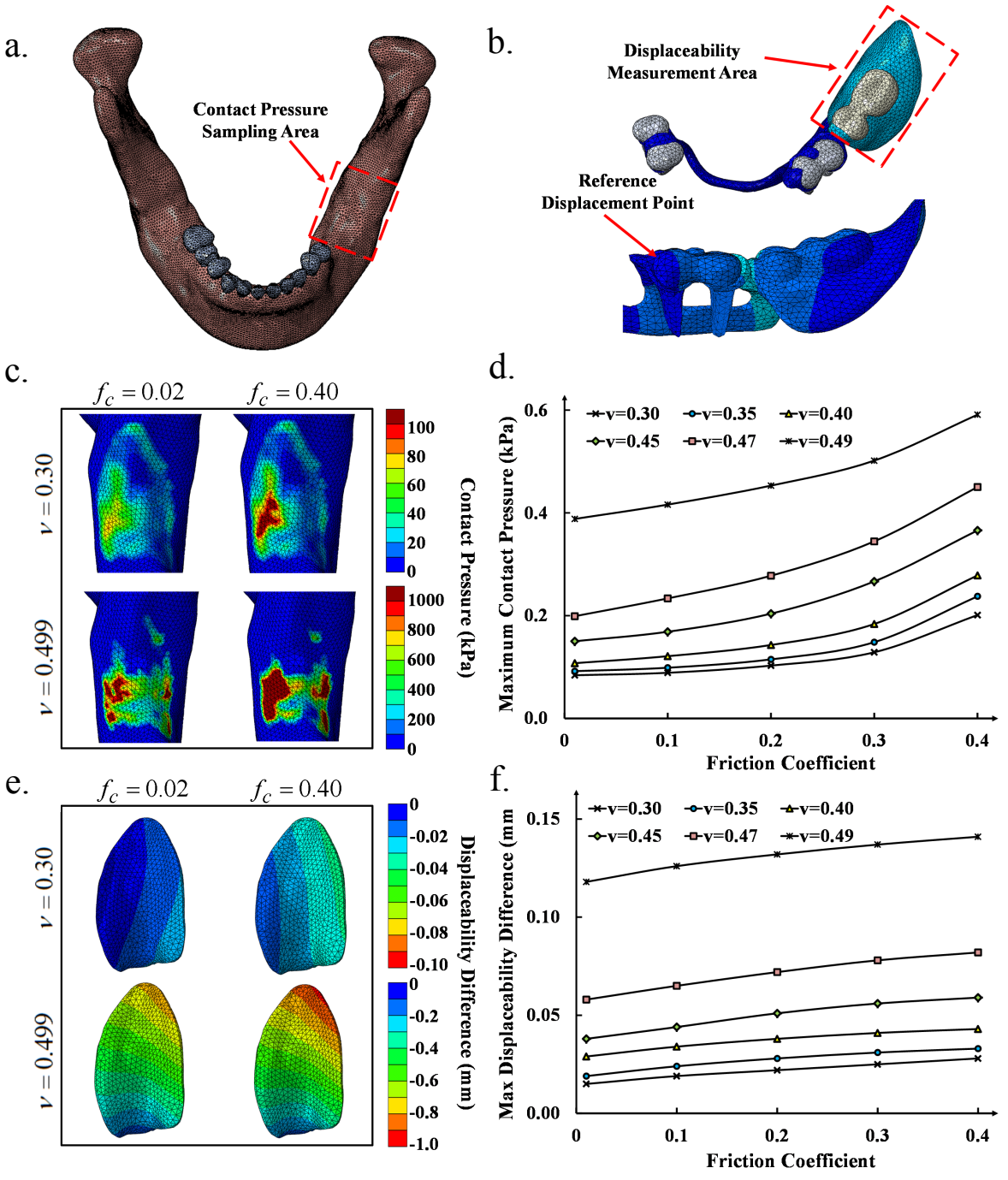

Figure 3-4 (a) Contact pressure measurement area underneath the RPD; (b) displaceability measurement area on the RPD; (c) the maximum contact pressure contours on mucosa for the four extreme cases; (d) the maximum contact pressure change with different Poisson's ratios and different friction coefficients; (e) the contours of displaceability difference with respect to the first premolar for the four extreme cases; (f) the maximum displaceability difference on the denture base with the different Poisson's ratios and friction coefficients.

Figure 3-4c compares the contact pressure contours for the four extreme combinations of the unknown parameters ($\nu = 0.30$ and 0.499; $f_c = 0.02$ and 0.40). It is evident that ν and f_c have significant impact on the mucosa responses, indicated by the changes in contact pressure distributions and their peak values. When the mucosa is modeled as highly incompressible but well lubricated ($\nu = 0.499$, $f_c = 0.02$), the maximum contact pressure can reach 1.8 MPa, 21 times that for the lowest Poisson's ratio case ($\nu = 0.30$). When $f_c = 0.40$, the predicted contact pressure reached 2.69 MPa. The maximum contact pressures are plotted versus f_c for different ν ranging from 0.30 to 0.49 in Figure 3-4d, at different friction coefficients, excluding $\nu = 0.499$ because of its unrealistic mucosal response in comparison with the experimental results. Increasing either Poisson's ratio or friction coefficient induces nonlinear increases in the maximum contact pressures.

Figure 3-4e illustrates the relative displacement on the denture base with respect to the 1st premolar, as the result of different mucosa displaceabilities. At $\nu = 0.30$ and $f_c = 0.02$, the lingual side of the denture base moved down 0.02 mm more than the premolar, as the smallest difference among all parameters. Obviously, ν plays a more dominant role in the tissue displaceability, and the maximum difference reaches 18 times. Figure 3-4f summarizes the maximum displaceability difference for individual cases. It is observed that the displaceability difference has nonlinear relationships to both Poisson's

ratio and friction coefficient, but the trend is concavely negative, different to contact pressure distributions (Figure 3-4d).

3.3.3 Response Surface and Minimum Deviation Determination

Since the high apparent Poisson's ratios ($\nu = 0.49$ and 0.499) generates unrealistic contact pressure contours with considerable deviations ($J(\nu, f_c) > 100$ kPa, Eq. 3) from the *in vivo* measurements, the associated sampling points are excluded from the RS modelling and subsequent parametric identification. Thus a total of 25 sample points (with 30 ROIs each) are considered for the construction of RS model.

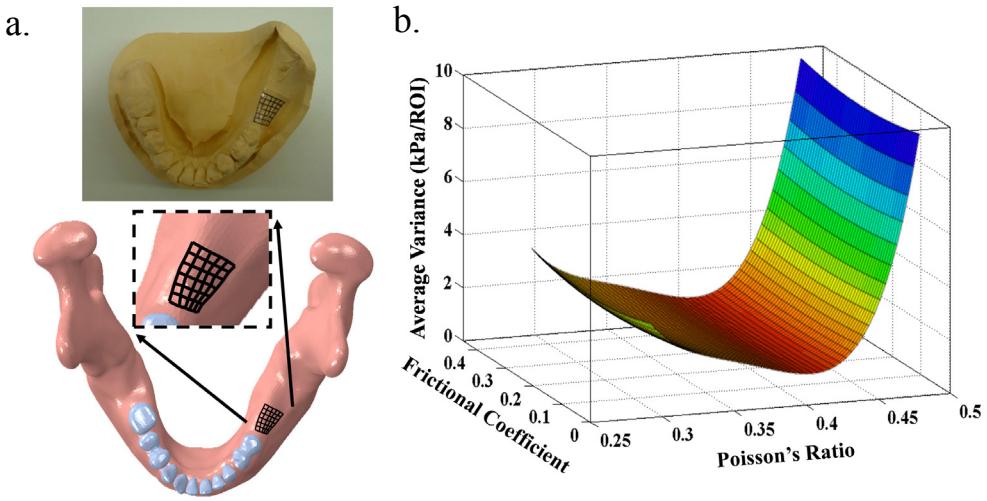

Figure 3-5 (a) The regions of interest (ROIs) indicated on the numerical model (lower sub-figure), corresponding to the sensing points of the in vivo contact pressure measurement (upper sub-figure); (b) the response surface model based on the 25 sampling points, over the given variable domains.

Figure 3-5a illustrates the corresponding ROIs (lower) in the FE model to the *in vivo* measurement areas (upper). Using the least square algorithm, the quartic-quadratic (ν - f_c, Eq. 4) model provides the best possible fit to the simulation outcomes, with an adjusted R^2=0.9997 and the residual standard error of 0.11 kPa. With The corresponding

polynomial coefficients are listed in Table 2. With this RS surrogate model, the minimum deviation within the given variable range is 1.57 kPa, for $\nu = 0.402$ and $f_c = 0.213$.

$$\begin{aligned} J(\nu, f_c) = {} & p_{00} + p_{10}\times\nu + p_{01}\times f_c + p_{20}\times\nu^2 + p_{11}\times\nu\times f_c \\ & + p_{02}\times f_c^2 + p_{30}\times\nu^3 + p_{21}\times\nu^2\times f_c + p_{12}\times\nu\times f_c^2 \\ & + p_{40}\times\nu^4 + p_{31}\times\nu^3\times f_c + p_{22}\times\nu^2\times f_c^2 \end{aligned} \quad (4)$$

Table 3-2 The coefficients of the response surface polynomial model (Eq. 4)

Coefficient	Value
p_{00}	8.14E+02
p_{10}	-9.06E+03
p_{01}	-6.25E+01
p_{20}	3.80E+04
p_{11}	3.36E+02
p_{02}	1.29E+02
p_{30}	-7.09E+04
p_{21}	-5.05E+02
p_{12}	-6.53E+02
p_{40}	4.96E+04
p_{31}	1.26E+02
p_{22}	8.34E+02

3.4 Discussion

A common clinical problem confronting prosthodontists is the design and maintenance of distal extension RPDs, because the mechanical supports required from the abutment teeth and residual ridge mucosa are quite different [48]. While optimal load transfer through the abutment teeth and the residual ridges is highly desirable; this has proven considerably difficult to realize as accurate values of mucosa properties have not been established [21]. There is no direct approach available for measuring the Poisson's ratio of the oral mucosa in a clinical scenario [19]. Although the previous studies [3, 20] attempted to derive the nonlinear moduli of mucosa via the same approach as hard tissues [49], data regarding its volumetric deformation has not been specifically identified. More importantly, the effect of the apparent Poisson's ratio has been largely disparaged because of the lack of data [21]. Our study has on the other hand clearly demonstrated the importance of Poisson's ratio to both the contact pressure distribution and mucosa displaceability, within the assumed range of Poisson's ratios suggested in the early FE studies [16, 26, 29].

From a mechanical aspect, solid evidence has shown that Poisson's ratio could alter the cushioning effect [50], thereby preventing both compressive and shearing damage. This cushioning effect of the masticatory mucosa comes from its hierarchical vascular structure and internal permeability. A stratified squamous keratinized epithelium covers the underlying tissues, tightly bonded by collagenous connective tissue [51]. A fluid-rich vascular network forms in the underlying tissues, and the permeability determines how fast the interstitial fluid can be transferred from a loaded area to its surrounding unstressed mucosal periosteum [4, 52, 53]. Both of these factors can be affected by aging, physiological conditions, and therapeutic treatments [27-30, 51-54]. Consequently, the

altered overall cushioning effect reflects the change in its apparent Poisson's ratio and other biomechanical material properties.

The friction coefficient between the denture material and mucosa has drawn some attention [31, 44]. It is directly linked to the mucosa-denture interaction and the stability of a denture [16, 26, 29]. It is important that the denture provides sufficient wettability by forming a superior lubricating layer over the supporting mucosa to reduce friction and minimize patient discomfort [55]. However, the prevalence of xerostomia (lack of saliva) in denture wearers can lead to inflamed and traumatic ulcerations with elevated circumferential fibrous tissue, which can further develop into an epulis fissuratum [56-58]. Thus, the friction coefficient acts as a critical indicator for denture design.

At the current stage of this study, the elementary stress-strain behaviour of the mucosa was adopted from a group of average patients based on the existing literature [17]. The mucosa condition can however vary significantly between individuals, and it also changes across different types of mucosa (e.g. masticatory, lining) within the same subject. It must be noted that further large scale patient-specific studies are needed to generate the statistical implications of these two parameters. Nevertheless, this study provides some biomechanical insights for the mucosal apparent Poisson's ratio and friction coefficient, which have not been adequately addressed in the literature to date.

3.5 Conclusions

This study established a FE based identification procedure for determining apparent Poisson's ratio of mucosa and the friction coefficient between the denture and oral mucosa. These two critical biomechanical parameters were determined by minimizing the discrepancy between the FE analyses and experimental tests of contact pressure. A combined quartic-quadratic response surface model was constructed to mathematically represent the deviation cost function with respect to the design variables of Poisson's ratio and friction coefficient. For this specific patient, we found that $\nu = 0.402$ and $f_c = 0.213$ achieved the closest fitting to the *in vivo* experimental results. After illustrating the importance and biomechanical insights of these two parameters, this chapter also established a non-invasive procedure for combining clinical analysis, biomechanics and dental materials studies in a patient-specific manner. The biomechanical parameters determined here will potentially generate more realistic simulations and biomechanical studies with potentially improved patient satisfaction.

Acknowledgement

This work is supported by Australian Research Council (ARC) and Australian Postgraduate Award (APA).

3.6 References

1. Klemetti, E., *A review of residual ridge resorption and bone density.* Journal of Prosthetic Dentistry, 1996. **75**(5): p. 512-514.
2. Ozan, O., et al., *The Effect of Removable Partial Dentures on Alveolar Bone Resorption: A Retrospective Study with Cone-Beam Computed Tomography.* Journal of Prosthodontics-Implant Esthetic and Reconstructive Dentistry, 2013. **22**(1): p. 42-48.
3. Sawada, A., et al., *Viscoelasticity of Human Oral Mucosa: Implications for Masticatory Biomechanics.* Journal of Dental Research, 2011. **90**(5): p. 590-595.
4. Ahmad, R., et al., *Three dimensional quantification of mandibular bone remodeling using standard tessellation language registration based superimposition.* Clin Oral Implants Res, 2013. **24**(11): p. 1273-1279.
5. Mori, S., et al., *Effect of continuous pressure on histopathological changes in denture-supporting tissues.* Journal of Oral Rehabilitation, 1997. **24**(1): p. 37-46.
6. Isobe, A., et al., *The influence of denture supporting tissue properties on pressure-pain threshold: –Measurement in dentate subjects–.* Journal of Prosthodontic Research, 2013. **57**(4): p. 275-283.
7. Ogawa, T., et al., *Pressure-pain threshold of oral mucosa and its region-specific modulation by pre-loading.* Journal of Oral Rehabilitation, 2003. **30**(11): p. 1062-1069.
8. Compagnoni, M.A., R.F.d. Souza, and C.R. Leles, *Kinesiographic study of complete denture movement related to mucosa displacement in edentulous patients.* Pesquisa Odontológica Brasileira, 2003. **17**: p. 356-361.
9. Sonune, S.J., S. Singh, and S. Dange, *Displaceable Tissue: A Clinical Challenge treated with Palliative Approach.* International Journal of Prosthodontics & Restorative Dentistry, 2013. **2**(1): p. 34.
10. Bae, K.H., et al., *A comparison of oral health related quality of life between complete and partial removable denture-wearing older adults in Korea.* Journal of Oral Rehabilitation, 2006. **33**(5): p. 317-322.
11. Celebic, A., et al., *The patient's and the therapist's evaluation of complete denture therapy.* Collegium Antropologicum, 2000. **24**: p. 71-77.
12. Tallgren, A., *Alveolar bone loss in denture wearers as related to facial morphology.* Acta Odontol Scand, 1970. **28**(2): p. 251-70.
13. Wright, P.S., et al., *The effects of fixed and removable implant-stabilised prostheses on posterior mandibular residual ridge resorption.* Clinical Oral Implants Research, 2002. **13**(2): p. 169-174.
14. Akazawa, H. and K. Sakurai, *Changes of blood flow in the mucosa underlying a mandibular denture following pressure assumed as a result of light clenching.* Journal of Oral Rehabilitation, 2002. **29**(4): p. 336-340.
15. Kydd, W.L., C.H. Daly, and D. Nansen, *Variation in the response to mechanical stress of human soft tissues as related to age.* Journal of Prosthetic Dentistry, 1974. **32**(5): p. 493-500.

16. Kanbara, R., et al., *Three-dimensional finite element stress analysis: The technique and methodology of non-linear property simulation and soft tissue loading behavior for different partial denture designs.* Dental Materials Journal, 2012. **31**(2): p. 297-308.

17. Kishi, M., *Experimental studies on the relation between area and displacement of loading surfaces in connection with displaceability in the mucosa of edentulous alveolar ridge under pressure.* Shika gakuho. Dental science reports, 1972. **72**(6).

18. Scapino, R.P., *Biomechanics of Prehensile Oral Mucosa.* Journal of Morphology, 1967. **122**(2): p. 89-&.

19. Lacoste-Ferre, M.H., et al., *Dynamic mechanical properties of oral mucosa: Comparison with polymeric soft denture liners.* Journal of the Mechanical Behavior of Biomedical Materials, 2011. **4**(3): p. 269-274.

20. Wakabayashi, N. and T. Suzuki, *Patient-specific finite element analysis of viscoelastic masticatory mucosa.* Journal of dental biomechanics, 2013. **4**.

21. Inoue, K., et al., *Viscoelastic properties of oral soft tissue. 1. A method of determining elastic modulus of oral soft tissue.* Dent Mater J, 1985. **4**(1): p. 47-53.

22. Cheng, S., et al., *Viscoelastic properties of the tongue and soft palate using MR elastography.* Journal of Biomechanics, 2011. **44**(3): p. 450-454.

23. Goktas, S., J.J. Dmytryk, and P.S. McFetridge, *Biomechanical Behavior of Oral Soft Tissues.* Journal of Periodontology, 2011. **82**(8): p. 1178-1186.

24. Kydd, W.L. and C.H. Daly, *The biologic and mechanical effects of stress on oral mucosa.* Journal of Prosthetic Dentistry, 1982. **47**(3): p. 317-29.

25. Yatabe, M., *Study on measurement of dynamic viscoelasticity of maxillary mucosa.* Kokubyo Gakkai zasshi. The Journal of the Stomatological Society, Japan, 1991. **58**(1): p. 74-94.

26. Zmudzki, J., G. Chladek, and J. Kasperski, *Single Implant-Retained Dentures: Loading of Various Attachement Types under Oblique Occlusal Forces.* Journal of Mechanics in Medicine and Biology, 2012. **12**(5).

27. Östlund, S.G., *Saliva and denture retention.* The Journal of Prosthetic Dentistry, 1960. **10**(4): p. 658-663.

28. Turner, M., L. Jahangiri, and J.A. Ship, *Hyposalivation, xerostomia and the complete denture - A systematic review.* Journal of the American Dental Association, 2008. **139**(2): p. 146-150.

29. Zmudzki, J., G. Chladek, and J. Kasperski, *The influence of a complete lower denture destabilization on the pressure of the mucous membrane foundation.* Acta of Bioengineering and Biomechanics, 2012. **14**(3): p. 67-73.

30. Upadhyay, S.R., L. Kumar, and J. Rao, *Fabrication of a functional palatal saliva reservoir by using a resilient liner during processing of a complete denture.* The Journal of prosthetic dentistry, 2012. **108**(5): p. 332-5.

31. Ranc, H., et al., *Friction coefficient and wettability of oral mucosal tissue: Changes induced by a salivary layer.* Colloids and Surfaces a-Physicochemical and Engineering Aspects, 2006. **276**(1-3): p. 155-161.

32. Rungsiyakull, C., et al., *Surface morphology optimization for osseointegration of coated implants.* Biomaterials, 2010. **31**(27): p. 7196-7204.

33. Field, C., et al., *Prediction of mandibular bone remodelling induced by fixed partial dentures.* Journal of Biomechanics, 2010. **43**(9): p. 1771-1779.

34. Kubo, K., et al., *Development of in vivo measuring system of the pressure distribution under the denture base of removable partial denture.* Journal of prosthodontic research, 2009. **53**(1): p. 15-21.

35. Li, W., et al., *Fibre reinforced composite dental bridge. Part II: numerical investigation.* Biomaterials, 2004. **25**(20): p. 4995-5001.

36. Li, W., et al., *Towards automated 3D finite element modeling of direct fiber reinforced composite dental bridge.* Journal of Biomedical Materials Research Part B: Applied Biomaterials, 2005. **74B**(1): p. 520-528.

37. Bergomi, M., et al., *Hydro-mechanical coupling in the periodontal ligament: A porohyperelastic finite element model.* Journal of Biomechanics, 2011. **44**(1): p. 34-38.

38. Wang, H.Y., et al., *Effects of rigid and nonrigid extracoronal attachments on supporting tissues in extension base partial removable dental prostheses: a nonlinear finite element study.* J Prosthet Dent, 2011. **105**(5): p. 338-46.

39. Verri, F.R., et al., *Evaluation of bone insertion level of support teeth in class I mandibular removable partial denture associated with an osseointegrated implant: a study using finite element analysis.* Implant Dent, 2011. **20**(3): p. 192-201.

40. Chen, J., et al., *Multiscale design of surface morphological gradient for osseointegration.* Journal of the Mechanical Behavior of Biomedical Materials, 2013. **20**: p. 387-97.

41. Sato, Y., et al., *Finite element analysis of stress relaxation in soft denture liner.* Journal of Oral Rehabilitation, 2000. **27**(8): p. 660-663.

42. Hart, R.T., et al., *Modeling the Biomechanics of the Mandible - a 3-Dimensional Finite-Element Study.* Journal of Biomechanics, 1992. **25**(3): p. 261-286.

43. Korioth, T.W.P., D.P. Romilly, and A.G. Hannam, *3-Dimensional Finite Element Stress-Analysis of the Dentate Human Mandible.* American Journal of Physical Anthropology, 1992. **88**(1): p. 69-96.

44. Prinz, J.F., R.A. de Wijk, and L. Huntjens, *Load dependency of the coefficient of friction of oral mucosa.* Food Hydrocolloids, 2007. **21**(3): p. 402-408.

45. Lin, D., et al., *Design optimization of functionally graded dental implant for bone remodeling.* Composites Part B-Engineering, 2009. **40**(7): p. 668-675.

46. Hou, S.J., et al., *Multiobjective optimization of multi-cell sections for the crashworthiness design.* International Journal of Impact Engineering, 2008. **35**(11): p. 1355-1367.

47. Bradley, N., *The response surface methodology*, in *Department of Mathematical Sciences*. 2007, Indiana University: South Bend. p. 36-38.

48. Igarashi, Y., et al., *Stress distribution and abutment tooth mobility of distal-extension removable partial dentures with different retainers: an in vivo study.* J Oral Rehabil, 1999. **26**(2): p. 111-6.

49. Kinney, J.H., S.J. Marshall, and G.W. Marshall, *The mechanical properties of human dentin: A critical review and re-evaluation of the dental literature.* Critical Reviews in Oral Biology & Medicine, 2003. **14**(1): p. 13-29.

50. Wang, Y.C. and R. Lakes, *Analytical parametric analysis of the contact problem of human buttocks and negative Poisson's ratio foam cushions.* International Journal of Solids and Structures, 2002. **39**(18): p. 4825-4838.

51. Squier, C.A. and M.J. Kremer, *Biology of Oral Mucosa and Esophagus.* JNCI Monographs, 2001. **2001**(29): p. 7-15.

52. Lesch, C.A., et al., *The Permeability of Human Oral Mucosa and Skin to Water.* Journal of Dental Research, 1989. **68**(9): p. 1345-1349.

53. Thelin, W.R., et al., *The oral mucosa as a therapeutic target for xerostomia.* Oral Diseases, 2008. **14**(8): p. 683-689.

54. Squier, C.A., *The Permeability of Oral Mucosa.* Critical Reviews in Oral Biology & Medicine, 1991. **2**(1): p. 13-32.

55. Waters, M.G., R.G. Jagger, and G.L. Polyzois, *Wettability of silicone rubber maxillofacial prosthetic materials.* J Prosthet Dent, 1999. **81**(4): p. 439-43.

56. Bogucki, Z.A., *Clinical aspects of the use of dental adhesive materials in patients with chronic xerostomia.* Gerodontology, 2013. **30**(2): p. 162-6.

57. Rashmikant, U.S., K. Lakshya, and R. Jitendra, *Fabrication of a Functional Palatal Saliva Reservoir by Using a Resilient Liner during Processing of a Complete Denture.* Journal of Prosthetic Dentistry, 2012. **108**(5): p. 332-335.

58. Turner, M., L. Jahangiri, and J.A. Ship, *Hyposalivation, xerostomia and the complete denture: a systematic review.* J Am Dent Assoc, 2008. **139**(2): p. 146-50.

Chapter 4: Mechanobiological Bone Reaction Quantified by Positron Emission Tomography

This chapter investigates instantaneous mandibular bone metabolism at various time points induced by removable partial denture (RPD) insertion. This behaviour was observed by correlating 18F-fluoride positron emission tomography (PET) image data with the calculated mechanical stimuli in the residual ridge. The resultant mechanobiological response was analysed using a 3D finite element (FE) model derived from the computerized tomography (CT) images of a specific patient under the mastication loading. This approach reveals the effectiveness of PET to determine bone metabolic activity associated with mechanical stimuli, and the results provide for the first time biomechanical insights into the association of tracer uptake with bone remodelling. Good correlation was found between bone metabolism and mechanical stimuli induced following RPD insertion. It was shown that PET enables detection of current bone metabolic activity, which is strongly associated with changed mechanical stimuli, in a much shorter duration than a conventional X-ray that quantify the summation of bone remodelling. The non-destructive nature of PET/CT scan and FEA is able to provide an effective means to clinical examination and monitoring of various denture treatments.

Associated Publications:

1. Hanako Suenaga, **Junning Chen**, Keiichiro Yamaguchi, Wei Li, Keiichi Sasaki, Michael Swain, Qing Li. **Mechanobiological Bone Reaction Induced by Removable Partial Denture Quantified by PET (18F) Imaging and Finite Element Modeling**. Submitted to *Journal of Dental Research*.

4.1 Introduction

While dentures have had a long history of successful usage in clinical dentistry, the manner, in which mastication induced load is supported by the soft gingival tissue overlying the bony ridges of the oral cavity, is an unnatural situation and has significant clinical consequences. This not only causes pain and discomfort, but also leads to bone resorption, typically occurring on the residual ridge beneath a mal-adapting denture base [1]. As widely accepted in previous studies [2-5], mechanical stimuli give rise to bone remodelling activities, either apposition or resorption, as implied by Wolff's rule. Therefore, it is important to investigate the mechanobiological responses induced, thereby controlling it through biomechanical design of dental prosthesis.

While X-rays have been commonly utilized to evaluate the bone quality in clinical practice [6-11], which enables detecting 30-50% changes in bone mineral; this technique is difficult to identify short term responses [12]. Nuclear medicine scanning techniques, such as bone scintigraphy, single-photon emission computerized tomography, and 18F-fluoride Positron Emission Computerized Tomography (PET), on the other hand, can identify subtle functional variations prior to the major structural change detectable by X-ray [13]. Recently, 18F-fluoride PET has received critical attention for its improved resolution and shorter waiting time for earlier clinical evaluation than other approaches [14-18].

The sensitivity of nuclear medicine scanning techniques to quantify increased bone turnover associated with stress injury has drawn attention in clinical practice [18]. Various *in vivo* human studies have been undertaken to evaluate stress fractures [19, 20]. Although all these studies acknowledged the role played by mechanical forces and its influence in bone metabolic activities, none of them have quantified or confirmed a correlation between tracer uptake and bone mechanical stimulus [21].

As no direct or non-destructive *in vivo* approach has been reported for directly measuring mechanical stimuli on humans, the finite element (FE) method provides and is considered an effective alternative [22-25]. With advances in clinical computerized tomography (CT), sophisticated 3D anatomy can be precisely modeled, reflecting patient-specific details possible with such studies [26]. In addition, with the increased computational power available it enables more realistic models of tissue behaviour, including simulating complicated responses in a nonlinear manner [22].

This study investigates the relationship between bone metabolism observed by 18F-fluoride PET image and mechanical stimuli of the mandible the supporting residual ridge induced by insertion of removable partial denture (RPD). 18F-fluoride PET imaging technique is used to quantify the change of bone metabolism in the residual ridge underneath denture base before and after RPD treatment. The corresponding FE analyses are conducted for the measured occlusal forces *in vivo* to quantify mechanical responses. Different mechanobiological stimuli determined from FE analyses are then quantitatively related to the standardized uptake values (SUV) of PET in the regions of interest (ROI). This study reveals the effectiveness of applying PET to predict bone metabolic activity associated with mechanical stimuli, and provides us with biomechanical insights into the association of tracer uptake with bone remodelling.

4.2 Materials and Methods

4.2.1 18F-fluoride PET/CT Imaging and Reconstruction

The subject was a 66-year-old female patient in the prosthodontic clinic of Tohoku University Hospital, Japan. The research protocols for this study were approved by the ethics committees at both the Tohoku University Graduate School of Dentistry and Sendai Kousei Hospital.

The subject's mandibular left molars and right second molar were missing and she chose a unilateral distal extension RPD to replace her left molars (Figure 4-1a and 1b). PET/CT scans were performed before (pre-insertion) and 6 weeks after (post-insertion) the RPD insertion, by using an 18F-fluoride PET/CT imaging scanner (Discovery ST Elite, GE Healthcare Japan Co., Tokyo, Japan). Signed consent forms were obtained from the subject after full explanation of the procedures. The emission in 3D acquisition mode with spatial resolutions of 2.0, 2.0, and 3.27 mm in radial, tangential, and axial directions commenced 75 mins after intravenous injection of 37 MBq 18F-fluoride. Occlusal forces on the dental arches were measured using pressure sensitive films (Dental PrescaleTM, Fuji Photo Film Co., Tokyo, Japan).

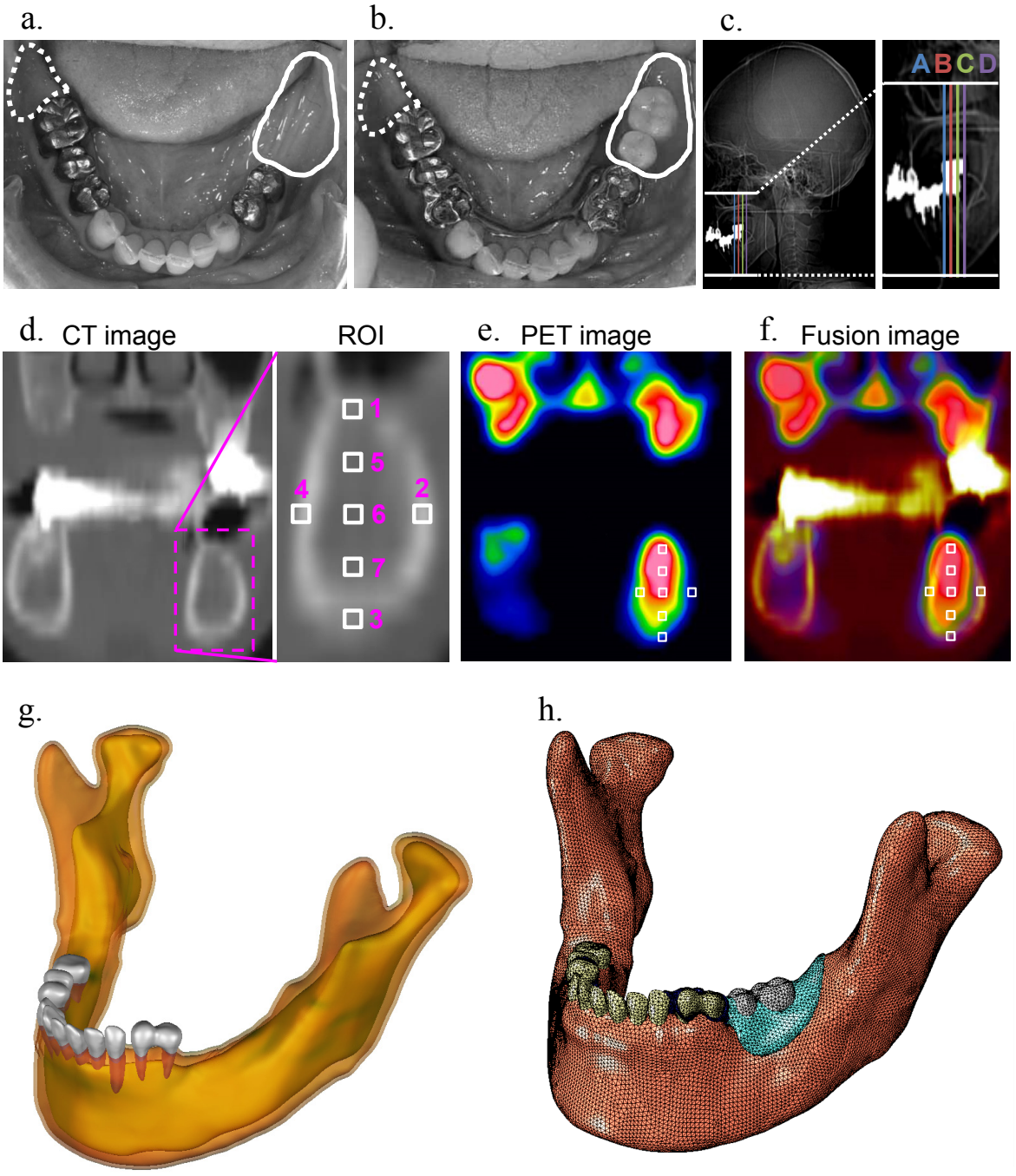

Figure 4-1 Intraoral view of mandible, coronal multiple planar reconstruction (MPR) and placement of regions of interests (ROIs), with patient-specific finite element modelling. (a) Intraoral view of mandible without denture; (b) Intraoral view of mandible with denture; (c) Locations of the four coronal planes for MPR; (d) Reconstructed CT image on the patient jaw with white rectangles to specify ROI; (e) The corresponding PET image to CT; (f) fusion image created from CT and PET; (g) the transparent view of the patient jaw model before denture insertion, maroon - mucosa, brown - cortical, yellow - cancellous, grey - teeth; (h) the geometric model with non-uniform rational B-spline（NURBS) for the patient jaw after

virtual insertion, pink - mucosa, yellow – native teeth, silver - artificial teeth, cyan - denture base, black - denture frame (cortical and cancellous bones are invisible in this view).

The PET and CT data were further processed and fused using medical image viewer software (EV Insite R, PSP Co., Tokyo, Japan), which allows detection and alignment of anatomic landmarks between the different cross-sectional examinations (Figure 4-1c-1f). Four coronal images were selected across the left residual ridge under the RPD of interest, by using the multiple planar reconstruction (MPR) procedure. These images were ordered from mesial, A, to distal, D (Figure 4-1c). Seven cubic regions of interests, with 2 mm size, were placed on each image. Four of them were positioned over the cortical bone as shown in Figure 4-1d (1: alveolar crest, 2: buccal side, 3: base of mandible, 4: lingual side) and remainders (5-7) were positioned in cancellous bone between 1 and 3. SUVs, reflecting accumulation of 18F-fluoride, and the CT values were measured for each ROI. The SUV expresses the ratio of the amount of 18F-fluoride in a certain ROI compared with a situation where the 18F-fluoride is distributed equally over the entire body.

2.4.2 Finite Element Modelling

The CT image stack of the subject was segmented in ScanIP Ver. 4.3 (Simpleware Ltd, Exeter, UK), based on their Hounsfield unit (HU) thresholds. 11 masks were created for the individual teeth, cortical bone, and cancellous bone. Due to the low contrast, the mucosa was constructed by offsetting the outer layer of cortical bone with 4 pixels, providing about 1.2 mm average thickness [12]. All masks were then exported to 3D parametric modelling software Rhinoceros 4.0 (Robert McNeel & Associates, Seattle USA) to create geometric models for the pre-insertion condition (Figure 4-1e) with non-uniform rational B-spline (NURBS) representation.

A CT image of RPD was obtained by using a duplicated denture specifically made for scanning, which consists of pure titanium, scanning resin for denture base, and radio-opaque teeth [27]. After performing the image registration using isosurfaces to the subject CT, another 3 masks were created for the denture frame, denture base, and artificial teeth, following the same approach as abovementioned. The subject and denture masks were assembled for the virtual denture insertion, as the post-insertion condition (Figure 4-1f).

Both models for the pre- and post-insertion conditions were meshed in ABAQUS 6.9.2 (Dassault Systèmes, Tokyo Japan), with the adaptive mesh control set to a maximum elemental size of 0.5 mm for hybrid formulated tetrahedral elements (C3D4H). The corresponding ROIs to the PET images were defined based on the same coordinates in these models. After a mesh convergence test similar to our previous studies [28, 29], the final meshes comprised 4,337,113 and 5,278,816 elements (2,287,506 and 2,784,185 degrees of freedom) for the pre- and post-insertion models, respectively.

As a critical and nonlinear material [30-32], the mucosa is modeled as being hyperelasticity based on literature data [23]. The denture-mucosa contact was modeled with a low frictional coefficient of 0.1 to mimic normal oral lubrication conditions [33, 34]. Occlusal forces were applied to each corresponding teeth as measured clinically, differently for pre- and post-insertion. Boundary conditions were prescribed to the distal ends of condyles and the muscular forces were derived from occlusal forces [35].

Different mechanical stimuli, i.e. von Mises stress (VMS), equivalent strain (ESN), and strain energy density (SED), were considered in this study. Linear regression analysis was performed to examine their relationship with SUV in this patient-specific case.

4.3 Results

4.3.1 Occlusal Force

The occlusal force measured on individual teeth is summarized in Figure 4-2a and 2b, for pre-/post-insertion. Before denture insertion, the total occlusal forces were considered as 175.6 and 176.2 N for the left- and right-hand sides of the dental arch, respectively. RPD insertion altered the load distribution (Figure 4-2b), increasing the total force to 215.8 N (left) and 191.6 N (right) at post-insertion with adjustment.

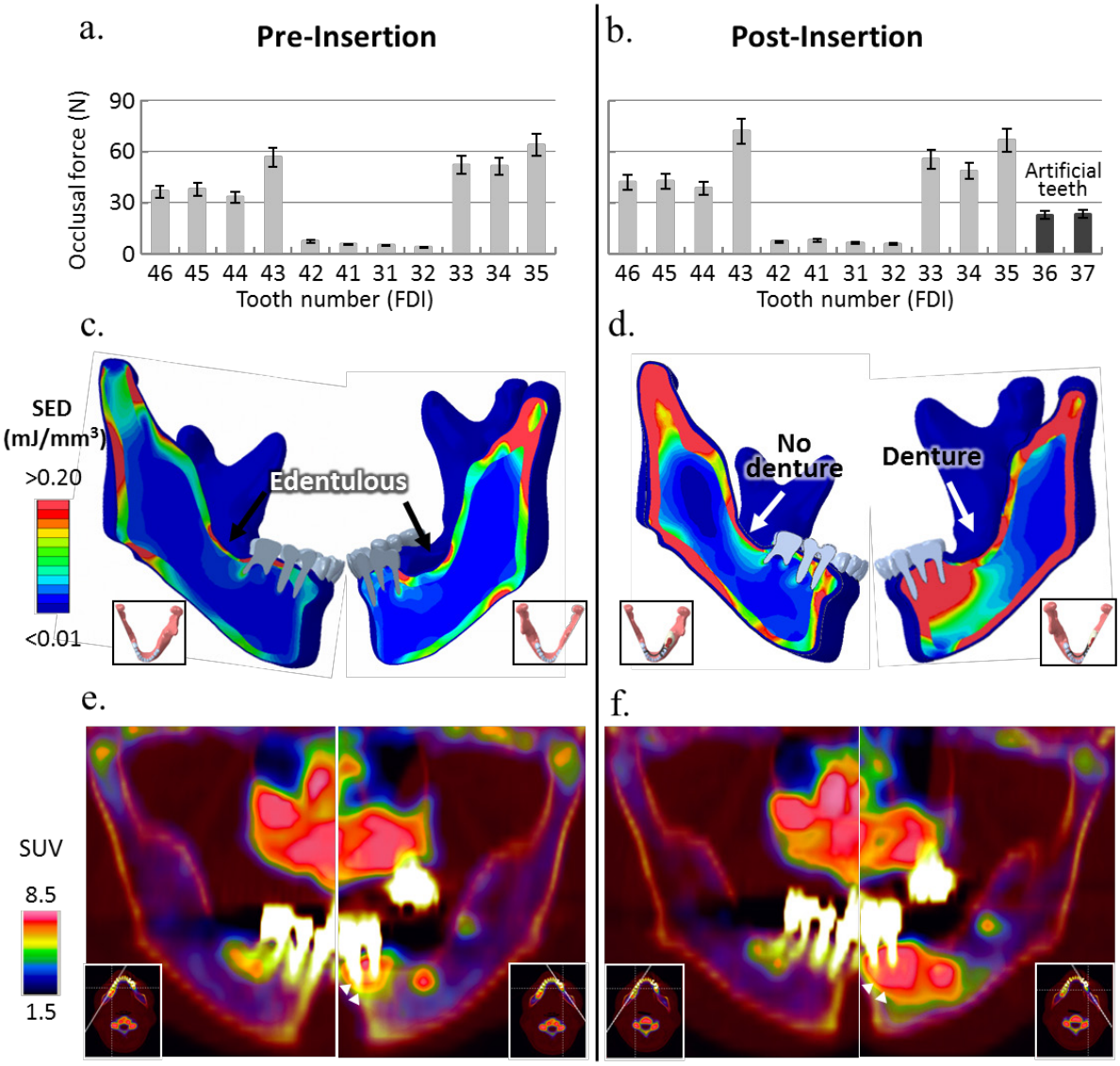

Figure 4-2 The comparison between pre-insertion (a, c, e) and post-insertion (b, d, f) of the RPD, for their influence on occlusal force distributions (a & b), the mechanobiological stimuli (c & d) as determined from FEA in the form of strain energy densities (SED), and standard uptake value (SUV) distributions (e & f) on PET/CT fusion MPR images.

4.3.2 Mechanobiological stimuli

SED is plotted on the oblique planes through both the left and right residual ridges at pre-insertion (Figure 4-2c) and post-insertion (Figure 4-2d), respectively. As the occlusal force increased, mechanical stimuli of all three forms (VMS, ESN and SED) increased. Most obviously, the mechanical stimuli increased in the left residual ridge and around the root of left premolars, compared to the right side. SED is the most sensitive stimulus following denture insertion, in which its maximum ramped up by 25 times in Week 6 in the cortical and 21 times in cancellous bone.

4.3.3 Bone metabolic activity

Consistent with distribution of mechanical stimuli after denture insertion, the right edentulous area maintained an almost constant level of metabolic activity, whereas the SUVs on the left residual bone beneath the denture base increased (Figure 4-2e and 2f). The SUVs around the roots of the left premolars, direct abutment teeth (Teeth 34 and 35), were more significantly affected by the RPD insertion than the indirect abutment teeth (Teeth 44 and 45), showing an enlarged area of high bone metabolic activity (white triangles).

To compare mechanical stimuli with SUV more quantitatively, Figure 4-3 summarizes the volume-averaged ROI values of VMS (1st row) and SUV (2nd row) for pre-insertion (left column) and post-insertion (right column). VMS in cancellous bone (ROI number 5-7) were lower than those in cortical bone (ROI number 1-4), whereas SUV shows the opposite trend.

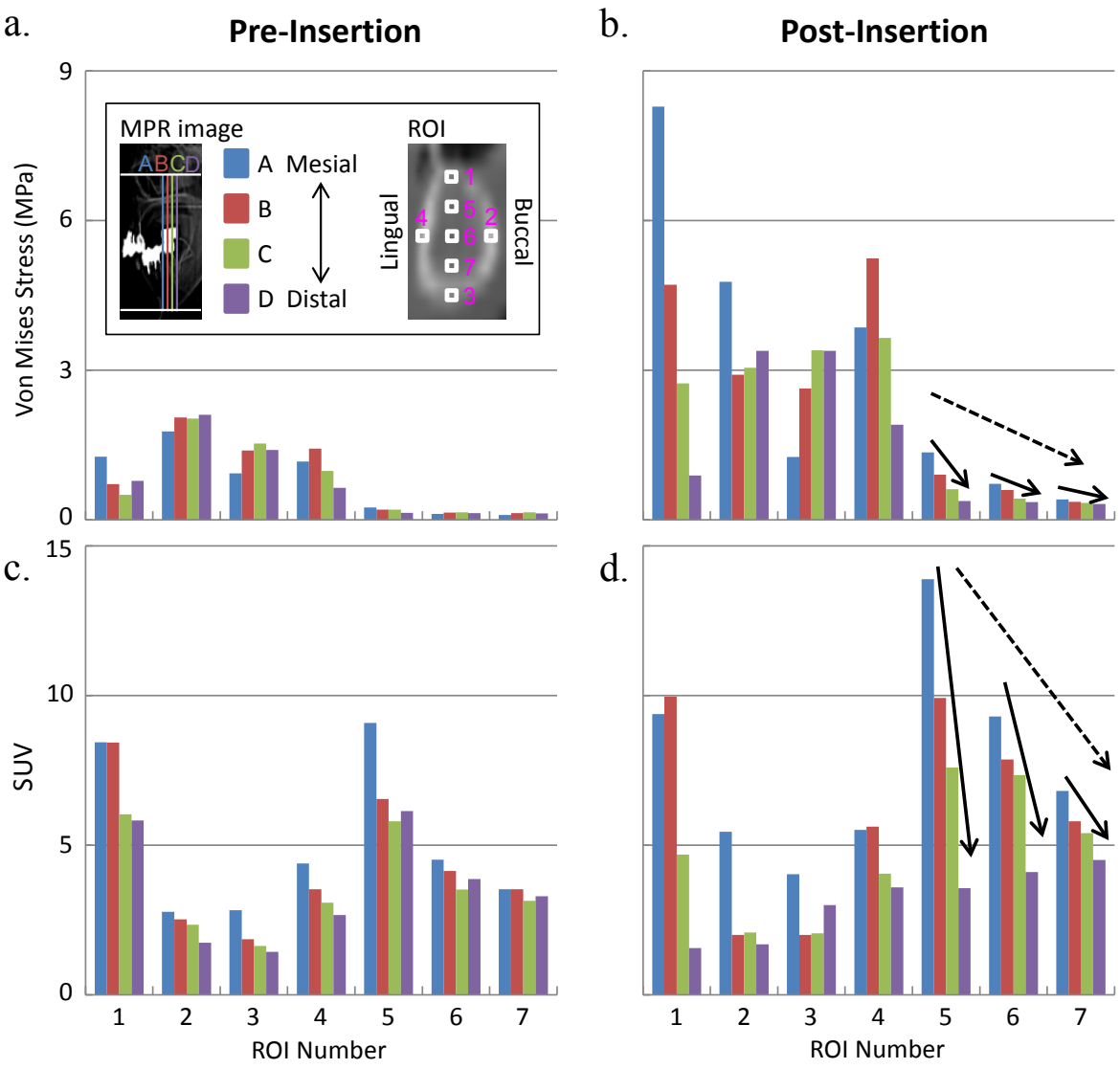

Figure 4-3 von Mises stress (1st row) of individual regions of interest (ROI 1 - 28), and the corresponding standard uptake values (SUVs) from PET scan (2nd row), at pre-insertion (left column) and post-insertion (right column) of the RPD.

The VMS of cancellous bone has two clear trends after denture insertion (Figure 4-3b: ROI number 5-7). Firstly, in the same MPR plane, VMS decreased as the number of ROI increased, or in other words, reducing from the top of residual ridge towards the bottom, as shown by the dashed arrow in Figure 4-3b. Secondly, for the same ROI, the VMS became lower distally (slice number A to D), as shown by solid arrows. The SUV also exhibited similar position dependent tendencies, as shown by solid and dashed arrows in Figure 4-3d.

4.4 Discussion

After the intravenous injection of 18F-fluoride, some of it diffuses through the bone capillaries into the bone extracellular fluid. From there, the 18F-fluoride ions exchange with hydroxyl groups in the hydroxyapatite at the surface of bone crystals forming fluoroapatite mainly at sites of bone remodelling with high turnover. Thus, the uptake of 18F-fluoride reflects blood flow and osteoblastic activity, and high SUV implies high bone turnover [16, 36]. On the other hand, mechanically stimulated osteoclasts regulate osteoblastic activity [37]. Therefore, 18F-fluoride PET scanning is highly sensitive to increased bone turnover associated with mechanical stimuli. Previous animal studies have shown that the tracer uptake in loaded bone regions is generally proportional to the degree of injury [18] and the tracer uptake in bone around an implant increased depending on magnitude of applied loading [38]. In this study, the increased applied occlusal force after denture insertion induced higher mechanical stimuli in the residual bone, and SUV increased in the region of the residual ridge with higher mechanical stimuli.

To further investigate the association between SUV and mechanobiological stimuli quantitatively, Figure 4-4 shows the SUV plotted against the VMS, EVS, and SED. The SUV was generally higher in cancellous than cortical bone at the same levels of VMS and SED (Figure 4-4a and 4c). This is because the cortical bone has a much lower surface area than cancellous bone [26], and 18F-fluoride ion exchange is dependent on the surface area of bones. Furthermore, the densities and Young's moduli in these two types of bones are quite different, reflecting different distribution patterns of mechanical stimulus [3, 39]. Therefore, the cortical and cancellous bones were analyzed separately using linear regression methods as plotted in Figure 4-4.

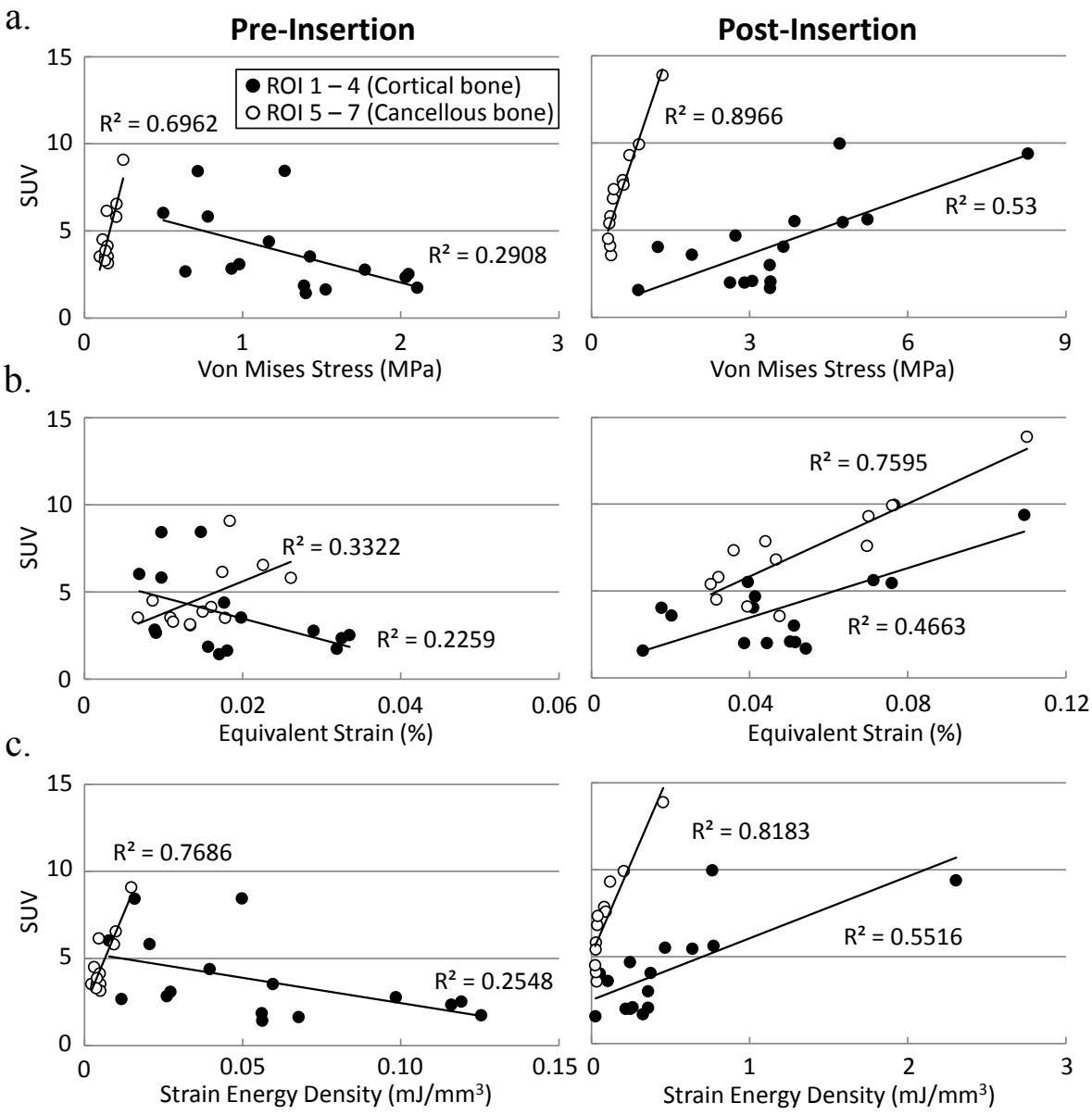

Figure 4-4 Linear regression analysis between SUVs in regions of interest (total 28 ROIs: 7 ROIs on each MPR image A to D) and the corresponding mechanobiological stimuli in different forms, including von Mises stress (1st row), equivalent strain (2nd row), and the strain energy density (3rd row), in both cortical (filled dots) and cancellous (open circles) bones before (left column) and after (right column) RPD insertion.

As shown in Figure 4-4a and 4c, the SUV had clear dependences on VMS and SED in the cancellous bone, especially after denture insertion ($R^2 > 0.8$, $p < 0.01$). These results indicate that bone metabolism interpreted by 18F-fluoride PET is directly proportional to VMS and SED in cancellous bone. On the other hand, there were no strong relationships

between SUV and mechanical stimuli in the cortical bone ($R^2 < 0.55$). The spatial resolution of PET was limited at 2 mm, as this was the minimum size for ROIs. The ROIs in cortical bone area may include not only the cortical but also the cancellous region, and even residual ridge mucosa. The much lower Hounsfield Unit (HU) values in the corresponding CT scan confirms this concern (e.g. ROI 1 on MPR plane A, 490.4 $\pm$ 395.8 HU), and this factor can attribute to the poor correlations observed for cortical bone.

As the subject had had the same edentulous conditions and occlusal activities for more than 8 years before the RPD insertion in this experiment, the mandible should have adapted to the occlusal force associated homeostasis of apposition and resorption, which is referred as a 'lazy zone' in the Wolff's law [4, 5]. At this stage, the physiological factors, such as diet, calcium and hydroxyapatite balance, hormones etc., were more dominant in a systematic level than the mechanically induced perturbation of metabolism [40-45]. Furthermore, the pilot study [13] demonstrated that SUV initially increased at 4-6 weeks after the RPD treatment, reflecting bone's response to the change in mechanical environment; and then decreased at 13 weeks, indicating that the SUV change induced by RPD insertion was temporary, which was much shorter than the 8 years of the subject's clinical record. Thus, at pre-insertion, SUV is considered to reflect more the effects of physiological factors than the mechanical stimuli induced by RPD treatment. The insertion of RPD, on the other hand, altered the occlusal load distribution on the dental arch as measured *in vivo*, consequently varying the stimulus distribution patterns. Therefore, there were higher determination coefficients between SUV and all quantified mechanical stimuli after denture insertion, in both the cortical and the cancellous bone.

In contrast to the long delay required in the case of X-ray to quantify bone augmentation or resorption, this study demonstrated that PET scans are able to detect bone metabolic change in a much shorter duration, which is strongly correlated with mechanical

stimuli. Currently, 18F-fluoride PET has been mainly utilized to evaluate bone tumour, osseous metastasis, or metabolic bone diseases [46]. The current combined PET-FEA technique, while not specifically evaluated in the previous studies, may be useful to detect false-positive outcomes during screening for these diseases. This procedure may also be useful to detect clinical conditions such as temporomandibular disorder, occlusal trauma or fatigue fracture of the jaw at an early stage.

Despite the high discriminatory opportunities of 18F-fluoride PET/CT, it is not yet as widely used as bone scintigraphy. Although other types of PET tracer are already commercially available, 18F-fluoride positron tracer must be manufactured in-house just prior to usage. Therefore, it may take a while before this technique becomes more widely procedural in a dental clinical setting. Meanwhile, this study focuses on a representative subject to determine a preliminary relationship between SUV and mechanical stimuli. Further large scale clinical studies are certainly warranted to provide the statistical implications of these correlations, which is however beyond the scope of this study.

4.5 Conclusion

This study demonstrated the relevance of the combined PET-FEA technique to examine the relationship between mandibular bone metabolism and modified mechanical stimuli induced by RPD insertion. Using this technique, it was shown that PET scans detect current bone metabolic change and in a much shorter duration than possible with X-rays. It was also shown that the bone metabolic change is strongly correlated with induced mechanical stimuli. It was found that bone metabolism interpreted by 18F-fluoride PET is strongly proportional to VMS and SED in the cancellous bone.

Acknowledgement

This work was supported by Australian Research Council (ARC, the Discovery and Fellowship schemes), Australian Postgraduate Award (APA), Grants-in-Aid for Young Scientists (B) (24792057) (2012-2013) and for Scientific Research (C) (26462912) (2014-) from the Ministry of Education, Culture, Sports, Science and Technology of Japan.

4.6 References

1. Carlsson, G.E., *Responses of jawbone to pressure.* Gerodontology, 2004. **21**(2): p. 65-70.
2. Chen, J., et al., *Multiscale design of surface morphological gradient for osseointegration.* Journal of the Mechanical Behavior of Biomedical Materials, 2013. **20**: p. 387-97.
3. Rungsiyakull, C., et al., *Surface morphology optimization for osseointegration of coated implants.* Biomaterials, 2010. **31**(27): p. 7196-7204.
4. Lin, D., et al., *Mandibular bone remodeling induced by dental implant.* Journal of Biomechanics, 2010. **43**(2): p. 287-293.
5. Lin, D., et al., *Dental implant induced bone remodeling and associated algorithms.* Journal of the Mechanical Behavior of Biomedical Materials, 2009. **2**(5): p. 410-432.
6. Brkovic-Popovic, S., et al., *Radiographic changes in alveolar bone height on overdenture abutments: a longitudinal study.* Gerodontology, 2008. **25**(2): p. 118-123.
7. Jacobs, R., et al., *Maxillary bone-resorption in patients with mandibular implant-supported overdenture or fixed prostheses.* Journal of Prosthetic Dentistry, 1993. **70**(2): p. 135-140.
8. Kordatzis, K., P.S. Wright, and H.J.A. Meijer, *Posterior mandibular residual ridge resorption in patients with conventional dentures and implant overdentures.* International Journal of Oral & Maxillofacial Implants, 2003. **18**(3): p. 447-452.
9. Kreisler, M., et al., *Residual ridge resorption in the edentulous maxilla in patients with implant-supported mandibular overdentures: An 8-year retrospective study.* International Journal of Prosthodontics, 2003. **16**(3): p. 295-300.
10. Lopez-Roldan, A., et al., *Bone resorption processes in patients wearing overdentures. A 6-years retrospective study.* Medicina Oral Patologia Oral Y Cirugia Bucal, 2009. **14**(4): p. E203-E209.
11. Xie, Q.F., J. Wolf, and A. Ainamo, *Quantitative assessment of vertical heights of maxillary and mandibular bones in panoramic radiographs of elderly dentate and edentulous subjects.* Acta Odontologica Scandinavica, 1997. **55**(3): p. 155-161.
12. Ahmad, R., et al., *Three dimensional quantification of mandibular bone remodeling using standard tessellation language registration based superimposition.* Clin Oral Implants Res, 2013. **24**(11): p. 1273-1279.
13. Suenaga, H., et al., *Time course of bone metabolism at the residual ridge beneath dentures observed using 18F-fluoride positron emission computerized-tomography/computed tomography (PET/CT).* Annals of Nuclear Medicine, 2012. **26**(10): p. 817-822.
14. Fischer, D.R., et al., *Assessment of successful incorporation of cages after cervical or lumbar intercorporal fusion with [(18)F]fluoride positron-emission tomography/computed tomography.* Eur Spine J, 2011. **20**(4): p. 640-8.

15. Groves, A.M., et al., *Non-[18F]FDG PET in clinical oncology.* Lancet Oncol, 2007. **8**(9): p. 822-30.

16. Even-Sapir, E., et al., *18F-Fluoride positron emission tomography and positron emission tomography/computed tomography.* Semin Nucl Med, 2007. **37**(6): p. 462-9.

17. Lim, R., et al., *Early experience with fluorine-18 sodium fluoride bone PET in young patients with back pain.* J Pediatr Orthop, 2007. **27**(3): p. 277-82.

18. Silva, M.J., et al., *In vivo skeletal imaging of 18F-fluoride with positron emission tomography reveals damage- and time-dependent responses to fatigue loading in the rat ulna.* Bone, 2006. **39**(2): p. 229-36.

19. Li, J.L., et al., *Imaging bone microdamage in vivo with positron emission tomography.* Bone, 2005. **37**(6): p. 819-824.

20. Slipman, C.W., et al., *Osseous stress reaction in a rower diagnosed with positron emission tomography (PET): a case report.* Pain physician, 2001. **4**(4): p. 336-42.

21. Draper, C.E., et al., *Patients with patellofemoral pain exhibit elevated bone metabolic activity at the patellofemoral joint.* Journal of Orthopaedic Research, 2012. **30**(2): p. 209-213.

22. Kanbara, R., et al., *Three-dimensional finite element stress analysis: The technique and methodology of non-linear property simulation and soft tissue loading behavior for different partial denture designs.* Dental Materials Journal, 2012. **31**(2): p. 297-308.

23. Wang, H.-y., et al., *Effects of rigid and nonrigid extracoronal attachments on supporting tissues in extension base partial removable dental prostheses: a nonlinear finite element study.* Journal of Prosthetic Dentistry, 2011. **105**(5): p. 338-346.

24. Archangelo, C.M., et al., *Periodontal ligament influence on the stress distribution in a removable partial denture supported by implant: a finite element analysis.* Journal of Applied Oral Science, 2012. **20**(3): p. 362-368.

25. Muraki, H., et al., *Finite element contact stress analysis of the RPD abutment tooth and periodontal ligament.* Journal of Dentistry, 2004. **32**(8): p. 659-665.

26. Field, C., et al., *Prediction of mandibular bone remodelling induced by fixed partial dentures.* Journal of Biomechanics, 2010. **43**(9): p. 1771-1779.

27. Suenaga, H., et al., *Validate Mandible Finite Element Model under Removable Partial Denture (RPD) with In Vivo Pressure Measurement.* Applied Mechanics and Materials, 2014. **553**: p. 322-326.

28. Li, W., et al., *Fibre reinforced composite dental bridge. Part II: numerical investigation.* Biomaterials, 2004. **25**(20): p. 4995-5001.

29. Li, W., et al., *Towards automated 3D finite element modeling of direct fiber reinforced composite dental bridge.* Journal of Biomedical Materials Research Part B: Applied Biomaterials, 2005. **74B**(1): p. 520-528.

30. Picton, D.C.A. and D.J. Wills, *Viscoelastic properties of periodontal-ligament and mucosa-membrane.* Journal of Prosthetic Dentistry, 1978. **40**(3): p. 263-272.

31. Bridges, T., G. King, and A. Mohammed, *The effect of age on tooth movement and mineral desntiy in the alveolar tissues of the rat.* American Journal of Orthodontics and Dentofacial Orthopedics, 1988. **93**(3): p. 245-250.

32. Sawada, A., et al., *Viscoelasticity of Human Oral Mucosa: Implications for Masticatory Biomechanics.* Journal of Dental Research, 2011. **90**(5): p. 590-595.

33. Prinz, J.F., R.A. de Wijk, and L. Huntjens, *Load dependency of the coefficient of friction of oral mucosa.* Food Hydrocolloids, 2007. **21**(3): p. 402-408.

34. Sajewicz, E., *Effect of saliva viscosity on tribological behaviour of tooth enamel.* Tribology International, 2009. **42**(2): p. 327-332.

35. Korioth, T.W.P., D.P. Romilly, and A.G. Hannam, *3-Dimensional Finite Element Stress-Analysis of the Dentate Human Mandible.* American Journal of Physical Anthropology, 1992. **88**(1): p. 69-96.

36. Czernin, J., N. Satyamurthy, and C. Schiepers, *Molecular mechanisms of bone 18F-NaF deposition.* J Nucl Med, 2010. **51**(12): p. 1826-9.

37. Taylor, A.F., et al., *Mechanically stimulated osteocytes regulate osteoblastic activity via gap junctions.* Am J Physiol Cell Physiol, 2007. **292**(1): p. C545-52.

38. Sasaki, H., et al., *Bone Metabolic Activity Around Dental Implants Under Loading Observed Using Bone Scintigraphy.* International Journal of Oral & Maxillofacial Implants, 2008. **23**(5): p. 827-834.

39. Junning Chen, W.L., Michael Swain, Ali Darendeliler, Qing Li *A Periodontal Ligament Driven Bone Remodeling Algorithm for Orthodontic Tooth Movement.* Journal of Biomechanics, 2014. **In Press**.

40. Ambrus, C., et al., *Bone mineral density in patients on maintenance dialysis.* International Urology and Nephrology, 2010. **42**(3): p. 723-739.

41. Black, D.M., et al., *The effects of parathyroid hormone and alendronate alone or in combination in postmenopausal osteoporosis.* New England Journal of Medicine, 2003. **349**(13): p. 1207-1215.

42. Marx, R.E., et al., *Bisphosphonate-induced exposed bone (osteonecrosis/osteopetrosis) of the jaws: Risk factors, recognition, prevention, and treatment.* Journal of Oral and Maxillofacial Surgery, 2005. **63**(11): p. 1567-1575.

43. Parfitt, A.M., et al., *Relationships between surface, volume, and thickness of iliac trabecular bone in aging and in osteoporosis - implaications for the microanatomic and cellular mechanisms of bone loss.* Journal of Clinical Investigation, 1983. **72**(4): p. 1396-1409.

44. Payne, J.B., et al., *Longitudinal alveolar bone loss in postmenopausal osteoporotic/osteopenic women.* Osteoporosis International, 1999. **10**(1): p. 34-40.

45. Wu, C., et al., *Dietary Pseudopurpurin Improves Bone Geometry Architecture and Metabolism in Red-Bone Guishan Goats.* Plos One, 2012. **7**(5).

46. Grant, F.D., et al., *Skeletal PET with 18F-fluoride: applying new technology to an old tracer.* J Nucl Med, 2008. **49**(1): p. 68-78.

Chapter 5: Investigation of Mucosa-Induced Residual Ridge Resorption between Implant-Retained Overdenture (IRO) and Complete Denture (CD)

Different types of prosthodontic prostheses can lead to different tissue reactions. This chapter investigates the residual ridge resorption (RRR) induced by an implant-retained overdenture (IRO) and associated biomechanics, compared to a conventional complete denture (CD) without implants. Cone beam computerized tomography (CBCT) is applied to quantify RRR in a three-dimensional manner after one year of treatment with either IROs (20 subjects) or CDs (9 subjects). A 3D FE model is created from a set of representative scan images for each treatment type to analyse the relevant biomechanics. Clinically, IRO leads to at least twice the RRR compared with CD and this could be due to higher hydrostatic stress and less effective energy absorption capabilities of the mucosa underneath the IRO. While implants associated with the overdentures provide patients the capability of exerting more biting forces, they could potentially concentrate hydrostatic stress and cause higher RRR compared to a conventional CD.

Associated Publications:

1. Rohana Ahmad, Junning Chen, Mohamed I. Abu-Hassan, Qing Li, Michael V. Swain. **Investigation of Mucosa-Induced Residual Ridge Resorption between Implant-retained Overdenture and Complete Denture**. *The International Journal of Oral & Maxillofacial Implants*, 2014. Accepted.

5.1 Introduction

Current evidence from bone remodelling studies relevant to complete dentures (CDs) and implant-retained overdentures (IROs) strongly advocate functional pressure as one of the most important etiological factors for residual ridge resorption (RRR) [1-5]. When two implants are used to retain dentures, bite forces can increase considerably [6-10] but generally lead to more severe RRR [11, 12] in the posterior region of the mandible distal to the implants compared to a conventional complete denture. With implant-supported overdentures (using four or more implants), reduced resorption [13-15] and even bone apposition [16-20] has been observed in the posterior region of the mandible as less pressure is exerted on the soft tissue mucosa and the underlying bone as most of the increased mastication forces are transferred to the implants.

When soft tissue mucosa underneath the denture base is compressed, blood flow which supplies nutrients to and removes metabolites from the bone is affected, potentially leading to an incidence of resorption [21, 22]. Maruo et al. [23] demonstrated that the amount of RRR versus the pressure induced blood flow rate exhibits a simple linear regression ($R = 0.766$). As most denture wearers are in their late middle age, the blood supply to the mandible mainly takes place from the subperiosteal plexus of vessels and therefore is very susceptible to diminished circulation under denture pressure [24]. The blood pressure in the venous capillary of the subperiosteal plexus is quite low, within the range of 15 mmHg (venous) to 35 mmHg (arterial), equivalent to 2.0-4.7 kPa [25].

When the epithelial layer of the mucosa is subjected to load, there will be cellular swelling, increased nuclear size and intercellular oedema [26]. This inflammatory response of the cells and surrounding tissue may contribute to a change in the permeability of the mucosal tissue which may further compromise blood circulation. If the hydrostatic pressure that develops in the mucosa underneath the denture exceeds the blood pressure in

the mucosa blood vessels, blood flow will be decreased and may even temporarily cease altogether as a result of a combination of active arteriolar closure and passive capillary obstruction [27]. However, there has been limited exploration from a clinical perspective to quantify the correlation between hydrostatic pressure and resultant RRR.

This chapter aims to investigate RRR induced by two types of dentures, namely CD and IRO, in clinical application across a one-year interval and correlate it to the hydrostatic stress and other associative biomechanics namely the contact surface deformation and strain energy absorption. We hypothesize that the hydrostatic stress plays a significant role in RRR and its magnitude is influenced by the bite force exerted on the denture and the resultant contact surface deformation in the mucosa as well as the strain energy absorption capabilities of the mucosa underneath the dentures. The established association of RRR with hydrostatic pressure will assist development of critical insights into the mechanism of RRR taking place for different types of dentures. To be noted, this piece of work was carried out before Chapter 3, and the discovery from Chapter 3, such as the Poisson's ratio and the friction coefficient of the mucosa, is not reflected in this chapter. Instead, the material properties adopted in this study are from existing literature studies.

5.2 Materials and Methods

5.2.1 Denture Fabrication and CBCT Imaging

Ethics approval to carry out this study was obtained from the Ethics Committee of Universiti Teknologi MARA, Malaysia (600-RMI (5/1/6) 20th April 2009). All recruited patients had diagnostic Cone Beam Computerized Tomography images of the mandible taken before the provision of new CDs. A duplicate denture containing barium sulphate was worn during imaging to enable clear definition of the bone, mucosa and dentures from which RRR patterns and the mucosa thickness could be analysed in a 3D manner.

For those patients with enough bone for placement of implants (11 or 13 mm implants were used), two implants (Ankylos® implants, Dentsply, Friadent, Germany) were placed in the canine regions of the mandible. After two months, the implants were exposed and telescopic male abutments attached (Ankylos® SynCone® Dentsply, Friadent, Germany). The mandibular denture was converted to an overdenture by incorporating the corresponding female metal sleeves inside its fitting surface. Both groups of patients had the second CBCT images taken for bone measurement after one year. There were 20 patients in the IRO group (12 females and 8 males) and 9 patients for the CD's (3 females and 6 males). Their age ranged from 52-79 years old at recruitment, average age was 67 years old. The antagonistic jaw for both treatment groups is also edentulous and restored with conventional complete denture. Among the exclusion criteria is that a patient should not have any extraction within the last 6 months. As for history of denture usage, it varies from no experience to almost 25 years of denture wearing.

The CBCT images were taken with an i-CAT (Imaging Sciences International, Hatfield, Pa) machine which was set at 120 kVp, 18.45 mAs, 20-second acquisition time, 13 cm field of view and a voxel size of 0.30 mm. The DICOM files of the sectional images were acquired and stored to a portable hard driver for quantitative and modelling analyses.

5.2.2 Biting Force and Bone Volume Change

Once patients were comfortable wearing their prostheses, they had their unilateral maximum bite force measured. They were asked to bite on a 200 N compression load cell (LMB-A-200N, Kyowa, Japan) placed in the molar region as hard as they possibly could. The load cell was connected to a data logger (PCD-300B, Kyowa, Japan) and a computer. Each bite recording lasted for 10 seconds and the measurements were carried out three times on each side of the jaw. The patients were allowed a 5 minute rest between the recordings. They were not given any feedback on their bite force and were not allowed to see the recordings. The highest recorded force was taken as the maximum bite force.

The 3D models of the initial diagnostic and at one year post treatment were superimposed in Mimics program version 14.1 (Materialise NV, Leuven Belgium) and subsequently exported into 3-matics program version 5.1 (Materialise NV, Leuven Belgium) to produce colour maps that reveal the magnitude of the RRR that have occurred after a period of one year [28]. The RRR results for both IRO and CD scenarios were quantified by measuring the changes in bone volume between the pre- and post-treatment models. The region of interest was from about 5 mm distal to the implants up to the retromolar area just anterior to the ascending ramus.

5.2.3 3D Finite Element Modelling and Simulation

Two male participants, one from IRO and the other from the CD group who are of similar age (62 years old), and scored the highest maximum bite force values in their respective treatment group were selected as representative models for finite element analysis. A complete 3D model of the mandible, mucosa and denture was created from their diagnostic CBCT images. The patient's CT image stacks at the pre-treatment conditions were imported into ScanIP Ver. 4.3 (Simpleware Ltd, Exeter, UK) for

segmentation as shown in Figure 5-1. Three individual masks were created to present the mandibular bone, denture and mucosa based on the gray-values of each pixel, normalised to a range from 0 to 255, and the thresholds of each mask were determined by sampling the localized counts (Figure 5-1a right). Due to the relative low density of the oral mucosa compared to other oral tissues, its image was improved by offsetting the contrast of the outer layer of the cortical bone by 5 pixels thus producing mucosa of a minimum thickness of 1 mm.

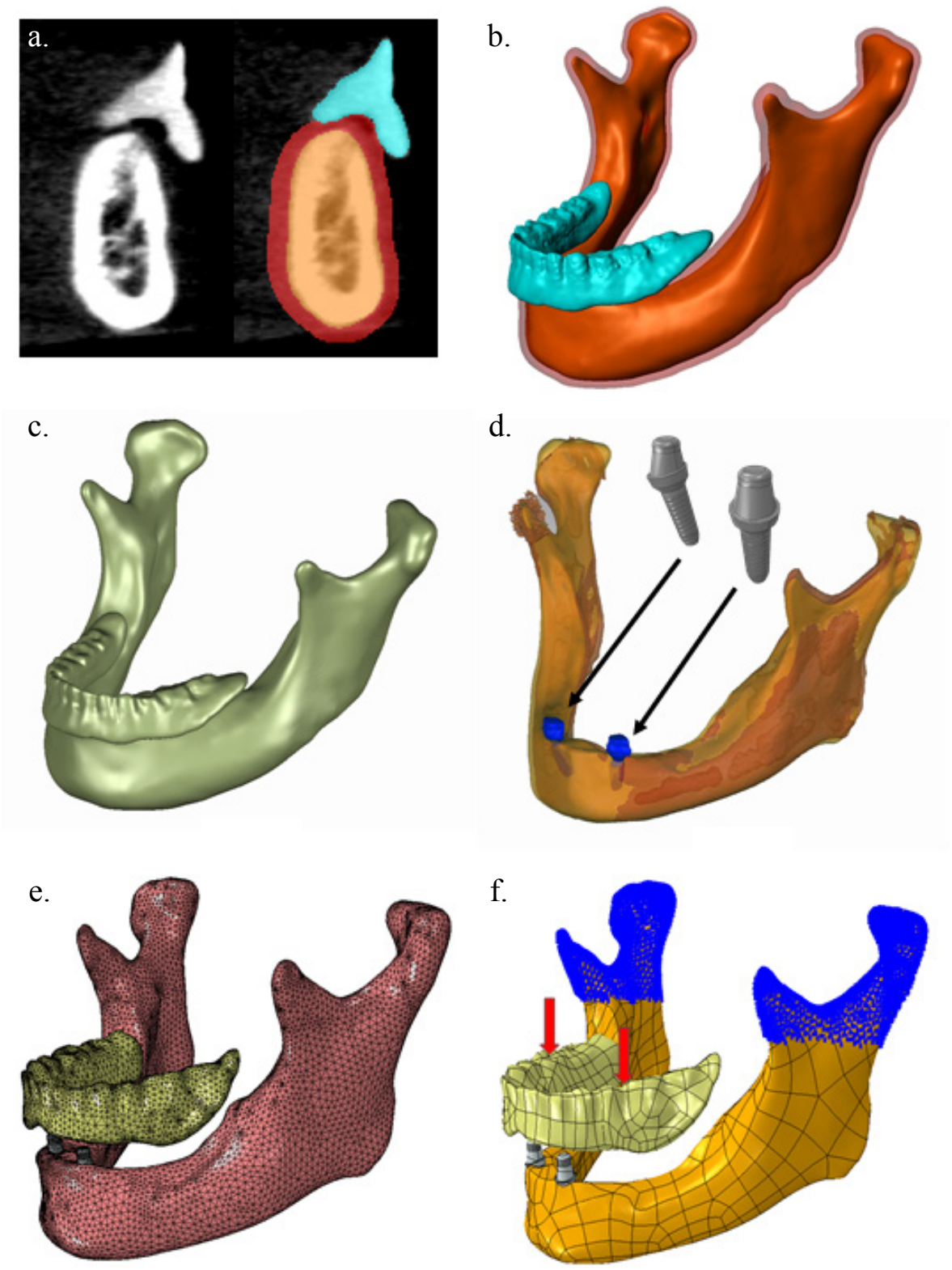

Figure 5-1 Finite element modelling procedures. (a) a cross-section of CBCT image showing the different Hounsfield Unit values of the denture, mandibular bone and the soft tissue mucosa; (b) 3D masks created for each structure, denture (azure), mucosa (pink), and jaw bone (orange), in STL format; (c) solid models created by NURBS in IGES format; (d) superimposition required to position the implants for the implant-retained denture, including

(diagnostic) pre-treatment scan (light orange), 1-year follow-up (dark red), implants (dark blue), and implant models (grey); (e) final model imported and meshed in ABAQUS 6.9.2; (f) boundary and loading condition assigned to the model, as chewing forces (red arrows) and fixation (blue nodes), while mucosa is hidden from the picture.

All three masks in each image stack were then exported in STL format and further processed using 3D parametric modelling software Rhinoceros 4.0 (Robert McNeel & Associates, Seattle USA) as shown in Figure 5-1b to create geometric models. The surface mesh on the masks formed a scaffold for constructing free-form parametric surfaces by using the non-uniform rational B-spline (NURBS) function (Figure 5-1c). The manipulated surfaces were then solidified and exported as IGES files for finite element modelling in ABAQUS 6.9.2 (Dassault Systèmes, Tokyo Japan).

In ABAQUS 6.9.2, the adaptive mesh control was set to have a maximum elemental size of 1 mm with the maximum deviation factor set at 0.05 for the curvature control in all components as shown in Figure 5-1e. Further mesh refinement was set to 0.5 mm on the interfaces between denture and mucosa. After a mesh convergence test similar to our previous studies [29, 30], the final mesh comprises 669,042 (376,974 degrees of freedom) and 727, 743 (423, 598 degrees of freedom, Figure 5-1e) tetrahedral elements for the CD and IRO models, respectively.

For the IRO, one extra step was required to place a pair of dental implants into the model. The implants, consisting of fixtures and abutments, were modelled in SolidWorks 2012 (Dassault Systèmes Solidworks Corp., Massachusetts USA). To ensure the correct locations of the fixtures, the CT scan at one year after placement was superimposed onto the pre-treatment model in Rhinoceros 4.0, where the implant models were matched to the fixtures mask (Figure 5-1d).

The material properties of cortical and cancellous bones were considered to be isotropic and linear elastic as used in previous studies [31-33]. The mechanical properties

of titanium alloy (Ti6Al4V) implant fixtures and that of the denture was obtained from O'Brien [32] and Satoh et al. [34] and the mucosa from Isaksson et al. [33] (this study was performed prior to Chapter 3; therefore, the material properties were adopted from literature). These detailed values are summarized in Table 1, and all the mechanical properties were assumed to be homogeneous and isotropic [35, 36].

Table 5-1 Material properties of the implant screws, mandibular bone, mucosa and denture

	Screw	Cortical Bone	Cancellous Bone	Mucosa	Denture
Young's Modulus (MPa)	110, 000	15,750	1, 970	1	2,650
Poisson Ratio	0.350	0.325	0.325	0.167	0.30

In both treatment cases, the cortical and cancellous bones were considered bonded as occurs for their biological function. For the IRO, the fixtures were assumed to be fully locked by tissue ingrowths from the surrounding bone structure [37-39], by assigning a full tie constraint in ABAQUS. Both the dentures were slightly off-set from the mucosa surface of the jaw and the displacement was generated upon loading. As such, the denture model was allowed to initiate the surface-to-surface contact between the denture and mucosa.

As suggested from previous clinical studies by Gibbs et al. [40] a localised load was applied to each side of the dentures using 40% of the measured maximum bite force in the participants by assuming a nearly symmetric loading condition as in Figure 5-1f. The load was applied in the vicinity of the first molar, in a vertical direction. This loading scenario has been considered as isometric bilateral biting of the mandible in the literature [41], and similar magnitudes of force have been adopted for mandibular loading in other finite element analyses [42-45].

The boundary conditions were prescribed to the distal ends of the condyles where they are connected to the joints with the maxilla. Early FEA studies have shown that the rotational degrees of freedom have limited effects on the local stress distribution if it is remote from this boundary [41]. Thus, full kinematic constraints of all degrees of freedom are applied here to effectively prevent rigid body motion of the mandibular model [35, 41].

5.2.4 Hydrostatic Stress and Strain Energy

As one of the primary indications to the prosthesis induced interference, the hydrostatic stress in the mucosa is determined by using a FORTRAN subroutine (UVARM - User Defined Output Field Requirement) in ABAQUS. It is derived by the one third of the sum of the principal and formulated as below:

$$\sigma_{hydro} = \frac{1}{3}\left(\sigma_1 + \sigma_2 + \sigma_3\right) = \frac{1}{3}\left(\sigma_{xx} + \sigma_{yy} + \sigma_{zz}\right) \tag{1}$$

In order to further assess the overall cushioning role that the mucosa plays under these two different prosthetic configurations, the absorption of strain energy in mucosa was used for measuring the severity of the disturbance brought to the mucosa under compression. As defined in Eq. (2), the total strain energy density was calculated by summing the products of stress and strain component in all elements (*n* is the total number of elements in the mucosa under stress).

$$\mathrm{SED} = \frac{\sum_{i=0}^{n} \langle \sigma_i \rangle : \langle \varepsilon_i \rangle V_i}{2\sum_{i=0}^{n} V_i} = \frac{1}{2\sum_{i=0}^{n} V_i} \times \sum_{i=0}^{n} \left[\begin{Bmatrix} \sigma_{xx} \\ \sigma_{yy} \\ \sigma_{zz} \\ \sigma_{xy} \\ \sigma_{xz} \\ \sigma_{yz} \end{Bmatrix}_i \cdot \begin{Bmatrix} \varepsilon_{xx} \\ \varepsilon_{yy} \\ \varepsilon_{zz} \\ 2\varepsilon_{xy} \\ 2\varepsilon_{xz} \\ 2\varepsilon_{yz} \end{Bmatrix}_i V_i \right] \tag{2}$$

5.3 Results

5.3.1 Maximum Biting Forces and Bone Volume Change

The maximum bite force in the participants with IROs was 172 N, which is nearly twice that of the CD wearers (95 N). The average bite forces during the entire duration (10 seconds) were 110 ± 32 N and 63 ± 15 N, respectively. The individual data of bite forces and bone volume changes are summarised in Table 2 (CD) and Table 3 (IRO). In the FE models, the load used for each case was 40% of those peak values, which is 68.8 N for IRO and 38.3 N for CD.

RRR was first measured in terms of the percentage change in bone volume that has taken place after a period of one year of wearing the prostheses. RRR occurred predominantly on the denture bearing areas, occlusally in the molar region and more lingually in the premolar area. The mean decrease in bone volume associated with IROs was -3.8% ± 4.5 which is around twice that of CDs (-1.9% ± 0.4), corresponding to the twice average bite forces in the former than the latter.

Table 5-2 Maximum Biting Force and Bone Volume Change of CD participants

CD Patient ID	Gender	Bite force	% Bone Volume change after 1st Year
1	M	60	-2.1
2	M	45	-2.3
3	F	62	-2.4
4	F	57	-2.3
5	M	56	-1.9
6	F	60	-1.8
7	M	62	-1.2
8	M	67	-1.9
9	M	102	-1.4
Mean		**63 ± 15.7**	**-1.9 ± 0.4**

Table 5-3 Maximum Biting Force and Bone Volume Change of IRO participants

IRO Patient ID	Gender	Bite force (N)	% Bone Volume change after 1st Year
1	F	91	-5.0
2	M	69	-1.0
3	M	88	-7.8
4	M	199	-5.3
5	F	100	-1.0
6	F	154	-0.8
7	F	145	-7.5
8	F	121	-7.9
9	F	117	-5.1
10	F	86	-15.9
11	F	84	-8.1
12	M	110	-4.4
13	F	123	2.1
14	F	137	-0.7
15	M	96	-1.3
16	F	85	-4.2
17	M	76	-2.4
18	F	75	-0.7
19	M	113	3.7
20	M	137	-2.9
Mean		**110 ± 32**	**-3.8 ± 4.5**

In Figure 5-2a and 5-2c, the residual ridge thickness changes were plotted for the CD and the IRO configurations, respectively. The scale ranges from -2.0 mm to +2.0 mm, for the bone resorption and apposition. Between them, the white colour indicates minor or no change. Under the CD, the white colour is dominant across the entire base contact, with a little pink for the minor ridge height reduction. In contrast, red and maroon colours at the posterior ends of the IRD indicate severe bone resorption, whereas some extent of bone apposition occurs around the two implants anteriorly.

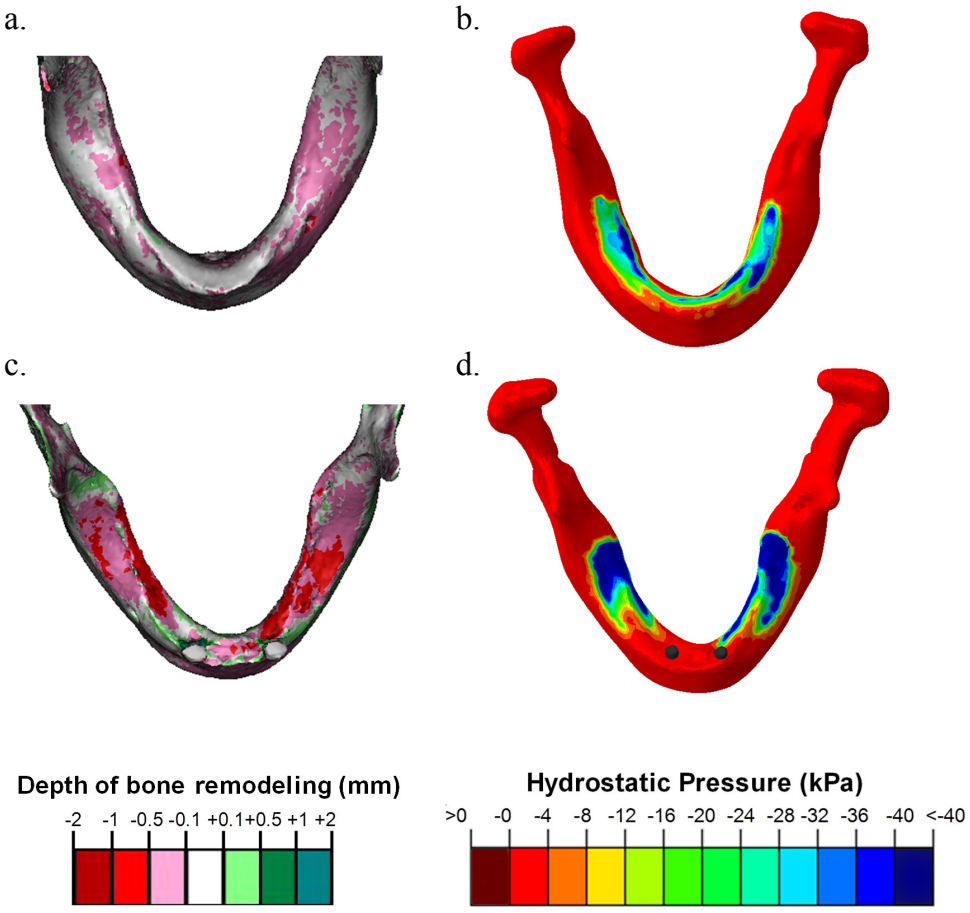

Figure 5-2 (a) The residual ridge resorption with the complete denture without implants under 76.6 N, and (b) its corresponding distribution of hydrostatic stress on the mucosa. (c) The residual ridge resorption with the implant-retained overdenture under 137.6 N and (d) its corresponding distribution of hydrostatic stress on the mucosa. (For hydrostatic stress, the colour Maroon indicates Tensile Stress; Red: Neutral Zone; Green: Close to Systolic Pressure; and Dark Blue: Highest Compressive. For residual ridge resorption, the reddish scales indicates bone resorption and the greenish scales, bone deposition).

5.3.2 Hydrostatic Stress Distribution

Based on the finite element outcomes of these two patient cases, the hydrostatic stress contours of the mucosa under the CD (Figure 5-2b) and the IRO (Figure 5-2d) are compared. In these two plots, the dark blue indicates the most severe compressive pressure under the denture bases, and the red colour shows the least effect as a neutral status (neither compressive nor tensile). The green regions designate a medium range of the

compressive pressure, close to the systolic blood pressure (140 mmHg, approximately 19 kPa).

The mucosa under a CD demonstrates a fairly low and uniform hydrostatic stress distribution from anterior to the posterior part of the residual ridge. In contrast, the hydrostatic stress magnitude in the mucosa under the IRO is higher and the distribution appears to be concentrated on the occlusal and lingual surfaces of the residual ridge in the molar and premolar regions respectively. For the individual patient, the volumetric average of hydrostatic stress over the contact region is -34.53 ± 8.07 kPa for the IRO, and -23.32 ± 0.81 kPa for the CD, representing a 32.5% reduction. The peak stress values also reduced from 128.5 kPa for IRO to 66.1 kPa for CD between these two cases.

When the contours of hydrostatic stress are compared with the contours of RRR, good agreements between the hydrostatic pressure contours and RRR can be observed for both the IRO and CD cases. For the CD, the low FE hydrostatic pressure correlates well with the minimal RRR observed after one year. For the IRO, the areas with high hydrostatic pressures correspond very well with areas of predominant resorption, which are on the occlusal and lingual surfaces of the residual ridge in the molar and premolar regions respectively.

5.3.3 Contact Surface Deformation and Energy Absorption

From FE modelling, the total compressed contact areas between the mucosa and denture in these two cases are calculated as 4608.7 mm^2 (CD) and 2833.4 mm^2 (IRO), respectively. By combining the contact status and the surface normal deformation, Figure 5-3 compares the deformation of these contact surfaces of the CD (Figure 5-3a) with the IRO (Figure 5-3b). With a total force of 76.6 N over the CD, the peak contact deformation of the mucosa is 0.58 mm in the normal direction. It is seen that the entire contact region

(2,762 nodes under contact) deforms fairly uniformly, with an area averaged deformation of 0.16 ± 0.06 mm, which agrees very well with the hydrostatic pressure contour. For the IRO, while the total biting force (137.6 N) applied was about 1.8 times of the CD, the peak contact deformation is 1.19 mm, more than double that of the CD in the posterior region of the denture. Nevertheless, the corresponding area averaged deformation is 0.32 ± 0.23 mm (over 1,708 nodes under contact), approximately double that for the CD.

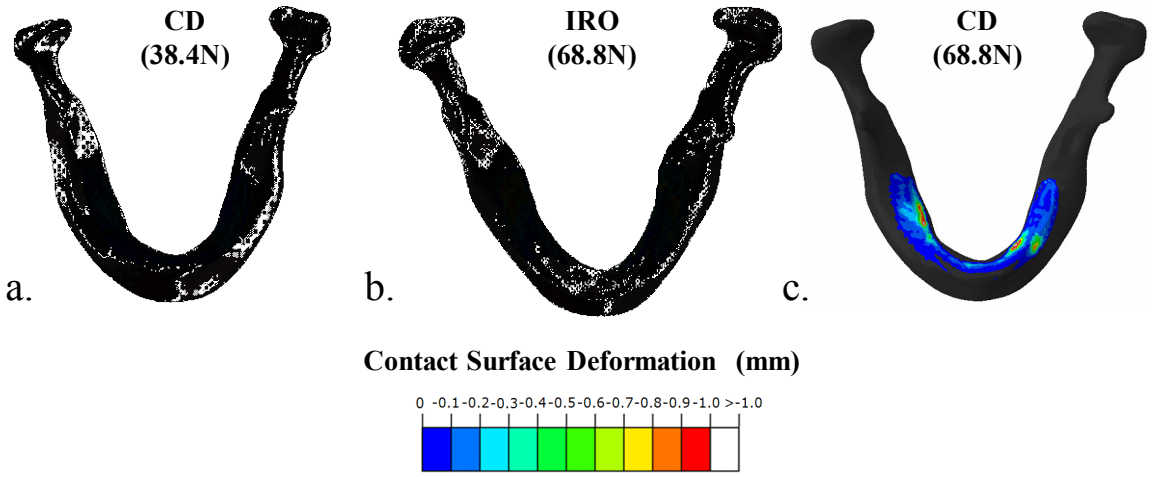

Figure 5-3 Contact surface deformation on the mucosa: (a) complete denture under 38.4N load, (b) implant-retained over denture under 68.8N load and (c) complete denture under similar higher load as overdenture with 68.8N. Larger contact deformation could be observed with the IRO even though similar higher load is used for complete denture. The contact surface deformation colour scale indicates: black: no contact formation, blue: minimal deformation, red: large deformation, white: severe deformation beyond 1mm.

When equal load of 137.6 N (68.8 N on each side) was applied for both IRO and CD case, the increasing biting force on the CD certainly leads to further mucosal deformation, but does not change the deformation pattern significantly (Figure 5-3c). Furthermore, the same biting force still caused the larger maximum deformation on IRO than CD, showing more concentrated disturbance to the local mucosa.

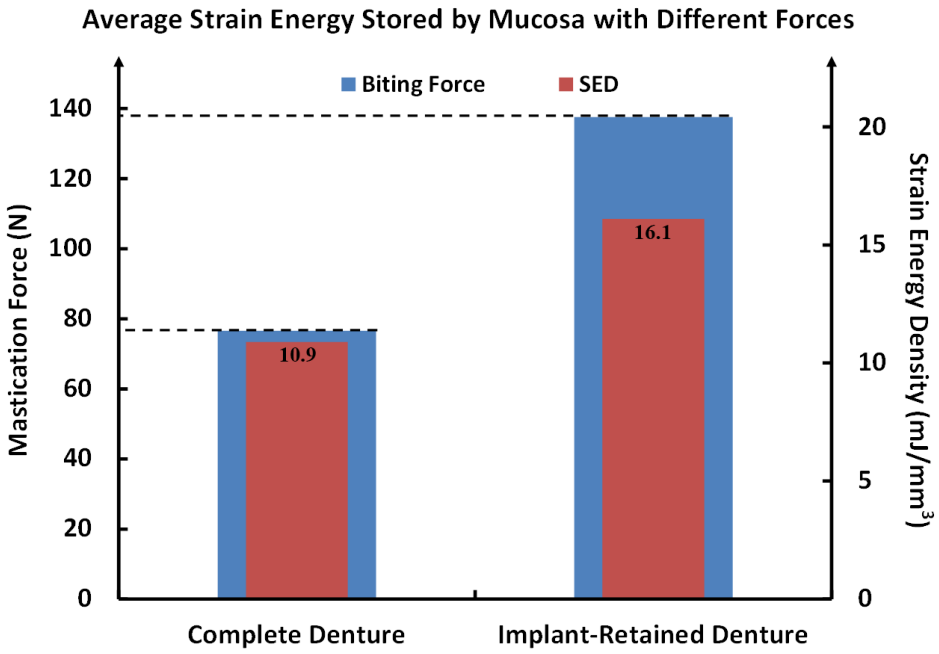

Figure 5-4 Strain energy absorbed by mucosa under different treatment strategies, while experiencing different loads.

Figure 5-4 graphs the energy absorption results at their respective mastication loads. Despite the load ratio of 1.8:1, it is found that, the mucosa beneath the IRO only stores 47.8% more strain energy on average than the CD due to the localized hydrostatic stress concentration as presented in Figure 5-2.

5.4 Discussion

Mechanical loading is recognized as one of the major causes of bone apposition and resorption in denture wearers [1-5]. The hydrostatic stress in mucosa has been considered a key factor that disturbs local microcirculation of tissues surrounding the bone, thereby affecting its mineralization pathway [46-48]. In this study, the hydrostatic stress distributions generated from the patient-specific 3D finite element models showed a good correlation with the in-vivo measurements of RRR in two different clinical treatment scenarios, namely CD and IRO. The clear visualisation of hydrostatic stress could provide biomechanical evidence of how the hydrostatic stress may affect the local blood supply in mucosa.

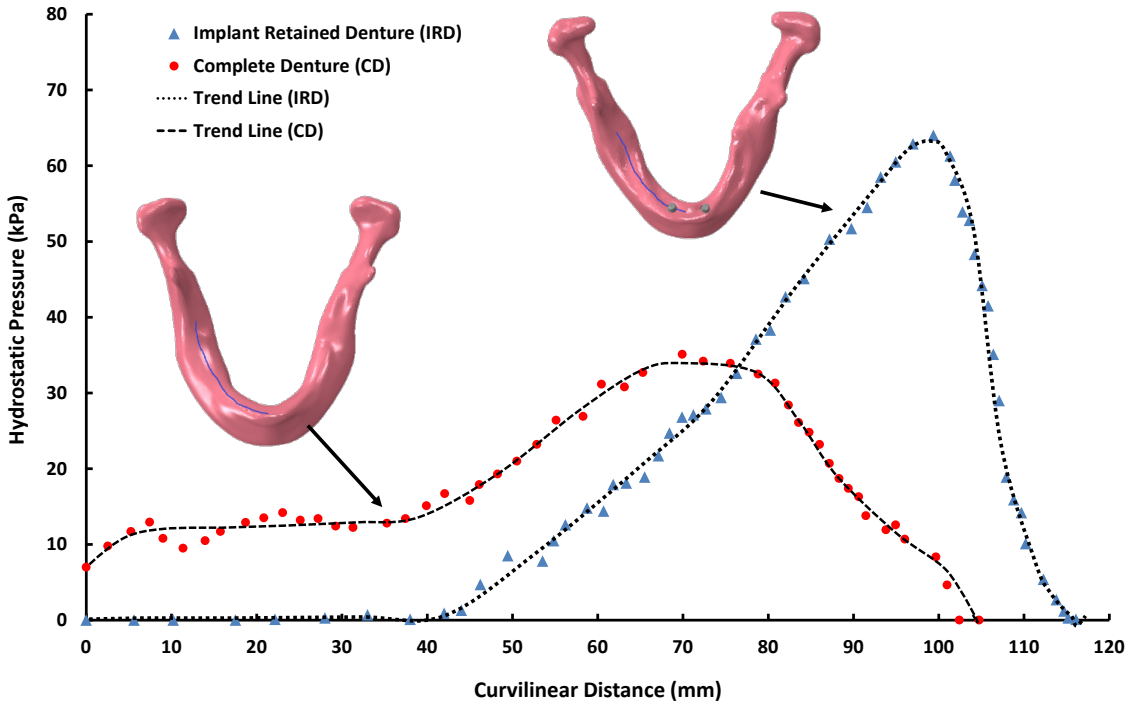

Figure 5-5 Hydrostatic pressure that develops along the interface between the denture and mucosa along the right hand side of the mandible, measured from the mid plane of the mucosa along the residual ridge and following the curvilinear coordinates (seen on the residual ridge surface of the mandible models).

To further illustrate the difference in hydrostatic pressure observed between these two treatment scenarios, the corresponding hydrostatic stresses on the contact interface between the mucosa and the denture are plotted in Figure 5-5, in which the curvilinear distance is measured from the centre of the incisors to the retromolar area along the residual ridge. As the mandibles exhibit the symmetrical similarity along the sagittal plan, the right hand side of the mandibles was plotted. It can be seen that the distribution of hydrostatic stresses along the mucosa-residual ridge interface differs considerably between the IRO and CD cases. The CD develops a relatively more even pressure distribution and its average is about 17.7 ± 4.81 kPa, which attributes to much lower RRR, as quantified in Figure 5-2a. The localized pressure increases to a level around 30 kPa in the loading area, which appears to cause a certain extent of RRR in the same location. In contrast, the IRO generates an uneven distribution of hydrostatic pressure. The pressure rises sharply in the posterior area and the peak values are about twice of the CD. The mastication force, based upon clinical measurement, for the IRO case is 1.8 times that of CD case, but the resultant peak hydrostatic stress leads to a 2-fold difference along this contour path. Interestingly, the area below the trend line, which is a measure of the effective force supported by the mucosa, of the IRO is only 1.13 times that of the CD, indicating that a substantial portion of the mastication force has been borne by the implants.

Another possible explanation for the current clinical observations may be that a much smaller denture bearing area is available to support the IRO posteriorly compared to the CD that has the entire interface as the denture bearing area for sharing the load (Figure 5-2). The average denture bearing area of contact after deformation was found to be 4608.7 mm^2 for CD and 2833.4 mm^2 for the IRO, which are fairly close to those reported in literatures, around 4000 mm^2 in the former and about half that in the latter.[22] When two implants are placed in the canine regions, the mucosa area available posteriorly to support

the overdenture is further reduced to about half from our in-vivo measurements. The longer the interabutment distance anteriorly, the smaller the mucosa area available for supporting the denture posteriorly. When combined with the higher bite force that is typically associated with the IRO, the smaller contact area may cause more localized RRR (twice as that of the CD). Furthermore, by virtue of the IRO design, free rotation during function may result in enhanced posterior loading.[49] Since the conventional CD could move around during functioning, there may be not a particular area with highly concentrated stress as happens in the IRO situation.

When an IRO was made to be mainly mucosa-borne, some portion of the masticatory force will be shared by the implants anteriorly. This is evidenced by the extremely low hydrostatic pressure recorded in the mucosa in the anterior region in the distance from 0 to 41 mm seen in Figure 5-5, where the implant is located. Upon moving in a posterior direction, the hydrostatic pressure increases steadily and has a peak at the first molar area where the biting force is exerted. For the CD, although hydrostatic pressure is found to reach its peak also at the molar region, the peak value is much lower than that in the IRO and the hydrostatic pressure is more uniformly distributed across the entire denture bearing area.

The outcome of energy absorption analysis implies that the mucosa under the CD stores deformation energy more efficiently than that under an IRO. This implies that an IRO may enable a patient to achieve a higher biting force, but could likely induce RRR around the posterior region of the mandible, due to the unevenly distributed hydrostatic pressure and the cushion effect in terms of energy absorption efficiency.

Although the IRO generates more localized RRR than the CD, the benefits of higher mastication forces with implants should be taken into consideration. It must be pointed out that the current implementation of implants follow conventional clinical

experience and there is considerable room for optimising the implant locations, length, angle, and other factors to transfer the load onto the mucosa more uniformly, leading to improved stress distribution and energy absorption efficiency.

It must be acknowledged that there are several limitations associated with the FE modelling in this study. First, a pair of bilateral biting forces was used instead of unilateral in the FE analysis, which does not represent how human mouth commonly functions. Second, only vertical force on a single tooth was applied in the analysis, further investigation is necessary to explore the effects from multiple teeth loading or different force directions (e.g. transverse). Furthermore, the bone density value in the CBCT scan cannot be calibrated to make a heterogeneous FE model. As Field et al.[50] suggested, a heterogeneous material distribution can affect potential bone remodelling activities. In this study, identical material properties have been applied to these two cases, enabling similar baseline for comparison purposes, and the heterogeneous effect will be considered in future studies. The mechanical properties of the other critical component, namely the mucosa, adopt values from literature for the same purpose; however, its individual variance may require attention. Future work can be done to optimise the arrangement of the IRO, including fixture position, length, abutment angle, et cetera, to generate a more uniformly distributed hydrostatic pressure. With the development in computerized tomography scan technology, there is potential to develop a patient-specific treatment plan[50] in clinical application, which may provide the least disturbance to blood flow in the mucosa to suit individual residual ridge condition.

5.5 Conclusions

Within the limitation of this 3D FE and short term clinical study involving twenty nine participants, it may be concluded that the IRO leads to at least twice the RRR as compared with the CD and this could be due to the higher hydrostatic stress associated with the IRO. While implants provide the capability of exerting more biting forces, they potentially concentrate hydrostatic stress and promote RRR.

Acknowledgement

This work is supported by Australian Research Council (ARC), Malaysian Ministry of Higher Education (ERGS/1/2013/SKK11/UiTM/02/01), Australia-Malaysia Institute (AMI), and Australian Postgraduate Award (APA).

5.6 References

1. Mori, S., et al., *Effect of continuous pressure on histopathological changes in denture-supporting tissues.* Journal of Oral Rehabilitation, 1997. **24**(1): p. 37-46.
2. Imai, Y., et al., *A histomorphometric analysis on bone dynamics in denture supporting tissue under continuous pressure.* J Oral Rehabil, 2002. **29**(1): p. 72-9.
3. Pietrokovski, J., J. Harfin, and F. Levy, *The influence of age and denture wear on the size of edentulous structures.* Gerodontology, 2003. **20**(2): p. 100-105.
4. Canger, E.M. and P. Çelenk, *Radiographic evaluation of alveolar ridge heights of dentate and edentulous patients.* Gerodontology, 2012. **29**(1): p. 17-23.
5. Blum, I.R. and J.F. McCord, *A clinical investigation of the morphological changes in the posterior mandible when implant-retained overdentures are used.* Clinical Oral Implants Research, 2004. **15**(6): p. 700-8.
6. Sposetti, V.J., et al., *Bite force and muscle activity in overdenture wearers before and after attachment placement.* The Journal of Prosthetic Dentistry, 1986. **55**(2): p. 265-273.
7. Haraldson, T., et al., *Oral function in subjects with overdentures supported by osseointegrated implants.* European Journal of Oral Sciences, 1988. **96**(3): p. 235-242.
8. Geertman, M.E., et al., *Two-center clinical trial of implant-retained mandibular overdentures versus complete dentures-chewing ability.* Community Dent Oral Epidemiol, 1996. **24**(1): p. 79-84.
9. Fontijn-Tekamp, F.A., et al., *Bite forces with mandibular implant-retained overdentures.* J Dent Res, 1998. **77**(10): p. 1832-9.
10. Fontijn-Tekamp, F.A., et al., *Biting and chewing in overdentures, full dentures, and natural dentitions.* Journal of Dental Research, 2000. **79**(7): p. 1519-24.
11. Finger, I.M. and L.R. Guerra, *Prosthetic Considerations in Reconstructive Implantology.* Dental Clinics of North America, 1986. **30**(1): p. 69-83.
12. Jacobs, R., et al., *Posterior jaw bone resorption in osseointegrated implant-supported overdentures.* Clinical Oral Implants Research, 1992. **3**(2): p. 63-70.
13. Assad Ahmed, S., M.A. Abd El-Dayem, and M. Badawy Magdy, *Comparison between mainly mucosa-supported and combined mucosa-implant-supported mandibular overdentures* Implant Dentistry 2004. **13**(4): p. 386-94
14. de Jong, M.H.M., et al., *Posterior Mandibular Residual Ridge Resorption in Patients with Overdentures Supported by Two or Four Endosseous Implants in a 10-year Prospective Comparative Study.* International Journal of Oral & Maxillofacial Implants, 2010. **25**(6): p. 1168-1174.
15. Elsyad, M.A. and A.A. Habib, *Implant-Supported Versus Implant-Retained Distal Extension Mandibular Partial Overdentures and Residual Ridge Resorption: A 5-Year Retrospective Radiographic Study in Men.* International Journal of Prosthodontics, 2011. **24**(4): p. 306-313.

16. Powers, M.P., et al., *The Transmandibular Implant - from Progressive Bone Loss to Controlled Bone Growth.* Journal of Oral and Maxillofacial Surgery, 1994. **52**(9): p. 904-910.

17. Keller, E.E., *Reconstruction of the severely atrophic edentulous mandible with endosseous implants: A 10-year longitudinal study.* Journal of Oral and Maxillofacial Surgery, 1995. **53**(3): p. 305-320.

18. Davis, W.H., et al., *Using restorations borne totally by anterior implants to preserve the edentulous mandible.* J Am Dent Assoc, 1999. **130**(8): p. 1183-9.

19. Reddy, M.S., et al., *Mandibular growth following implant restoration: Does Wolff's law apply to residual ridge resorption?* International Journal of Periodontics & Restorative Dentistry, 2002. **22**(4): p. 315-322.

20. Wright, P.S., et al., *The effects of fixed and removable implant-stabilised prostheses on posterior mandibular residual ridge resorption.* Clinical Oral Implants Research, 2002. **13**(2): p. 169-174.

21. Kydd, W.L., C.H. Daly, and D. Nansen, *Variation in the response to mechanical stress of human soft tissues as related to age.* Journal of Prosthetic Dentistry, 1974. **32**(5): p. 493-500.

22. Sawada, A., et al., *Viscoelasticity of Human Oral Mucosa: Implications for Masticatory Biomechanics.* Journal of Dental Research, 2011. **90**(5): p. 590-595.

23. Maruo, Y., et al., *Stress distribution prevents ischaemia and bone resorption in residual ridge.* Archives of Oral Biology, 2010. **55**(11): p. 873-878.

24. Bradley, J.C., *The clinical significance of age-changes in the vascular supply to the mandible.* International Journal of Oral Surgery, 1981. **10**: p. 71-76.

25. Sherwood, L., ed. *Human Physiology: From Cells to Systems.* . 7th ed. 2008, Brooks Cole Cengage Learning: Canada. 352.

26. Kydd, W.L. and C.H. Daly, *The biologic and mechanical effects of stress on oral mucosa.* Journal of Prosthetic Dentistry, 1982. **47**(3): p. 317-29.

27. Ashton, H., *Effect of increased tissue pressure on blood flow.* Clinical Orthopaedics and Related Research, 1975(113): p. 15-26.

28. Ahmad, R., et al., *Three dimensional quantification of mandibular bone remodeling using standard tessellation language registration based superimposition.* Clinical Oral Implants Research, 2012: p. n/a-n/a.

29. Li, W., et al., *Fibre reinforced composite dental bridge. Part II: numerical investigation.* Biomaterials, 2004. **25**(20): p. 4995-5001.

30. Li, W., et al., *Towards automated 3D finite element modeling of direct fiber reinforced composite dental bridge.* Journal of Biomedical Materials Research Part B: Applied Biomaterials, 2005. **74B**(1): p. 520-528.

31. Carr, M.E. and S.L. Carr, *Fibrin structure and cocentration alter clot elastic-modulus but do not alter platelet-mediated force development.* Blood Coagulation & Fibrinolysis, 1995. **6**(1): p. 79-86.

32. O'Brien, W.J., *Dental Materials and Their Selection*. 2008, Michigan: Quintessence Publishing Co, Inc.

33. Isaksson, H., C.C. van Donkelaar, and K. Ito, *Sensitivity of tissue differentiation and bone healing predictions to tissue properties.* Journal of Biomechanics, 2009. **42**(5): p. 555-564.

34. Sato, Y., et al., *Finite element analysis of stress relaxation in soft denture liner.* Journal of Oral Rehabilitation, 2000. **27**(8): p. 660-663.

35. Korioth, T.W.P., D.P. Romilly, and A.G. Hannam, *3-Dimensional Finite Element Stress-Analysis of the Dentate Human Mandible.* American Journal of Physical Anthropology, 1992. **88**(1): p. 69-96.

36. Li, W., et al., *Computational Biomechanics of Bone's Responses to Dental Prostheses - Osseointegration, Remodeling and Resorption*, in *9th World Congress on Computational Mechanics and 4th Asian Pacific Congress on Computational Mechanics*, N. Khalili, et al., Editors. 2010.

37. Lin, D., et al., *Mandibular bone remodeling induced by dental implant.* Journal of Biomechanics, 2010. **43**(2): p. 287-293.

38. Lin, D., et al., *Dental implant induced bone remodeling and associated algorithms.* Journal of the Mechanical Behavior of Biomedical Materials, 2009. **2**(5): p. 410-432.

39. Chen, J., et al., *Multiscale design of surface morphological gradient for osseointegration.* Journal of the Mechanical Behavior of Biomedical Materials, 2013. **20**: p. 387-97.

40. Gibbs, C.H., et al., *Occlusal forces during chewing and swallowing as measured by sound transmission.* The Journal of Prosthetic Dentistry, 1981. **46**(4): p. 443-449.

41. Hart, R.T., et al., *Modeling the Biomechanics of the Mandible - a 3-Dimensional Finite-Element Study.* Journal of Biomechanics, 1992. **25**(3): p. 261-286.

42. Maeda, Y. and W.W. Wood, *Finite Element Method Simulation of Bone Resorption Beneath a Complete Denture.* Journal of Dental Research, 1989. **68**(9): p. 1370-1373.

43. Barão, V.A.R., et al., *Effect of different mucosa thickness and resiliency on stress distribution of implant-retained overdentures-2D FEA.* Computer Methods and Programs in Biomedicine, 2008. **92**(2): p. 213-223.

44. Assunção, W.G., et al., *Comparison of stress distribution between complete denture and implant-retained overdenture-2D FEA.* Journal of Oral Rehabilitation, 2008. **35**(10): p. 766-774.

45. Chowdhary, R., K. Lekha, and N.P. Patil, *Two-dimensional finite element analysis of stresses developed in the supporting tissues under complete dentures using teeth with different cusp angulations.* Gerodontology, 2008. **25**(3): p. 155-161.

46. Burger, E.H., J. Kleinnulend, and J.P. Veldhuijzen, *Mechanical-Stress and Osteogenesis in vitro.* Journal of Bone and Mineral Research, 1992. **7**: p. S397-S401.

47. Loboa, E.G., G.S. Beaupre, and D.R. Carter, *Mechanobiology of initial pseudarthrosis formation with oblique fractures.* Journal of Orthopaedic Research, 2001. **19**(6): p. 1067-1072.

48. Aspenberg, P. and H. Van der Vis, *Migration, particles, and fluid pressure - A discussion of causes of prosthetic loosening.* Clinical Orthopaedics and Related Research, 1998(352): p. 75-80.

49. Naert, I., et al., *Prosthetic Aspects of Osseointegrated Fixtures Supporting Overdentures - a 4-Year Report.* Journal of Prosthetic Dentistry, 1991. **65**(5): p. 671-680.

50. Field, C., et al., *Prediction of mandibular bone remodelling induced by fixed partial dentures.* Journal of Biomechanics, 2010. **43**(9): p. 1771-1779.

Chapter 6: A Comparative Study on Complete and Implant Retained Denture Treatments: A Biomechanics Perspective Biomechanics of Oral Mucosa

While an implant-retained overdenture allows edentulous patients to achieve higher occlusal forces than the conventional complete dentures, the biomechanical influences have not been thoroughly investigated. Clinically, there is limited knowledge and means for predicting localized bone remodeling after denture treatment with and without implant support. As an extension to Chapter 4, this chapter provides an *in-silico* approach to exploring the treatment effects on the oral mucosa and identifying potential resorption of residual ridge under three different denture configurations in a patient-specific manner. Despite the improved stability and enhanced masticatory function, implant-retained overdentures have demonstrated higher hydrostatic stress in mucosa at the posterior ends of the mandible due to a cantilever effect, than with complete dentures. Hydrostatic pressure in the mucosa, as shown in Chapter 4, is a critical indicator and correlated well with clinically measured bone resorption, pointing to more severe mandibular ridge resorption posteriorly with implant-retained overdentures. This study provides a biomechanical basis for denture treatment planning to improve long-term clinical outcomes with minimal residual ridge resorption.

Associated Publications:

1. Junning Chen, Rohana Ahmad, Michael V. Swain, Wei Li, Hanako Suenaga, and Qing Li. **Comparing Contact Pressure Induced by a Conventional Complete Denture and an Implant-Retained Overdenture**. *Applied Mechanics and Materials*, 2014(553): p. 384-89.

2. Junning Chen, Rohana Ahmad, Wei Li, Hanako Suenaga, Michael Swain, Qing Li. **A Comparative Study on Complete and Implant Retained Denture Treatments – A Biomechanics Perspective**. Submitted to *Journal of Biomechanics*.

6.1 Introduction

Residual ridge resorption is a progressive phenomenon harmful to a patient's oral health, and has been reported to continue even 25 years post-extraction of teeth, which severely compromises prosthetic support and retention for satisfactory functioning of conventional complete dentures [1, 2]. To overcome these problems, implants have been increasingly used to retain complete dentures and have demonstrated to be a successful treatment alternative for edentulous patients with mandibular denture predicament [3-6]. Despite these clear benefits, there have been reports concerning severe residual ridge resorption associated with implant-retained overdentures [7, 8]. The biomechanical differences of these different configurations have not yet been clearly addressed in terms of their association to possible clinical outcomes.

The functional pressure, namely interstitial fluid pressure (IFP) or hydrostatic pressure, in the mucosa has been indicated as one of the most important etiological factors accounting for the residual ridge resorption [8, 9]. Such highly vascularized soft tissue plays a critical role in distributing masticatory force from the dentures to the underlying bony ridge [9-11] over a larger denture-supporting tissue interface, thereby alleviating stress concentration. The aging edentulous mandible is mainly supported by the periosteal plexus of blood vessels and is therefore very susceptible to diminished circulation under denture-induced contact pressure, which may reduce nutrient supply and metabolite removal in the supporting bone [12]. Specifically, the resultant hydrostatic pressure may exceed the systolic pressure and disturb local circulation in surrounding periosteal tissue, potentially causing bone resorption [13].

Clinically limited *in vivo* techniques exist for evaluating the disturbance induced by denture insertion to the mucosa. Despite recent findings correlating hydrostatic pressure to soft-tissue induced bone resorption, the biomechanical effects of a denture pressing on the

mucosa still remains poorly understood [14, 15]. This prevents effective prediction of possible bone remodeling after denture insertion in clinical practice as there have been few adequate clinical methods for examining the associated biomechanics. Finite element (FE) methods on the other hand have shown compelling advantages in biomechanical analysis and surgical planning. With advanced clinical computerized tomography (CT), sophisticated 3D FE models allow precise capturing of both anatomical and biomaterial features of an individual patient, thereby faithfully reflecting the case-specific bone profile and density distribution [16]. Complex soft-tissue responses can be mimicked in a nonlinear manner to more realistically reflect biomechanical behaviour [17].

This study aims to evaluate the differences in mucosal hydrostatic pressure of these three different (namely, complete, two and four implant-retained) denture treatments in a patient-specific setting. A 3D heterogeneous FE model was created based on clinical CT scans. The mucosa is characterized as a nonlinear (hyperelastic) material derived from clinical data. Visual insertion of the prostheses was tested under a clinically measured occlusal load (63 N) in the vicinity of the first molars. The simulated treatment results with two implant-retained overdentures were validated clinically against a one year follow-up study for the specific patient. Furthermore, increased occlusal forces reported in the literature were also attempted on these models to examine their consequences. The finite element analysis procedure allows comparison of different treatment options by correlating the biomechanical responses to clinical outcomes, thereby establishing an *in-silico* approach to evaluate different denture designs for reducing potential residual ridge resorption.

6.2 Materials and Methods

6.2.1 Patient Data Acquisition and Modeling

The patient CT image was stored in DICOM format (Figure 6-1a, 3D rendering) and imported into ScanIP Ver. 4.3 (Simpleware Ltd, Exeter, UK) for segmentation based on Hounsfield Unit (HU) thresholds. Three segmented masks (bone, mucosa, and denture) were further processed in 3D parametric modeling software Rhinoceros 4.0 (Robert McNeel & Associates, Seattle USA) to create geometric models with non-uniform rational B-spline (NURBS) (Figure 6-1b).

In order to enable meaningful comparison, the same denture profile (Figure 6-1b) is considered here for all three different configurations during virtual insertion. For the overdentures retained by two implants (Figure 6-1c), the implants were placed in the vicinity of the canine on each side of the jaw; and by four implants (Figure 6-1d), they were placed equidistant within the interforamina region, as adopted clinically [11, 18]. The final assemblies were exported to ABAQUS 6.9.2 (Dassault Systèmes, Tokyo Japan) for FE meshing (Figure 6-1e). To ensure the numerical accuracy, an adaptive mesh was employed and a mesh convergence test was carried out, similarly to our previous studies [19, 20]. For these different cases, the final meshes contain 2,614,854 (complete), 2,864,871 (two implants), and 3, 188, 247 (four implants) degrees of freedom (D.O.F.) using quadratic tetrahedral elements with hybrid formulation (C3D10H) to ensure smoothness of contact boundaries for the nonlinear analysis.

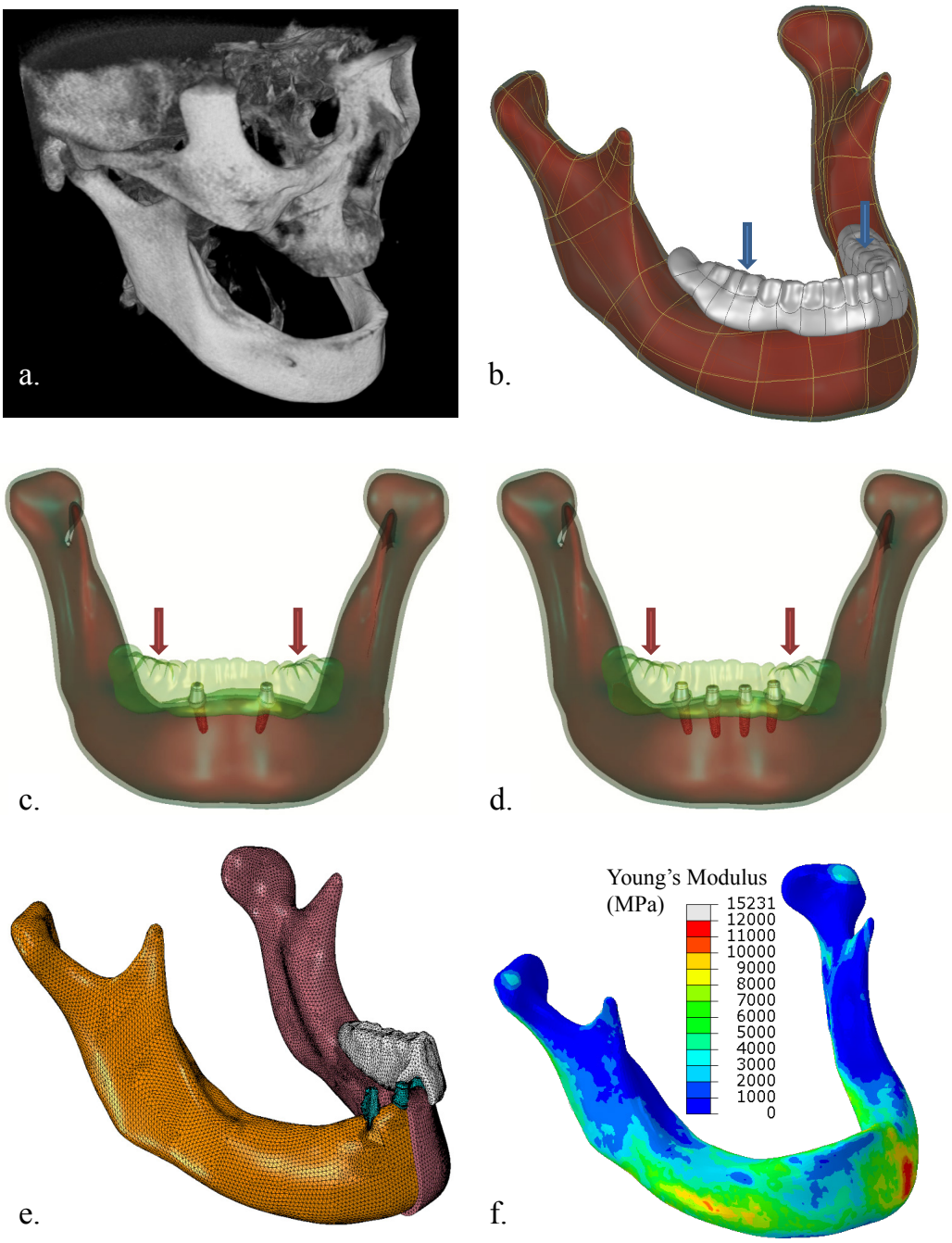

Figure 6-1 Patient-specific FE model with denture fitting. (a) volume-render CT scan of a patient's lower jaw during initial treatment consultation; (b) solidified model with NURBS representation (osseous tissue (red), mucosa (transparent brown), and denture (opaque white), as well as mastication forces (blue); (c) and (d) virtual implantation for over-denture systems (left: 2-implants and right: 4-implants): osseous tissue (maroon), mucosa (transparent brown), denture (transparent green), and screws (grey), as well as mastication forces (red); (e) final model (the 4-implant retained overdenture system is shown here) imported and meshed in ABAQUS 6.9.2, with partially sectioned mucosa (pink), denture (white), screws (cyan), and full osseous tissue (orange); (f) heterogeneous material properties of osseous tissues assigned based on the HU values from the CT scan data.

Clinical treatment was conducted independently to the FE analysis in this study, and the subject chose the two-implant retained overdenture treatment. A follow-up scan was performed one year after the overdenture insertion. The second image stack was processed in the same manner as the initial one, after registration of their isosurfaces. Differences between these two sets of measurement data allowed us to determine bone remodeling and correlate the outcomes with the FEA results [11].

6.2.2 Material Property Interpretation and Assignment

While linear elastic and homogenous material models have been widely assumed in most previous FE studies [21-23], such assumptions may not adequately replicate complex tissue responses or interaction [17]. In this study, the jaw bone was characterized with heterogeneous material properties as per the HU values to more precisely reflect the anatomical variation in density and modulus, which could potentially affect load-deformation response. The jaw HU values vary from -300 to 1500. The associated mineral densities of 0.72 g/cm^3 and 1.86 g/cm^3 were adopted from literature for cancellous and cortical bones, respectively, corresponding to the maximum (HU_{max}) and minimum (HU_{max}) values [24]. The apparent mineral density ρ_{app} is interpolated linearly against the HU value, and their relationship can be formulated as,

$$\rho_{\text{app}} = \rho_{\text{min}} + \rho_{\text{diff}} \times \frac{(HU - HU_{\text{min}})}{(HU_{\text{max}} - HU_{\text{min}})} \tag{1}$$

where ρ_{min} denotes the minimum density and ρ_{diff} indicates the difference between the maximum and minimum densities.

To correlate the Young's modulus E to the apparent mineral density ρ_{app} from CT data, Eq. (2) was adopted [25] considering the jaw bone as a two-phase porous material [26]

at a low strain rate $\dot{\varepsilon}_e$. The determined heterogeneous material properties were assigned to the Gaussian integration point in each element (Figure 6-1f).

$$E = 3790\dot{\varepsilon}_e^{0.06}\rho_{app}^3 \quad (2)$$

The mucosa has been reported to have a nonlinear response under mechanical loading [10, 27, 28]. The hyperelastic constitutive material model was adopted in this study, which defines the strain energy (U_ε) stored in a unit volume as a function of the strain at a point in the material. This strain energy driven behaviour was derived via a least-square fitting of the clinical data [28], as plotted in Figure 6-2 (solid dots with dash lines), and a third order ($N = 3$) Ogden strain energy equation [29] provides the closest match (Eq. (3), a solid curve in Figure 6-2). The material parameters are summarised in Table 1. Other materials adopt linear elastic and homogeneous properties from previous studies [21, 30, 31].

$$U = \sum_{i=1}^{N} \frac{2\mu_i}{\alpha_i^2}(\bar{\lambda}_1^{\alpha_i} + \bar{\lambda}_2^{\alpha_i} + \bar{\lambda}_3^{\alpha_i} - 3) + \sum_{i=1}^{N} \frac{1}{D_i}(J^{el} - 1)^{2i} \quad (3)$$

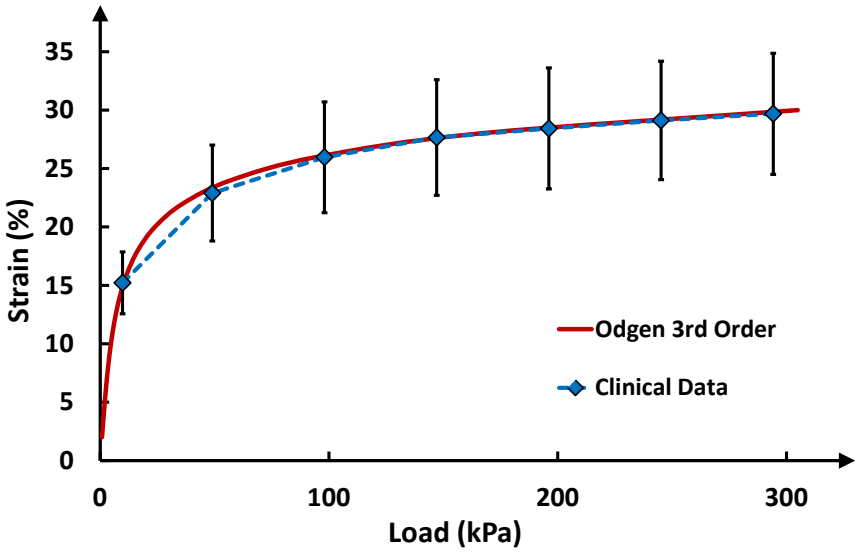

Figure 6-2 Determination of the non-linear hyperelastic behaviour of mucosa based on clinical data: the blue dash line indicates clinical measurements of mucosa deformation under

various loading magnitudes with a range across a group of patients [28], and the red solid line presents the fitting curve of the 3rd order Ogden strain energy equation with respect to these data.

Table 6-1 Material Parameters for 3rd Order Ogden Strain Energy Equation

i	μ_i	α_i	D_i
1	3.26E-02	8.41	12.47
2	7.88E-04	25.00	0
3	1.03E-03	-18.94	0

6.2.3 Mastication Scenario

For the implant retained overdentures, the screw threads were assumed to be fully locked with the surrounding bone through osseointegration [21, 23, 32, 33]. The Augmented Lagrangian algorithm was adopted to simulate the denture-mucosa contact, with a low frictional coefficient assumed as 0.1 to mimic lubrication in the oral environment [34]. A pair of localized masticatory loads was applied to both sides of the denture in the vicinity of the first molar, along the tooth root direction (nearly vertical in this subject). This loading scenario is referred to as isometric bilateral biting in literature [35], by assuming a nearly symmetric loading condition. The average voluntary biting force (63 N) was measured clinically, and was applied onto the dentures; and similar magnitudes have been reported for mandibular loading in other FE studies [36-39]. The kinematic boundary conditions were prescribed to the distal ends of the condyles [35, 40].

6.3 Results

6.3.1 Hydrostatic Pressure in Mucosa

The hydrostatic pressure contours on the mucosa are plotted in Figure 6-3, comparing all three different denture configurations, on both the external surface (between denture base and mucosa, (a) - (c)) and the periosteal surface (between mucosa and bone, sectioned views through axial planes (d) - (f)). The heterogeneous residual ridge led to non-uniform distribution of hydrostatic stress for local stiffness variances, even under a well-fitted denture base of the patient. These pressure contours exhibit a bilateral profile due to the biting activity considered, but the distribution patterns differed noticeably between the complete denture and the implant retained ones, particularly in the anterior-posterior direction, as the implants generated more cantilever effects.

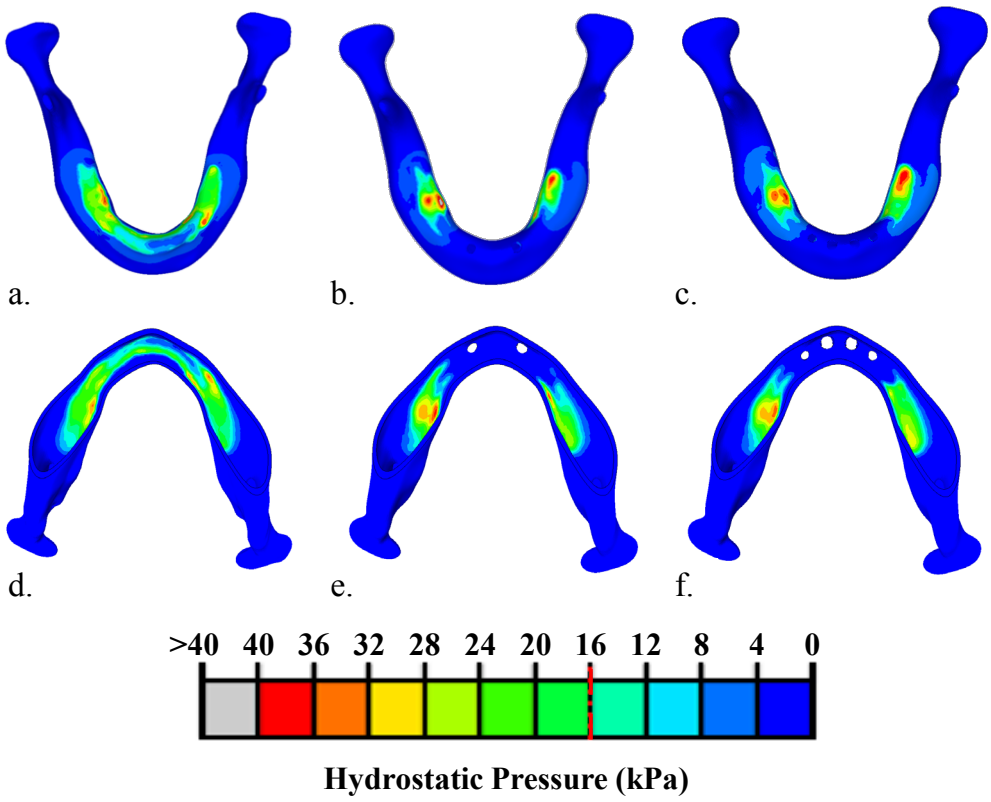

Figure 6-3 The hydrostatic pressure contours on the mucosa mandibular contact surfaces ((a) - (c)) and periosteal surfaces ((d) - (f)) induced by three different denture treatments

(complete, 2-implant retained, 4-implant retained): blue - low pressures; green - around systolic pressure; red - high pressures.

The occlusal load was transferred to the entire residual ridge under the complete denture with a contact surface area of 1926 mm^2 and the volume average of hydrostatic pressure at 10.6 ± 0.8 kPa (Figure 6-3a). For the implant retained configurations, the contact areas reduced to 73.4% (two implants, 1412.9 mm^2) and 60.1% (four implants, 1155.8 mm^2), respectively; and the corresponding volume average of hydrostatic pressures were 14.3 ± 0.9 kPa and 13.3 ± 0.9 kPa (Figure 6-3b & c).

The peak hydrostatic stress in the complete denture was 33.4 kPa, whereas it was 43.6 kPa for the two-implant retained overdenture and 39.9 kPa for the four-implant one. More severe stress concentration can be observed at the posterior ends of the mandible in the two implant cases, resulting from substantial cantilever deflection during mastication. With two extra implants, the structure became more rigid, leading to slight pressure reduction on the mucosa by 8.6%.

6.3.2 Occlusal load distribution

Compared to the complete denture, the implants played important roles in supporting the overdenture and transferring load directly to the bone. Due to the bone morphology and internal heterogeneity, the left and right implants also contributed to different extents of load bearing. Figure 6-4 depicts the calculated load proportions distributed onto the mucosa and implants. For a complete denture, the mastication load was entirely transferred to the mucosa, whilst for the two- and four-implant retained overdentures, only 63.9% and 62.1% of the mastication load were respectively borne by the mucosa.

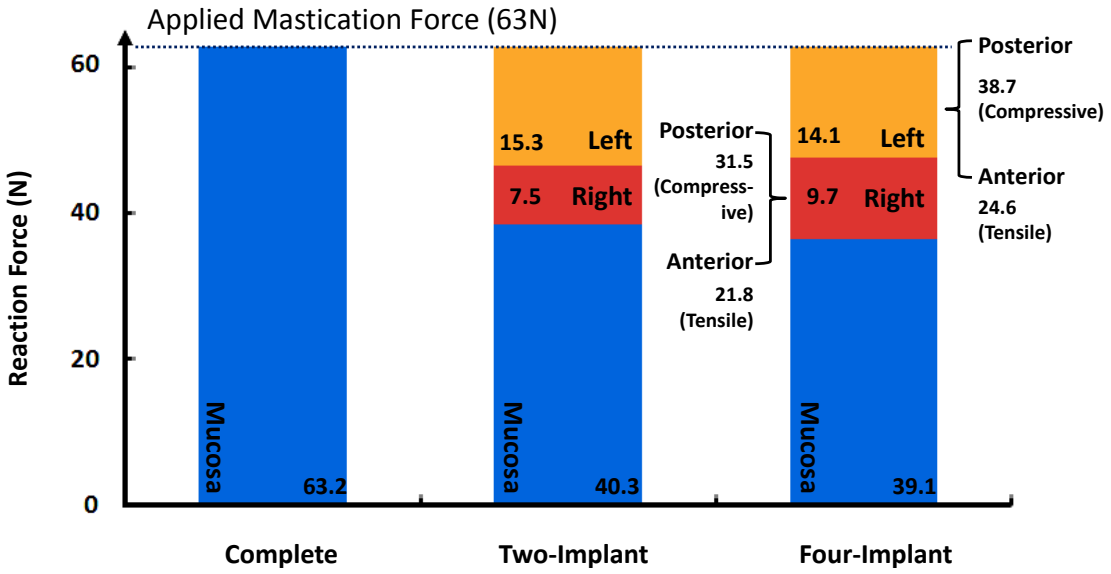

Figure 6-4 This figure compares the load distributions for each denture case, as induced by mastication (63 N). Blue - compressive load entirely supported by the mucosa; red - compressive load shared by the left implant(s); orange - compressive load borne by the right implant(s), as well as their individual components for four-implant one.

In the two-implant case, the left implant carried nearly twice load of the right one (15.3 vs 7.5 N) in this specific patient, opposite to the pressure pattern developed on the mucosa as shown in Figure 6-3b. This difference was reduced by an extra pair of implants in the four-implant case, showing an improved balance along the sagittal plane (net loads of 14.1 N at left and 9.7 N at right). Due to the cantilever effect and associated bending moment incurred in the four-implant retained overdenture, the anterior implants experience tensile pull-out forces to balance the bending moment at the posterior end of denture, whereas the posterior pair carried more than 3 times the compressive load than the two-implant case. The force balance in the anterior and posterior pairs increased the structural rigidity, transferring less occlusal load directly to the posterior end of mandible, as seen in the reduction of hydrostatic pressure in the mucosa (Figure 6-3c).

6.3.3 Denture stability

The vertical displacements along the cusps of the dentures were plotted in Figure 6-5 to examine stability of the dentures. The minimum vertical displacement was found as

1.66 mm (complete), 1.91 mm (two implants), and 1.34 mm (four implants), respectively. The left posterior regions of all these three configurations exhibited more displacements than the right hand side.

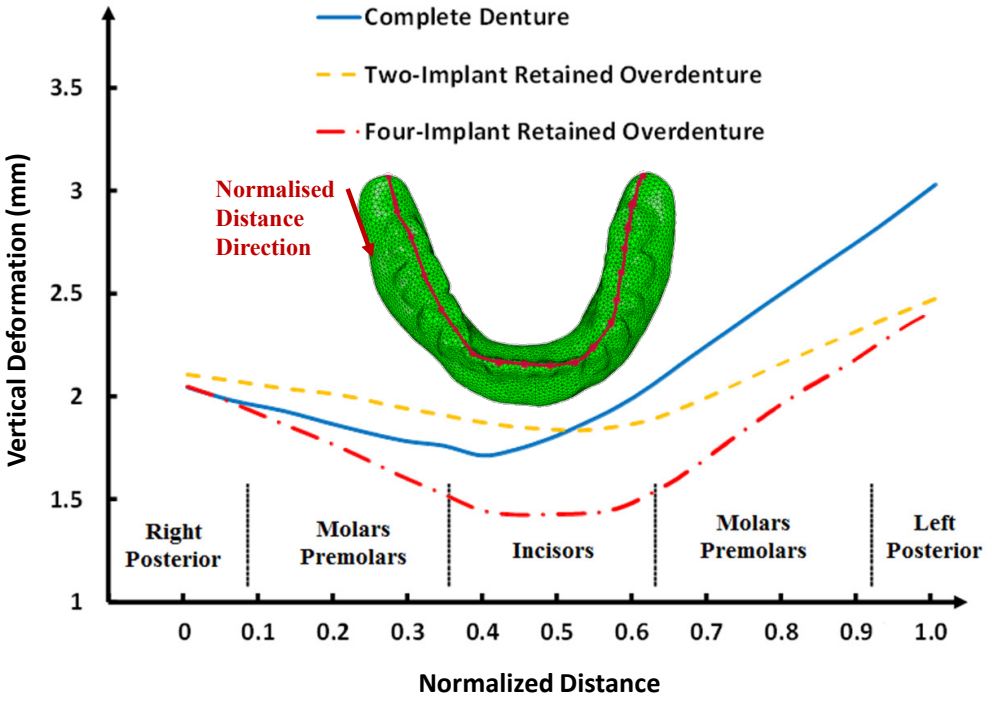

Figure 6-5 The vertical displacement of each denture configuration is plotted along the normalized arch path distance consisting of all artificial tooth cusps and posterior ends of denture cushion, as indicated by the red line on the top of the denture model. The corresponding denture regions are labelled over the normalized distance.

The minimum deformation of the complete denture occurred around the canine on the right-side, reflecting a non-symmetrical deflection in the given jaw, consistent with the non-symmetric hydrostatic pressure contours (Figure 6-3a).

Reduced denture deformation was found around the anterior region of the denture retained with more implants. The implant-retained configurations also demonstrated much smaller differences between the left and right sides, as well as between the posterior and anterior ridges. Lower displacement levels and more symmetric deflection and stress patterns indicated better stability during mastication.

6.4 Discussion

6.4.1 Correlation to Clinical Outcomes

In the course of clinical treatment, this specific subject received the two-implant retained overdenture with a follow-up scan after one year [11]. These two scans were registered based on their isosurfaces that have the same HU values. The density difference between these two scans was plotted in Figure 6-6a, as a measure of bone remodeling activity [41]. The cyan-blue regions indicated bone resorption, whereas the yellow-red regions suggested bone apposition. The grey regions showed that the bone density increases by more than 0.7 g/cm^2 (the two grey circular areas on the anterior ridge were replaced by the implants after a year). The black region at the posterior end of the right mandible arm was the site of most severe bone resorption with the maximum density reduction of 0.92 g/cm^2.

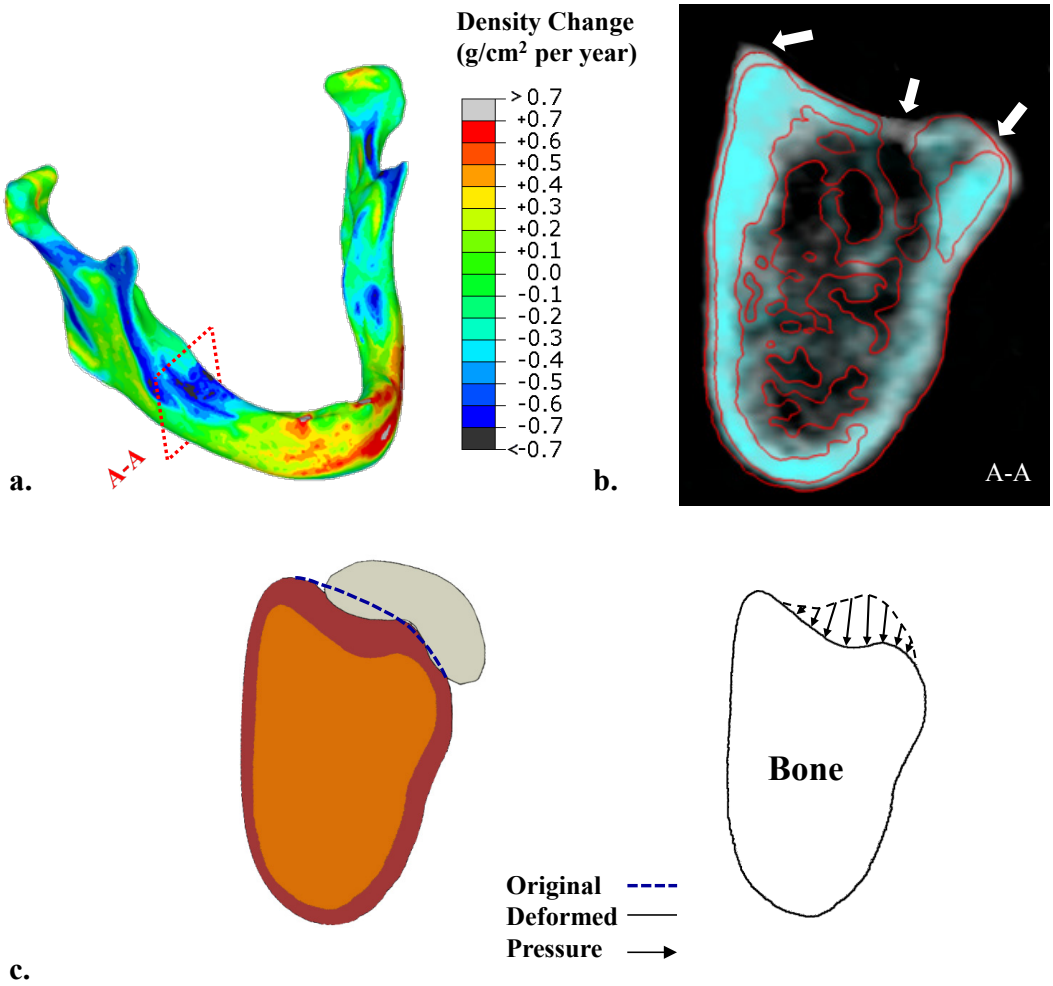

Figure 6-6 (a) The density differences between the initial and 1-year follow-up scans plotted in 3D manner, as determined by Eq. (1); (b) A 2D cross-sectional view of the CT scans were extracted at the posterior end of patient's mandible, where the most severe bone resorption occurred, as indicated by region A-A in (b), grey scale - the initial scan, cyan scale - the follow-up scan, red lines - isolines of HU thresholds for the cortical bone from the follow-up scan; (c) Left: the deformed and original (dashed) surface profiles are compared in the region A-A, orange - bone, red - mucosa, grey - denture; Right: the schematic hydrostatic pressure distribution over the periosteal membrane on the bone surface, as interpolated from the FE modeling.

As the region of major interest is the posterior mandible, 2D coronal slice of the CT scans was selected in Section A-A (Figure 6-6b), in which the grey scale represented the initial scan, and the overlapping cyan was the second scan after one year. The red profiles were the isolines presenting the HU thresholds (i.e. 0-700-1300 HU) of the second scan, to highlight the borders between each region. On both the buccal and lingual sides of the

residual ridge, the bone surface profile was well preserved. In contrast, the bone profile dropped along the contacting mucosal surface at the upper profile of the residual ridge, where three white arrows identify the region of most extensive bone resorption. At the middle arrow, the bone density decreased sharply along the periosteal-mucosal surface the bone profile was substantially lowered.

The deformed mucosa profile in Section A-A was depicted on the left hand side of Figure 6-6c (in black), to compare with the original shape (in dashed blue). The resultant hydrostatic pressure acting on the periosteal membrane was plotted on the right hand side in Figure 6-6c, where the longest vector (peak pressure) located at the same place as where the most severe bone resorption occurred (Figure 6-6a). It is found that the simulated hydrostatic pressure in the mucosa was a good predictive indicator of bone resorption at the posterior end.

Comparison of the FE modeling with clinical outcomes exhibited excellent correlation between the magnitude of hydrostatic pressure in the surrounding soft tissue and the underlying bone density changes, with consequent the bone profile variance (Figure 6-6). While most researchers have agreed that mastication forces were mainly responsible for bone remodeling beneath dental prosthesis [41-45], the associated biological mechanisms have remained inconclusive. Some studies suggested that bone resorption may be triggered mechanically by either low or overly high stress levels inside the jaw bone [16, 22, 46], while others have suggested that the soft tissue mucosa could play a much more critical role in driving bone resorption [9, 27, 37, 47]. In the present study, the regions concerned most with severe bone resorption (e.g. Section A-A in Figure 6-6), the hard-tissue driven bone remodeling stimulus, e.g. the effective strain [16, 48] or strain energy density [32, 33], was unable to be correlated with the observed bone resorption; instead, the stimulus in the surrounding fluid-rich vascular mucosa tissue, such

as hydrostatic pressure (Figure 6-3), appeared to be more relevant to the bone's turnover responses.

6.4.2 Increasing Occlusal Loads

Previous clinical studies have also reported higher bite forces in implant-retained overdentures compared with the complete dentures. Two independent studies by Geckili et al.[49] and Ahmad et al.[11] measured the maximum biting force (MBF) on average around 110 N for the patients with two implants; and comparable results (150 N) were obtained by Fontijin-Tekamp et al. [50]. Increased voluntary biting forces were also observed with more implants, reaching above 400 N on average [51], while lower MBFs were also reported in clinical trials from very elderly subjects with implant-retained overdentures [52].

Akin to the diverse range of MBFs reported in the literature, different conclusions were drawn on the effects of implants. Despite observed rising MBF with the increasing number of implants [51], there was little difference demonstrated with or without implants after 4-year adaptation [49]. Wismeijer et al. [53] claimed a simple overdenture retained by two implants was sufficient to improve functionality.

To understand the role of the number of implants at different force levels, the effects of increasing biting forces were explored within a conservative range (up to 140 N). Figure 6-7 plots the implant contribution to load sharing in the implant-retained overdentures. It was found that the implants were carrying nearly half of the mastication force at 140 N, rising from about one third, for both treatment cases. Meanwhile, the peak hydrostatic pressures in the mucosa increased much less significantly. Both trends plateaued at the higher forces, and the increased load-bearing capacity of implants was gradually compromised.

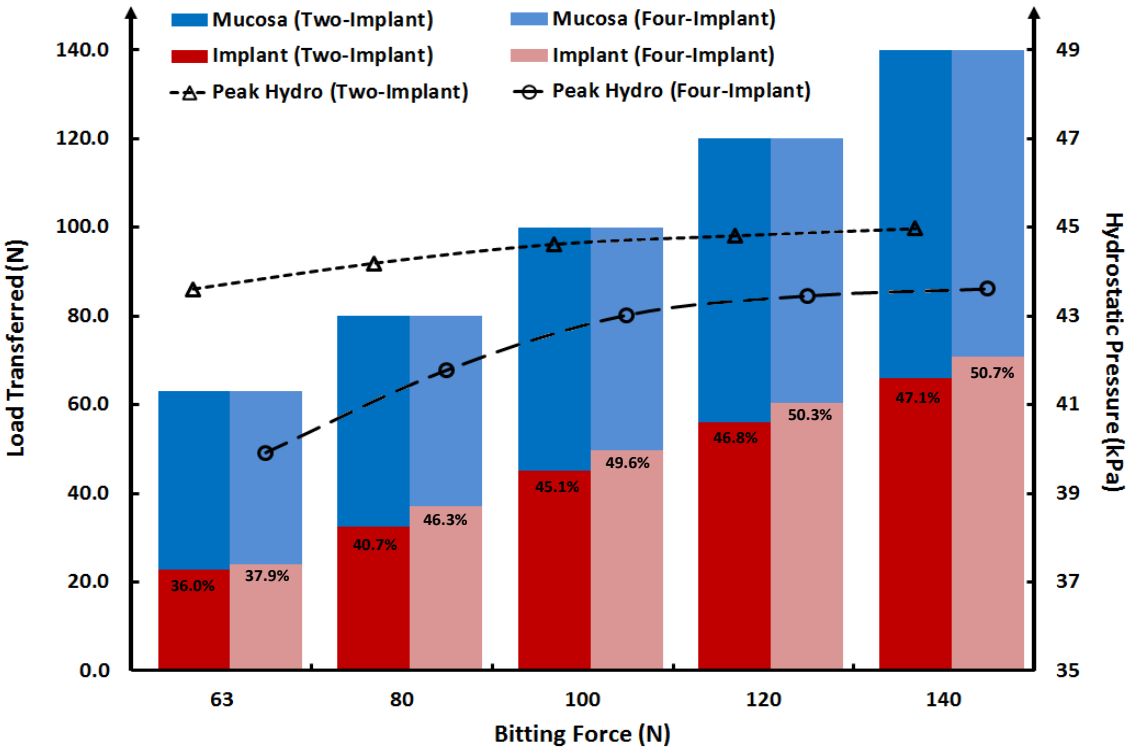

Figure 6-7 This figure compares the contributions of load sharing between two- and four-implant retained overdentures, as well as the peak hydrostatic pressure, at different force levels ranging from 63 N, measured in this study, to a conservative maximum value (140 N).

6.4.3 Clinical Implications

In this study, the complete denture exhibited the most uniform distribution of the occlusion load, with the maximum contact surface of all the three different designs. The implant-retained overdentures transferred less than two thirds of the 63N load to the mucosa, with significantly reduced contact areas, consistent with previous clinical findings [10, 11]. Although implant-retained cases delivered improved stability during mastication [11, 54], as shown in more symmetric hydrostatic pressures and deflections, the downside was the stress concentrated more posteriorly [7, 55, 56], where the cantilever effect was revealed to be a major cause [29, 43, 47].

Despite their appealing benefits, implant-retained overdentures are not free of accompanying clinical complications that require specific attention. Shortening the denture

arms was considered to reduce the posterior bone resorption [43]. Adding metal frame or wires in the denture can increase the overall rigidity of dentures [57]. These ideas can be further explored by using the FE procedure established in this study, thereby examining the overall biomechanical effectiveness of implant-retained overdentures and developing a patient specific optimized design.

6.5 Conclusions

This study explored the biomechanical basis associated with bone remodeling utilizing different denture treatments; namely complete dentures, and two or four implant retained overdentures in a patient-specific case. The 3D heterogeneous jaw bone model was created based on the patient's CT data, and a hyperelastic model of mucosa derived from the *in-vivo* data. The FE modeling results for one of these denture systems (two implant-retained) was correlated to our one year clinical follow-up study.

Acknowledgement

This work is supported by Australian Research Council (ARC), Malaysian Ministry of Higher Education (ERGS/1/2013/SKK11/UiTM/02/01), Australia-Malaysia Institute (AMI), and Australian Postgraduate Award (APA).

6.6 References

1. Atwood, D.A., *Reduction of Residual Ridges - Major Oral Disease Entity.* Journal of Prosthetic Dentistry, 1971. **26**(3): p. 266-79.
2. Tallgren, A., *The continuing reduction of the residual alveolar ridges in complete denture wearers: a mixed-longitudinal study covering 25 years.* Journal of Prosthetic Dentistry, 1972. **27**(2): p. 120-32.
3. Attard, N.J. and G.A. Zarb, *Long-term treatment outcomes in edentulous patients with implant overdentures: The Toronto study.* International Journal of Prosthodontics, 2004. **17**(4): p. 425-433.
4. Fueki, K., et al., *Effect of implant-supported or retained dentures on masticatory performance: A systematic review.* The Journal of Prosthetic Dentistry, 2007. **98**(6): p. 470-477.
5. Rashid, F., et al., *The effectiveness of 2-implant overdentures - a pragmatic international multicentre study.* Journal of Oral Rehabilitation, 2011. **38**(3): p. 176-184.
6. Barao, V.A.R., et al., *Comparison of different designs of implant-retained overdentures and fixed full-arch implant-supported prosthesis on stress distribution in edentulous mandible - A computed tomography-based three-dimensional finite element analysis.* Journal of Biomechanics, 2013. **46**(7): p. 1312-1320.
7. Jacobs, R., et al., *Posterior jaw bone resorption in osseointegrated implant-supported overdentures.* Clinical Oral Implants Research, 1992. **3**(2): p. 63-70.
8. Blum, I.R. and J.F. McCord, *A clinical investigation of the morphological changes in the posterior mandible when implant-retained overdentures are used.* Clinical Oral Implants Research, 2004. **15**(6): p. 700-8.
9. Mori, S., et al., *Effect of continuous pressure on histopathological changes in denture-supporting tissues.* Journal of Oral Rehabilitation, 1997. **24**(1): p. 37-46.
10. Sawada, A., et al., *Viscoelasticity of Human Oral Mucosa: Implications for Masticatory Biomechanics.* Journal of Dental Research, 2011. **90**(5): p. 590-595.
11. Ahmad, R., et al., *Three dimensional quantification of mandibular bone remodeling using standard tessellation language registration based superimposition.* Clin Oral Implants Res, 2013. **24**(11): p. 1273-1279.
12. Bradley, J.C., *The clinical significance of age changes in the vascular supply to the mandible.* International Journal of Oral Surgery, 1981. **10**: p. 71-76.
13. Maruo, Y., et al., *Stress distribution prevents ischaemia and bone resorption in residual ridge.* Archives of Oral Biology, 2010. **55**(11): p. 873-878.
14. Kim, S.H., et al., *Hydrostatic Pressure can Control Osteogenesis and Osteoclastogenesis when Stromal Cells and Osteoclast Precursor Cells are Cocultured.* Tissue Engineering and Regenerative Medicine, 2010. **7**(4): p. 388-394.
15. Aspenberg, P. and H. van der Vis, *Fluid pressure may cause periprosthetic osteolysis - Particles are not the only thing.* Acta Orthopaedica Scandinavica, 1998. **69**(1): p. 1-4.

16. Field, C., et al., *Prediction of mandibular bone remodelling induced by fixed partial dentures.* Journal of Biomechanics, 2010. **43**(9): p. 1771-1779.

17. Kanbara, R., et al., *Three-dimensional finite element stress analysis: The technique and methodology of non-linear property simulation and soft tissue loading behavior for different partial denture designs.* Dental Materials Journal, 2012. **31**(2): p. 297-308.

18. Clelland, N.L., et al., *Comparison of strains transferred to a bone simulant among implant overdenture bars with various levels of misfit.* Journal of prosthodontics, 1995. **4**(4).

19. Li, W., et al., *Fibre reinforced composite dental bridge. Part II: numerical investigation.* Biomaterials, 2004. **25**(20): p. 4995-5001.

20. Li, W., et al., *Towards automated 3D finite element modeling of direct fiber reinforced composite dental bridge.* Journal of Biomedical Materials Research Part B: Applied Biomaterials, 2005. **74B**(1): p. 520-528.

21. Chen, J., et al., *Multiscale design of surface morphological gradient for osseointegration.* Journal of the Mechanical Behavior of Biomedical Materials, 2013. **20**: p. 387-97.

22. Li, W., et al., *Computational Biomechanics of Bone's Responses to Dental Prostheses - Osseointegration, Remodeling and Resorption*, in *9th World Congress on Computational Mechanics and 4th Asian Pacific Congress on Computational Mechanics*, N. Khalili, et al., Editors. 2010.

23. Rungsiyakull, C., et al., *Surface morphology optimization for osseointegration of coated implants.* Biomaterials, 2010. **31**(27): p. 7196-7204.

24. Zaw, K., et al., *Rapid identification of elastic modulus of the interface tissue on dental implants surfaces using reduced-basis method and a neural network.* Journal of Biomechanics, 2009. **42**(5): p. 634-641.

25. Carter, D.R. and W.C. Hayes, *Compressive Behaviour of Bone as a 2-Phase Porous Structure.* Journal of Bone and Joint Surgery-American Volume, 1977. **59**(7): p. 954-962.

26. Rho, J.Y., R.B. Ashman, and C.H. Turner, *Youngs Modulus of Trabecular and Cortical Bone Material - Ultrasonic and Microtensile Measurements.* Journal of Biomechanics, 1993. **26**(2): p. 111-119.

27. Kydd, W.L. and C.H. Daly, *The biologic and mechanical effects of stress on oral mucosa.* Journal of Prosthetic Dentistry, 1982. **47**(3): p. 317-29.

28. Kishi, M., *Experimental studies on the relation between area and displacement of loading surfaces in connection with displaceability in the mucosa of edentulous alveolar ridge under pressure.* Shika gakuho. Dental science reports, 1972. **72**(6).

29. Bergomi, M., et al., *Hydro-mechanical coupling in the periodontal ligament: A porohyperelastic finite element model.* Journal of Biomechanics, 2011. **44**(1): p. 34-38.

30. O'Brien, W.J., *Dental Materials and Their Selection*. 2008, Michigan: Quintessence Publishing Co, Inc.

31. Sato, Y., et al., *Finite element analysis of stress relaxation in soft denture liner.* Journal of Oral Rehabilitation, 2000. **27**(8): p. 660-663.

32. Lin, D., et al., *Mandibular bone remodeling induced by dental implant.* Journal of Biomechanics, 2010. **43**(2): p. 287-293.

33. Lin, D., et al., *Dental implant induced bone remodeling and associated algorithms.* Journal of the Mechanical Behavior of Biomedical Materials, 2009. **2**(5): p. 410-432.

34. Prinz, J.F., R.A. de Wijk, and L. Huntjens, *Load dependency of the coefficient of friction of oral mucosa.* Food Hydrocolloids, 2007. **21**(3): p. 402-408.

35. Hart, R.T., et al., *Modeling the Biomechanics of the Mandible - a 3-Dimensional Finite-Element Study.* Journal of Biomechanics, 1992. **25**(3): p. 261-286.

36. Maeda, Y. and W.W. Wood, *Finite Element Method Simulation of Bone Resorption Beneath a Complete Denture.* Journal of Dental Research, 1989. **68**(9): p. 1370-1373.

37. Barão, V.A.R., et al., *Effect of different mucosa thickness and resiliency on stress distribution of implant-retained overdentures-2D FEA*. Computer Methods and Programs in Biomedicine, 2008. **92**(2): p. 213-223.

38. Assunção, W.G., et al., *Comparison of stress distribution between complete denture and implant-retained overdenture-2D FEA*. Journal of Oral Rehabilitation, 2008. **35**(10): p. 766-774.

39. Chowdhary, R., K. Lekha, and N.P. Patil, *Two-dimensional finite element analysis of stresses developed in the supporting tissues under complete dentures using teeth with different cusp angulations.* Gerodontology, 2008. **25**(3): p. 155-161.

40. Korioth, T.W.P., D.P. Romilly, and A.G. Hannam, *3-Dimensional Finite Element Stress-Analysis of the Dentate Human Mandible.* American Journal of Physical Anthropology, 1992. **88**(1): p. 69-96.

41. Klemetti, E., *A review of residual ridge resorption and bone density.* Journal of Prosthetic Dentistry, 1996. **75**(5): p. 512-514.

42. Klemetti, E., L. Lassila, and V. Lassila, *Biometric design of complete dentures related to residual ridge resorption.* Journal of Prosthetic Dentistry, 1996. **75**(3): p. 281-284.

43. Bergendal, T. and B. Engquist, *Implant-supported overdentures: A longitudinal prospective study.* International Journal of Oral & Maxillofacial Implants, 1998. **13**(2): p. 253-262.

44. Fontijn-Tekamp, F.A., et al., *Biting and chewing in overdentures, full dentures, and natural dentitions.* Journal of Dental Research, 2000. **79**(7): p. 1519-24.

45. Krishnan, V. and Z.e. Davidovitch, *Cellular, molecular, and tissue-level reactions to orthodontic force.* American Journal of Orthodontics and Dentofacial Orthopedics, 2006. **129**(4): p. 469.e1-469.e32.

46. Jahangiri, L., et al., *Current perspectives in residual ridge remodeling and its clinical implications: A review.* Journal of Prosthetic Dentistry, 1998. **80**(2): p. 224-237.

47. Assad Ahmed, S., M.A. Abd El-Dayem, and M. Badawy Magdy, *Comparison between mainly mucosa-supported and combined mucosa-implant-supported mandibular overdentures* Implant Dentistry 2004. **13**(4): p. 386-94

48. Field, C., et al., *Influence of tooth removal on mandibular bone response to mastication.* Archives of Oral Biology, 2008. **53**(12): p. 1129-1137.

49. Geckili, O., et al., *Comparison of patient satisfaction, quality of life, and bite force between elderly edentulous patients wearing mandibular two implant-supported overdentures and conventional complete dentures after 4 years.* Special care in dentistry : official publication of the American Association of Hospital Dentists, the Academy of Dentistry for the Handicapped, and the American Society for Geriatric Dentistry, 2012. **32**(4): p. 136-41.

50. Fontijn-Tekamp, F.A., et al., *Bite forces with mandibular implant-retained overdentures.* Journal of Dental Research, 1998. **77**(10): p. 1832-1839.

51. Baca, E., et al., *In vivo evaluation of occlusalcontact area and maximum bite force in patients with various types of implant-supported prostheses.* Acta Odontologica Scandinavica, 2013. **71**(5): p. 1181-1187.

52. Müller, F., et al., *Implant-supported Mandibular Overdentures in Very Old Adults: A Randomized Controlled Trial.* Journal of Dental Research, 2013.

53. Wismeijer, D., et al., *Patient satisfaction with implant-supported mandibular overdentures: A comparison of three treatment strategies with ITI-dental implants.* International Journal of Oral and Maxillofacial Surgery, 1997. **26**(4): p. 263-267.

54. Goodacre, C.J., et al., *Clinical complications with implants and implant prostheses.* Journal of Prosthetic Dentistry, 2003. **90**(2): p. 121-132.

55. Kordatzis, K., P.S. Wright, and H.J.A. Meijer, *Posterior mandibular residual ridge resorption in patients with conventional dentures and implant overdentures.* International Journal of Oral & Maxillofacial Implants, 2003. **18**(3): p. 447-452.

56. Kreisler, M., et al., *Residual ridge resorption in the edentulous maxilla in patients with implant-supported mandibular overdentures: An 8-year retrospective study.* International Journal of Prosthodontics, 2003. **16**(3): p. 295-300.

57. Drago, C. and K. Howell, *Concepts for Designing and Fabricating Metal Implant Frameworks for Hybrid Implant Prostheses.* Journal of Prosthodontics-Implant Esthetic and Reconstructive Dentistry, 2012. **21**(5): p. 413-424.

Chapter 7: Three-Dimensional Contact Shape Optimisation and Free-Form Fabrication for Removable Partial Dentures: A New Paradigm for Prosthetic CAD/CAM

This chapter aims to develop a fully automatic procedure for shape optimisation of a removable partial denture (RPD) base, to minimize the contact pressure on the mucosa and avoid associated clinical complications. A contact optimisation algorithm was developed based on the bi-directional evolutionary structural optimisation (BESO) technique. Both initial and optimized dentures were prototyped by 3D printing and tested with fitting silicone and pressure sensitive film. Despite the commonality of clinical complications induced by dentures, there has, as yet, been no quantitative method available for appropriate denture base adaptation. Our procedure provides a novel CAD-CAM method for digitalised denture adjustment. The integration of digitalized modelling, optimisation and free-form fabrication enables more efficient clinical adaptation. The customized optimal denture design is expected to have considerable clinical benefits including minimizing pain/discomfort and potentially reduce long-term residual ridge resorption.

Associated Publications:

1. Junning Chen, Hanako Suenaga, Wei Li, Michael Swain, Qing Li. **Three-Dimensional Contact Shape Optimisation and Free-Form Fabrication for Removable Partial Dentures – A New Paradigm for Prosthetic CAD/CAM**. Submitted to *the Journal of Prosthodontic Dentistry*.
2. Junning Chen, Rohana Ahmad, Michael V. Swain, Wei Li, Hanako Suenaga, and Qing Li. **Comparing Contact Pressure Induced by a Conventional Complete Denture and an Implant-Retained Overdenture**. *Applied Mechanics and Materials*, 2014(553): p. 384-89.

7.1 Introduction

Denture treatments have been widely applied in dental practice to restore oral function of the edentulous group [1-3]. Mal-adapted dentures can induce clinical complications associated with the inappropriate load transfer from the dental prosthesis to oral tissues, leading to pain and discomfort in patients [4-6], thus compromising their quality of life [7-9]. In more severe cases, subsequent residual ridge bone resorption may develop [1, 10, 11].

During mastication, the oral mucosa plays a critical role in distributing occlusal loads from the denture to the underlying bony ridge [12-15]. The contact pressure developed over this highly vascular tissue is one of the most important etiological factors causing the clinical complications [5, 15-19]. With aging, the mandibular arches are found to become even more susceptible to the excessive contact pressure under the denture, which disturbs local blood supply to the underlying bone, triggering nerve pain [20] and potentially resulting in bone resorption [21].

Conventionally, clinical denture fabrication is performed using either a cast/press mould or an artificial model [22-25], followed by time-consuming manual correction and adjustment [26]. Early studies have shown that bone is a heterogeneous material with local anatomical property variations, affecting load transfer and strain [3, 16]. The soft tissue also influences the denture masticatory load distribution [13-15]. Meanwhile, the accuracy of denture adaptation may vary significantly with different fabrication techniques [23]. Recent developments of *in vivo* measurement techniques allow determining the contact pressure beneath dentures [27], providing more insight into clinical adaptation. However, its accuracy essentially relies on the tactile sensor, and the clinical practicability remains unclear because of its complex setup.

The finite element (FE) method has demonstrated compelling advantages for biomechanical analysis and surgical planning [28-31]. When combined with clinical cone beam computed tomography (CBCT), precise 3D morphologies can be modeled accurately with both anatomical and physiological features of an individual patient [3]. In addition, increasing computational power enables more realistic models of tissue behaviour, including complex nonlinear biomaterial responses [28]. Furthermore, computational design allows one to optimize the shape of an engineering structure based on FE models and has been applied for addressing design issues involving sophisticated contact problems [32-36]. Following the success achieved in engineering, the denture shape can potentially be optimized to minimize clinical complications induced by contact pressure [37]. This numerical approach also provides compatibility with digital manufacturing, known as a computer-aided design and computer-aided manufacturing (CAD-CAM) system, for ensuring controllable consistency and standardized accuracy [38-40].

This study aims to develop a fully automatic algorithm for denture-mucosa contact optimisation in a patient-specific removable partial denture by minimizing the peak contact pressure developed. A 3D heterogeneous FE model is first created based on clinical CT data, with the mucosa modeled as a nonlinear (hyperelastic) material in response to mastication. Both pressure-induced pain and hydrostatic pressure in the mucosa are examined with the initial and optimal contact surfaces. Both dentures were prototyped using a 3D printer, and further tested with existing clinical examination methods, to verify the effectiveness of the proposed procedure *in vitro*. From an engineering perspective, this study develops a novel procedure by the integration of FE based automatic design optimisation and the digital free-form fabrication (3D printing). From a clinical perspective, this novel technique automates patient-specific denture adaptation with quantitative guidelines for denture adjustment and correction in less time, subject to mastication. From

a patient's perspective, the optimized denture would potentially minimize pain/discomfort and reduce long-term residual ridge resorption, thereby maximising intervals between subsequent denture adjustments.

7.2 Materials and Methods

7.2.1 Patient Data Acquisition and Modelling

The CT image was segmented in ScanIP Ver. 4.3 (Simpleware Ltd, Exeter, UK) based on Hounsfield unit (HU) thresholds, to form polygonal surface meshes for two sets of models. Using non-uniform rational B-splines (NURBS), free-form parametric surfaces were reconstructed from these meshes, and geometric models were solidified in the 3D parametric modelling software Rhinoceros 3.0 (Robert McNeel & Associates, Seattle USA) (Figure 7-1a).

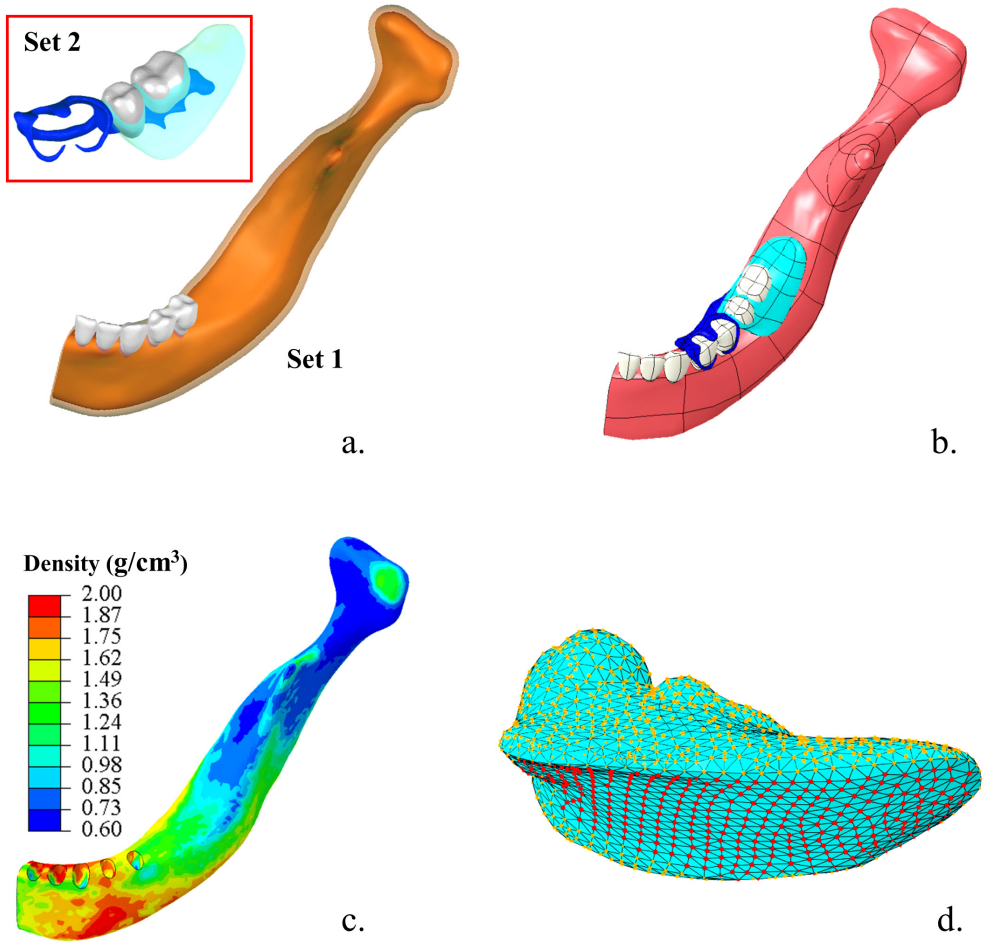

Figure 7-1 The model is created based on patient's clinical data. (a) Two sets of masks created separately (Set 1: white - teeth, orange - bone, transparent pink - mucosa, grey - teeth; Set 2: grey - artificial teeth, transparent cyan - denture base, blue - denture frame); (b) Both models are solidified by using NURBS after visual insertion of RPD; (c) Assignment of heterogeneous material property of the bone based on HU value; (d) The nodes highlighted in

red on the denture base are allowed to be modified during bi-directional evolutionary shape optimisation (BESO), and the orange ones are fixed to maintain the denture functionality.

The prescribed RPD of the subject was duplicated with a titanium frame, a scanning resin denture base, and radiopaque artificial teeth, for the scanning purpose. The RPD image stack was initially processed in the same manner as the subject's jaw. The virtual insertion was then performed utilizing the surface contour registration between the supporting crowns and the denture rest in this software (Figure 7-1b). The denture base was further modified to create an exact match to the jaw bone surface by Boolean operations in Rhinoceros 3.0. Through this approach, the 3D baseline model optimisation commences with an initial 'perfect-surface-match' (without mastication).

The final model was meshed in ABAQUS 6.9.2 (Dassault Systèmes, Waltham USA), with the built-in global adaptive mesh. To ensure sufficient numerical accuracy, a mesh convergence test was performed on this model as in our previous studies [41, 42]. The final mesh contains 186,213 degrees of freedom (D.O.F.) with 328,066 tetrahedral elements in the hybrid formulation (C3D4H) to preserve the continuity and smoothness of the contact pressure in the nonlinear analysis.

Clinical treatment was conducted independently to the FE analysis in this study, and the subject chose the two-implant retained overdenture treatment. A follow-up scan was performed one year after the overdenture insertion. The second image stack was processed in the same manner as the initial one, after registration of their isosurfaces. Differences between these two sets of measurement data allowed us to determine bone remodelling and correlate the outcomes with the FEA results [14].

7.2.2 Material Assignment and Masticatory Scenario

Although linear elastic and homogenous material models have been widely assumed in most FE studies [43-46], such assumptions may not adequately replicate

complex tissue responses [28]. In this study the mandibular bone was characterized as a heterogeneous material based on the HU values, reflecting the variation of localized modulus and load deflection [43, 45]. The apparent bone density ρ_{app} is interpolated linearly against the HU value as in Eq. (1), with the thresholds of 1.86 g/cm^3 and 0.72 g/cm^3 for cortical and cancellous bones, respectively [47] (the resultant bone density contour in Figure 7-1c).

$$\rho_{app} = \rho_{\min} + (\rho_{\max} - \rho_{\min}) \times \frac{(HU - HU_{\min})}{(HU_{\max} - HU_{\min})} \tag{1}$$

$$E = 3790 \dot{\varepsilon}_e^{0.06} \rho_{app}^3 \tag{2}$$

$$U = \sum_{i=1}^{M} \frac{2\mu_i}{\alpha_i^2} (\bar{\lambda}_1^{\alpha_i} + \bar{\lambda}_2^{\alpha_i} + \bar{\lambda}_3^{\alpha_i} - 3) + \sum_{i=1}^{N} \frac{1}{D_i} (J^{el} - 1)^{2i} \tag{3}$$

Eq. (2) established by Carter and Hayes [48] was adopted here to correlate the Young's modulus E to the apparent density ρ_{app}, A FORTRAN subroutine in the User Defined Field (USDFLD) was employed to assign these heterogeneous material properties to the individual material integration point of every element in ABAQUS.

A hyperelastic constitutive material model was adopted for the mucosa to better represent its nonlinear response under mechanical loading [13, 49, 50]. This material model depends upon the strain energy (U_ε) stored per unit volume as a function of the instantaneous strain at a point of the material, and was derived from the clinical data documented by Kishi [50] via least-squares fitting. A third order Ogden strain energy constitutive model equation [51] was determined to provide the closest match (Eq. (3)), where $\bar{\lambda}_i$ are the deviatoric principal stretches obtained from the principal stretches, M (= 3

in this case) is the order of the fitting equation. Table 1 summarizes all the material properties, including μ_i, α_i, and D_i for the hyperelastic model [3, 43, 46].

Table 7-1 Material properties of the implant screws and denture

Material		**Young's Modulus (MPa)**		**Poisson's Ratio**
Bone		Heterogeneous		0.3
Denture Frame		110, 000		0.35
Denture Base		2,650		0.30
Artificial Tooth		140, 000		0.28
Tooth		84, 100		0.20
Mucosa		Hyperelastic		0.47
(Ogden 3rd)	i	μ_i	α_i	D_i
	1	3.26E-02	8.41	12.47
	2	7.88E-04	25.00	0
	3	1.03E-03	-18.94	0

A localized masticatory force was applied in the vicinity of the first molar approximately in a vertical direction with a magnitude of 130 N [52]. The Augmented Lagrangian algorithm was adopted to simulate the denture-mucosa contact, with a low frictional coefficient assumed at 0.1 to mimic typical lubrication in the oral environment [53, 54]. The boundary conditions were prescribed to the distal condyle with full kinematic constraints and the sagittal plane with symmetric constraints [55, 56].

7.2.3 Bi-directional Evolutionary Structural Optimisation Algorithm

The evolutionary structural optimisation (ESO) algorithm is a heuristic and non-gradient approach that mimics the adaptability of natural structures iteratively, and has proven effective to handle both nonlinear and non-differentiable contact problems [32]. As its further development, bi-directional evolutionary structural optimisation (BESO) allows

material addition to where it is most needed, and material removal from where it is most redundant concurrently. The BESO method has been demonstrated to be more robust and efficient than ESO [32, 57]. Treating individual elements as design variables, BESO creates non-smooth zigzag boundaries in the design domain that prevents it from creating a functional shape providing meaningful and realistic contact [32, 58].

To tackle this problem, the conventional BESO approach is significantly modified here, in which the cloud of surface nodes is utilized to define the design domain for implementing the optimisation. The surface mesh in Figure 7-1d indicates where these boundary nodes are in the initial design domain, and two groups of these nodes are highlighted in red (i.e. free-to-move nodes and capable of being optimized) and black (constrained to maintain the functionality of a denture) groups, respectively.

The clinical expectation is to optimize the denture-mucosa contact surface thereby avoiding undesirable concentrations of contact pressure over the entire contact profile (denoted as $g(x,y,z)$). Mathematically, this may be simply formulated as in Eq. (4). In order to implement an effective BESO approach, this objective function is further revised by reducing the overall deviation of the contact pressure shown in Eq. (5), which reduces the magnitude of the upper extremes and improves the effectiveness of the lower extremes over the entire contact region.

$$\min f(g(x,y,z)) = \min \sigma_{\max}(g(x,y,z)) \tag{4}$$

$$\min f'(g(x,y,z)) = \min \sqrt{\frac{1}{N}\sum_{i=0}^{N}(\sigma_i - \bar{\sigma}_{Iter=0})^2} \tag{5}$$

where N denotes the total nodal number in the design domain; σ_i is the nodal contact pressure. Target contact pressure $\bar{\sigma}$ is obtained from the average at the initial step (virgin model with Iter = 0), to balance material removal and addition. The convergence

criterion is set so that the average of 5 contiguous objective function changes (Δf) is less than 1% (Eq. (6)).

$$\frac{1}{5}\sum_{i=n}^{n+5}\Delta f_i'(g(x,y,z)) \le 1\% \tag{6}$$

The interfacial contact surface g is modified by implementing nodal movement $\boldsymbol{\delta}(x,y,z)$ in Eq. (7), to effectively redistribute the contact pressure. Increasing the initial distance between the contact pairs will reduce the pressure, whilst reducing the initial distance will enable them to share more load. While the surface nodes are kept the same to maintain both the functional group and design domain, the internal domain is remeshed every iteration based on the modified surface nodes, to avoid over-stretched elements.

As in Eq. (7), the magnitude of modification is proportional to the relative deviation between nodal contact pressures and target average pressure. The direction of the nodal movement is determined by the normal vector of each individual surface node in a three-dimensional space. The change speed is controlled by the modification rate, denoted as *MR* here. Four different constant modification rates, 0.01, 0.005, 0.002, and 0.001, are first attempted. An adaptive modification rate controlled by the maximum contact pressure ratio as defined in Eq. (8) is also proposed to improve the convergence, where the initial modification rate is set to $MR_{Initial} = 1\%$ in the case below. For clarification, the complete contact based BESO procedure is depicted in the flowchart shown in Figure 7-2.

$$\boldsymbol{\delta_i}(x,y,z) = -MR \cdot (\frac{\sigma_i - \overline{\sigma}}{\overline{\sigma}})\tilde{\boldsymbol{n}}_{(x,y,z)} \tag{7}$$

$$MR^{\,Adaptive}_{Iter=i} = MR_{Initial} \cdot (\frac{\sigma^{\,Max}_{Iter=i}}{\sigma^{\,Max}_{Iter=0}}) \tag{8}$$

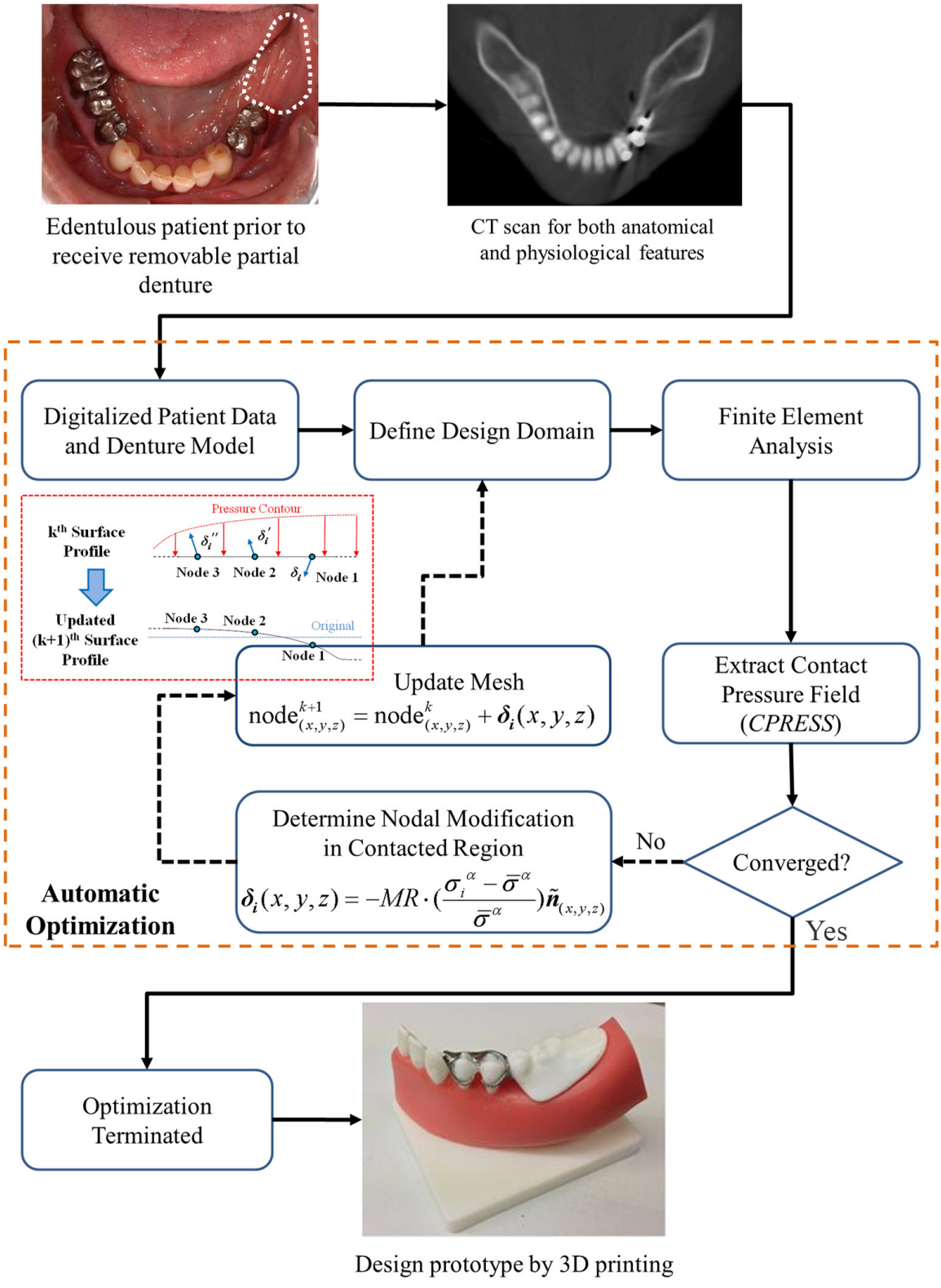

Figure 7-2 The flow chart illustrates the contact-based BESO procedure for optimisation of removable partial denture contact surface.

7.2.4 Design Prototype and in vitro Test

Conventional subtractive manufacturing has been widely applied to fabricate dentures and there have been several reports describing its usage [38]. The other option available using CAD-CAM is additive manufacturing, with 3D printing technology, and its novel potential is gradually being recognized [59], but few reports are currently available for dental prosthetic RPD. In this study, the subject's jaw model and both the initial and optimized RPDs were prototyped using 3D printing to demonstrate the complete integration of CAD with CAM through additive fabrication. Finally, the prototypes were used for *in vitro* tests to explore the outcomes of this computational design and manufacturing procedure. It is noted however, the precise *in vivo* mechanical behaviour cannot be obtained with these *in vitro* models; however, these *in vitro* tests can provide the same physical baseline without being influenced by physiological factors.

The jaw bone was printed with a stereolithography machine (Projet HD 3000, 3dsystems, Melbourne Australia) with 16 μm building layer thickness in Shore 90D polyurethane. The mucosa layer was moulded onto the rigid bone model, with Shore 15AF polyurethane. The metal frames of both dentures were printed with stainless steel 316 GP1 by direct metal laser sintering (EOSINT M 270, EOS, Ingleburn Australia) at 20 μm per building layer. The artificial crowns and cushion base were also over-moulded with Shore 30D polyurethane.

The loading test was performed with a universal testing machine (Instron 3360, Melbourne Australia) (resolution at 0.1N, ± 0.5 % accuracy). The loading rate was set to 0.1 mm/min, and the sampling frequency was at 20 Hz. Two typical clinical methods were used to examine the contact between the denture prototype and the jaw model. The first was to apply white silicone (GC Corporation, Tokyo Japan) for checking the fit, and the other one was using a pressure sensitive film (model 4LW, Fuji Film, Tokyo Japan).

7.3 Results

7.3.1 Modification Rate (MR) and Optimisation Convergence

MR is a critical parameter for determining whether or not and how fast the shape optimisation converges. A balance must be achieved between the rate of convergence and computational efficiency. Four different constant *MR*s and an adaptive *MR* (starting at 0.01) were attempted. Both the maximum contact pressure (MAX) and the standard deviation (SD) are plotted in Figure 7-3a and 3b against the iteration number.

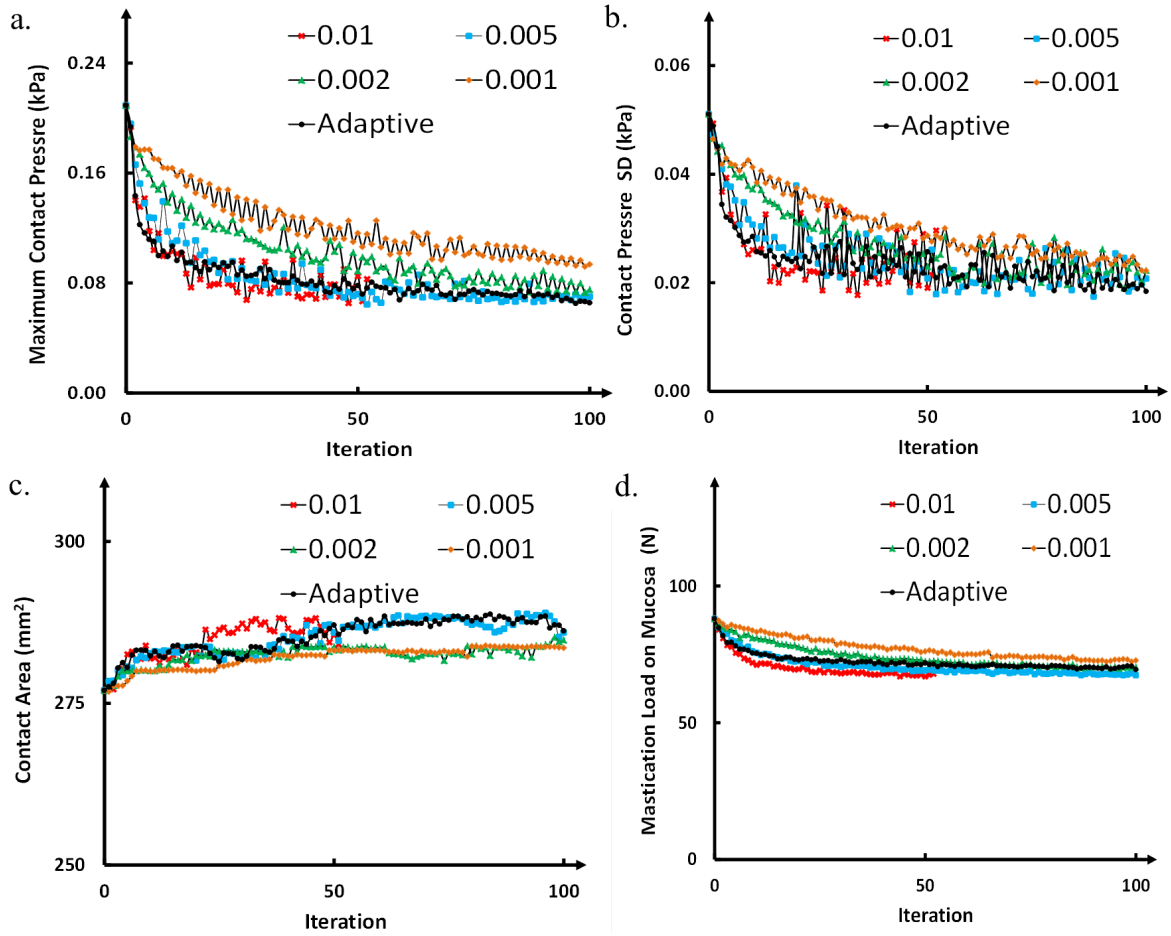

Figure 7-3 Convergence history, (a) the maximum contact pressure; (b) the contact pressure deviation (as objective function Eq. (5)); (c) the contact area, and (d) the load transferred from denture base through the optimisation with different modification rates (0.01: red cross, 0.005: blue square, 0.002: green triangle, 0.001: orange diamond, adaptive: black dot).

The larger modification rates (0.01 and 0.005) bring down both MAX and SD faster than the smaller ones (0.002 and 0.001) in the early iterations. However, the larger

the *MR*, the greater the oscillations in the objective curves. A non-smooth contact surface was finally generated by *MR*=0.01, leading to a singularity resulting in termination at Iteration 53. Two smaller *MR*s (0.005, and 0.002) still fluctuate substantially beyond 80 iterations and barely show SD convergence. The smallest *MR* (0.001) provides the smoothest trend in both MAX and SD; however, it takes many more iterations to approach convergence.

The adaptive *MR* demonstrated a better balance by taking advantages from both large and small *MR*s to provide the best efficiency and robustness of convergence. Within the first 10 iterations, the adaptive *MR* enables the reduction of both MAX and SD by over 50% from the initial design. The subsequent iterations go through a smooth convergence trend, meeting the criterion (Eq. (6)) at Iteration 93. At the end of optimisation, the maximum contact pressure is reduced from 209.2 kPa to 65.6 kPa (that is by 69%), and the uniformity is improved from ± 50.3 kPa to ± 18.4 kPa (by 63%).

Meanwhile, the other concerns associated with optimisation reside in the variation of the contact area and the total load transferred from the denture base to mucosa tissue, as plotted in Figure 7-3c and 3d, respectively. All five *MR*s exhibit small increases in the contact area, as the nature of the BESO algorithm attempts to balance material removal and deposition. Besides, some proportion of the load is shifted from the denture base in the initial design onto the supportive abutment teeth (premolars) via the clasps in the optimal design. All *MR*s converge to a similar level around 70 N out of the total load (130 N), with about 13% reduction from the initial design.

7.3.2 Denture Modification and Contact Pressure

Figure 7-4a presents the optimal denture shape generated from the adaptive *MR*, where the maximum extent of material addition amounts to 382 um and the maximum

material removal is 224 um. In the case of a cantilever, most material is added near the denture clasp end, whereas the thickness is reduced at the distal end, to reduce the overloading. In addition, the buccal side of the denture is optimized to share more load than the lingual side in this specific patient case.

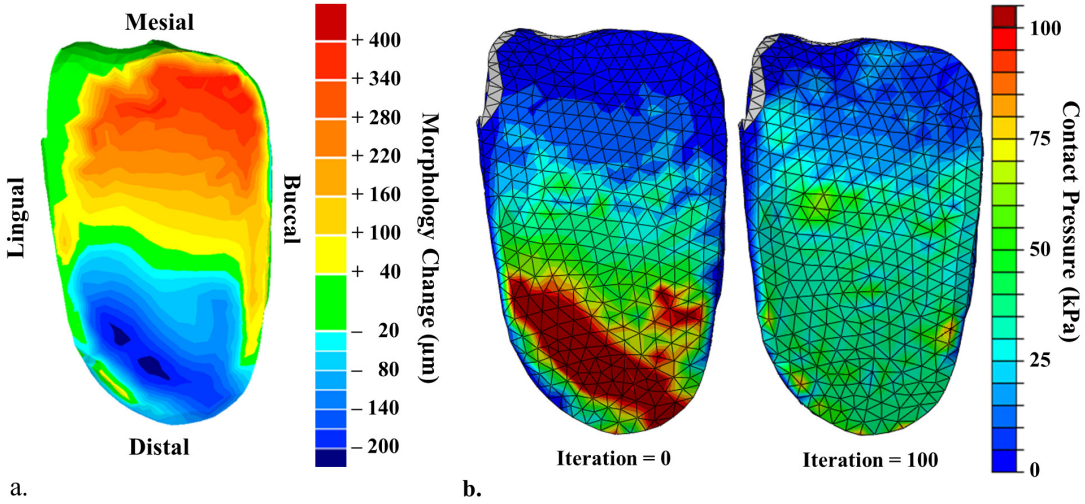

Figure 7-4 (a) The modification made to the denture base through the evolutionary shape optimisation with an adaptive modification rate; the maximum material deposition and removal are 382 and 224 um respectively; (b) The contact pressure contours on the initial denture base (left) and the optimized denture base (right).

Figure 7-4b shows the contact pressure contours on the denture base before and after the optimisation, which clearly exhibit the reduction of pressure concentration severity and improvement in its uniformity. The initial high pressure region is largely redistributed more uniformly over the entire contact region. It is seen that not just the mesial area, but also the edges of the denture base achieve the improved contact conditions after the optimisation, allowing more effective and smoother load transfer to the mucosa.

7.3.3 in vitro Loading Test

Figure 7-5a shows the prototyped jaw (upper) alone and with the optimal denture fitted (lower). Figure 7-5b illustrates the loading setup for the *in vitro* test, and in this figure, the pressure film was inserted between the jaw model and the denture prototype.

The *in vitro* test aimed only to verify the effectiveness of the shape optimisation and additive fabrication for these models.

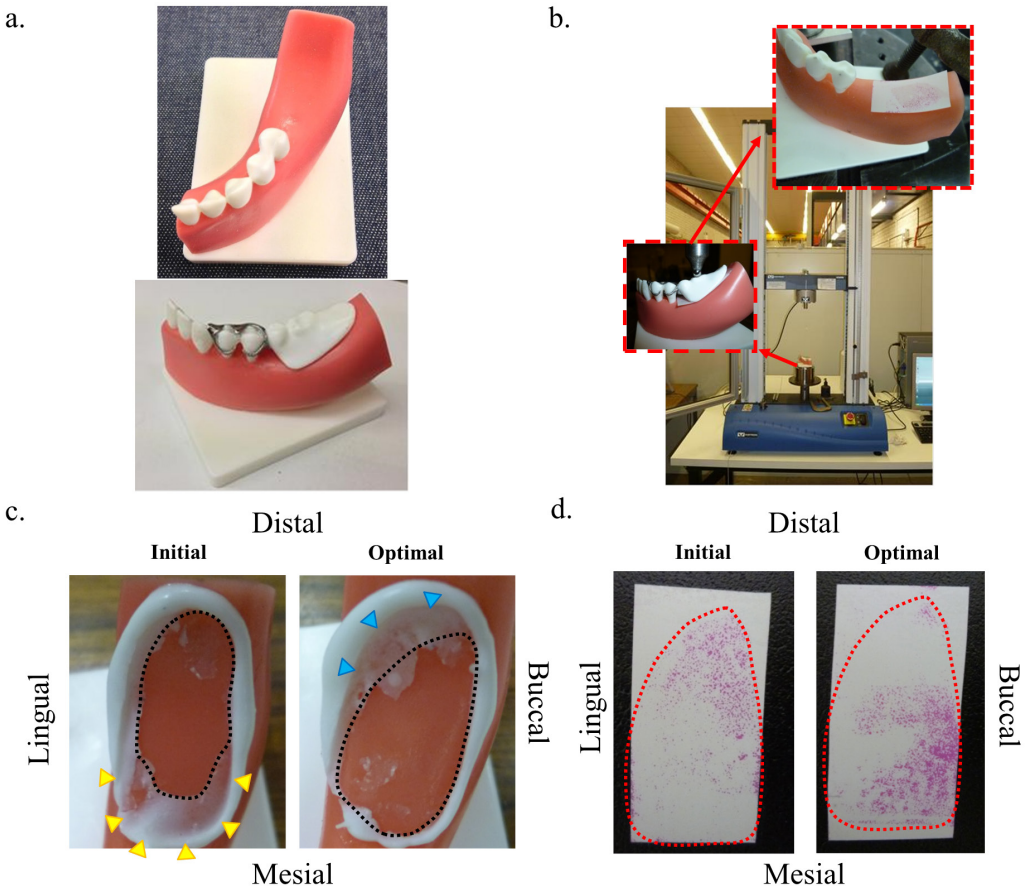

Figure 7-5 Prototypes and in vitro test. a) The subject jaw model (upper) and the optimized denture (lower); b) in vitro loading test performed under Instron, with a pressure sensitive firm between the denture and the jaw; c) the fitting white silicone test; d) the pressure sensitive film test.

The white silicone fitting outcomes are shown in Figure 7-5c, and a tight contact in this test squeezed silicone out to create a blank area (black dash line) under loading. In the initial denture, a medium layer of silicone indicated insufficient use on the mesial end, as highlighted by the yellow triangles. Through optimisation, the supportive contact area was expanded in the mesial direction, while some distal areas became less effective, indicated by the blue triangles, in these models. Consistent trends were observed with the pressure sensitive film test in Figure 7-5d. The initial denture led to stress concentration at the distal end, and this load was re-distributed towards the mesial direction through the optimisation.

7.4 Discussion

The oral mucosa, being a supportive tissue, is found to be mechanically and physiologically responsive to functional pressure during mastication. While the biomechanics underpinning its behaviour is not fully understood [60], previous research has revealed that high contact pressure can trigger pain in the oral mucosa [27, 61, 62]. To quantify this, a pressure-pain threshold (PPT) relationship was defined as a lowest pressure that causes pain, which links the objective stimulus (contact pressure) to the subjective response (pain). The validity and reliability of this *in vivo* approach using pressure algometers have been developed [60, 63], showing a positive outcome associated with this technique.

Figure 7-6a compares the maximum contact pressure obtained from clinical PPT data reported in the literature along with our FE modelling. All the literature data showed a moderate range of standard deviations, which reflects the consistency and reliability of using the pressure algometers in the individual tests [60, 63]. As Ogimoto et al. suggested, PPT depends on the loading rate; and slower loading rates generally result in the lowest threshold [60], which agrees with other *in vivo* studies [61, 63]. The mucosa is a fluid-rich tissue and its viscoelasticity generates nonlinear responses, in which a faster impact stiffens the tissue and develops higher pressures [13, 49, 50, 64, 65]. For a conservative estimate of pressure, all literature data adopted in Figure 7-6a were tested under a low loading rate less than 0.05N/sec.

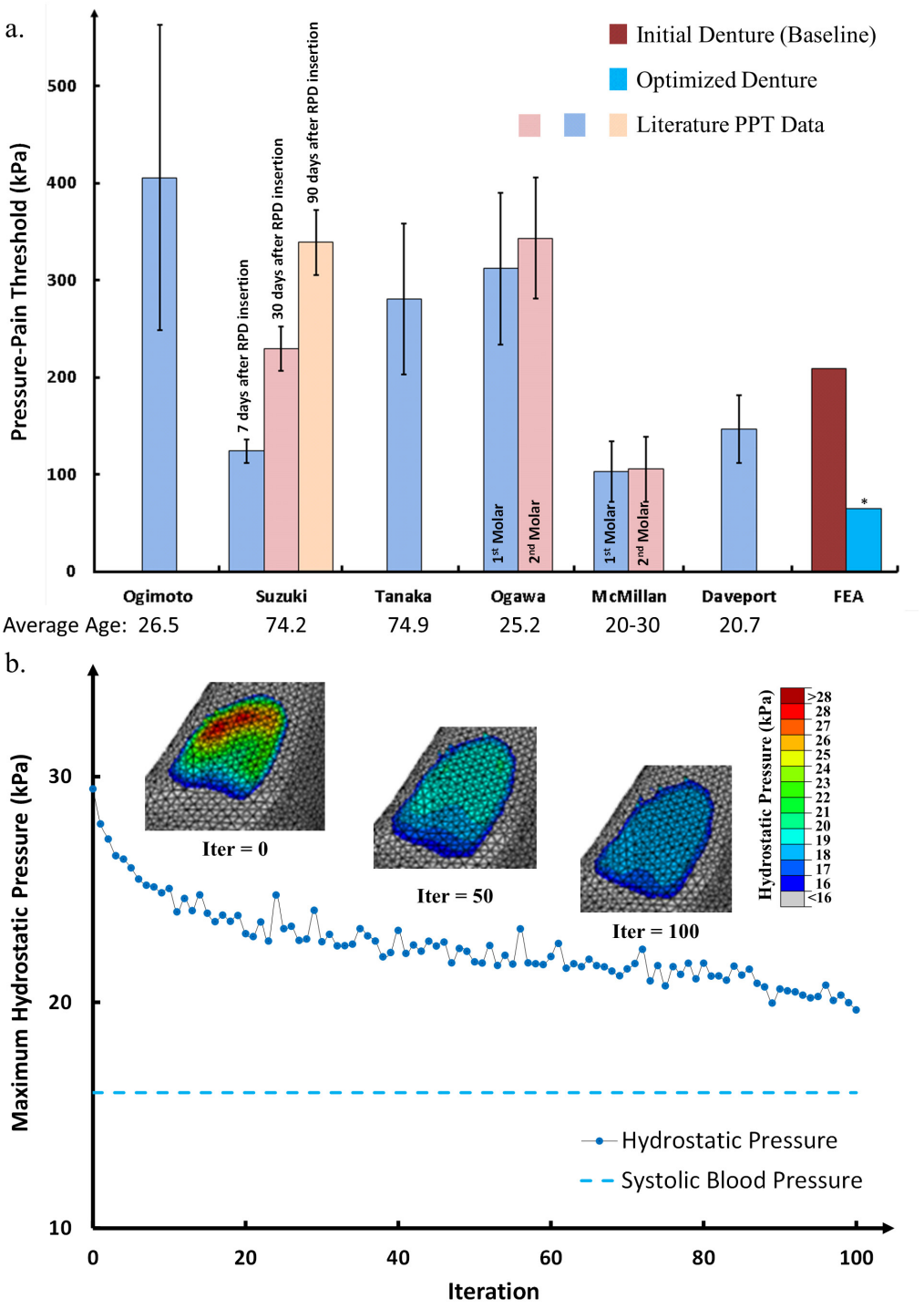

Figure 7-6 (a) The maximum contact pressures induced by both initial and optimised dentures are compared to clinical pressure-pain thresholds (PPTs) over the distal region of the mandible. The maximum contact pressure (*) under the optimised denture is significantly lower than available PPTs from literature ($p < 0.01$). (b) Hydrostatic pressure induced by the removable partial denture insertion through the optimisation procedure, which indicates the reduction of disturbance severity to the blood circulation.

Other factors, such as loading position [60, 61, 66, 67] and pre-loading history [6] [20], also affect PPT. We considered that the distal region is of major interest in the location of RPD. A short-term loading history caused insignificant change in PPT [6], but the tolerance ramps up with longer loading time [20]. Age is another factor, and it may influence PPT. A general trend indicates that younger people have higher PPT, whereas the oral mechanosensitivity was found to decrease with age [68] though exceptions were found in both young and old age groups [20, 61]. For this reason, data from various age groups have been shown in Figure 7-6a.

Although the initial FE denture model (baseline) provides a 'perfect' morphological match to the mucosa, the maximum contact pressure (209.2 kPa) lies in the mid-range of PPTs. After the optimisation, the maximum contact pressure is reduced by nearly 70% to 65.6 kPa, which falls well below most PPTs ($p < 0.01$, ANOVA [69]).

Apart from the immediate pain and discomfort, the long term concern with high contact pressure is the consequential bone resorption, caused by raised interstitial fluid pressure (IFP) or hydrostatic pressure [15, 17, 18]. The aging edentulous mandible is mainly supported by the periosteal plexus of blood vessels and therefore are very sensitive to a diminished level of circulation under occlusal load, resulting in reduced nutrient supply to and metabolite removal from the supporting mandibular bone [70]. The resultant hydrostatic pressure, which may exceed the local systolic pressure, disturbs local blood supply to the surrounding periosteal tissue, potentially leading to bone resorption [21]. Experimental observations have shown that 50 kPa pressure can reduce the blood flow rate to only 21% within 5 seconds, and further reduction to 15% after 30 seconds [71]. The recovery time can be four times longer than the loading time, and the ratio of biting to recovering time increases with more frequent mastication [71]. The continuously loaded epithelial cells and surrounding tissues, undergoing an inflammatory response, contribute

to a variation in permeability of the mucosal tissue, and further compromising circulation [49, 72]. More recent studies have shown that hydrostatic pressure controls osteogenesis and osteoclastogenesis [73, 74], and bone resorption has been observed at high hydrostatic pressure regions under certain types of dentures [14].

Figure 7-6b shows the hydrostatic pressure distribution on the mucosa through the optimisation process. The maximum hydrostatic pressure was 29.5 kPa for the initial denture, and it decreased to 19.6 kPa (33.5% reduction) after optimisation, where the green-red colour (medium to severe disturbance) disappears. More importantly, the distribution has become more uniform on the residual ridge and along both mesial-distal and lingual-buccal directions, indicated by the expanded light blue (low disturbance) regions. The magnitude of the hydrostatic pressure indicates the severity of induced disturbance to local blood circulation, and shows in the above figure that the initial high disturbance along the lingual side is eased and more evenly disturbed over the entire contact surface with optimisation. Within the defined contact area and the maximum voluntary occlusal force, the average pressure cannot decrease below the systolic pressure (16 kPa). Further expanding the contact area or modifying the denture fixation design may more effectively reduce the hydrostatic pressure to a lower level; these alternative approaches are the basis for further study.

The conventional fabrication method has shown its effectiveness with clinical predictability for more than a century [75]. With the growing aging group and the increasing demand for denture treatments [2, 76], this approach is facing severe challenges because of its labour-intensive nature, especially with the shortage of dentists and dental laboratory staff [76]. Its disadvantages are being gradually exposed, such as the need for a minimum of 4 or 5 treatment visits with additional post-insertion follow-ups, high laboratory expenses and time cost, lack of intimate iteration with soft tissues, and reliance

on technique and experience [38]. The proposed computer based optimisation and additive fabrication procedure may ameliorate these downsides with quantitative guidelines, customized optimal treatment, standardized accuracy, reliable reproducibility, and reduced cost, through a computationally automatic process of scan-design-manufacturing.

Apart from BESO, there may be other shape optimisation algorithms available to minimize contact stress concentration. From a design perspective, configuration with softer or stiffer materials has also been applied in the modification for denture adaptation [77], and gradient materials may have potential to provide further improved pressure contours over the contact morphology. While the effectiveness of these methods is worth testing for comparison; it is beyond the scope of this study.

3D additive manufacturing for multiple materials was adopted in the prototyping stage. The prototypes have a certain manufacturing error involving thermal shrinkage, relative low resolution (16μm) and differences between real human oral tissue and printable surrogate materials in the jaw model. The *in-vitro* validation tests were performed with such prototype models and the results of the contact conditions could have been affected. Nevertheless, this study showcased a feasible new approach from diagnosed scan, computational design to additive manufacturing of removable partial dentures (RPD), thereby providing technological potential for other dental prosthetic treatments in the future.

7.5 Conclusions

This study proposed a fully automatic design optimisation and additive fabrication procedure for removable partial dentures (RPD). The bi-directional evolutionary structural optimisation (BESO) technique was revised to accommodate contact optimisation problems, in which the material is removed from the high contact pressure region to lessen the stress concentration and added to under-loaded regions to enhance loading-bearing capacity. In this study, the contact pressure is related to the pressure-pain threshold (PPT) associated with patients' denture usage. It is found that the optimized denture base is able to deliver a more even pressure distribution and reduce the pressure well below all PPTs available from clinical studies in the literature (with sufficient statistical significance). More importantly, the overloaded region was largely reduced via the optimisation and a lower hydrostatic pressure was generated, which could potentially reduce associated long term bone resorption. This proposed computational contact optimisation and additive fabrication procedure is of considerable promise for other dental prostheses, thereby providing quantitative guidelines and computer aided design and manufacturing in the dental clinic for an individual patient.

Acknowledgement

This work is supported by Australian Research Council (ARC) and Australian Postgraduate Award (APA).

7.6 References

1. Klemetti, E., *A review of residual ridge resorption and bone density.* Journal of Prosthetic Dentistry, 1996. **75**(5): p. 512-514.
2. Ozan, O., et al., *The Effect of Removable Partial Dentures on Alveolar Bone Resorption: A Retrospective Study with Cone-Beam Computed Tomography.* Journal of Prosthodontics-Implant Esthetic and Reconstructive Dentistry, 2013. **22**(1): p. 42-48.
3. Field, C., et al., *Prediction of mandibular bone remodelling induced by fixed partial dentures.* Journal of Biomechanics, 2010. **43**(9): p. 1771-1779.
4. Carlsson, G.E., *Responses of jawbone to pressure.* Gerodontology, 2004. **21**(2): p. 65-70.
5. Isobe, A., et al., *The influence of denture supporting tissue properties on pressure-pain threshold: –Measurement in dentate subjects–.* Journal of Prosthodontic Research, 2013. **57**(4): p. 275-283.
6. Ogawa, T., et al., *Pressure-pain threshold of oral mucosa and its region-specific modulation by pre-loading.* Journal of Oral Rehabilitation, 2003. **30**(11): p. 1062-1069.
7. Kuo, H.C., et al., *The association of responsiveness in oral and general health-related quality of life with patients' satisfaction of new complete dentures.* Quality of Life Research, 2013. **22**(7): p. 1665-1674.
8. Bae, K.H., et al., *A comparison of oral health related quality of life between complete and partial removable denture-wearing older adults in Korea.* Journal of Oral Rehabilitation, 2006. **33**(5): p. 317-322.
9. Celebic, A., et al., *The patient's and the therapist's evaluation of complete denture therapy.* Collegium Antropologicum, 2000. **24**: p. 71-77.
10. Tallgren, A., *Alveolar bone loss in denture wearers as related to facial morphology.* Acta Odontol Scand, 1970. **28**(2): p. 251-70.
11. Wright, P.S., et al., *The effects of fixed and removable implant-stabilised prostheses on posterior mandibular residual ridge resorption.* Clinical Oral Implants Research, 2002. **13**(2): p. 169-174.
12. Kydd, W.L., C.H. Daly, and D. Nansen, *Variation in the response to mechanical stress of human soft tissues as related to age.* Journal of Prosthetic Dentistry, 1974. **32**(5): p. 493-500.
13. Sawada, A., et al., *Viscoelasticity of Human Oral Mucosa: Implications for Masticatory Biomechanics.* Journal of Dental Research, 2011. **90**(5): p. 590-595.
14. Ahmad, R., et al., *Three dimensional quantification of mandibular bone remodeling using standard tessellation language registration based superimposition.* Clin Oral Implants Res, 2013. **24**(11): p. 1273-1279.
15. Mori, S., et al., *Effect of continuous pressure on histopathological changes in denture-supporting tissues.* Journal of Oral Rehabilitation, 1997. **24**(1): p. 37-46.

16. Sato, T., et al., *Threshold for bone resorption induced by continuous and intermittent pressure in the rat hard palate.* Journal of Dental Research, 1998. **77**(2): p. 387-392.

17. Imai, Y., et al., *A histomorphometric analysis on bone dynamics in denture supporting tissue under continuous pressure.* J Oral Rehabil, 2002. **29**(1): p. 72-9.

18. Blum, I.R. and J.F. McCord, *A clinical investigation of the morphological changes in the posterior mandible when implant-retained overdentures are used.* Clinical Oral Implants Research, 2004. **15**(6): p. 700-8.

19. Hara, T., et al., *Effect of occlusal pressure on the histopathological changes in denture supporting tissues.* Journal of Oral Rehabilitation, 1996. **23**(6): p. 363-371.

20. Suzuki, Y., et al., *Pressure pain threshold of mucosa after tooth extraction under removable denture bases.* The European journal of prosthodontics and restorative dentistry, 2011. **19**(4): p. 184-6.

21. Maruo, Y., et al., *Stress distribution prevents ischaemia and bone resorption in residual ridge.* Archives of Oral Biology, 2010. **55**(11): p. 873-878.

22. Saito, M., et al., *Stress distribution of abutments and base displacement with precision attachment- and telescopic crown-retained removable partial dentures.* Journal of Oral Rehabilitation, 2003. **30**(5): p. 482-487.

23. Lee, C.-J., et al., *Comparative adaptation accuracy of acrylic denture bases evaluated by two different methods.* Dental Materials Journal, 2010. **29**(4): p. 411-417.

24. Laughlin, G.A., et al., *A comparison of palatal adaptation in acrylic resin denture bases using conventional and anchored polymerization techniques.* Journal of Prosthodontics, 2001. **10**(4).

25. Rodrigues, R.C.S., et al., *Retention and stress distribution in distal extension removable partial dentures with and without implant association.* Journal of prosthodontic research, 2013. **57**(1): p. 24-9.

26. Liebenberg, W.H., *Removable partial denture abutment restoration: a case report illustrating a new direct technique.* Quintessence Int, 1995. **26**(3): p. 175-9.

27. Kubo, K., et al., *Development of in vivo measuring system of the pressure distribution under the denture base of removable partial denture.* Journal of prosthodontic research, 2009. **53**(1): p. 15-21.

28. Kanbara, R., et al., *Three-dimensional finite element stress analysis: The technique and methodology of non-linear property simulation and soft tissue loading behavior for different partial denture designs.* Dental Materials Journal, 2012. **31**(2): p. 297-308.

29. Wang, H.-y., et al., *Effects of rigid and nonrigid extracoronal attachments on supporting tissues in extension base partial removable dental prosthesis: a nonlinear finite element sutdy.* Journal of Prosthetic Dentistry, 2011. **105**(5): p. 338-346.

30. Archangelo, C.M., et al., *Periodontal ligament influence on the stress distribution in a removable partial denture supported by implant: a finite element analysis.* Journal of Applied Oral Science, 2012. **20**(3): p. 362-368.

31. Muraki, H., et al., *Finite element contact stress analysis of the RPD abutment tooth and periodontal ligament.* Journal of Dentistry, 2004. **32**(8): p. 659-665.

32. Li, W., et al., *An evolutionary approach to elastic contact optimization of frame structures.* Finite Elements in Analysis and Design, 2003. **40**(1): p. 61-81.

33. Li, W., et al., *An evolutionary shape optimization for elastic contact problems subject to multiple load cases.* Computer Methods in Applied Mechanics and Engineering, 2005. **194**(30-33): p. 3394-3415.

34. Li, W., et al., *An evolutionary shape optimization procedure for contact problems in mechanical designs.* Proceedings of the Institution of Mechanical Engineers Part C-Journal of Mechanical Engineering Science, 2003. **217**(4): p. 435-446.

35. Li, Q., et al., *Evolutionary shape optimization for stress minimization.* Mechanics research communications, 1999. **26**(6): p. 657-664.

36. Li, Q., et al., *Stress based optimization of torsional shafts using an evolutionary procedure.* International Journal of Solids and Structures, 2001. **38**(32-33): p. 5661-5677.

37. Chang, C.C., M.Y. Lee, and S.H. Wang, *Digital denture manufacturing-An integrated technologies of abrasive computer tomography, CNC machining and rapid prototyping.* International Journal of Advanced Manufacturing Technology, 2006. **31**(1-2): p. 41-49.

38. Bidra, A.S., T.D. Taylor, and J.R. Agar, *Computer-adided technology for fabricating complete dentures: systematic review of historical background, current status, and future perspectives.* Journal of Prosthetic Dentistry, 2013. **109**(6): p. 361-366.

39. Butscher, A., et al., *New depowdering-friendly designs for three-dimensional printing of calcium phosphate bone substitutes.* Acta Biomaterialia, 2013. **9**(11): p. 9149-9158.

40. Butscher, A., et al., *Structural and material approaches to bone tissue engineering in powder-based three-dimensional printing.* Acta Biomaterialia, 2011. **7**(3): p. 907-920.

41. Li, W., et al., *Fibre reinforced composite dental bridge. Part II: numerical investigation.* Biomaterials, 2004. **25**(20): p. 4995-5001.

42. Li, W., et al., *Towards automated 3D finite element modeling of direct fiber reinforced composite dental bridge.* Journal of Biomedical Materials Research Part B: Applied Biomaterials, 2005. **74B**(1): p. 520-528.

43. Chen, J., et al., *Multiscale design of surface morphological gradient for osseointegration.* Journal of the Mechanical Behavior of Biomedical Materials, 2013. **20**: p. 387-97.

44. Li, W., et al., *Computational Biomechanics of Bone's Responses to Dental Prostheses - Osseointegration, Remodeling and Resorption*, in *9th World Congress on Computational Mechanics and 4th Asian Pacific Congress on Computational Mechanics*, N. Khalili, et al., Editors. 2010.

45. Rungsiyakull, C., et al., *Surface morphology optimization for osseointegration of coated implants.* Biomaterials, 2010. **31**(27): p. 7196-7204.

46. Sato, Y., et al., *Finite element analysis of stress relaxation in soft denture liner.* Journal of Oral Rehabilitation, 2000. **27**(8): p. 660-663.

47. Zaw, K., et al., *Rapid identification of elastic modulus of the interface tissue on dental implants surfaces using reduced-basis method and a neural network.* Journal of Biomechanics, 2009. **42**(5): p. 634-641.

48. Carter, D.R. and W.C. Hayes, *Compressive Behaviour of Bone as a 2-Phase Porous Structure.* Journal of Bone and Joint Surgery-American Volume, 1977. **59**(7): p. 954-962.

49. Kydd, W.L. and C.H. Daly, *The biologic and mechanical effects of stress on oral mucosa.* Journal of Prosthetic Dentistry, 1982. **47**(3): p. 317-29.

50. Kishi, M., *Experimental studies on the relation between area and displacement of loading surfaces in connection with displaceability in the mucosa of edentulous alveolar ridge under pressure.* Shika gakuho. Dental science reports, 1972. **72**(6).

51. Bergomi, M., et al., *Hydro-mechanical coupling in the periodontal ligament: A porohyperelastic finite element model.* Journal of Biomechanics, 2011. **44**(1): p. 34-38.

52. Itoh, H., et al., *Effects of periodontal support and fixed splinting on load transfer by removable partial dentures.* The Journal of Prosthetic Dentistry, 1998. **79**(4): p. 465-471.

53. Prinz, J.F., R.A. de Wijk, and L. Huntjens, *Load dependency of the coefficient of friction of oral mucosa.* Food Hydrocolloids, 2007. **21**(3): p. 402-408.

54. Sajewicz, E., *Effect of saliva viscosity on tribological behaviour of tooth enamel.* Tribology International, 2009. **42**(2): p. 327-332.

55. Hart, R.T., et al., *Modeling the Biomechanics of the Mandible - a 3-Dimensional Finite-Element Study.* Journal of Biomechanics, 1992. **25**(3): p. 261-286.

56. Korioth, T.W.P., D.P. Romilly, and A.G. Hannam, *3-Dimensional Finite Element Stress-Analysis of the Dentate Human Mandible.* American Journal of Physical Anthropology, 1992. **88**(1): p. 69-96.

57. Huang, X. and Y.M. Xie, *Convergent and mesh-independent solutions for the bi-directional evolutionary structural optimization method.* Finite Elements in Analysis and Design, 2007. **43**(14): p. 1039-1049.

58. Rozvany, G.I.N., *A critical review of established methods of structural topology optimization.* Structural and Multidisciplinary Optimization, 2009. **37**(3): p. 217-237.

59. Inokoshi, M., M. Kanazawa, and S. Minakuchi, *Evaluation of a complete denture trial method applying rapid prototyping.* Dental Materials Journal, 2012. **31**(1): p. 40-46.

60. Ogimoto, T., et al., *Pressure-pain threshold determination in the oral mucosa: validity and reliability.* Journal of Oral Rehabilitation, 2002. **29**(7): p. 620-626.

61. McMillian, A.S., *Pain-pressure threshold in human gingivae.* Journal of Orofacial Pain, 1995. **9**(1): p. 44-50.

62. Davenpor, J.C., *Pressure-pain thresholds in oral cavity in man.* Archives of Oral Biology, 1969. **14**(11): p. 1267-&.

63. List, T., M. Helkimo, and R. Karlsson, *Influence of pressure rates on the reliability of a pressure threshold meter.* Journal of Craniomandibular Disorders, 1991. **5**(3): p. 173-178.

64. Scapino, R.P., *Biomechanics of Prehensile Oral Mucosa.* Journal of Morphology, 1967. **122**(2): p. 89-&.

65. Wakabayashi, N. and T. Suzuki, *Patient-specific finite element analysis of viscoelastic masticatory mucosa.* Journal of dental biomechanics, 2013. **4**.

66. Ogawa, T., et al., *Mapping, profiling and clustering of pressure pain threshold (PPT) in edentulous oral mucosa.* Journal of Dentistry, 2004. **32**(3): p. 219-228.

67. Tanaka, M., et al., *Denture wearing and strong bite force reduce pressure pain threshold of edentulous oral mucosa.* Journal of Oral Rehabilitation, 2004. **31**(9): p. 873-878.

68. Teranaka, S., et al., *Age-related changes in oral mechanosensitivity of symptom-free subjects.* Journal of medical and dental sciences, 2008. **55**(1): p. 61-9.

69. Mycroft, R.H., D.C. Mitchell, and J. Kay, *An evaluation of statistical procedures for comparing an individual's performance with that of a group of controls.* Cognitive Neuropsychology, 2002. **19**(4): p. 291-299.

70. Bradley, J.C., *The clinical significance of age changes in the vascular supply to the mandible.* International Journal of Oral Surgery, 1981. **10**: p. 71-76.

71. Akazawa, H. and K. Sakurai, *Changes of blood flow in the mucosa underlying a mandibular denture following pressure assumed as a result of light clenching.* Journal of Oral Rehabilitation, 2002. **29**(4): p. 336-340.

72. Ashton, H., *Effect of increased tissue pressure on blood flow.* Clinical Orthopaedics and Related Research, 1975(113): p. 15-26.

73. Kim, S.H., et al., *Hydrostatic Pressure can Control Osteogenesis and Osteoclastogenesis when Stromal Cells and Osteoclast Precursor Cells are Cocultured.* Tissue Engineering and Regenerative Medicine, 2010. **7**(4): p. 388-394.

74. Aspenberg, P. and H. van der Vis, *Fluid pressure may cause periprosthetic osteolysis - Particles are not the only thing.* Acta Orthopaedica Scandinavica, 1998. **69**(1): p. 1-4.

75. Jacob, R.F., *The traditional therapeutic paradigm: Complete denture therapy.* Journal of Prosthetic Dentistry, 1998. **79**(1): p. 6-13.

76. Hill, E.E. and L.C. Breeding, *Who Is Teaching Undergraduate Prosthodontics in US Dental Schools, 2007?* Journal of Prosthodontics-Implant Esthetic and Reconstructive Dentistry, 2009. **18**(2): p. 195-198.

77. Kocabalkan, E. and M. Turgut, *Variation in blood flow of supporting tissue during use of mandibular complete dentures with hard acrylic resin base and soft relining: A preliminary study.* International Journal of Prosthodontics, 2005. **18**(3): p. 210-213.

Chapter 8: A Periodontal Ligament Driven Remodelling Algorithm for Orthodontic Tooth Movement

While orthodontic tooth movement (OTM) gains considerable popularity and clinical success, the roles played by relevant tissues involved, particularly periodontal ligament (PDL), remain an open question in biomechanics. This study develops a soft-tissue induced external (surface) remodelling procedure in a form of power law formulation by correlating time-dependent simulation *in-silico* with clinical data *in-vivo* (p<0.05), thereby providing a systematic approach for further understanding and prediction of OTM. The biomechanical stimuli, namely hydrostatic stress and displacement vectors experienced in PDL, are proposed to drive tooth movement through an iterative hyperelastic finite element analysis (FEA) procedure. This algorithm was found rather indicative and effective to simulate OTM under different loading conditions, which is of considerable potential to predict therapeutical outcomes and develop a surgical plan for sophisticated orthodontic treatment.

Associated Publications:

1. Junning Chen, Wei Li, Michael V. Swain, Ali M. Darendeliler, and Qing Li. **A periodontal ligament driven remodeling algorithm for orthodontic tooth movement**. *Journal of biomechanics*, 2014. 47(7): p. 1689-1695.

8.1 Introduction

Orthodontic tooth movement (OTM) is based upon the ability of periodontal ligament (PDL) reaction to appropriate mechanical loading for a remodelling process within dental alveolar bone. OTM relies on a complex set of mechanical stimuli that triggers specific biological reactions in the tissues around the targeted tooth, thereby moving the tooth to a more desired position [1]. The 'pressure-tension theory' [2, 3] suggests that tooth movement is a consequence of generating mechanical compression on one side of PDL for bone resorption, and tension on the other side for bone apposition [3], in which normal strain in PDL was taken as the mechanical stimulus. The studies confirmed the critical role played by PDL [4, 5], which enabled the evaluation of clinical outcomes under a range of orthodontic forces. Nevertheless, the biomechanics behind OTM remains an open question.

Finite element (FE) methods have shown compelling advantages in biomechanical analysis for OTM process [2, 6, 7], which allows incorporating anatomical, physiological, heterogeneous variance of individuals [3]. Middleton et al. (1996), Boucauel et al. (1999, 2000) and others [8] pointed out that the mechanical stimuli within PDL were more relevant to OTM than those in the surrounding bones, as the mechanical responses to orthodontic force in alveolar bone are far below typical thresholds for remodelling to occur. With advances in clinical computerized tomography (CT), sophisticated 3D FE models can be created to precisely quantify biomechanical responses to the initial application of orthodontic force. However, it remains under-studied as to the understanding of how such responses change during tooth movement and how to simulate OTM in a time-dependent fashion.

This article aims to address the abovementioned issues through developing an iterative FE procedure driven by a new remodelling rule, in which hydrostatic stress within

the PDL and the resultant interfacial displacement are considered as remodelling stimuli to account for tooth movement. To determine the remodelling parameters, the proposed remodelling simulation is correlated with the clinical data. The remodelling procedure established enables us to gain biomechanical insights into the time-dependent process and explore the effects of different orthodontic loading *in silico*.

8.2 Materials and Methods

8.2.1 Clinical Data Acquisition

14 healthy teenagers (5 boys, 9 girls; mean age, 15.8 years; range from 13.0 to 19.5 years old) who required bilateral extraction of the maxillary first premolars and retraction of the maxillary canines during their orthodontic treatment were recruited. All subjects and their parents or guardians consented to participation after receiving verbal and written explanations (ethics approval: SSWAHS X06-0062 and EK: 358). All the participants had no previous orthodontic or orthopedic treatment histories, no craniofacial anomalies, no previously reported or observed dental treatment on the canine, or any existing medical conditions. After a minimum 3-month consolidation of post-extraction, the distal retraction of maxillary canines was performed with a force of either 0.5 N (namely 50 grams in orthodontics, a light force) or 3.0 N (300 grams, a heavy force) for each subject, respectively. Measurements were made from the orthodontic impression moulds every 28 days from beginning of canine retraction and 4 impressions per patient were obtained at different time points for assessments.

8.2.2 Finite Element Modelling

CT images (in DICOM format) were captured on one average subject (0.2 mm per pixel resolution) through standard orthodontic measurement. The images were segmented in ScanIP 4.3 (Simpleware Ltd, Exeter UK) (Figure 8-1a). Masks of teeth, PDLs, cortical bone, and cancellous bone were created based on their respective Hounsfield unit (HU) (Figure 8-1b). Half of the maxilla was set as the region of interest (ROI) for its approximate symmetry in the sagittal plane. 14 masks (STL format) were further processed in Rhinoceros 4.0 (Robert McNeel & Associates, Seattle USA), to create geometric models with free-form surfaces in non-uniform rational B-splines (NURBs) (Figure 8-1c). The

solidified models were imported to ABAQUS 6.9.2 (Dassault Systèmes, Tokyo Japan) as IGES files. The unstructured quadratic tetrahedral elements (C3D10H) were used to smoothly capture the anatomical sophistication with an adaptive mesh in a seed size of 2 mm, where mesh-refinement was applied to all 6 PDL regions involved (Figure 8-1d). Unlike an initial analysis, the remodelling required updating mesh to follow tooth movement. The average number of elements was 250,000, of which around 40,000 were dedicated to the PDLs. The mesh density was validated through a convergence test as per our previous studies [9, 10] .

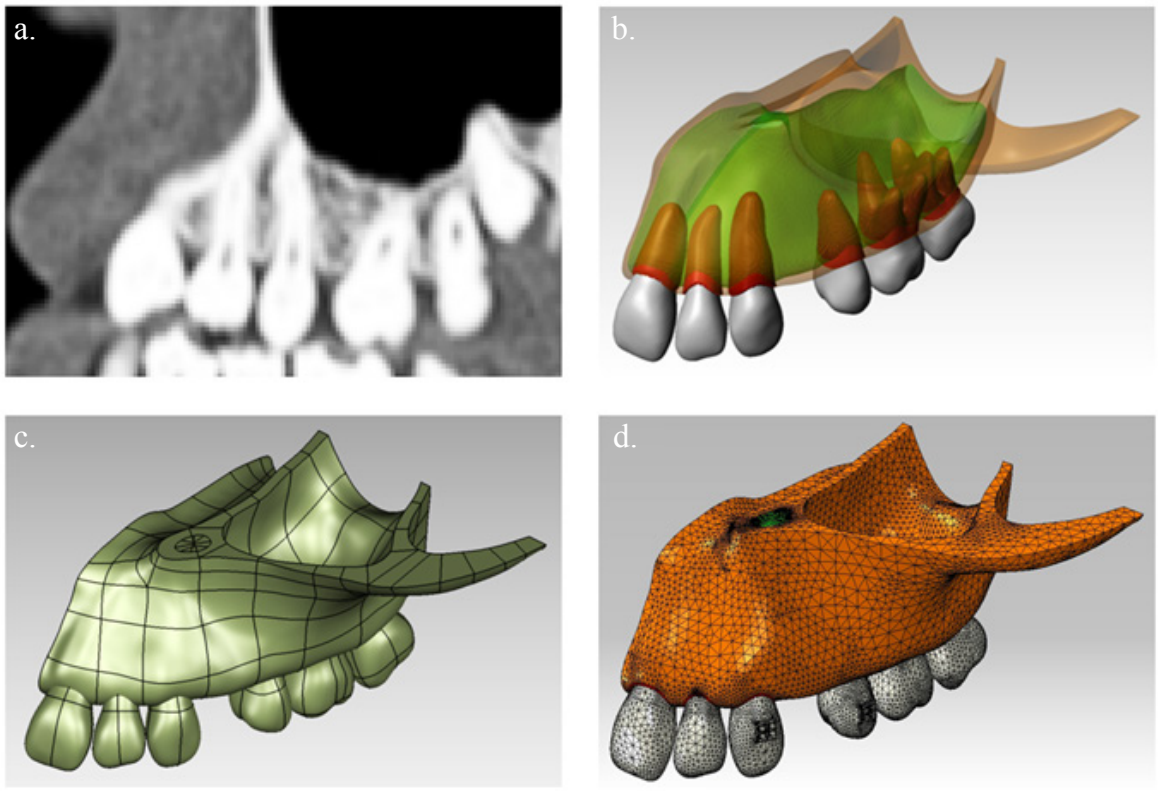

Figure 8-1 (a) CT images captured in DICOM format; (b) Masks created for each individual component in ScanIP; (c) NURBS surfaces created in Rhinoceros to form solidified geometric models; (d) Meshed FE models in ABAQUS for analysis

8.2.3 Material Property and Loading Scenario

The non-linear hyperelastic model was adopted for PDL by fitting the strain-stress curve [2], in which the strain energy potential equation (Marlow Model) was interpolated in ABAQUS. The retracted canine was simplified as a rigid body for its negligible deformation compared to PDL. Elastic properties (Table 1) were assigned to the remaining regions in the model [7, 11, 12].

Symmetric boundary conditions were prescribed to the sagittal plane; and full constraints were applied to the coronal and transverse sectional planes (Figure 8-2a). The orthodontic force (every 0.5 N from 0.5 N to 3 N, individually) was directly applied through the bracket on the canine surface, pointing towards the second premolar bracket (Figure 8-2b). The load direction kept updating step-wise but the magnitude remained constant to simulate an ideal orthodontic spring [13]. Other factors, such as friction and slipping in the arch wire, or variations in other teeth, have not been considered here for simplification.

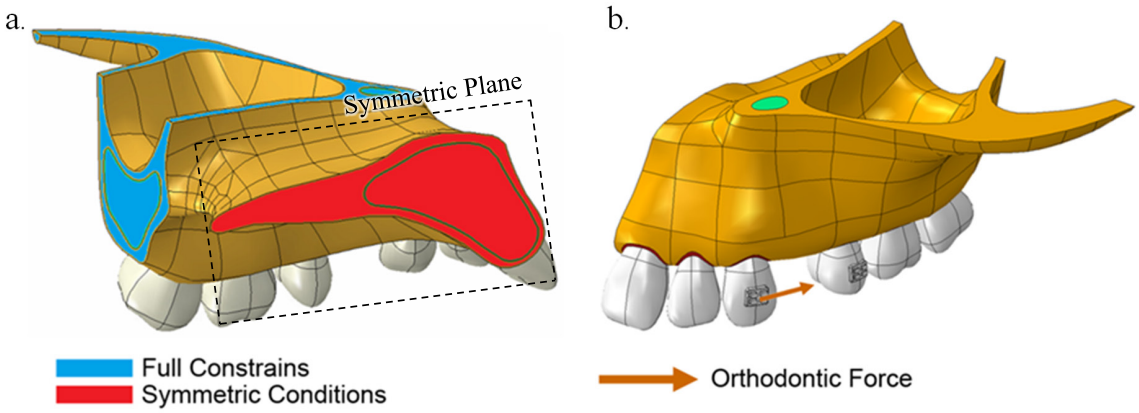

Figure 8-2 (a) Boundary conditions assigned to the final assembly; (b) orthodontic force applied onto the canine pointing towards the 2nd pre-molar

8.2.4 Mechanical Stimulus and Remodelling Algorithm

Physiologically, blood capillaries in the PDL region are exposed to stress and strain induced by orthodontic forces. A certain level of hydrostatic pressure σ_H (Eq. (1)) could

collapse capillaries partially or completely, affecting periodontal interstitial fluid [14] and causing dysfunction of PDL [11]. Therefore, sustained exposure to compression instigates osteoclast recruitment, leading to bone resorption on the compression side [15]. During orthodontic treatment, the volume-averaged hydrostatic pressure $\overline{\sigma}_H$ (Eq. (2)) in PDL indicates the degree of overall disturbance to blood supply [16, 17]. The previous studies showed that the capillary pressure varies in the root [18]. The upper range of capillary blood pressure, σ_L^* = 4.7 kPa (35 mmHg) [14, 19], was adopted here as a threshold to trigger the remodelling activities [11].

$$\sigma_H = \frac{1}{3}(\sigma_{xx} + \sigma_{yy} + \sigma_{zz}) \tag{1}$$

$$\overline{\sigma}_H = \frac{\sum_e \sigma_H^e V^e}{\sum_e V^e} \tag{2}$$

Furthermore, the localized PDL displacement at the interface between the tooth and PDL was considered to direct tooth movement [8, 15, 20], in which the unit vector **n** was computed as Eq. (3). In this equation, **u** was the nodal displacement and $\mathbf{u}^{\max}$ indicated the maximum. The unit vectors on the surface nodes preserved a constant tooth profile.

$$\mathbf{n} = \frac{\mathbf{u}}{|\mathbf{u}^{\max}|} \tag{3}$$

A power law model is proposed in Eq. (4) to determine tooth movement vector $\Delta\mathbf{d}$ over a time interval Δt [1, 21, 22], in which the hydrostatic pressure above the threshold σ_L^* quantifies the magnitude of tooth movement and the displacement vector determines the movement direction. Coefficient *a* and exponent *b*, in the formula, denote the remodelling parameters, determined by correlating with the clinical measurements using the least-square technique.

$$\Delta \mathbf{d} = \begin{cases} 0, & \text{if } \bar{\sigma}_H \le \sigma_L^* \\ a(\bar{\sigma}_H - \sigma_L^*)^b \mathbf{n} \cdot \Delta t, & \text{if } \bar{\sigma}_H > \sigma_L^* \end{cases} \quad (4)$$

8.2.5 Computer Simulation

Each loop of simulation consists of two steps. (1) The initial meshed model was assigned specific loading condition through ABAQUS pre-processing, followed by FE simulation in ABAQUS kernel, in which the mechanical stimulus is determined in post-processing; (2) If the stimulus is above the threshold, the tooth moves by the distance determined in Eq. (4). If the maximum number of loops (M = 12 weeks here) is not reached, the geometry of the model should be updated and a re-meshing be performed to assure the mesh quality for the next loop. This iterative procedure is depicted as a flowchart in Figure 8-3.

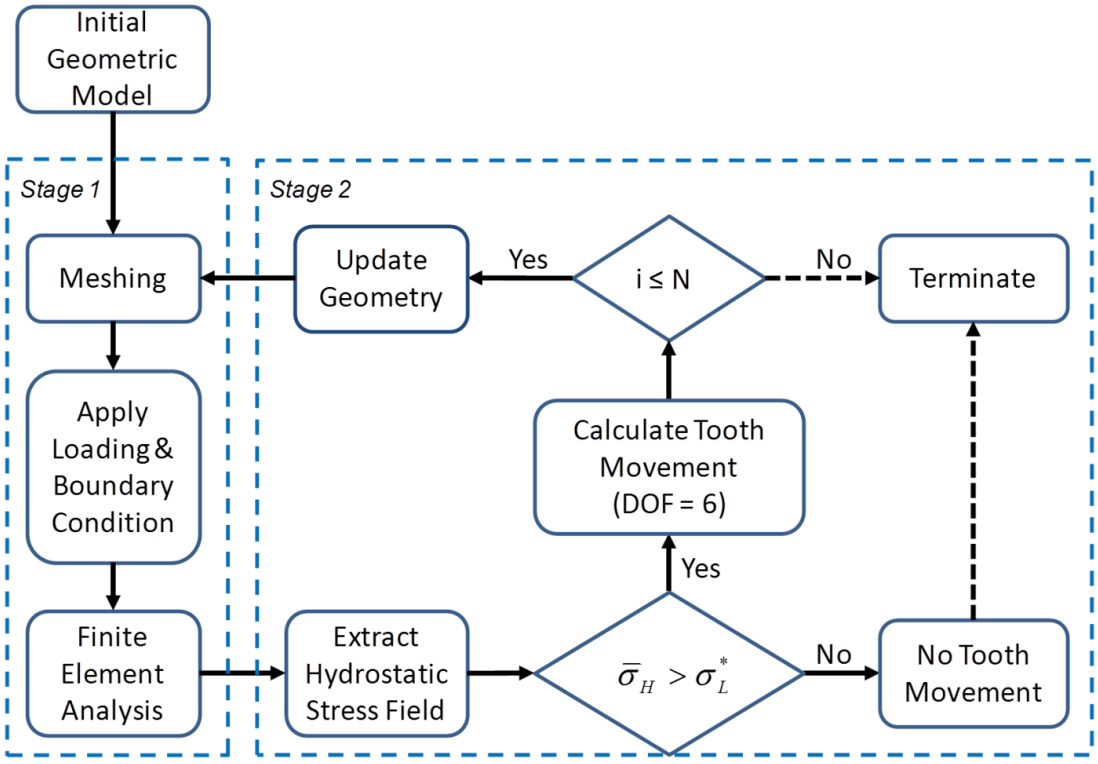

Figure 8-3 Flow chart of tooth movement algorithm consisting of two stages: (1) meshing, loading and finite element analysis; (2) hydrostatic stress, strain to determine tooth movement and update model geometry

The translation was measured at the tooth centroid, taken as the approximate centre of resistance (CR), as the physical CR kept changing as the tooth moved. The rotation was calculated around the central axis (CA) pointing from the apex to centre of canine cusp. The tipping angles were calculated from this CA relative to lingual and posterior directions on the transverse plane.

8.3 Results

8.3.1 Tooth Movement under Light Force (0.5 N)

As shown on the left side of Figure 8-4, clinical measurements were performed from the impression moulds at Weeks 0, 4, 8, and 12 for this average subject modeled under the light orthodontic force of 0.5 N. The right hand side images in Figure 8-4 are the snapshots of tooth movement simulated at the corresponding time points. Clinical and computational results exhibit very good agreement in translation towards the posterior direction.

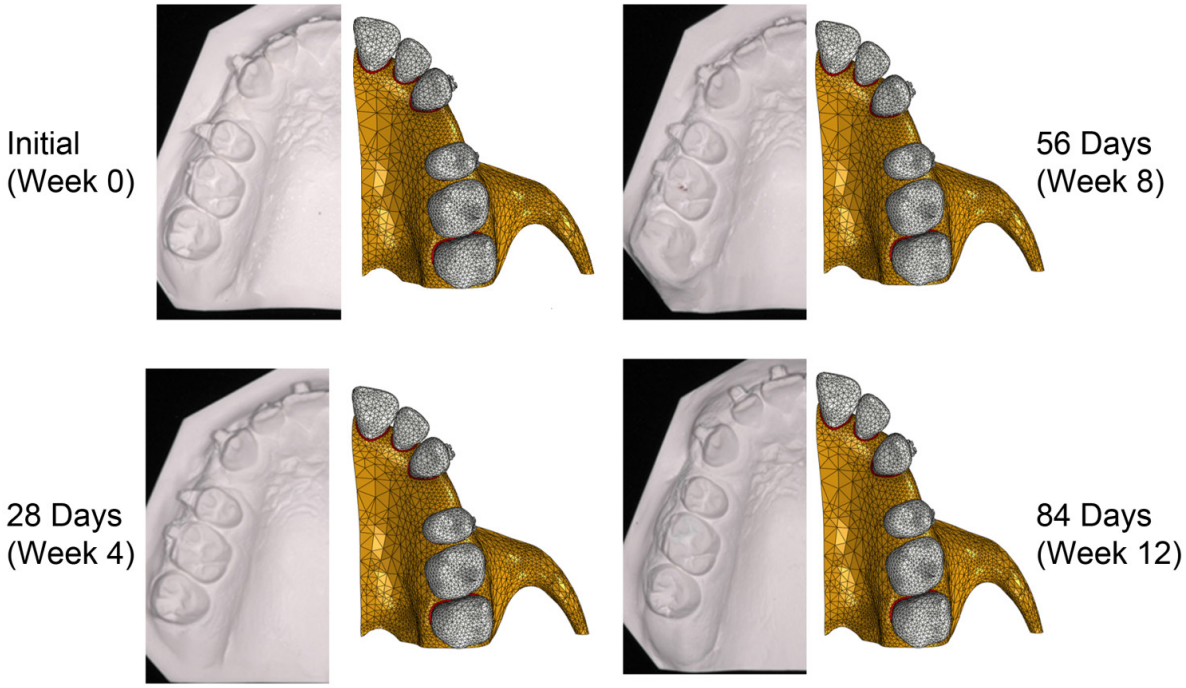

Figure 8-4 Visualisation of orthodontic tooth movement with correlation to clinical data at different time points (Initial, Week 4, Week 8, and Week 12)

The translational and rotational rates of movement are plotted against time in Figure 8-5 (a) and (b), respectively. The crosses on the blue dashed line indicate the average speed over every four-week interval (denoting in T1, T2, and T3 respectively) in our clinical study, and the error bars present the standard deviation of these 14 patients' data. The translation (normality test, $p < 0.001$) slowed down from 0.175 ± 0.094

mm/week in T1 to 0.143 ± 0.072 mm/week in T2, and remains almost constant in T3 (0.148 ± 0.083 mm/week). The rotational speeds also slowed down from 0.323 ± 0.543 °/week (normality test, $p < 0.05$) in T1, to 0.073 ± 0.255 °/week and 0.063 ± 0.178 °/week in T2 and T3 (normality test, $p < 0.001$), respectively.

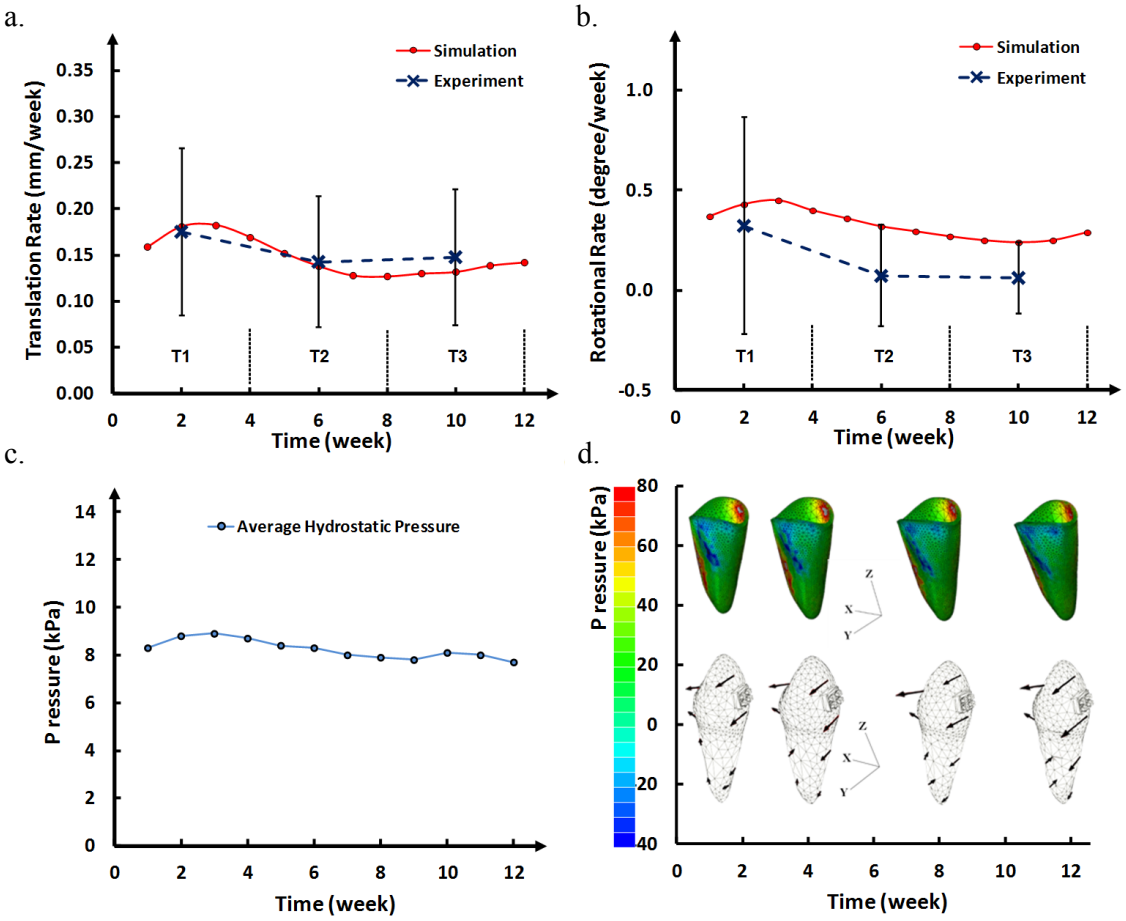

Figure 8-5 Comparison between clinical (blue dash line) and computational (red line) results in the resultant translational (a) and rotational (b) movement; average hydrostatic pressure change during 12 weeks (c); hydrostatic pressure contour of canine PDL and resultant nodal displacement of canine surface in Week 0, 4, 8, and 12 (d), all under the light force of 50 g

The simulation showed the similar trend to the clinical observation, under one-sample t test (single-tailed). The dominant movement occurred in the posterior translation with 12-week average at 0.147 ± 0.008 mm/week ($p < 0.01$ for Week 4, $p < 0.005$ for Week 8 &12), with the small transverse movement towards the buccal side (-0.013 ± 0.009 mm/week). Neither intrusion nor extrusion is significant (0.001 ± 0.015 mm/week). On the

other hand, the simulated canine underwent more rotation and tipping than clinical scenarios. The rotation along the central axis turned the canine bracket further facing the second premolar (from buccal towards posterior, 0.33 ± 0.07 º/week), and the tipping rate towards the posterior direction (the second premolar) was 0.52 ± 0.04 º/week, which was more substantial than the buccal direction (-0.20 ± 0.10 º/week). While the simulated translation agreed well with the averages from our clinical measurements, the simulated rotation rates were at the upper range of those clinically measured ($p < 0.01$ for Week 4, $p < 0.05$ for Weeks 8 and 12).

The average hydrostatic pressure was plotted in Figure 8-5 (c), and it decreased slightly (8.24 ± 0.41 kPa) under a constant orthodontic force over the time. While the canine PDL profile changed over Weeks 1, 4, 8, and 12 as exhibited in Figure 8-5 (c) (the upper row), the hydrostatic pressure did not decay during tooth movement. Figure 8-5 (c) (the lower row) also shows the normalized displacement profile on the canine surface at eight representative points, where the arrow length and direction indicate the magnitude and direction of movement. During the early stage of OTM, displacements on the buccal surface were larger than that on the lingual surface, leading to rotation, but this difference reduced over time. Meanwhile, larger displacements in the crown than those around the root lead to tipping, which accumulated through the 12 weeks, as reflected in the change of PDL orientation (more tilting by week 12).

8.3.2 Tooth Movement under Heavy Forces (1-3 N)

A range of heavier orthodontic forces was also applied to the same model to examine the effects of force magnitudes on OTM. In Figure 8-6 (a) and (b), the absolute distances to the original canine location and the average speeds are plotted. Increasing forces raised the OTM rates, but our model indicated that the rise was gradually compromised. At 0.5 N, the average speed was 0.148 mm/week, leading to the final

movement of 1.77 mm over the 12 weeks. A doubled load (1 N) boosts the speed to 0.227 mm/week (1.53 times faster) with a final distance of 2.72 mm. Whereas, 3 N force (6 times) only increased the moving rate to 0.324 mm/week (2.19 times), yielding final movement 3.88 mm. Comparing the heavier forces, 2.5 and 3 N, there was very marginal difference (0.15 mm) by the end of 12 weeks.

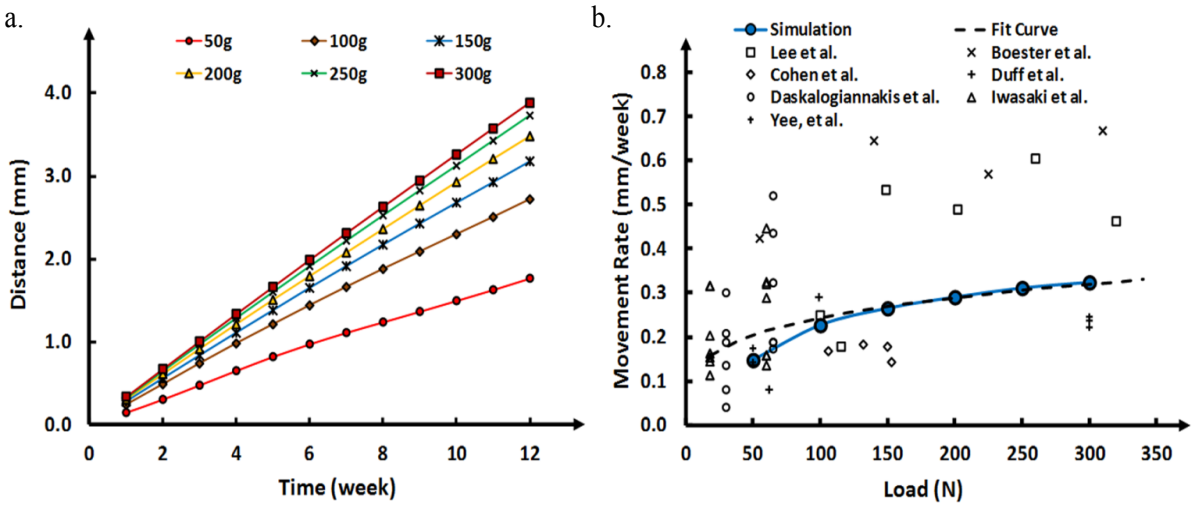

Figure 8-6 (a) Total displacements of the canine under various orthodontic loadings (50-300 gram) in 12 weeks; (b) available clinical data of orthodontic tooth movement speed against different loadings

8.4 Discussion

This subject also received a 3 N orthodontic force on the contralateral side, as part of the clinical experiment, which allows us to focus on biomechanics by excluding gene, biology and life style variance from patient to patient. The outcome is graphed in Figure 8-5(d) together with the simulated prediction for a validation purpose, which showed a good agreement. The difference during the first 4 weeks was suspected to be caused by dental arch wire slipping, leading to insufficient load transfer at heavy force scenarios [23].

Early studies suggested anisotropic nature of bone [24, 25], thus a sensitivity analysis was performed to quantify the effects on approximation from the isotropy to anisotropy (scaled to the same average modulus) [26]. Figure 8-5(c) compared the volume-averaged hydrostatic pressures from the orthotropic model with those from the isotropic model, indicating an average difference of 5.7 %. Upon more specific anisotropic data available, this gap can be minimized by tweaking the remodelling parameters.

To make the remodelling parameters more applicable, six other human studies with similar conditions were considered for general orthodontic treatment. 42 data points were taken collectively from these reports as plotted in Figure 8-6 (b). The remodelling parameters were derived by the least square fitting (black dashed) for Eq. (4), i.e. coefficient a = 1.45 and exponent b= 0.249, by which the simulated tooth movement rates were plotted with a blue line in Figure 8-6 (b). Note that while the fitting curve provided a relatively weak match to these scattered clinical data (R^2 = 0.13), as the individual variances and separate studies could have affected the outcomes dramatically; the general trend can be still observed, and the correlation was stronger than suggested in the literature (R^2 = 0.06) [27].

In the literature, a wide range of optimal forces have been documented. Lee [28] suggested a range from 1.5 to 2.6 N (150 - 260 grams), leading to the maximum rate of 0.61 mm/week. Whereas 3.54 to 3.75 N was found in another clinic report, with a resultant movement rate from 0.86 to 1.37 mm/week [29]. Similar to our simulation, several other studies showed less significant effect with increasing orthodontic forces [22, 30]. Non-linear regression analysis by Ren et al. [27] even showed a decreased movement rate at extremely large forces. Within a conservative force range considered in this study ($\leqslant$ 3 N), the OTM rate showed a similar trend to the abovementioned clinical studies and the early mathematical model [1]. Although the force range adopted in this study has not appeared to make movement rates achieve a plateau, the movement rates delivered by the heavier forces (e.g. 2.5 and 3 N) were fairly close to each other. Nevertheless, the highest force exhibited the fastest tooth movement rate and peaked at 0.340 mm/week.

While this study addressed the critical biomechanical determinants and appropriately modeled OTM process, there are limitations. First, the model provides a phenomenological link of orthodontic force to OTM on an anatomical level. Biological events at the molecular level and corresponding pathways have not been considered [31, 32]. Biochemical activities and genomic regulation [31, 33, 34] on the cellular level, including bone remodelling induced by cellular activities during OTM [35, 36], were important but beyond the scope of this study. Second, applied forces beyond the range in this study may induce more complications with respect to cell mechanics and physiology [3, 37-41], requiring further investigation for a more in-depth understanding so as to modify the procedure established. Third, while the average subject from a group of 14 patients was modeled to establish a conceptual framework accounting for soft-tissue driven remodelling with a considerable statistical significance, it has not particularly differentiated anatomical and physiological variances between individual patients. The

clinical studies, including ours, have however shown notable differences between subjects [42, 43], due to various factors [44-47]. Thus it would be more indicative and statistically meaningful to create all individual patients' models for remodelling analyses. With further understanding of biomechanics from the *in-vivo* studies [48, 49], the proposed OTM algorithm can be refined and potentially used for patient-specific analysis and development of a surgical treatment plan.

8.5 Conclusions

In this study, a procedure of soft-tissue driven bone remodelling has been established for simulating orthodontic tooth movement (OTM) in a time-dependent manner. A novel 3D finite element (FE) based surface remodelling algorithm is proposed through a power law formulation, in which the hydrostatic stress within periodontal ligament (PDL) triggers tooth movement. A specific *in vivo* study was conducted for deriving the remodelling parameters, enabling the model to have a statistically meaningful correlation. Increasing orthodontic force was found to raise remodelling rate but its effect was compromised at heavier forces. The proposed soft tissue driven surface remodelling algorithm provides a novel means for understanding the biomechanical responses associated with OTM. It should be noted that the 3D FE model adopted herein was created directly from human CBCT data *in-vivo*, and the remodelling parameters were derived from a combined source of the clinical maxillary data reported in the literature and our own specific human study. Within the limitations, it is anticipated that this approach has relevant clinical implications for OTM prediction and surgical planning, potentially optimizing the procedure of orthodontic force application, while minimizing side effects (e.g. orthodontic root resorption induced by heavy force).

Acknowledgement

This work is supported by Australian Research Council (ARC) and Australian Postgraduate Award (APA).

8.6 References

1. Quinn, R.S. and D.K. Yoshikawa, *A reassessment of force magnitude in orthodontics.* American Journal of Orthodontics and Dentofacial Orthopedics, 1985. **88**(3): p. 252-260.
2. Cattaneo, P.M., M. Dalstra, and B. Melsen, *The finite element method: a tool to study orthodontic tooth movement.* Journal of Dental Research, 2005. **84**(5): p. 428-433.
3. Ren, Y.J., J.C. Maltha, and A.M. Kuijpers-Jagtman, *Optimum force magnitude for orthodontic tooth movement: A systematic literature review.* Angle Orthodontist, 2003. **73**(1): p. 86-92.
4. Jones, M.L., et al., *A validated finite element method study of orthodontic tooth movement in the human subject.* Journal of orthodontics, 2001. **28**(1): p. 29-38.
5. Middleton, J., M. Jones, and A. Wilson, *The role of the periodontal ligament in bone modeling: The initial development of a time-dependent finite element model.* American Journal of Orthodontics and Dentofacial Orthopedics, 1996. **109**(2): p. 155-162.
6. Middleton, J., M.L. Jones, and A.N. Wilson, *3-dimensional analysis of orthodontic tooth movement.* Journal of Biomedical Engineering, 1990. **12**(4): p. 319-327.
7. Field, C., et al., *Mechanical responses to orthodontic loading: A 3-dimensional finite element multi-tooth model.* American Journal of Orthodontics and Dentofacial Orthopedics, 2009. **135**(2): p. 174-181.
8. Qian, Y., Z. Liu, and Y. Fan, *Numerical simulation of canine bodily movement.* International Journal for Numerical Methods in Biomedical Engineering, 2010. **26**(2): p. 157-163.
9. Li, W., et al., *Fibre reinforced composite dental bridge. Part II: numerical investigation.* Biomaterials, 2004. **25**(20): p. 4995-5001.
10. Li, W., et al., *Towards automated 3D finite element modeling of direct fiber reinforced composite dental bridge.* Journal of Biomedical Materials Research Part B: Applied Biomaterials, 2005. **74B**(1): p. 520-528.
11. Hohmann, A., et al., *Correspondences of hydrostatic pressure in periodontal ligament with regions of root resorption: A clinical and a finite element study of the same human teeth.* Computer Methods and Programs in Biomedicine, 2009. **93**(2): p. 155-161.
12. Lettry, S., et al., *Quality assessment of the cortical bone of the human mandible.* Bone, 2003. **32**(1): p. 35-44.
13. Yee, J.A., et al., *Rate of tooth movement under heavy and light continuous orthodontic forces.* American Journal of Orthodontics and Dentofacial Orthopedics, 2009. **136**(2).
14. Kristiansen, A.B. and K.J. Heyeraas, *Micropuncture measurements of interstitial fluid pressure in the rat periodontal ligament.* Proceedings of the Finnish Dental Society. Suomen Hammaslaakariseuran toimituksia, 1989. **85**(4-5): p. 295-300.

15. Bourauel, C., D. Vollmer, and A. Jager, *Application of bone remodeling theories in the simulation of orthodontic tooth movements.* Journal of orofacial orthopedics, 2000. **61**(4): p. 266-79.

16. Sarrafpour, B., et al., *Finite element analysis suggests functional bone strain accounts for continuous post-eruptive emergence of teeth.* Archives of Oral Biology, 2012. **57**(8): p. 1070-1078.

17. Sarrafpour, B., et al., *Tooth eruption results from bone remodelling driven by bite forces sensed by soft tissue dental follicles: a finite element analysis.* PloS one, 2013. **8**(3): p. e58803-e58803.

18. Field, C., et al., *Prediction of mandibular bone remodelling induced by fixed partial dentures.* Journal of Biomechanics, 2010. **43**(9): p. 1771-1779.

19. Hohmann, A., et al., *Periodontal ligament hydrostatic pressure with areas of root resorption after application of a continuous torque moment - A study using identical extracted maxillary human premolars.* Angle Orthodontist, 2007. **77**(4): p. 653-659.

20. Bourauel, C., et al., *Simulation of orthodontic tooth movements. A comparison of numerical models.* Journal of orofacial orthopedics, 1999. **60**(2): p. 136-51.

21. Hixon, E.H., et al., *Optimal force differential force and anchorage.* American Journal of Orthodontics, 1969. **55**(5): p. 437-&.

22. Boester, C.H. and L.E. Johnston, *Clinical investigation of concepts of differential and optimal force in cannie retraction.* Angle Orthodontist, 1974. **44**(2): p. 113-119.

23. Olson, J.E., et al., *Archwire vibration and stick-slip behavior at the bracket-archwire interface.* American Journal of Orthodontics and Dentofacial Orthopedics, 2012. **142**(3): p. 314-322.

24. O'Mahony, A.M., et al., *Anisotropic elastic properties of cancellous bone from a human edentulous mandible.* Clinical Oral Implants Research, 2000. **11**(5): p. 415-421.

25. Pithioux, M., P. Lasaygues, and P. Chabrand, *An alternative ultrasonic method for measuring the elastic properties of cortical bone.* Journal of Biomechanics, 2002. **35**(7): p. 961-968.

26. Natali, A.N., E.L. Carniel, and P.G. Pavan, *Modelling of mandible bone properties in the numerical analysis of oral implant biomechanics.* Computer Methods and Programs in Biomedicine, 2010. **100**(2): p. 158-165.

27. Ren, Y.J., et al., *Optimum force magnitude for orthodontic tooth movement: A mathematic model.* American Journal of Orthodontics and Dentofacial Orthopedics, 2004. **125**(1): p. 71-77.

28. Lee, B.W., *Relationship between tooth-movement rate and estimated pressure applied.* Journal of Dental Research, 1965. **44**(5): p. 1053-&.

29. Lee, B.W., *The force requirements for tooth movement, Part I: Tipping and bodily movement.* Aust Orthod J., 1995. **13**(4): p. 238-48.

30. Daskalogiannakis, J. and K.R. McLachlan, *Canine retraction with rare earth magnets: An investigation into the validity of the constant force hypothesis.* American Journal of Orthodontics and Dentofacial Orthopedics, 1996. **109**(5): p. 489-495.

31. Masella, R.S. and M. Meister, *Current concepts in the biology of orthodontic tooth movement.* American Journal of Orthodontics and Dentofacial Orthopedics, 2006. **129**(4): p. 458-468.

32. Matsumoto, T., et al., *The Role of Osteocytes in Bone Resorption during Orthodontic Tooth Movement.* Journal of Dental Research, 2013. **92**(4): p. 340-345.

33. Davidovitch, Z., et al., *Neurotransmitters, cytokines, and the control of alveolar bone remodelling in orthodontics.* Dental Clinics of North America, 1988. **32**(3): p. 411-435.

34. Reitan, K., *Effects Of Force Magnitude And Direction Of Tooth Movement On Different Alveolar Bone Types.* The Angle Orthodontist, 1964. **34**(4): p. 244-255.

35. King, G.J., S.D. Keeling, and T.J. Wronski, *Histomorphometric study of alveolar bone turnover in orthodontic tooth movement.* Bone, 1991. **12**(6): p. 401-409.

36. Melsen, B., *Biological reaction of alveolar bone to orthodontic tooth movement.* The Angle Orthodontist, 1999. **69**(2): p. 151-158.

37. Wennstrom, J.L., et al., *Some periodontal tissue-reactions to orthodontic tooth movement in monkeys.* Journal of Clinical Periodontology, 1987. **14**(3): p. 121-129.

38. Krishnan, V. and Z.e. Davidovitch, *Cellular, molecular, and tissue-level reactions to orthodontic force.* American Journal of Orthodontics and Dentofacial Orthopedics, 2006. **129**(4): p. 469.e1-469.e32.

39. Harris, D.A., A.S. Jones, and M.A. Darendeliler, *Physical properties of root cementum: Part 8. Volumetric analysis of root resorption craters after application of controlled intrusive light and heavy orthodontic forces: A microcomputed tomography scan study.* American Journal of Orthodontics and Dentofacial Orthopedics, 2006. **130**(5): p. 639-647.

40. von Böhl, M. and A.M. Kuijpers-Jagtman, *Hyalinization during orthodontic tooth movement: a systematic review on tissue reactions.* The European Journal of Orthodontics, 2009. **31**(1): p. 30-36.

41. King, G.J. and W. Fischlschweiger, *The Effect of Force Magnitude on Extractable Bone Resorptive Activity and Cemental Cratering in Orthodontic Tooth Movement.* Journal of Dental Research, 1982. **61**(6): p. 775-779.

42. Rees, J.S. and P.H. Jacobsen, *Elastic modulus of the periodontal ligament.* Biomaterials, 1997. **18**(14): p. 995-999.

43. Borak, L., et al., *Bilinear elastic property of the periodontal ligament for simulation using a finite element mandible model.* Dental Materials Journal, 2011. **30**(4): p. 448-454.

44. Yamane, A., *The effect of age on the mechanical properties of the periodontal ligament in the incisor teeth of growing young rats.* Gerodontology, 1990. **9**(1-3): p. 9-16.

45. Shibata, T., et al., *Mechanical behavior of bovine periodontal ligament under tension-compression cyclic displacements.* European Journal of Oral Sciences, 2006. **114**(1): p. 74-82.

46. Fill, T.S., et al., *Experimentally determined mechanical properties of, and models for, the periodontal ligament: critical review of current literature.* Journal of dental biomechanics, 2011. **2011**: p. 312980-312980.

47. Boyd, R.L., et al., *Periodontal implications of orthodontic treatment in adults with reduced or normal periodontal tissues versus those of adolescents.* American Journal of Orthodontics and Dentofacial Orthopedics, 1989. **96**(3): p. 191-198.

48. Poppe, M., C. Bourauel, and A. Jager, *Determination of the elasticity parameters of the human periodontal ligament and the location of the center of resistance of single-rooted teeth a study of autopsy specimens and their conversion into finite element models.* Journal of orofacial orthopedics, 2002. **63**(5): p. 358-70.

49. Drolshagen, M., et al., *Development of a novel intraoral measurement device to determine the biomechanical characteristics of the human periodontal ligament.* Journal of Biomechanics, 2011. **44**(11): p. 2136-2143.

Chapter 9: Multiscale design of surface morphological gradient for osseointegration

Rapid and stable osseointegration has become of major concern for the design of implantable prostheses, which in turn has stimulated continuous development of new implantable materials and structures. This chapter promotes a graded configuration of a bead/particle coated porous surface for implants by exploring how its micromechanical features determine osseointegration through a multiscale modelling technique. A typical dental implantation setting is exemplified for investigation, using the remodelling parameters determined from a systematic review of bone-implant-contact (BIC) ratio published in the literature. The global responses of a macroscale model are obtained through 48 month remodelling simulation, which form the basis for the 27 graded microscopic models created with different particle diameters of 30, 50 and 70 μm. The osseointegration responses are evaluated in terms of BIC ratio and averaged 10% peak Tresca shear stress (PTS). The multiobjective optimisation was performed to simultaneously maximize BIC ratio and minimize PTS for achieving the best possible overall outcome. Due to strong competition between these two design objectives, a Pareto front is generated. In order to make a proper trade-off, the minimum distance (optimal-to-Utopia) selection criterion is considered. This study provides a novel surface configuration and design methodology for an individual patient that allows optimizing the topographical gradient for a desirable patient-specific biomechanical environment to promote osseointegration.

Associated Publications:

1. **Junning Chen**, Chaiy Rungsiyakull, Wei Li, Yuhang Chen, Michael V. Swain, Qing Li. **Multiscale design of surface morphological gradient for osseointegration**. *Journal of the Mechanical Behavior of Biomedical Materials*, 2013. 20: p. 387-97.

2. Chaiy Rungsiyakull, **Junning Chen**, Pimduen Rungsiyakull, Wei Li, Michael V. Swain, Qing Li. **Bone's Responses to Different Designs of Implant Supported Fixed Partial Dentures**. *Biomechanics and Modeling in Mechanobiology*. Accepted.

3. Wei Li, Daniel Lin, **Junning Chen**, Zhongpu Zhang, Zhipeng Liao, Michael Swain, Qing Li. **Role of Mechanical Stimuli in Oral Implantation**. *Journal of Biosciences and Medicines*, 2014. 2: p. 63-68.

4. Joseph Cadman, Che-Cheng Chang, **Junning Chen**, Yuhang Chen, Shiwei Zhou, Wei Li, Qing Li. **Bioinspired lightweight cellular materials - Understanding effects of natural variation on mechanical properties**. *Materials Science and Engineering: C*, 2013. 33(6): p. 3146-3152.

5. Wei Li, **Junning Chen**, Chaiy Rungsiyakull, Zhongpu Zhang, Michael Swain, Qing Li. **Multiscale Remodelling for Topographical Optimization in Coated Porous Implants**. *Biomaterials for Implants and Scaffolds*, Springer, 2013.

9.1 Introduction

Over the last two decades, titanium endosseous implants have become well accepted as effective management devices for restoring oral functions in the orofacial structures [1-3]. Titanium and its alloys are of proven mechanical properties and biocompatibility favoured by osseointegration that is the key for implants to anchor into the host bone [2-4]. Nevertheless, there are still some biomechanical drawbacks for titanium implants, such as limited or delayed bone growth into or around the implant surface [2, 3, 5]. In order to enhance osseointegration, various physical and chemical surface treatment technologies have been developed to achieve desirable surface morphologies [3, 6]. A porous implant surface provides considerably more space to promote cell attachment and tissue ingrowth, thereby facilitating a higher level of bone-implant interaction for cell migration and osteoblast adhesion to the implant surfaces [3, 5, 7]. As a result, a more even shear stress can be transferred across the interface, leading to a more uniform stimulation of the surrounding tissues for the establishment of osseointegration and biomechanical binding. The performance of porous surface relies on a number of topographical features, including porosity, pore/particle size, pore orientation, etc.

Various in vivo empirical studies have been carried out to determine the effects of these factors [2, 3, 7-10]. In general, increasing porosity to a certain extent can provide a greater space to enable more efficient nutrient delivery and metabolite removal for cellular activities, thereby better promoting bone mineralisation and stabilisation over a shorter period [2, 6, 11-13]. Shen and Brinson developed computational models to determine the effects of porosity and particle sizes of porous titanium [2, 6, 13] and their subsequent study modelled the bone's responses to surface morphology [14]. Rungsiyakull et al. found the combinations of particle sizes and porosities at 100 μm - 65% and 38 μm - 82.5%

could be favoured for cortical and cancellous bone remodelling under uniform surface morphology settings, respectively [15].

Nevertheless, these existing studies have considered nearly uniform morphology across the porous thickness, in which there is no systematic variation in pore or particle size and porosity except for microscopic randomness. Beside this, there is a new opportunity to improve bone osseointegration and remodelling by adopting graded surface morphology that has been proposed as a potential upgrade to existing uniform coated implants [3]. Over the past decade, material scientists and engineers have been attempting to develop different morphological gradients to lower the mismatch of mechanical properties, especially the elastic modulus, and thereby improve osseointegration between bone and implant [16-20]. A few empirical studies have been carried out to evaluate biocompatibilities and advantages of graded surfaces in promoting bone ingrowth [5, 18]. Computational models of axially graded hydroxyapatite-titanium solid implants were proposed by Lin et al for a macroscopic level of material design [5, 19-21], and some rather indicative results were generated to achieve an optimal gradient for osseointegration [18]. However, all these studies focused on macroscopic responses and considered only the axial gradients with solid composites. Very few reports have been available to model a graded porous surface morphology in the radial direction through examination of the microscopic responses and none has genuinely searched for an optimal radial gradient to date.

This study aims to provide a multiscale study for bone remodelling responses and provide an approach to examining the effects of different combinations of particles/beads for a graded surface morphology, with sizes varying from 30 to 70 μm. As one of the most critical indicators for implant success, osseointegration is measured in terms of ongoing Bone-Implant Contact (BIC) ratio and an averaged level of top 10% Tresca shear stress

(PTS) in the peri-implant regions. Based on the remodelling results obtained, the response surface method is adopted to formulate the osseointegration outcomes in terms of gradient parameters, thereby determining an optimal gradient configuration of the particle coating.

9.2 Materials and Methods

9.2.1 Multiscale Finite Element (FE) Modelling

With rapid development of fabrication technologies for micro- and/or nanostructured materials, traditional monoscale finite element analysis (FEA) became inadequate to capture detailed interaction between biomaterials and tissues effectively. In order to tackle this problem, multiscale analysis techniques have been developed by bridging macroscale (global) homogenized materials to microscale (local) heterogeneous structures, enabling more insightful analysis [16, 18, 22]. Multiscale modelling has been used to simulate how bone is related to internal structures and implant compositions [23, 24], how trabecular bone remodels for correlating to empirical data [25], and how surface morphology affects local cancellous and cortical osseointegration [26].

This paper concerns a non-threaded implant to better restrict our attention on the specific effect of surface morphology gradient rather than other geometric features on osseointegration. To avoid the structural complexity of the 3D multiscale model and associative high computational costs for remodelling analyses [3], a 2D model capable of capturing the major biomechanical features in the occlusal loading scenario of mandible section is adopted in this study [27]. As a preliminary study on topographical gradients, the 2D model facilitates capturing many randomly-located particles/beads and pores in a reasonably dense mesh, requiring relatively lower computational cost for iterative remodelling simulations compared to the 3D version of multiscale models. Other computational pros and cons between 2D and 3D models can be consulted from literature [3].

The implant considered herein is coated through sintering dense beads and has a 5 degree taper angle [27] (Figure 9-1). This global model comprised an abutment and a ceramic crown as a typical dental implantation setting. A 202.23 N load was applied

vertically to the crown cusp with 2 mm horizontal offset from the centre to the buccal side [6]. Note that the details of microscopic morphology were not considered in the global model.

Microscale models were created by selecting a representative region of 1 mm × 1 mm in the cortical region, consisting of bone, implant, and a 300 μm transitional region between them, which presents a mixture of pores due to the bead morphology and connective tissues growing from host bone [3, 16]. To explore the effect of the coating gradient on osseointegration, this transitional area was separated into three layers with different combinations of particle sizes (specifically, 30, 50, and 70 μm in diameter [9, 28]) to form a graded surface morphology. Each layer has 3 candidate particle sizes, leading to $3\times3\times3=27$ different surface morphologies, including 24 graded and 3 uniform configurations. Note that current fabrication technologies have been capable of providing various porosities across a range from 30% to 70%, with which these implants can still have adequate mechanical properties for load-bearing and other biomechanical requirements [3, 29]. Thereby, the volume fraction (counted as area fraction in 2D) of implant beads was kept constant at 30% (highest available porosity) to focus more on the effects due to particle sizes and morphological gradient. Thus, 27 microscopic sample models were created to represent all possible gradients determined by the given design parameters. Linear triangular element was chosen to mesh macroscale and microscale models after a convergence test based on total strain energy [1].

9.2.2 Material Properties

In the macroscale model, the implant core adopted the properties of commercial titanium alloy, Ti6A14V [30], and the abutment and crown are zirconia [31]. The initial properties of the cortical and cancellous bones follow the empirical test done by Carr and O'Brien [32]. The first major assumption regarding materials properties was that the

Poisson's ratio of the same type of tissue does not vary with Young's modulus to simplify the analysis. Similarly in the micro models, the implant region and the cortical bone region adopt the same properties as those in the macro models, and the second assumption is that the transitional region is fully filled by a blood clot within 30 minutes of implantation [31, 33] and forms its initial status. All the material properties used in this simulation are summarized in Table 1, and were assumed to be linearly elastic and isotropic to simplify the remodelling analysis [34]. The minimum bone Young's modulus was set as 870 MPa and minimum density as 0.85 g/cm^3 to allow potential remodelling to low density tissues. Following the literature [3], the average density of cortical bone is allowed to approach its upper limit of 2.0 g/cm^3 [32].

Table 9-1 Initial Properties of Multiscale Models for Remodelling Simulation

Macroscale Model				
	Implant Core	Abutment/Crown	Cortical Bone	Cancellous Bone
Young's Modulus (MPa)	110,000[35]	201,000[31, 32]	1,970[32]	14.8 [33]
Poisson Ratio	0.35[31]	0.28[31]	0.33[32]	0.33 [33]

Microscale Model						
	Native Bone (Cortical)	Implant	Hosting Tissue (Blood Clots)	Mature Bone	Immature Bone	Soft Tissues
Young's Modulus (MPa)	1,970[31]	110,000[33]	0.001[31]	6000[34]	1000[36]	1[36]
Poisson Ratio	0.33[36]	0.3[33, 37]	0.33[31]	0.33[33, 34]	0.33[33, 37]	0.167[33, 37]

9.2.3 Multiscale Simulation

The empirical Wolff's rule forms the major governing equations for modelling the turnovers of cortical, cancellous bone, and connective tissues [3, 38]. In this simulation, the time increment was set to be a month, and the mechanical stimuli is the difference between an instant strain energy density (SED) per unit mass ($U^{(i)} = \sigma\varepsilon/2\rho$) and either an upper or lower reference SED per unit mass (U_l, U_u), which are 10% offset from their mean [3, 38-40]. The rates of bone apposition and resorption were presented by C_a and C_r, respectively [32, 38, 39]. Mechanical overload is also taken into account in this study, which can induce bone loss by presenting osteolysis if it exceeds the physiological limit [32, 38]. A quadratic term is added to the remodelling equation for such an adjusted Wolff's rule (see Figure 9-1) [7, 41-43].

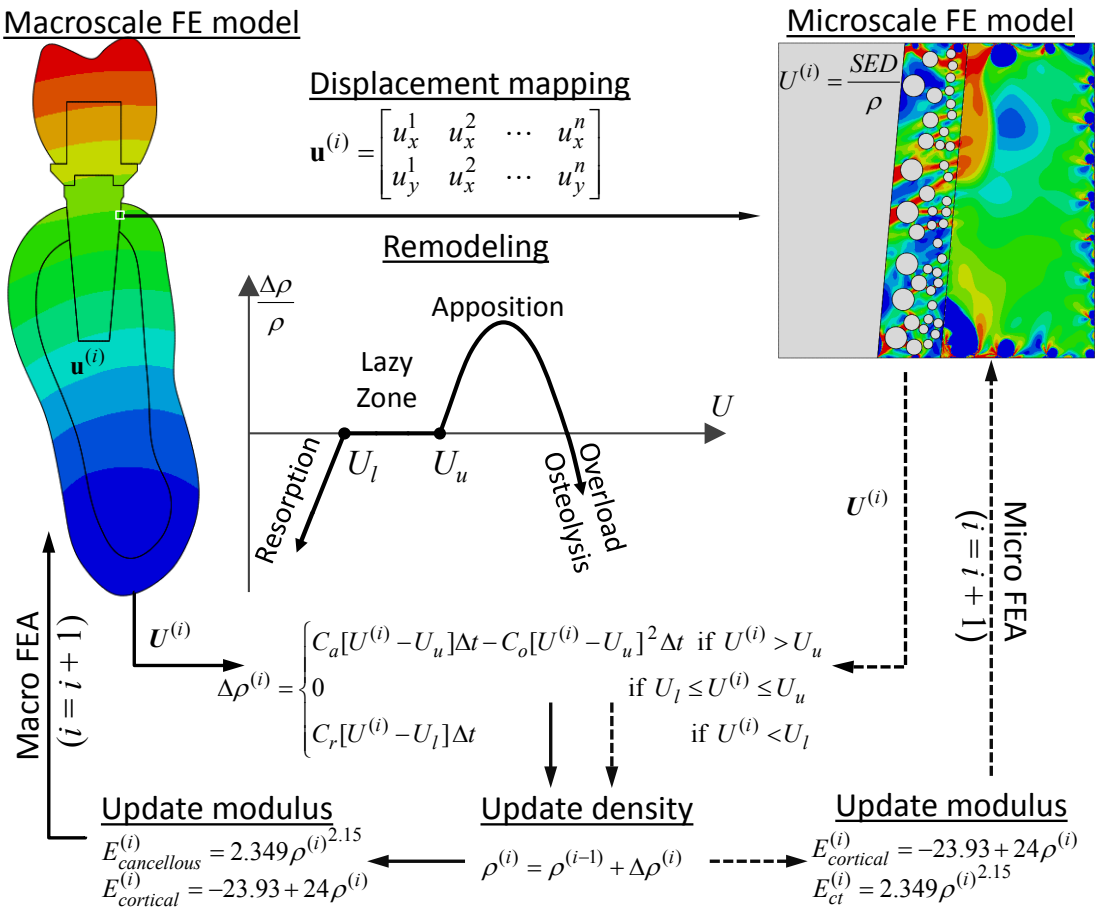

Figure 9-1 Remodelling Algorithm with the Adjusted Wolff's Law as the Major Governing Equation.

The upper and lower reference SED per unit mass were set at 0.000021 and 0.000033 J·cm^3/g, respectively [38, 44-46]. The remodelling rate coefficients, C_a, C_o, and C_r, were determined by matching the simulation results to the in-vivo data in terms of bone-implant-contact (BIC) ratios from the literature. The new bone density determined by the Wolff's rule updated Young's modulus of bony tissues [3]. In this study, the connective tissue will follow the cancellous remodelling equation because its Young's modulus is much lower than the threshold of cortical bone (6 GPa). Displacement fields generated in the macroscale model remodelling are mapped to the microscale models as the inputs. Both macroscale and microscale remodelling procedures were implemented in FORTRAN code through the ABAQUS user subroutine.

9.2.4 Design Optimisation

First, the bone-implant-contact (BIC) ratio is considered one of the primary measures of osseointegration, which measures the degree to which bone ingrows into and becomes mature within the pore space of the transitional region [3]. The BIC ratio can be determined by the proportion of elemental areas with Young's modulus higher than the threshold of mature bone (MB) to the total element area (AE) of connecting tissues as follows.

$$f_{BIC} = \%\text{BIC} = \frac{\text{Mature Bone Area}}{\text{All Elemental Areas}} \times 100\% = \frac{\sum_{i=1}^{MB} A_i}{\sum_{i=1}^{AE} A_i} \times 100\% \quad (1)$$

The other concern lies in whether the implant-bone interface can withstand mechanical loading without debonding failure. Indeed, the pull-out test has been an important method to test the extent of osseointegration in terms of shear resistance [36, 47]. For this reason, Tresca stress is adopted as another key measure of implant topography,

assessing how well the surface morphological gradient avoids the shear stress concentration. Note that the maximum Tresca stress in a single element may not be appropriate to determine the shear failure for an entire region, and to make it more statistically meaningful, the elemental Tresca stresses averaged out over 10% of the total volume with the highest stress concentration adopted. Therefore the overall risk of shear failure is measured as

$$f_{PTS} = \frac{\sum_{e=1}^{n} \text{Peak Tresca Stress (Top 10\%)} \times \text{Volume}}{\text{Total Volume of Top 10\% Tresca Stress}} = \frac{\sum_{e=1}^{n} \sigma_{Tre}^{e} \times V_{Tre}^{e}}{\sum_{e=1}^{n} V_{Tre}^{e}} \quad (2)$$

where n is the number of elements required to sum 10% of the total volume.

To seek an optimal design, the particle sizes in the three layers, α_1, α_2, and α_3, will be varied to determine if an optimal osseointegration outcome can be attained. To do so we introduce a multiobjective optimisation technique to maximize BIC and minimize PTS by using linearly weighted average (LWA) and multiple objective particle swarm optimisation (MOPSO) approaches, respectively.

The LWA method [29, 48-50] formulates a cost function comprised of the individual objectives in terms of the selected weighting factors ω_1 and ω_2 as,

$$\begin{cases} \min \mathrm{F}_{\mathrm{LWA}}(\alpha_1, \alpha_2, \alpha_3) = \omega_1 \dfrac{\mathrm{f}_{\mathrm{BIC}}^{\circ}}{\mathrm{f}_{\mathrm{BIC}}} + \omega_2 \dfrac{\mathrm{f}_{\mathrm{PTS}}}{\mathrm{f}_{\mathrm{PTS}}^{\circ}} \\ \text{s.t. } \omega_1 + \omega_2 = 1, \ (\omega_1 \geq 0, \omega_2 \geq 0) \\ 30\mu\mathrm{m} \leq \alpha_1, \alpha_2, \alpha_3 \leq 70\mu\mathrm{m} \end{cases} \quad (3)$$

To eliminate the dimensional difference in combining these two individual objective functions, a normalisation procedure was applied by using minimum f_{BIC}° and maximum f_{Tre}°.

The particle swarm optimisation (PSO) [3, 22, 51] method utilises the concept of crowding distance, which is of specific benefit on the basis of global best selection of dominated solutions from an external reference archive. This method allows a fast convergence, and has been successfully applied in a broad range of problems [52].

$$\begin{cases} \min \mathrm{F}_{\mathrm{MOPSO}}(\alpha_1, \alpha_2, \alpha_3) = \left[\mathrm{f}_{\mathrm{BIC}}^{-1}, \mathrm{f}_{\mathrm{PTS}} \right]^{\mathrm{T}} \\ \text{s.t.} \quad 30\mu\mathrm{m} \le \alpha_1, \alpha_2, \alpha_3 \le 70\mu\mathrm{m} \end{cases} \tag{4}$$

9.2.5 Response Surface Method (RSM)

It is non-trivial to establish the objective functions mentioned above. Surrogate modelling techniques such as RSM is considered an effective, and sometimes unique, alternative [3, 51-53]. Since the knowledge of the objective functions is rather limited; we attempted several different polynomial models to capture sophisticated mutual consequences from multiple variables [3, 22, 51]. As such, the most suitable response surface (RS) function was finally determined.

9.3 Results

In this study, bone remodelling response was simulated by using different pre-selected surface morphological gradients and their consequences over 48 months of healing, during which the host bone can ingrow into the void space and the corresponding osseointegration performance is measured by the BIC ratios and averaged peak Tresca stress (10% volume), respectively. After a certain period of initial healing, during which the bone could gradually achieve a dynamic equilibrium between apposition and resorption, the design parameters are considered less significant. The results in Month 6 and Month 48 were chosen as two critical indicators to measure short-term and long-term performance, respectively.

9.3.1 Bone-Implant-Contact (BIC) Ratio

The porosities of each layer in the graded surfaces were kept constant at 70% in this study. In other words, all the models in different layers had the same void space to allow tissue ingrowth. The BIC ratios are presented in units of %. All gradient configurations are presented in a form of (α_1-α_2-α_3), representing the particle sizes in different layers, in which α_1 is the layer closest to the implant core and α_3 is next to the host bone.

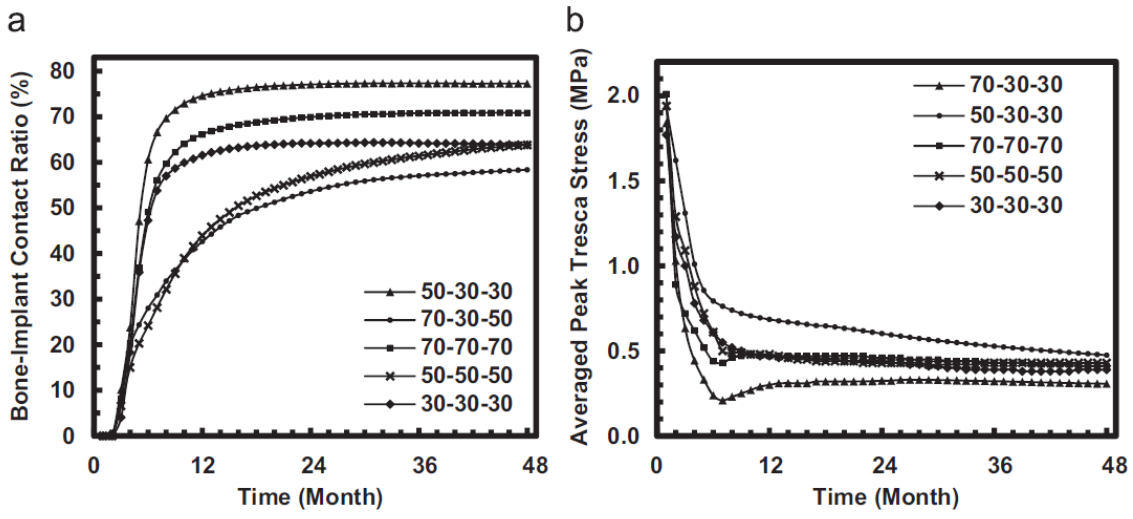

Figure 9-2 Highest/Lowest Bone-Implant Contact Ratios (a) and Average Peak Tresca Stresses in 27 Samples (b) Compared to Three Uniform Morphologies Over 48 Month Period.

Figure 9-2 (a) compares the two gradients having the highest and the lowest BIC ratios to the three uniform surface morphologies consisting of 30, 50 and 70 μm particles, and obviously they clearly demonstrate the effect of gradients on osseointegration rate. Gradient 50-30-30 shows superior bone mass gain over the entire simulation period than others, and it has 6.41% more bone mass than configuration 70-70-70 by Month 48, which is the best performer of all three uniform options. However, it is noted that not all graded surface morphologies increase the extent of osseointegration. Gradient 70-30-50 shows a reverse effect on osseous tissue ingrowth, although its initial gain over the first 8 months is higher than uniform configuration 50-50-50, which has the worst outcome of the uniform morphologies.

As shown in Figure 9-2 (a), all five surface morphologies presented have similar rates of mature bone deposition during the first three months of acute healing. However, there has been a significant difference in BIC outcomes after Month 6. Gradient 50-30-30 maintained a steep initial growth rate till the end of the first year and then commenced to plateau more quickly. In comparison the growth in Gradient 70-30-50, has a delayed commencement and a decrease at an earlier time point, but its growth is more gradual and smoother than Gradient 50-30-30, as it lasts for more than 3 years till the mature bone apposition comes into equilibrium. At the end of 48 months, the best and worst gradients ended up with around 20% difference in the BIC ratios.

9.3.2 Averaged Peak Tresca Stress (PTS)

The averaged PTS (10% of the total volume) is adopted as the other important indicator to measure the success of implantation in this study. Figure 9-2 (b) plots the overall highest and lowest Tresca stress evolutions of all the 27 gradients compared to

those induced by the three uniform morphologies. It is evident that Gradient 70-30-30 delivers the lowest stress concentration over 48 months. Note that the highest shear failure possibility appears to be in Gradient 50-30-30, and their similar gradients lead to a small difference of only 0.02 MPa at Month 48.

Considering the overall trend, the significant drops of PTS in the first 6 months indicate the rapid growth of osseous tissues, and the reductions are 86.9% for Gradient 70-30-30 and 58.5% for Gradient 50-30-30. Subsequently, these two gradients gradually converge by Month 48. A similar pattern occurs in the uniform surface morphologies which fall between the best and worst, having similar average shear stress at the equilibrium status (< 0.02 MPa at Month 48). The final difference between Gradients 70-30-30 and 50-30-30 at Month 48 is 0.17 MPa, which is approximately 10% of the initial stress concentration.

In contrast to the BIC outcomes, all gradients show a slower and more gradual convergence for PTS. From Figure 9-2 (b), the PTS rises after the sharp drops and then towards an equilibrium with time, instead of directly approaching steady state as in BIC (Figure 9-2 (a)). Based on the monthly data obtained, however, it is not possible to draw a direct relationship between BIC and PTS.

9.4 Discussion

9.4.1 Bone Remodelling Responses

Previous *in vivo* studies have been carried out to explore bone-implant contact problems, and the associated empirical data provides an approximate guide for determination of bone remodelling ratio, by interpreting the solid bone deposition through the object lifespan. Kim et al. performed an *in vivo* study on 30 implants in dog mandibles with three groups of materials with different surface finish [13]. In the roughest surface group, BIC reached 81.2% over 10 weeks. Since the test subjects were dogs, ten weeks is roughly equivalent to a year and an half of human life in their study. Similarly, Deporter et al investigated a porous-coated dental implant and showed 50% and 65% BIC in the buccal and lingual sides of dog mandible [17] (at 2.5 year equivalent human life). Beside dogs, rabbits are also popular animal models. Suzuki et al conducted a time-dependent study of implants into rabbit femurs separating them into smooth and rough surface groups [13]. BIC in the rough surface group reached 37%, 62%, and 78% in 6, 16, and 42 weeks, corresponding to human life of approximately 1, 2.5, and 7 years, respectively. Abron et al. also performed a study on rat tibiae and indicated an averaged BIC of 54% in 3 weeks [11], corresponding to 1.5 years of human life. Morra et al.'s *in vivo* study on rabbits' femoral diaphysis presented an averaged BIC of 62.75% in 12 weeks (2 year human life) [48]. BIC has also been considered in computational remodelling, for example, Lian et al. tested four different initial BICs (25, 50, 75 and 100%) without surface morphology [2]. After equilibrium, the final outcomes all lay in a range from 58 to 60% BIC.

A summary graph plot of BIC ratios from the literature against time (Figure 9-3) shows a rough progression trend for human osseointegration, in which fits a logarithmic function. It is noted that with the same set of correlated bone remodelling parameters, the comparison between individual graded and uniform surface morphologies becomes valid

and meaningful. The BIC outcomes for Gradients 50-30-30 and 70-30-50 show reasonable consistency with literature data; the former (best) exhibits improved performance above the fitting line and the latter (worst) fall below it for most of the time.

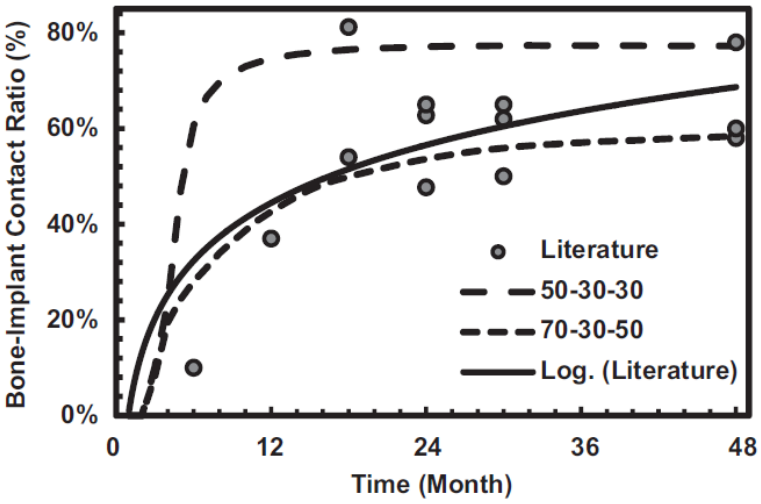

Figure 9-3 Interpreted Bone-Implant Contact Ratios from Empirical Studies for a Trend Line Compared to the Best (50-30-30) and the Worst (70-30-50) Remodelling Simulation Outcomes in Two Surface Gradients.

The bone conditions of individual patients may vary considerably, and the corresponding remodelling parameters will certainly affect the simulation outcomes. However, the main focus of this paper resides in establishing a new computational procedure and revealing a fact that different surface gradients lead to different osseointegration outcomes under the same external loading condition. Using the design protocol established here, a study can be performed to create a patient-specific surface gradient, meeting individual needs. Meanwhile, this approach can be extended to a 3D model by including a peripheral gradient for an implant with more sophisticated coating variables.

9.4.2 Response Surface Functions

The sample data provides the essential information to extrapolate design analysis and optimisation. Based on the above remodelling results, the assessment criteria, BIC and

PTS, are related to the design variables of coating parameters in each layer as (α_1, α_2, α_3,). In order to evaluate the fitness of response surface (RS) models, 3 different orders (linear, quadratic, and cubic) of polynomial functions were attempted by the least-square method. The R^2 and root mean square error (RMSE) between simulation and RS functions (Max & Min) are used to assess which polynomial is most accurate. As summarized in Table 2, the cubic polynomial function provides the best fits to both BIC and PTS for the two selected time points indicative of short and long term osseointegration (Months 6 and 48, respectively).

Table 9-2 Response Surface Models (Polynomial) for Month 6 and 48

	Time	RS Model	R-sqr	Max	RSM* Max	Min	RSM* Min	RMSE**
BIC (%)	**Month 6**	**Linear**	0.8828		45.79		27.33	8.69
		Quadratic	0.9035	60.59	50.54	21.51	23.02	6.21
		Cubic	0.9536		59.15		21.83	4.30
	Month 48	**Linear**	0.9950		71.92		63.23	4.88
		Quadratic	0.9968	77.25	73.69	58.36	57.90	3.88
		Cubic	0.9983		76.95		56.66	2.88
PTS (10^5 Pa)	**Month 6**	**Linear**	0.9417		6.50		4.09	1.35
		Quadratic	0.9572	9.14	8.05	2.38	3.15	1.16
		Cubic	0.9647		8.89		2.84	1.06
	Month 48	**Linear**	0.9810		4.03		3.64	0.54
		Quadratic	0.9888	4.96	4.55	2.85	3.21	0.42
		Cubic	0.9942		4.83		3.04	0.31

RSM* **Response Surface Method Result**

RMSE** **Root Mean Square Error**

To clearly show the response surfaces, α_3 is set to 50 um representing an intermediate size of particles as an example for RSM. Figure 9-4(a)-(d) plots the BIC and PTS for Months 6 and 48, respectively. From the BIC perspective, the combinations of

medium particles in the inner layer (α_1) with large sizes in the mid layer (α_2) shows their advantages over the other configuration in both short term (Month 6 as in Figure 9-4(a)) and long term (Month 48 as in Figure 9-4(b)). Also the trend is affected by α_2 (mid layer) more significantly than α_1 (inner layer), and it declines rapidly in the reverse direction of α_2 axis, with a short term plateau for the medium size range. The benefit of using a medium-large combination becomes amplified in BIC as healing time progresses. Figure 9-4(a) and (b) also reflects that Gradient 70-30-50 (right bottom corner in the plots) is the worst performer in the design range over the simulation time considered.

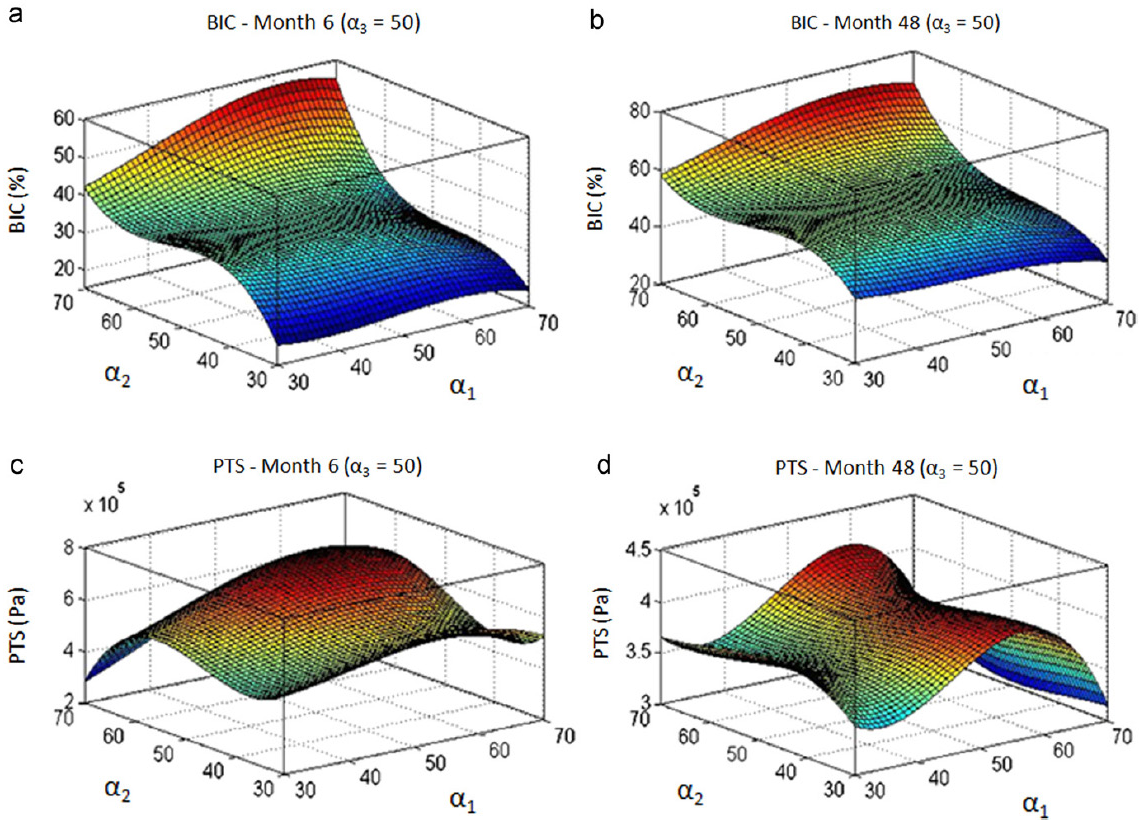

Figure 9-4 Response Surfaces Showing the Effects of Gradient Input α_1 and α_2 when α_3 is Set to 50 µm on BIC (a, b) and Averaged Peak Tresca Stress (c, d) at Month 6 and 48, respectively.

On the other hand, PTS shows more distinct patterns than BIC. From Figure 9-4(c), α_2 plays a more important role in the short term osseointegration than α_1; however, this is reversed in the long term as seen in Figure 9-4(d). The minimum PTS appears in the case

when small particles in the inner layer are combined with the large ones in the mid layer in Month 6, while it occurs at large-medium combinations at month 48. Similarly to BIC, the lowest PTS occurs around Gradient 70-30-50 which is close to Gradient 70-30-30 having the least failure chance.

Based on the RS functions obtained, we can determine the gradients for either maximum BIC or minimum PTS outcomes at both Month 6 and 48, respectively. It is noted that the gradient 62-70-50 has the highest BIC ratio of 61.4% by Month 6, at the same time with a high PTS of 0.54 MPa. In contrast, Gradient 70-30-70 has the lowest PTS of 0.29 MPa accompanied by least bone mass gain, leading to a BIC ratio of 29.8%. In Month 48, Gradient 30-30-32 leads to the maximum BIC ratio of 76.9% (0.34 MPa PTS), while Gradient 70-45-41 promotes the least PTS of 0.28 MPa (40.7% BIC). It appears that these two design criteria cannot be achieved concurrently.

9.4.3 Multiobjective Optimisation

Here we attempt to adopt multiobjective optimisation for maximizing BIC and minimizing PTS by using both linearly weighted average (LWA) and direct multiple objective particle swarm optimisation (MOPSO) methods.

In the LWA method, one of the weighting factors is raised by a small increment of 0.0005 in order to obtain the Pareto frontier, and resulting in 80, 000 Pareto points. From these 80 of them at uniform intervals are selected to plot Pareto fronts in Figure 9-5 (a) and (b) for 6 and 48 Months, respectively. The Pareto set is supposed to span the entire optimal solution space. It is observed, however, that highly concentrated regions appear for both Month 6 and Month 48 solutions, with a few isolated aggregates.

To tackle the non-uniform distribution problem that occurred in the LWA solutions, the multiobjective Particle Swarm Optimisation (MOPSO) method is adopted in line with

its special feature of generating a well-distributed Pareto solution [54]. Some 2, 000 Pareto points are generated through 1, 000 iterations, and 80 of them at uniform intervals are plotted in the same graph as that from the LWA method. Obviously, MOPSO is more effective than LWA in terms of the smoothness of the Pareto frontier and extent of uniformity in this design problem. As expected, MOPSO is much more widely distributed and all the LWA results are well located in the MOPSO Pareto frontier, which also reflects the effectiveness of these two approaches, although they differ as to integrity of outcomes.

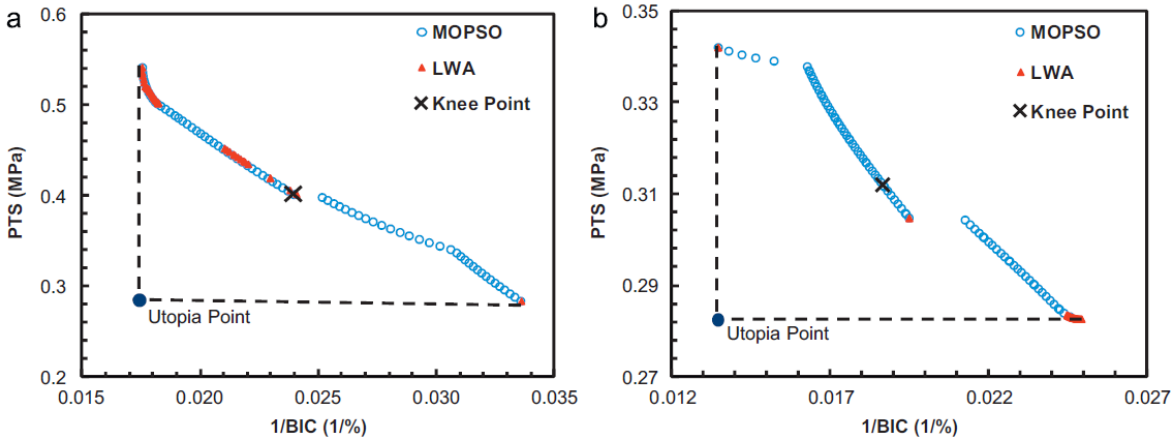

Figure 9-5 Pareto Set of Optimal Surface Gradient Parameters Based on Two Multiobjective Optimisation Schemes at Month 6 and 48. Any Point on the Pareto Frontiers Represents a Feasible Choice, and the MOPSO Method is More Effective than the LWA Method to Depict the Pareto Frontiers.

From the Pareto frontier generated by MOPSO, the maximum BIC ratio and the minimum PTS fall into the same outcomes as determined in Section 9.4.2. It is noted that to further improve either BIC or PTS one must sacrifice the corresponding counterpart along the Pareto frontier. For example, more acute and faster bone growth during early stages will be accompanied by higher peak stresses, and *vice versa*.

There is a Utopia point where the maximum BIC ratio and the minimum PTS occur at the same time; however this point was unable to be achieved in most design cases presented [3]. In theory, any point in the Pareto frontier can be a solution to a specific

morphological design providing different BIC ratio and PTS, and a full range of optima provides multiple choices for various balances between BIC ratio and PTS for clinical decision making. Based on the given selection criteria, a decision can be made for the most "satisfactory" solution, known as a knee point, in the Pareto set [3]. In this study, the minimum distance selection method (MDSM) is adopted for an optimal selection, as stated in Eq. (5).

$$\min D = \sqrt{\left(\frac{f_{BIC} - f_{BIC}^{L}}{f_{BIC}^{U} - f_{BIC}^{L}}\right)^2 + \left(\frac{f_{PTS} - f_{PTS}^{L}}{f_{PTS}^{U} - f_{PTS}^{L}}\right)^2} \tag{5}$$

In this equation, f_{BIC} and f_{PTS} are the objective functions, while f^L and f^U are their corresponding upper and lower thresholds in the design space concerned. An optimal gradient can thus be selected by minimising the distance between the point itself and the Utopia point. Within the limitations of this study, it is found that the coating with a moderate gradient near the largest particle size (70-70-62) represents an optimal solution to initial healing up to Month 6, giving a BIC outcome of 41.5% and PTS of 0.40 MPa. But for the long term healing, a graded coating with a combination of particle size of 37-70-68 is preferred, leading to a BIC ratio of 54.3% and PTS of 0.31 MPa. Note that with other selection criteria, such as "the maximum BIC ratio within a tolerated PTS range", it can lead to a different conclusion on the optimal choice.

9.4.4 Patient-Specific Design and Future Applications

Osseointegration process can be affected by both implant surface morphology and physiological conditions. For the latter, age, sex, race, genetics and other medical factors all contribute and have a bearing on bone responses to the implantation, leading to different osseointegration outcomes. This paper considers a particular set of remodelling parameters derived from literature to demonstrate how the surface topographical gradient

of an implant can be optimized for the same given mechanical and biological conditions. With sufficient patient data (e.g. from interval CT/MRI scans), this approach can be applied to individual subjects with their own remodelling parameters, aiming for a patient-specific design. To each patient, the predicted Pareto optima consists of a series of solutions at different balancing points between BIC ratio and PTS, and a clinic decision can be made based upon individual needs of a patient and clinical expectations.

Although this study considers a loaded dental implant as an example, the graded topographical configuration and corresponding design procedure can be extended to other applications of prosthetic fixation, such as orthopaedic osseointegration. A recent study has examined the macroscopic remodelling outcomes in terms of bone mass density and failure possibility of different prosthetic designs in hip replacements [55]. By applying the design procedure for graded topography proposed in this paper, the microscopic surface morphology could also be optimized for the hip prosthesis to meet individual patient needs.

Topology optimisation has proven an effective tool for microstructural design aiming to regulate effective material properties for bone remodelling applications [56]. Recent studies [57-59] demonstrated how to optimize the microstructural gradient of a hip replacement implant for achieving minimum bone resorption and clinical failure probability. Nevertheless, the technique presented in those studies is restricted to periodic microstructures and may be of limited relevance to random morphology as shown in this paper.

9.5 Conclusions

A novel application of multiscale modelling and remodelling analyses has been implemented in this study to optimize a graded porous surface morphology, by evaluating osseointegration outcomes in terms of bone-implant-contact (BIC) and averaged peak Tresca stress (PTS). The simulation results suggested that the size of particles in each surface layer determines bone ingrowth and shear stress distribution, and the optimized surface gradient can outperform uniform surface morphologies that have conventionally been adopted in most traditional implants. A cubic surrogate model is found to best correlate BIC and PTS with gradient parameters in this problem, and the RS plots are in good agreement with the sample simulation results, leading to different gradient optima for the highest BIC ratio or the minimum PTS at Month 6 and 48, respectively. Since the maximisation of BIC and minimisation of PTS cannot be achieved simultaneously, a multiobjective optimisation procedure was adopted here. Two different approaches, namely LWA and MOPSO, were used to generate Pareto solutions, from which MOPSO demonstrates its capability of dealing with concentrated regions of optimal solutions. By adopting the minimum distance selection method (TMDSM), Gradients 70-70-62 and 37-70-68 are selected by minimising the distance to the Utopia point as the most "satisfactory" solutions for short term and long term healing, respectively. With sufficient patient information, a private case study can be done by following this procedure to generate a range of optimal solutions, allowing a material engineer and clinician to choose a patient-specific surface morphology for clinic application. With different optimal selection criteria, a different solution may be obtained. Prior to such clinical application further animal studies need to be performed to verify the multiscale model and graded porous implant surface approach proposed. These future investigations can also be used to optimize

porosity gradients under other design criteria [60] or with other materials, thereby providing different implant-tissue interaction (e.g. [61]).

Acknowledgement

This work is supported by Australian Research Council (ARC) and Australian Postgraduate Award (APA).

9.6 References

1. Dewidar, M.M. and J.K. Lim, *Properties of solid core and porous surface Ti-6Al-4V implants manufactured by powder metallurgy.* Journal of Alloys and Compounds, 2008. **454**(1-2): p. 442-446.
2. Morra, M., et al., *Surface engineering of titanium by collagen immobilization. Surface characterization and in vitro and in vivo studies.* Biomaterials, 2003. **24**(25): p. 4639-4654.
3. Rungsiyakull, C., et al., *Surface morphology optimization for osseointegration of coated implants.* Biomaterials, 2010. **31**(27): p. 7196-7204.
4. O'Brien, W.J., *Dental materials and their selection*. 4th ed. 2008, Hanover Park, IL: Quintessence Pub. Co. xiii, 425 p.
5. Kunzler, T.P., et al., *Systematic study of osteoblast and fibroblast response to roughness by means of surface-morphology gradients.* Biomaterials, 2007. **28**(13): p. 2175-2182.
6. Vaillancourt, H., R.M. Pilliar, and D. McCammond, *Finite element analysis of crestal bone loss around porous-coated dental implants.* Journal of Applied Biomaterials, 1995. **6**(4): p. 267-282.
7. Esposito, M., et al., *Biological factors contributing to failures of osseointegrated oral implants (I). Success criteria and epidemiology.* European Journal of Oral Sciences, 1998. **106**(1): p. 527-551.
8. Okazaki, K., et al., *Physical characteristics of Ti-6Al-4V implants fabricated by electrodischarge compaction.* Journal of Biomedical Materials Research, 1991. **25**(12): p. 1417-1429.
9. Xue, W., et al., *Processing and biocompatibility evaluation of laser processed porous titanium.* Acta Biomaterialia, 2007. **3**(6): p. 1007-1018.
10. Anil, S., et al., *Chapter 4: Dental implant surface enhancement and osseointegration*, in *Implant dentistry - a rapidly evolving practice*, I. Turkyilmaz, Editor. 2011, InTech: Rijeka. p. 86-90.
11. Suzuki, K., K. Aoki, and K. Ohya, *Effects of surface roughness of titanium implants on bone remodeling activity of femur in rabbits.* Bone, 1997. **21**(6): p. 507-514.
12. Itala, A.I., et al., *Pore diameter of more than 100 mu m is not requisite for bone ingrowth in rabbits.* Journal of Biomedical Materials Research, 2001. **58**(6): p. 679-683.
13. Bradley, N., *The response surface methodology*, in *Department of Mathematical Sciences*. 2007, Indiana University: South Bend. p. 36-38.
14. Shen, H., H. Li, and L.C. Brinson, *Effect of microstructural configurations on the mechanical responses of porous titanium: A numerical design of experiment analysis for orthopedic applications.* Mechanics of Materials, 2008. **40**(9): p. 708-720.
15. Shen, H. and L.C. Brinson, *A numerical investigation of porous titanium as orthopedic implant material.* Mechanics of Materials, 2011. **43**(8): p. 420-430.

16. Lin, D., et al., *Bone remodeling induced by dental implants of functionally graded materials.* Journal of Biomedical Materials Research Part B-Applied Biomaterials, 2010. **92B**(2): p. 430-438.

17. Kim, S.J., et al., *Comparison of implant stability after different implant surface treatments in dog bone.* Journal of Applied Oral Science, 2010. **18**(4): p. 415-420.

18. Yang, J. and H.-J. Xiang, *A three-dimensional finite element study on the biomechanical behavior of an FGBM dental implant in surrounding bone.* Journal of Biomechanics, 2007. **40**(11): p. 2377-2385.

19. Yang, Y.Z., et al., *Morphological behavior of osteoblast-like cells on surface-modified titanium in vitro.* Biomaterials, 2002. **23**(5): p. 1383-1389.

20. Yang, Y.Z., et al., *Preparation of graded porous titanium coatings on titanium implant materials by plasma spraying.* Journal of Biomedical Materials Research, 2000. **52**(2): p. 333-337.

21. Chen, C.C., et al., *Characterization of functionally graded hydroxyapatite/titanium composite coatings plasma-sprayed on Ti alloys.* Journal of Biomedical Materials Research Part B-Applied Biomaterials, 2006. **78B**(1): p. 146-152.

22. Lin, D., et al., *Design optimization of functionally graded dental implant for bone remodeling.* Composites Part B-Engineering, 2009. **40**(7): p. 668-675.

23. Podshivalov, L., A. Fischer, and P.Z. Bar-Yoseph, *3D hierarchical geometric modeling and multiscale FE analysis as a base for individualized medical diagnosis of bone structure.* Bone, 2011. **48**(4): p. 693-703.

24. Podshivalov, L., A. Fischer, and P.Z. Bar-Yoseph, *Multiscale FE method for analysis of bone micro-structures.* Journal of the Mechanical Behavior of Biomedical Materials, 2011. **4**(6): p. 888-899.

25. Fritsch, A., C. Hellmich, and L. Dormieux, *Ductile sliding between mineral crystals followed by rupture of collagen crosslinks: Experimentally supported micromechanical explanation of bone strength.* Journal of Theoretical Biology, 2009. **260**(2): p. 230-252.

26. Buti, F., et al., *Bone Remodelling in BioShape.* Electronic Notes in Theoretical Computer Science, 2010. **268**: p. 17-29.

27. Romeed, S.A., S.L. Fok, and N.H.F. Wilson, *A comparison of 2D and 3D finite element analysis of a restored tooth.* Journal of Oral Rehabilitation, 2006. **33**(3): p. 209-215.

28. Traini, T., et al., *Direct laser metal sintering as a new approach to fabrication of an isoelastic functionally graded material for manufacture of porous titanium dental implants.* Dental Materials, 2008. **24**(11): p. 1525-1533.

29. Bobyn, J.D., et al., *The optimum pore size for the fixation of porous-surfaced metal implants by the ingrowth of bone.* Clin Orthop Relat Res, 1980(150): p. 263-70.

30. Li, W., et al., *Towards automated 3D finite element modeling of direct fiber reinforced composite dental bridge.* Journal of Biomedical Materials Research Part B: Applied Biomaterials, 2005. **74B**(1): p. 520-528.

31. O'Brien, W.J., *Dental Materials and Their Selection*. 2008, Quintessence Publishing Co, Inc: Michigan.

32. Lin, D., et al., *Mandibular bone remodeling induced by dental implant.* Journal of Biomechanics, 2010. **43**(2): p. 287-293.

33. Carr, M.E. and S.L. Carr, *Fibrin structure and cocentration alter clot elastic-modulus but do not alter platelet-mediated force development.* Blood Coagulation & Fibrinolysis, 1995. **6**(1): p. 79-86.

34. Riha, P., et al., *Elasticity and fracture strain of whole blood clots.* Clinical Hemorheology and Microcirculation, 1999. **21**(1): p. 45-49.

35. Chen, Y., S. Zhou, and Q. Li, *Microstructure design of biodegradable scaffold and its effect on tissue regeneration.* Biomaterials, 2011. **32**(22): p. 5003-5014.

36. Liu, X.Y. and G.L. Niebur, *Bone ingrowth into a porous coated implant predicted by a mechano-regulatory tissue differentiation algorithm.* Biomechanics and Modeling in Mechanobiology, 2008. **7**(4): p. 335-344.

37. Isaksson, H., C.C. van Donkelaar, and K. Ito, *Sensitivity of tissue differentiation and bone healing predictions to tissue properties.* Journal of Biomechanics, 2009. **42**(5): p. 555-564.

38. Lin, D., et al., *Dental implant induced bone remodeling and associated algorithms.* Journal of the Mechanical Behavior of Biomedical Materials, 2009. **2**(5): p. 410-432.

39. Keaveny, T.M., *Strength of Trabecular Bone*, in *Bone Mechanics Handbook*, S.C. Cowin, Editor. 2001, CRC Press LLC: Danvers. p. 7.

40. Frost, H.M., *Bone's mechanostat: A 2003 update.* The Anatomical Record Part A: Discoveries in Molecular, Cellular, and Evolutionary Biology, 2003. **275A**(2): p. 1081-1101.

41. Noble, B.S. and J. Reeve, *Osteocyte function, osteocyte death and bone fracture resistance.* Molecular and Cellular Endocrinology, 2000. **159**(1-2): p. 7-13.

42. Wernig, F. and Q. Xu, *Mechanical stress-induced apoptosis in the cardiovascular system.* Progress in Biophysics and Molecular Biology, 2000. **78**(2-3): p. 105-137.

43. Xie, M., et al., *Rabbit Annulus Fibrosus Cell Apoptosis Induced by Mechanical Overload via a Mitochondrial Apoptotic Pathway.* Journal of Huazhong University of Science and Technology-Medical Sciences, 2010. **30**(3): p. 379-384.

44. Tanaka, E., et al., *A mathematical model of bone remodelling under overload and its application to evaluation of bone resportion around dental implants.* Acta of Bioengineering and Biomechanics, 1999. **1**(1): p. 117-121.

45. Field, C., et al., *A comparative mechanical and bone remodelling study of all-ceramic posterior inlay and onlay fixed partial dentures.* Journal of Dentistry, 2012. **40**(1): p. 48-56.

46. Field, C., et al., *Prediction of mandibular bone remodelling induced by fixed partial dentures.* Journal of Biomechanics, 2010. **43**(9): p. 1771-1779.

47. Sollazzo, V., et al., *Zirconium oxide coating improves implant osseointegration in vivo.* Dental Materials, 2008. **24**(3): p. 357-361.

48. Abron, A., et al., *Evaluation of a predictive model for implant surface topography effects on early osseointegration in the rat tibia model.* Journal of Prosthetic Dentistry, 2001. **85**(1): p. 40-46.

49. Anderson, R.C., et al., *An evaluation of skeletal attachment to LTI pyrolytic carbon, porous titanium, and carbon-coated porous titanium implants.* Clin Orthop Relat Res, 1984(182): p. 242-57.

50. Feighan, J.E., et al., *The influence of surface-blasting on the incorporation of titanium-alloy implants in a rabbit intramedullary model.* J Bone Joint Surg Am, 1995. **77**(9): p. 1380-95.

51. Hou, S.J., et al., *Multiobjective optimization of multi-cell sections for the crashworthiness design.* International Journal of Impact Engineering, 2008. **35**(11): p. 1355-1367.

52. Raquel, C.R. and P.C. Naval, *An effective use of crowding distance in multiobjective particle swarm optimization*, in *GECCO 2005: Genetic and Evolutionary Computation Conference, Vols 1 and 2*, H.G. Beyer, Editor. 2005, Assoc Computing Machinery: New York. p. 257-264.

53. Padhye, N., et al., *Empirical comparison of MOPSO methods - guide selection and diversity preservation*, in *2009 Ieee Congress on Evolutionary Computation, Vols 1-5*. 2009, Ieee: New York. p. 2516-2523.

54. Lian, Z., et al., *Effect of bone to implant contact percentage on bone remodelling surrounding a dental implant.* International Journal of Oral and Maxillofacial Surgery, 2010. **39**(7): p. 690-698.

55. Sun, G.Y., et al., *Crashworthiness design of vehicle by using multiobjective robust optimization.* Structural and Multidisciplinary Optimization, 2011. **44**(1): p. 99-110.

56. Tomaszewski, P.K., et al., *Numerical analysis of an osseointegrated prosthesis fixation with reduced bone failure risk and periprosthetic bone loss.* Journal of Biomechanics, 2012. **45**(11): p. 1875-1880.

57. Adachi, T., et al., *Framework for optimal design of porous scaffold microstructure by computational simulation of bone regeneration.* Biomaterials, 2006. **27**(21): p. 3964-3972.

58. Chen, Y., S. Zhou, and Q. Li, *Computational design for multifunctional microstructural composites.* International Journal of Modern Physics B, 2009. **23**(6-7): p. 1345-1351.

59. Sturm, S., et al., *On stiffness of scaffolds for bone tissue engineering-a numerical study.* Journal of Biomechanics, 2010. **43**(9): p. 1738-1744.

60. Arabnejad Khanoki, S. and D. Pasini, *Multiscale design and multiobjective optimization of orthopedic hip implants with functionally graded cellular material.* Journal of biomechanical engineering, 2012. **134**(3): p. 031004.

61. Natali, A.N., et al., *Investigation of the integration process of dental implants by means of a numerical analysis.* Dental Materials, 1997. **13**(5-6): p. 325-332.

Chapter 10: Characterisation of Anisotropic Elasticity and Diffusivity in Injection-Moulded Porous Titanium for Dental and Orthopaedic Application

With the same target of enhancing osseointegration, as stated in Chapter 9, using a porous titanium implant has been shown as an alternative. This paper introduces the novel injection moulding fabrication technique and then systemically characterises the fabricated samples. Surface morphology is firstly examined using a scanning electron microscope (SEM) and then a micro-computational topology (μ-CT) scan is performed to non-invasively capture its subsurface 3D microscopic features. The porosity and the pore sizes are determined statistically based on the μ-CT image analysis. The minimum size of a representative volume element (RVE) of the scans is determined by convergence tests. Based on FE models created from these RVEs, homogenisation methods determine the microscopic heterogeneity in their anisotropic elasticity and oxygen diffusivity.

Associated Publications:

1. **Junning Chen**, Zhongpu Zhang, Liangjian Chen, Wei Li, Michael V. Swain, Qing Li. **Injection-Moulded Porous Titanium Dental Implant and Characterization Modeling**. Submitted to *Dental Materials*.
2. **Junning Chen**, Liangjian Chen, Wei Li, Michael V. Swain, and Qing Li. **Porous Titanium Implant and Micro-CT Based Characterization of Sub-Surface Morphology**. *PRICM – 8*. John Wiley & Sons, Inc., 2013: p. 1579-1586.

10.1 Introduction

Endosseous implants made of titanium and its alloys have been widely used for orthopaedic and dental application in load-bearing scenarios [1-3]. As the most prevalent materials, their proven biocompatibility is favoured by osseointegration [2, 4]. Sandblasting and acid etching are the current gold standard for the surface treatment, and have shown advantages in improving osseointegration with increased surface roughness [5, 6]. However, these surface features are limited in several microns, and there are still some biomechanical drawbacks, including stress-shielding and insufficient bone-implant bonding, to prevent more satisfactory clinical outcomes [2, 7, 8]. A porous implant substrate is capable of reducing stress-shielding, by increasing the porosity and alternating the 3D microstructure to reduce the local material property mismatch [1, 2, 9]. It also provides considerably more space to promote cell attachment and tissue ingrowth with the increased contact surface area, thereby facilitating a higher level of bone-implant interaction for osteoblast adhesion [2, 8, 10]. Advanced technologies, such as microwave sintering and plasma spraying, have been developed for fabricating desired morphological surfaces for implants [1, 4, 8, 11, 12].

Although these technologies are able to create a highly porous implant surface with sufficient interconnection, they have limited control on the porosity and poor integrity with post-machining process [1, 9, 12, 13]. As a novel fabrication method in implant dentistry, metal injection moulding has been demonstrated to have superior control on porosity and pore size, giving a near-net-shape with a high open-pore ratio of 98% for mass scale production [9]. This type of porous structure was often found anisotropic and micro-heterogeneous, of which the localised material properties are primarily determined by its microstructure [14-18]. The heavy laboratory expense of fabricating this novel material limits the repetitive testing on consistent samples to have statistic meaning, while

computational simulation accelerate the analysis with various mathematical models built in the last few decades [14-16, 19-21]. With the rapid evolution in micro-computational tomography (μCT) technology, imaging of the microstructure becomes available to provide precise and detailed finite element models for numerical analysis [14, 15].

The principal elastic moduli are the critical indication of material property mismatch, for bone tissue ingrowth and mechanical stress-induced apoptosis [22-24]. The shear moduli are the key measurement to the micro motion of the implant with respect to the host bone, which may cause initial instability and lack of bone ingrowth [25]. The diffusivity has shown its critical role in initial wound healing and vascular formation [26-28]. For the above reasons, these material properties are important factors in evaluating biomechanical potential of an implant media.

This paper briefly introduces the novel fabrication technique of this porous titanium implant by injection moulding, and systemically examines the samples under scanning electron microscope (SEM) and micro-computational tomography (μCT), for its surface morphology and subsurface 3D micro structure. The CT images are further processed to determine its porosity and pore sizes statistically. The minimum size of a representative volume element (RVE) of this material is determined by a convergence tests. Finite element models are then created based on the CT scans for homogenisation analysis, to determine the microscopic heterogeneity in elasticity and diffusivity. The outcomes will be compared to literature data in both the mechanical and biological aspects, to reveal its potential for dental and orthopaedic application.

10.2 Materials and Methods

10.2.1 Material Fabrication, Imaging, and Modelling

The porous titanium substrate was created using hydrogenation-dehydrogenation titanium (HDH Ti) powder with particle sizes less than 77 μm and sodium chloride (NaCl) powder less than 290 μm, at a volume fraction ratio of 6:4. A multi-component binder consisted of high density polyethylene (HDPE), paraffin wax (PW), polyethylene glycol (PEG), and stearic acid (SA), and was used to mix the powders. The mixture at 155 ºC is injected into a 30 ºC mould at 100 MPa, around a solid titanium core inside (3 mm in diameter) (Figure 10-1a). Organic components in the formed compact are removed by methylene dichloride at 37 ºC, and the space holder (NaCl) is removed a water bath, followed by a thermal debinding at 720 ºC in argon gas. More details can be explored in the report by Chen et al. [9].

For the surface morphology characteristics, the finished samples are firstly examined under a scanning electron microscope, Hitachi S-4500 (Australia Centre for Microscopy & Microanalysis, Sydney Australia). The accelerating voltage is set to 15 kV, and the working distance is set to 17 mm. Three arch sections are cut from the porous implant samples (Figure 10-1a & b), with a radius of 1.5 mm, a base width of 1.2 mm, and a length of 2 mm. Each sample is scanned by μCT, MicroXCT-400 (Xradia Inc, USA) with a resolution at 4.02μm per pixel, and 988 slices of DICOM images are reconstructed for each scan. Preliminary image processing and feature recognition are performed in Avizo Fire (FEI Visualization Sciences Group, Burlington USA) for the pore size and porosity. All statistical analysis in this paper is performed in IBM SPSS Statistics Ver. 19 (IBM Cor., New York USA).

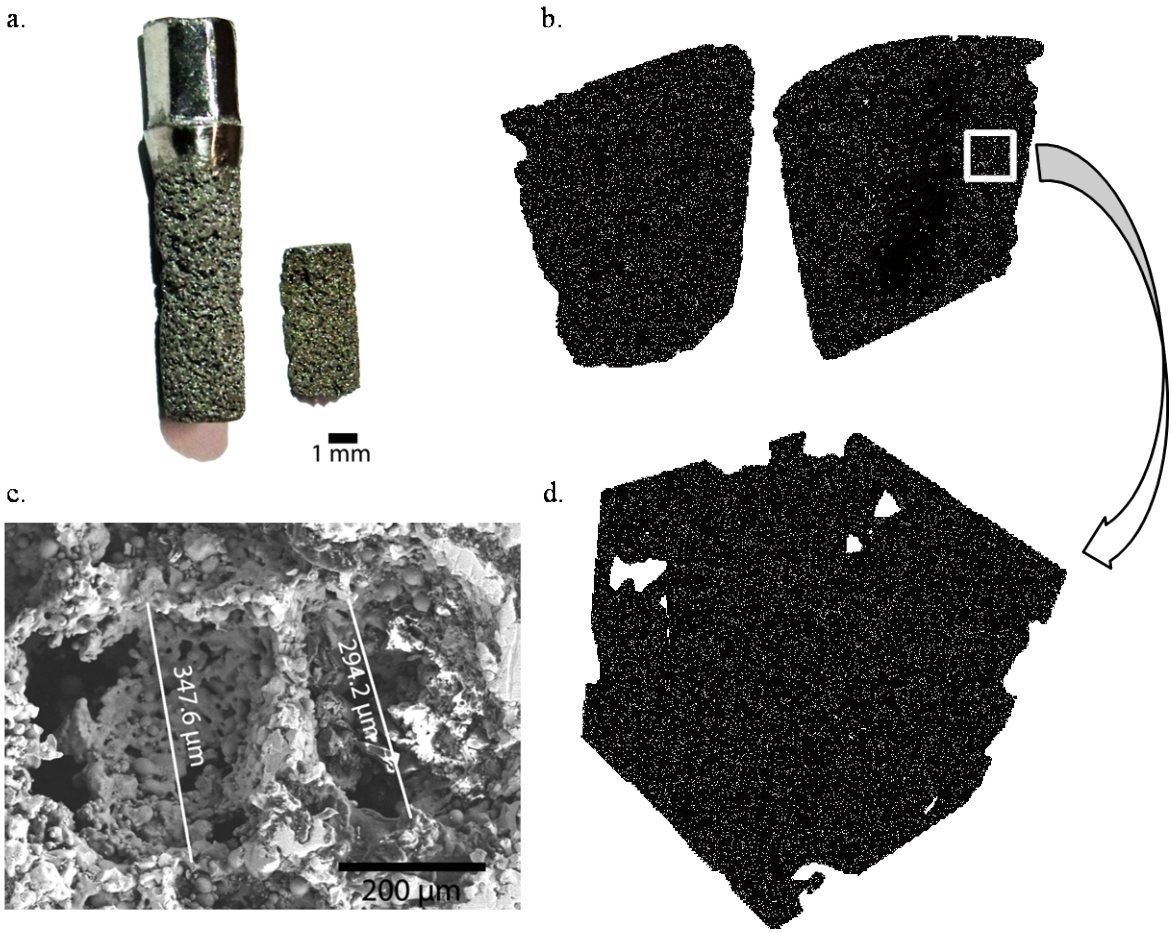

Figure 10-1 (a) Porous dental implant fabricated by injection moulding and a cut sample; (b) one cut sample reconstructed from CT images; (c) SEM image of the porous surface showing hierarchical features; (d) a RVE sample of 700 µm randomly selected from CT images, reconstructed and meshed into a finite element model.

The 3D mask for each sample is further reconstructed from the DICOM images in ScanIP (Simpleware Ltd, UK), and the meshed finite element models are exported to ABAQUS 6.9.1 (Dassault Systèmes Australia Pty Ltd, AU) for analysis. The microscopic structure is likely to behave differently to the overall macroscopic entirety, especially in the heterogeneous real-world materials; therefore, a representative volume element (RVE) must be determined to be capable of reflecting the macroscopic characteristics and properties [14-16, 29-31]. The common approach is to create a representing model with the minimum volume that is adequate to show the effective material characteristics and properties as the entire model. Cubic representative models with edge length varying from

300 μm to 700 μm are selected for a convergence test [30] on their overall porosities (%Por), and the homogenized first principal elastic modulus (E11, along the radial direction). 8 non-overlapping subdivisions of the implant samples are randomly selected for each length. Meanwhile, the numerical accuracy is ensured by a numeric convergence test [2, 32], to ensure adequate mesh densities and present the complex geometry accurately.

10.2.2 Effective Material Elastic Moduli

Until the dramatic increase of computational power recently, the direct computation of micro-material responses was hard to achieve [33]. Accordingly, the Hills-Voigt-Reuss bounds were developed to estimate the effective responses of a mixture of two materials [30, 33], which were improved by Hashin and Shtrikman (known as HS-Bounds) [34, 35]. Following this theory, the randomly distributed void is reasonable to be taken as a type of material with a very low elastic modulus approaching to 0 GPa with no tendency of maintaining its volume (Poisson's ratio =0). The two bounds for bulk and shear moduli can be stated in Eq. (1) to (4), where %Por is the same to void volume fraction, k and μ stand for bulk modulus and shear modulus, respectively.

$$k^*_{\text{low}} = \text{k}_{\text{void}} + \frac{(1 - \%\text{Por})}{\frac{1}{k_{\text{Ti}} - k_{\text{void}}} + \frac{3 \times \%\text{Por}}{3k_{\text{void}} + 4\mu_{\text{void}}}} \tag{1}$$

$$k^*_{\text{upper}} = \text{k}_{\text{Ti}} + \frac{\%\text{Por}}{\frac{1}{k_{\text{void}} - k_{\text{Ti}}} + \frac{3 \times (1 - \%\text{Por})}{3k_{\text{Ti}} + 4\mu_{\text{Ti}}}} \tag{2}$$

$$\mu^*_{\text{low}} = \mu_{\text{void}} + \frac{(1 - \%\text{Por})}{\frac{1}{\mu_{\text{Ti}} - \mu_{\text{void}}} + \frac{6 \times \%\text{Por}(k_{\text{void}} + 2\mu_{\text{void}})}{5\mu_{\text{void}}(3k_{\text{void}} + 4\mu_{\text{void}})}} \tag{3}$$

$$\mu^{*}_{\text{upper}} = \mu_{\text{Ti}} + \frac{\%\text{Por}}{\frac{1}{\mu_{\text{void}} - \mu_{\text{Ti}}} + \frac{6\times(1-\%\text{Por})(k_{\text{void}} + 2\mu_{\text{void}})}{5\mu_{\text{void}}(3k_{\text{Ti}} + 4\mu_{\text{Ti}})}} \quad (4)$$

The HS bounds provide a very wide range of estimation, and this approach does not consider other factors, such as microscopic geometry. Therefore, the homogenisation method based on the conservation of energy is adopted, which has shown successful predictions in numerical characterisations with experiments [34]. With an appropriate RVE volume selection, the effective micro-scale material properties should be able to describe the macroscopically homogeneous media with macro-stress and macro-strain fields [16]. This method satisfies the conditions for the Hill's energy theorem that the total stain energy U stored in an effective volume V′ must be equivalent to the strain energy U′ stored in the heterogeneous RVE volume V (Eq. (5)). Given a normal or shear load, the equivalent stress $\boldsymbol{\sigma}_{\Omega}$ and strain $\boldsymbol{\varepsilon}_{\Omega}$ can be determined from FE simulations, and the constitutive tensor Φ^{*} can be inversely solved from the governing equation (Eq. (6)). In this equation, each independent loading case will lead to six equations, hence resulting in total 36 equations.

$$\frac{1}{2}\int \boldsymbol{\sigma}_{\text{ij}} : \boldsymbol{\varepsilon}_{\text{ji}} \text{dV} = \frac{1}{2}(\boldsymbol{\sigma}_{\Omega} : \boldsymbol{\varepsilon}_{\Omega})\ \text{V} \quad (5)$$

$$\boldsymbol{\sigma}_{\Omega} = \Phi^{*} : \boldsymbol{\varepsilon}_{\Omega} \quad (6)$$

The general constitutive tensor contains 36 constants to illustrate the anisotropic material properties. As the major concerns are laid on the normal and shear moduli, this paper assumes that RVE model is orthotropic for the simplicity in solving, accepted by previous researches on cellular material or structure [14, 16, 33, 36-38]. The expanded constitutive equation can be expressed in Eq. (7) [38].

$$\begin{Bmatrix}\sigma_{11}\\ \sigma_{22}\\ \sigma_{33}\\ \sigma_{12}\\ \sigma_{13}\\ \sigma_{23}\end{Bmatrix}=\begin{bmatrix}C_{11} & C_{12} & C_{13} & & & \\ C_{21} & C_{22} & C_{23} & & \cdots & \\ C_{31} & C_{32} & C_{33} & & & \\ & & & C_{44} & & \\ & \cdots & & & C_{55} & \\ & & & & & C_{66}\end{bmatrix}\begin{Bmatrix}\varepsilon_{11}\\ \varepsilon_{22}\\ \varepsilon_{33}\\ \varepsilon_{12}\\ \varepsilon_{13}\\ \varepsilon_{23}\end{Bmatrix} \tag{7}$$

To generate the six independent loads, the usual choices on loading cases are shown in Eq. (8) for the corresponding RVE surfaces,

$$\boldsymbol{\sigma} \text{ or } \boldsymbol{\varepsilon}=\begin{bmatrix}\beta & 0 & 0\\ 0 & 0 & 0\\ 0 & 0 & 0\end{bmatrix},\begin{bmatrix}0 & 0 & 0\\ 0 & \beta & 0\\ 0 & 0 & 0\end{bmatrix},\begin{bmatrix}0 & 0 & 0\\ 0 & 0 & 0\\ 0 & 0 & \beta\end{bmatrix},\begin{bmatrix}0 & \beta & 0\\ \beta & 0 & 0\\ 0 & 0 & 0\end{bmatrix},\begin{bmatrix}0 & 0 & \beta\\ 0 & 0 & 0\\ \beta & 0 & 0\end{bmatrix},\begin{bmatrix}0 & 0 & 0\\ 0 & 0 & \beta\\ 0 & \beta & 0\end{bmatrix} \tag{8}$$

where β is a load parameter [30, 33, 39] to indicate the same magnitude or unit of 1 for the homogenisation purpose. Appropriate boundary conditions must be assigned to RVE models, and the effective responses calculated over a finite domain depend on the type of boundary conditions. Two basic types of boundary conditions are often adopted in analysis of heterogeneous material, with homogeneous boundary conditions in either controlled stress or strain fields [30, 40, 41]. One of them is to implement a uniform traction vector on the corresponding boundary ∂V according to

$$\mathcal{L}(\boldsymbol{x})=\sigma^{*}\cdot\boldsymbol{n}=\left(\frac{1}{\mathrm{V}}\int_{\mathrm{V}}\sigma d\mathrm{V}\right)\cdot\boldsymbol{n}\quad\text{at}\qquad\forall\boldsymbol{x}\in\partial\mathrm{V} \tag{9}$$

and is to be called static or Neumann uniform boundary condition (SUBC). The other one is to impose a displacement vector at all points belonging to the boundary ∂V according to

$$\mathcal{E}(\boldsymbol{x})=\varepsilon^{*}\cdot\boldsymbol{x}=\left(\frac{1}{\mathrm{V}}\int_{\mathrm{V}}\varepsilon d\mathrm{V}\right)\cdot\boldsymbol{n}\quad\text{at}\qquad\forall\boldsymbol{x}\in\partial\mathrm{V} \tag{10}$$

named as displacement or Dirichlet uniform boundary condition (KUBC). Both of these two methods have been performed in previous researches [14-16, 20, 36, 37, 40], and have a wide range of acceptance.

10.2.3 Oxygen Diffusivity and Distribution

Oxygen has been found to play a critical and rate-limiting role in wound healing and tissue growth [26-28]. The empirical studies have already shown that oxygen transportation and dissolution are complex problems in blood and tissues [42-45]. This paper aims to simulate how oxygen is transported by diffusion into the implant subsurface, before the vascular network forms in the porous voids. Two assumptions are made. Firstly, in the early stage of healing, the tissue and biofluid mixture in the voids can be considered as a uniform and homogenous material, which enables the analysis to focus on the implant microstructural effects [44, 46, 47]. Secondly, due to lack of vascular network and slow movement of biofluid, the transportation of oxygen by chemicals (metalloproteins, such as haemoglobin) and flow is negligible for the simplicity of diffusion analysis [28, 45].

A Kroghian model is employed to formulate the oxygen tension distribution at a steady-state [48], and the diffusion activity is driven by the gradient of its chemical potential [48, 49] that allows non-uniform diffusion in the base material. The mass conservation for the diffusing phase is stated as in Eq. (11), where V is the elemental volume whose surface is S, $\mathbf{n}$ is the outward normal to S, and $\mathbf{J}$ is the flux of concentration of the diffusion phase.

$$\int_{\mathrm{V}} \frac{dc}{dt} dV + \int_{\mathrm{S}} \mathbf{n} \cdot \mathbf{J} dS = 0 \tag{11}$$

Without driving fluid pressure or temperature, the concentration flux $\mathbf{J}$ can be simply defined as

$$J = -D \cdot \frac{\partial \phi}{\partial x} \tag{12}$$

where D(c, θ, f) is the diffusivity and ϕ is the normalised concentration. The diffusion coefficient of oxygen in various tissues and biofluid varies in a wide range from 1.4×10^{-5} to 3.6×10^{-5} cm^2/sec in previous *in vivo* studies [46], and a moderate diffusion rate of 2.0×10^{-5} cm^2/sec is adopted at full saturation. Similar to the conservation of energy in determining mechanical moduli, the effective oxygen diffusivity of the RVE is determined in Eq. (13) based on the conversation of mass at a steady state, in which the mass flow rate (MFR) in the volume is the same between the RVE and the homogeneous model. In this equation, the s_Ω is the equivalent solubility in the RVE and D_Ω is the effective diffusivity of oxygen.

$$-D_\Omega \cdot \frac{\partial \left(\int \phi_{high} dA - \int \phi_{low} dA \right)}{\partial x} = \int -D_i \cdot \frac{\partial \phi_i}{\partial x} dA \tag{13}$$

In the meantime, another well-known homogenisation method of determining diffusivity based on scaling is adopted, too. The effective diffusivity is the result of combining several geometrical features, such as pore shape, size, interconnectivity, porosity and specific surface area [50], which can be determined by homogenisation by asymptotic expansion [51]. Such formulation is also established on the same representative volume element concept that the structure of RVE is a lower level building block of the higher level organisation, which can be upscaled to obtain the effective properties of the upper level structure [51]. In this analysis, RVE represents the microscopic (y) level and the macroscopic (x) forms homogenised results for the entire material. This homogenisation method solves for flux correction driven by distributed nodal forces [51]. The governing equations (Eq. (14)-(16)) are as follows,

$$\nabla \cdot \left(a \nabla u \left(\mathrm{x}, \mathrm{y} \right) \right) + f = 0 \qquad \mathrm{x} \in \Omega \tag{14}$$

$$u\left(\mathrm{x}, \mathrm{y} \right) = u\left(\mathrm{x} \right) + \varepsilon u\left(\mathrm{y} \right) \tag{15}$$

$$\varepsilon = \frac{\mathrm{x}}{\mathrm{y}} \tag{16}$$

where a is the conductivity matrix, u is the transport quality, x is the macroscopic scale, y is the microscopic scale, f is the driving force, and ε is the scaling ratio. The effective conductivity matrix is computed by solving the following equations (Eq. (17)-(19)):

$$\nabla_{\mathrm{y}} \cdot \left(a\left(\mathrm{y} \right) \nabla_{\mathrm{y}} w_{\mathrm{j}} \left(\mathrm{y} \right) \right) = -\nabla_{\mathrm{y}} \cdot \left(a\left(\mathrm{y} \right) e_{\mathrm{j}} \right) \tag{17}$$

$$a_{\mathrm{ij}} = \int_{\mathrm{y}} a\left(\mathrm{y} \right) \left(\delta_{\mathrm{ij}} + \partial_{\mathrm{y_i}} w_{\mathrm{j}} \left(\mathrm{y} \right) \right) \mathrm{d}\mathrm{y} \tag{18}$$

$$\nabla \cdot \left(\mathrm{A} \nabla u\left(\mathrm{x} \right) \right) + f\left(\mathrm{x} \right) = 0 \tag{19}$$

where a(y) is the conductivity matrix of the material, w is the characteristic transport quality on a microscopic scale, e is an identity matrix with the same size as the number of modeling dimensions, x and y indicates it is a microscopic and a microscopic model respectively, a_{ij} is the effective conductivity coefficient in the matrix A, and δ is the Kronecker delta.

These equations are solved j times, each time for one column of e, to reconstruct the full effective conductivity matrix A. In a finite element analysis, the left hand side of Eq. (17) is treated as a body force while a(y) is taken as an identity matrix multiplied by the material conductivity coefficient. The simulation result is then ensembled by integration of w over the entire design domain according to Eq. (18). For a multi-scale

model, this upscaling process is repeated. Such procedure finally arrives at an uppermost level with a homogenised conductivity (Eq. (19)).

10.3 Result and Discussion

10.3.1 Pore Size and Distribution

Figure 10-1a shows the optical image of a fabricated implant and a section prepared for scanning, in which the macroscopic pores on surface are estimated from 0.20 to 0.45 mm in diameter. Further SEM scans reveal more detailed microscopic features of this porous media showing richly porous network as indicated in Figure 10-1c. The µ-CT images are reconstructed to form a 3D view of the sample section as in Figure 10-1b.

The feature recognition of the pores on the maximum internal distance (the largest diameter for irregular pore surfaces) is plotted in Figure 10-2 ($\rho < 0.005$). 100-200 µm pores are dominant in this porous media, and the major pore size distribution crosses a range from 50 to 400 µm. The average porosity in all three samples is 45.81 ± 3.02%.

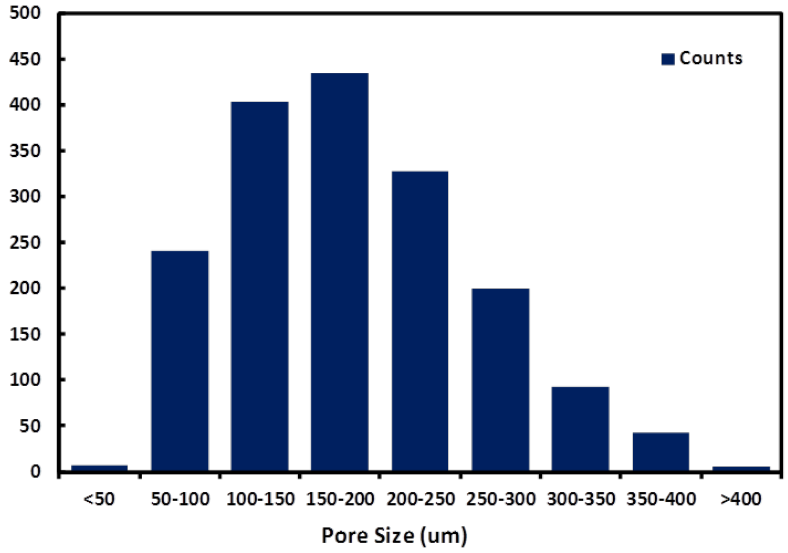

Figure 10-2 Pore size distribution in all scanned implant samples, varying from 50 to 400 µm, with 100 to 200 µm dominant.

10.3.2 Representative Volume Element (RVE)

Five sampling sizes (300 - 700 µm) are examined in the convergence test for the minimum size of RVE, based on the average and standard deviation of their first effective

principal modulus (E11) and porosity. Each sampling size has 8 non-overlapping samples. Figure 10-3a plots E11 and Figure 10-3b shows the porosity, against the total volumes of RVEs.

For E11 with two types boundary conditions, SUBC shows an increasing trend and KUBC indicates a decreasing trend along the tendency of converging. This merging pattern with increasing RVE sizes falls into a good agreement with previous studies [15, 30, 40], and the improved accuracy leads to the approach to a certain range of homogenised values. Both trend lines sit well in the range defined by HS bounds [34, 35, 38]. The porosity also shows well-settled trend towards 700 µm RVEs, close to the feature recognition result of all implant samples in Section 3.1. 700 µm RVE is adopted for further analysis with a sufficient geometric accuracy.

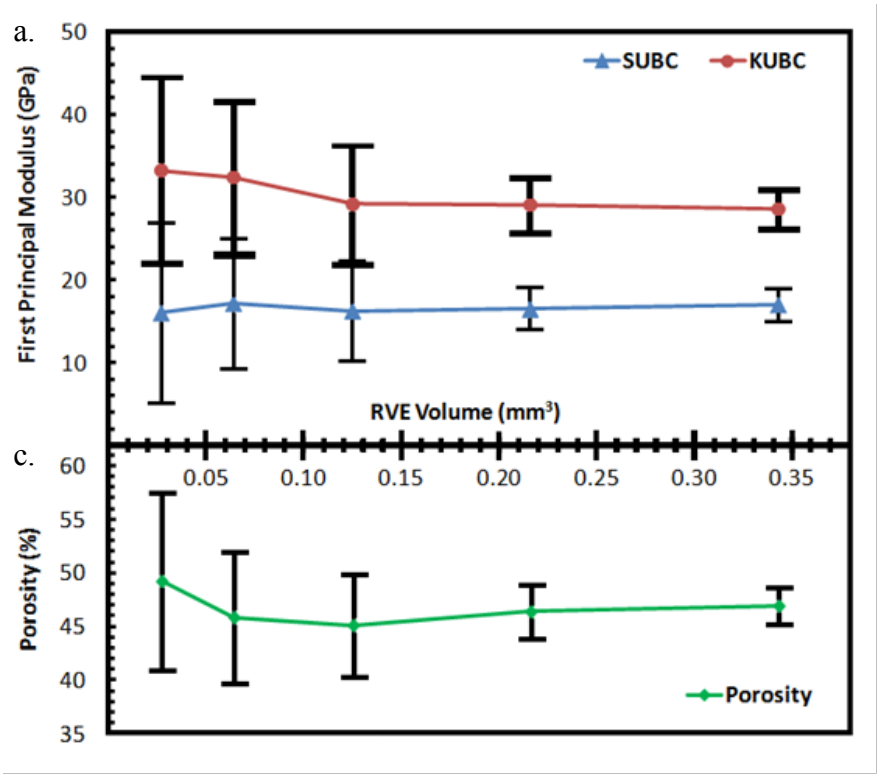

Figure 10-3 (a) Convergence test of RVE models with different volume sizes on the first principal elastic modulus (E11)) with SUBC (blue triangle), KUBC (red dot), and (b) the porosity (green rhombus).

For the 8 RVE samples with 700 μm, there are 993, 557 ± 39, 616 linear tetrahedral elements in average. This is equivalent to a mesh density of 0.34 ± 0.01 element per voxel, which is higher than similar studies [14, 20] to ensure its numeric accuracy.

10.3.3 Effective Elastic Moduli

The results of the effective elastic moduli have been summaries in Table 1, and the individual results for each sample are plotted in Figure 10-4 against their porosities. As revealed by the early researches [29, 30, 40], SUBC often underestimate the material stiffness without considering the neighbour units of the model, while KUBC lead to an over-estimated stiffness as the model is over-constrained. Nevertheless, these two sets of material moduli indicate a refined range of possible material properties than the Hashin and Shtrikman (HS) Bounds. There are other numerical methods available for special cases, such as periodic boundary conditions [16, 29, 39]; however, the Hill's energy theorem adopted in this paper suits the most general structures with high irregularity and complexity.

Table 10-1 Effective Elastic Moduli Determined by Homogenisation Method with Static Uniform and Kinematic Uniform Boundary Conditions

Modulus (GPa)	Static Uniform Boundary Condition	Kinematic Uniform Boundary Condition
E_{11}	16.99 ± 2.41	28.58 ± 1.96
E_{22}	15.89 ± 1.86	25.05 ± 1.21
E_{33}	13.39 ± 2.72	20.82 ± 4.15
G_{44}	4.64 ± 0.74	6.54 ± 0.51
G_{55}	4.22 ± 0.97	6.00 ± 0.99
G_{66}	4.06 ± 0.79	4.84 ± 0.92
Porosity	46.91 ± 1.83 %	

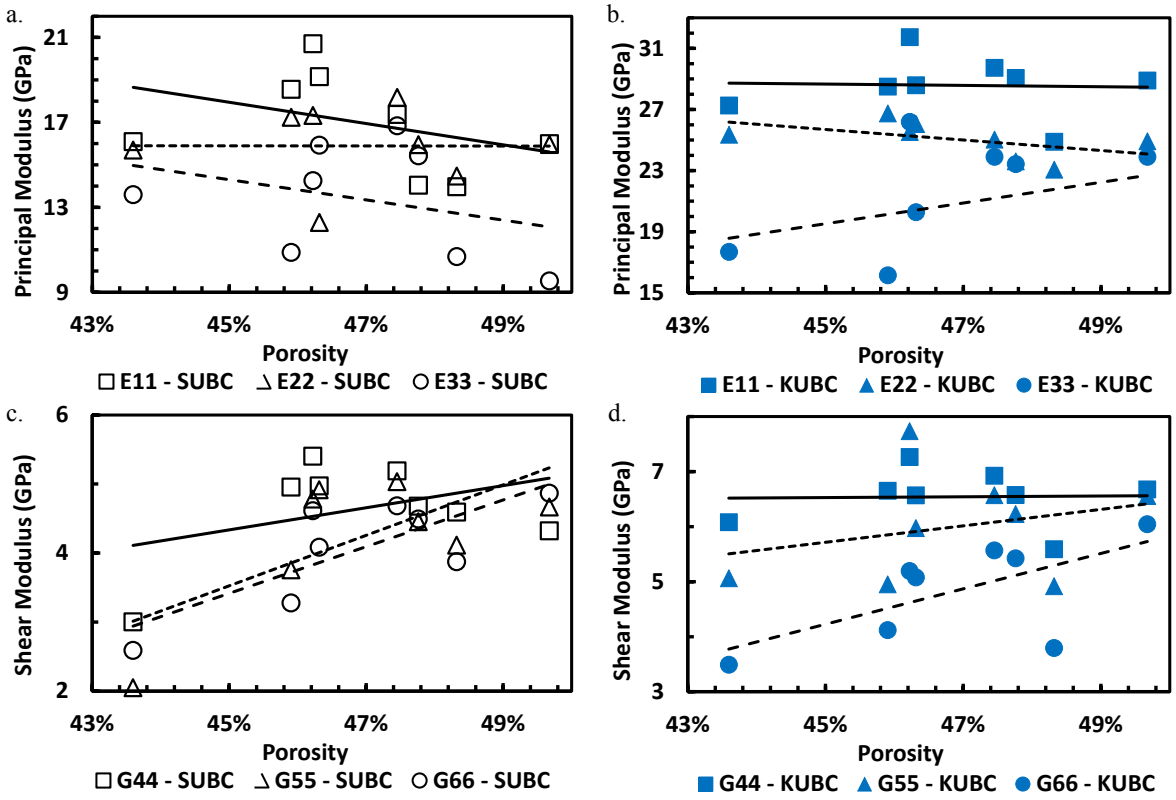

Figure 10-4 The effective principal moduli (a,b) and shear moduli (c,d) determined by the homogenisation method, with static uniform boundary conditions (left) and kinetic uniform boundary condition (right) over 8 REVs with 700 µm.

Both effective elastic moduli determined with SUBC and KUBC indicate that this porous media is stiffer in the radial and circumferential directions (E_{11} & E_{22}) than in the longitudinal direction (E_{33}) ($\rho < 0.005$). This porous media is orthotropic with considerable differences between the radial directions and the longitudinal direction. On contrast, G44 and G55 of the shear moduli are slightly larger than G66 with little difference ($\rho > 0.05$). Within a small range of porosity in the given samples, the variation of porosity could not demonstrate a clear effect on any elastic modulus difference (ρ-value > 0.05).

Young's modulus of cortical bone has been measured by various techniques, which varies from 14 to 25 GPa [52, 53], and cancellous bone has a broader range varying from 0.5 to over 4 GPa [53, 54]. Cortical bone has directional differences in elastic moduli, that the longitudinal direction is about 40% stiffer than the transverse in long bone [53]. The

elastic moduli determined in this study show a great potential to reduce the mechanical property mismatch to the local cortical and cancellous bone for dental and orthopaedic application, which reduce the chance of stress-shielding around the implant to cause implant failure in mid or long term [23, 24]. The current sample has a close match to the cortical bone, and the injection-moulding technique allows a wide range of porosity from 10 to 70% [9], which can further reduce the stiffness of this material with increasing porosity. The orthotropic behaviour of this porous media can be optimised by varying the microscopic structure to match the directional stiffness as the native bone, which will require further investigation and study.

10.3.4 Oxygen Diffusivity

Table 2 has summarised the average oxygen diffusivities of all 8 samples in the three directions and their standard deviations. Both methods by using conservation of mass and multi-scale homogenisation have come up with similar results. Different to the moduli found in Section 3.2, the oxygen diffusivity along the radial direction (D11) is higher than the circumferential and longitudinal directions (ρ-value < 0.001). This trend can also be seen in the individual plots of Figure 10-5, where the trend line of the diffusivity along the radial direction sits well above the other two. Within a consistent range of porosity, the porosity could not demonstrate a clear effect on the diffusivity variation (ρ-value > 0.05), similar to the findings in the effective moduli.

Table 10-2 Effective Diffusivity Determined by Conservation of Mass and Multi-Scale Homogenisation

Diffusivity (10^{-6} cm^2/sec)	Conversation of Mass	Multi-Scale Homogenisation
D11	3.08 ± 0.20	4.32 ± 0.28
D22	2.04 ± 0.31	2.58 ± 0.25
D33	1.99 ± 0.13	2.51 ± 0.34

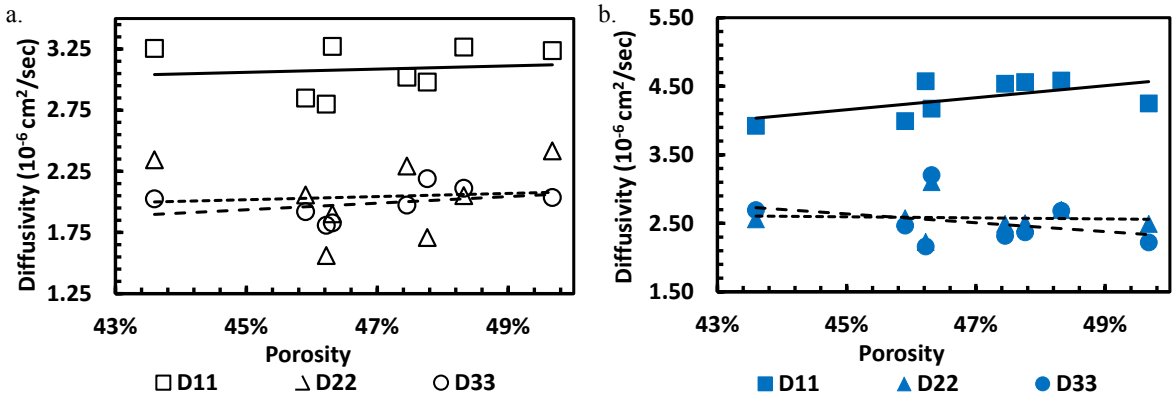

Figure 10-5 Diffusivity determined on RVE models of 700 µm based on conservation of mass method and multi-scale homogenisation method

Oxygen supply is always one of primal concerns in bone healing, growth and remodeling. In cortical bone, oxygen is transported through the vascular system in the Haversian and Volkmann's canals; however, there are very few reports addressing the oxygen diffusivity in either cortical or cancellous bone after implantation [48]. The *in vivo* oxygen diffusivity through a fresh bone was found at 2.31×10^{-5} cm^2/sec (0.02 mm^2/day) by using stain [55]. The conservation of mass method estimates that the initial oxygen diffusivity in this porous titanium media after implantation varies from the 8.7% to 13.3% of the native bone's diffusivity in different directions, and the multi-scale homogenisation finds that it varies from 10.9% to 18.7%. The directional differences have a potential to be further optimised for a higher radial diffusivity, which can reduce the change of necrosis caused by insufficient oxygen [56] and also benefit pre-vascular network formation with improved oxygen and nutrients delivery as well as waste removal [57]. Meanwhile, the majority of the void space is larger than 150 um as indicated in Figure 10-2, which provides sufficient space for vascular network ingrowth to assist further migration of osteoid and fibroblast [58]. These benefits may lead to early establish of bone-implant lock mechanism after implantation, and increase the long-term success rate.

10.4 Conclusions

A novel injection-moulding technique has been applied to fabricate a highly porous titanium media for orthopaedic and dental application. This paper has examined its macroscopic and microscopic features by CT and SEM scanning, and estimated its effective elastic moduli and oxygen diffusivity based on a representative element volume (RVE) in a finite element analysis. 8 cubic models with 700 μm length are created from the CT scans as the representative volumes after a convergence test based on the porosity and the first principal elastic modulus. The porosity of these RVE models falls into a good agreement with the SEM images and 3D feature analysis of the CT scans. By applying the two different types of boundary conditions (SUBC & KUBC), the strain energy equivalence provides a refined range of possible elastic moduli as a homogeneous media. The results suggest that this porous media can have a close-match to the mechanical property of local bones to reduce the chance of stress-shielding. Meanwhile, this material shows orthotropic behaviours which can be utilised to mimic native bone behaviours. The diffusivity, on the other hand, is determined by two different homogenisation methods showing similar results, and it is about 10 to 18% of the native bone which provides considerable oxygen transport for the initial pre-vascular network formation within sufficient spaces revealed by CT image analysis. Similarly, the diffusivity also demonstrates its orthotropic characteristics, where the radial direction oxygen transport can be further reinforced to promote cell migration and tissue ingrowth. The next stage of investigation can be done to link the fabrication inputs (particle size, ratio, etc.) to the mechanical and biological features of this type of media [59], and the optimisation of the gradients to trace the optimal strength and diffusivity is also an important direction [2]. Furthermore, the cellular response and local bone remodelling is an attractive region of

study, where both finite element analysis and medical study can be perform on this porous media [2, 59-61].

Acknowledgement

This work is supported by Australian Research Council (ARC) and Australian Postgraduate Award (APA).

10.5 References

1. Dewidar, M.M. and J.K. Lim, *Properties of solid core and porous surface Ti-6Al-4V implants manufactured by powder metallurgy.* Journal of Alloys and Compounds, 2008. **454**(1-2): p. 442-446.
2. Rungsiyakull, C., et al., *Surface morphology optimization for osseointegration of coated implants.* Biomaterials, 2010. **31**(27): p. 7196-7204.
3. Hayashi, K., et al., *Quantitative-analysis of invivo tissue responses to titanium-oxide-coated and hydroxyapatite-coated titanium-alloy.* Journal of Biomedical Materials Research, 1991. **25**(4): p. 515-523.
4. Kunzler, T.P., et al., *Systematic study of osteoblast and fibroblast response to roughness by means of surface-morphology gradients.* Biomaterials, 2007. **28**(13): p. 2175-2182.
5. Kim, H., et al., *The biocompatibility of SLA-treated titanium implants.* Biomedical Materials, 2008. **3**(2).
6. Li, D.H., et al., *Biomechanical comparison of the sandblasted and acid-etched and the machined and acid-etched titanium surface for dental implants.* Journal of Biomedical Materials Research, 2002. **60**(2): p. 325-332.
7. Piattelli, A., et al., *Histologic studies on osseointegration: Soft tissues response to implant surfaces and components. A review.* Dental Materials, 2011. **27**(1): p. 53-60.
8. Morra, M., et al., *Surface engineering of titanium by collagen immobilization. Surface characterization and in vitro and in vivo studies.* Biomaterials, 2003. **24**(25): p. 4639-4654.
9. Chen, L.-j., et al., *Porous titanium implants fabricated by metal injection molding.* Transactions of Nonferrous Metals Society of China, 2009. **19**(5): p. 1174-1179.
10. Vaillancourt, H., R.M. Pilliar, and D. McCammond, *Finite element analysis of crestal bone loss around porous-coated dental implants.* Journal of Applied Biomaterials, 1995. **6**(4): p. 267-282.
11. Esposito, M., et al., *Biological factors contributing to failures of osseointegrated oral implants (I). Success criteria and epidemiology.* European Journal of Oral Sciences, 1998. **106**(1): p. 527-551.
12. Traini, T., et al., *Direct laser metal sintering as a new approach to fabrication of an isoelastic functionally graded material for manufacture of porous titanium dental implants.* Dental Materials, 2008. **24**(11): p. 1525-1533.
13. Thieme, M., et al., *Titanium powder sintering for preparation of a porous functionally graded material destined for orthopaedic implants.* Journal of Materials Science-Materials in Medicine, 2001. **12**(3): p. 225-231.
14. Veyhl, C., et al., *Finite element analysis of the mechanical properties of cellular aluminium based on micro-computed tomography.* Materials Science and Engineering a-Structural Materials Properties Microstructure and Processing, 2011. **528**(13-14): p. 4550-4555.

15. Grimal, Q., et al., *A determination of the minimum sizes of representative volume elements for the prediction of cortical bone elastic properties.* Biomechanics and Modeling in Mechanobiology, 2011. **10**(6): p. 925-937.

16. Sun, C.T. and R.S. Vaidya, *Prediction of composite properties, from a representative volume element.* Composites Science and Technology, 1996. **56**(2): p. 171-179.

17. Kouznetsova, V., M.G.D. Geers, and W.A.M. Brekelmans, *Multi-scale constitutive modelling of heterogeneous materials with a gradient-enhanced computational homogenization scheme.* International Journal for Numerical Methods in Engineering, 2002. **54**(8): p. 1235-1260.

18. Belova, I.V., et al., *Analysis of anisotropic behaviour of thermal conductivity in cellular metals.* Scripta Materialia, 2011. **65**(5): p. 436-439.

19. Suzuki, K. and N. Kikuchi, *A homogenization method for shape and topology optimization.* Computer Methods in Applied Mechanics and Engineering, 1991. **93**(3): p. 291-318.

20. Torquato, S., et al., *Effective mechanical and transport properties of cellular solids.* International Journal of Mechanical Sciences, 1998. **40**(1): p. 71-82.

21. Hassani, B. and E. Hinton, *A review of homogenization and topology optimization I - homogenization theory for media with periodic structure.* Computers & Structures, 1998. **69**(6): p. 707-717.

22. Spoerke, E.D., et al., *A bioactive titanium foam scaffold for bone repair.* Acta Biomaterialia, 2005. **1**(5): p. 523-533.

23. Huiskes, R., H. Weinans, and B. Vanrietbergen, *The relationship between stress shielding and bone-resorption around total hip stems and the effects of flexible materials.* Clinical Orthopaedics and Related Research, 1992(274): p. 124-134.

24. Thelen, S., F. Barthelat, and L.C. Brinson, *Mechanics considerations for microporous titanium as an orthopedic implant material.* Journal of Biomedical Materials Research Part A, 2004. **69A**(4): p. 601-610.

25. Ramaniraka, N.A., et al., *Noncemented total hip arthroplasty: influence of extramedullary parameters on initial implant stability and on hone-implant interface stresses.* Revue De Chirurgie Orthopedique Et Reparatrice De L Appareil Moteur, 2000. **86**(6): p. 590-597.

26. Hunt, T.K., Zederfel.B, and Goldstic.Tk, *Oxygen and healing.* American Journal of Surgery, 1969. **118**(4): p. 521-&.

27. Lavan, F.B. and T.K. Hunt, *Oxygen and wound-healing.* Clinics in Plastic Surgery, 1990. **17**(3): p. 463-472.

28. Niinikos.J, J.E. Dunphy, and T.K. Hunt, *Oxygen supply in healing tissue.* American Journal of Surgery, 1972. **123**(3): p. 247-&.

29. Xia, Z.H., Y.F. Zhang, and F. Ellyin, *A unified periodical boundary conditions for representative volume elements of composites and applications.* International Journal of Solids and Structures, 2003. **40**(8): p. 1907-1921.

30. El Houdaigui, F., et al., *On the size of the representative volume element for isotropic elastic polycrystalline copper*. IUTAM Symposium on Mechanical

Behavior and Micro-Mechanics of Nanostructured Materials, ed. Y.L.Z.Q.S.W.Y.G. Bai. Vol. 144. 2007. 171-180.

31. Salahouelhadj, A. and H. Haddadi, *Estimation of the size of the RVE for isotropic copper polycrystals by using elastic-plastic finite element homogenisation.* Computational Materials Science, 2010. **48**(3): p. 447-455.

32. Hou, S.J., et al., *Multiobjective optimization of multi-cell sections for the crashworthiness design.* International Journal of Impact Engineering, 2008. **35**(11): p. 1355-1367.

33. Zohdi, T.I. and P. Wriggers, *An Introduction to Computational Micromechanics*. Lecture Notes in Applied and Computational Mechanics, ed. F. Pfeiffer and P. Wriggers. Vol. 20. 2005: Springer. 196.

34. Hashin, Z., *Analysis of composite-materials - a survey.* Journal of Applied Mechanics-Transactions of the Asme, 1983. **50**(3): p. 481-505.

35. Hill, R., *Elastic properties of reinforced solids - some theoretical principles.* Journal of the Mechanics and Physics of Solids, 1963. **11**(5): p. 357-372.

36. Liu, T., Z.C. Deng, and T.J. Lu, *Structural modeling of sandwich structures with lightweight cellular cores.* Acta Mechanica Sinica, 2007. **23**(5): p. 545-559.

37. Zhang, W., et al., *Using strain energy-based prediction of effective elastic properties in topology optimization of material microstructures.* Acta Mechanica Sinica, 2007. **23**(1): p. 77-89.

38. Torquato, S., *Random Heterogeneous Materials: Microstructure and Macroscopic Properties*. Interdisciplinary Applied Mathematics, ed. S.S. Antman. Vol. 16. 2001, New York: Springer-Verlag. 701.

39. Steven, G., *Homogenization and inverse homogenization for 3D composites of complex architecture.* Engineering Computations, 2006. **23**(3-4): p. 432-450.

40. Jiang, M., et al., *Scale and boundary conditions effects in elastic properties of random composites.* Acta Mechanica, 2001. **148**(1-4): p. 63-78.

41. Wang, C.Y., L. Feng, and I. Jasiuk, *Scale and Boundary Conditions Effects on the Apparent Elastic Moduli of Trabecular Bone Modeled as a Periodic Cellular Solid.* Journal of Biomechanical Engineering-Transactions of the Asme, 2009. **131**(12).

42. Austin, J.H., et al., *Studies of gas and electrolyte equilibria in blood. I. Technique for collection and analysis of blood, and for its saturation with gas mixtures of known composition.* Journal of Biological Chemistry, 1922. **54**(1): p. 121-147.

43. Sendroy, J., R.T. Dillon, and D.D. Van Slyke, *Studies of gas and electrolyte equilibria in blood - XIX. The solubility and physical state of uncombined oxygen in blood.* Journal of Biological Chemistry, 1934. **105**(3): p. 597-632.

44. Kawashiro, T., W. Nusse, and P. Scheid, *Determination of diffusivity of oxygen and carbon-dioxide in respiring tissue - results in rat skeletal-muscle.* Pflugers Archiv-European Journal of Physiology, 1975. **359**(3): p. 231-251.

45. Beard, D.A. and J.B. Bassingthwaighte, *Advection and diffusion of substances in biological tissues with complex vascular networks.* Annals of Biomedical Engineering, 2000. **28**(3): p. 253-268.

46. Macdouga.Jd and M. McCabe, *Diffusion coefficient of oxygen through tissues.* Nature, 1967. **215**(5106): p. 1173-&.

47. Tsai, A.G., et al., *Microvascular and tissue oxygen gradients in the rat mesentery.* Proceedings of the National Academy of Sciences of the United States of America, 1998. **95**(12): p. 6590-6595.

48. Zahm, A.M., et al., *Numerical modeling of oxygen distributions in cortical and cancellous bone: oxygen availability governs osteonal and trabecular dimensions.* American Journal of Physiology-Cell Physiology, 2010. **299**(5): p. C922-C929.

49. Young, A.M., et al., *Characterization of chlorhexidine-releasing, fast-setting, brushite bone cements.* Acta Biomaterialia, 2008. **4**(4): p. 1081-1088.

50. Truscello, S., et al., *Prediction of permeability of regular scaffolds for skeletal tissue engineering: A combined computational and experimental study.* Acta Biomaterialia, 2012. **8**(4): p. 1648-1658.

51. Hornung, U., *Homogenization and Porous Media*. Interdisciplinary Applied Mathematics. Vol. 6. 1997: Springer.

52. Rho, J.Y., T.Y. Tsui, and G.M. Pharr, *Elastic properties of human cortical and trabecular lamellar bone measured by nanoindentation.* Biomaterials, 1997. **18**(20): p. 1325-1330.

53. Turner, C.H., et al., *The elastic properties of trabecular and cortical bone tissues are similar: results from two microscopic measurement techniques.* Journal of Biomechanics, 1999. **32**(4): p. 437-441.

54. Rho, J.Y., R.B. Ashman, and C.H. Turner, *Youngs Modulus of Trabecular and Cortical Bone Material - Ultrasonic and Microtensile Measurements.* Journal of Biomechanics, 1993. **26**(2): p. 111-119.

55. Pfretzschner, H.U., *Fossilization of Haversian bone in aquatic environments.* Comptes Rendus Palevol, 2004. **3**(6-7): p. 605-616.

56. Watanabe, Y., et al., *Prediction of avascular necrosis of the femoral head by measuring intramedullary oxygen tension after femoral neck fracture.* Journal of Orthopaedic Trauma, 2007. **21**(7): p. 456-461.

57. Rouwkema, J., J. De Boer, and C.A. Van Blitterswijk, *Endothelial cells assemble into a 3-dimensional prevascular network in a bone tissue engineering construct.* Tissue Engineering, 2006. **12**(9): p. 2685-2693.

58. Yang, S.F., et al., *The design of scaffolds for use in tissue engineering. Part 1. Traditional factors.* Tissue Engineering, 2001. **7**(6): p. 679-689.

59. Chen, J., et al., *Multiscale design of surface morphological gradient for osseointegration.* Journal of the Mechanical Behavior of Biomedical Materials, 2013. **20**: p. 387-97.

60. Lin, D., et al., *Design optimization of functionally graded dental implant for bone remodeling.* Composites Part B-Engineering, 2009. **40**(7): p. 668-675.

61. Shen, H. and L.C. Brinson, *A numerical investigation of porous titanium as orthopedic implant material.* Mechanics of Materials, 2011. **43**(8): p. 420-430.

Chapter 11: Conclusion

This chapter provides a closure to the PhD studies by summarising the findings and outcomes in prosthodontics, orthodontics, and dental implantology, with recommendations for future studies in the associated areas.

This PhD thesis explored a broad range of diverse projects covering three major clinical areas, prosthodontics, orthodontics and dental implantology. All these projects focused on the design analysis and optimisation of dental prostheses. The basis for the analysis depended upon understanding the fundamental biomechanics and potential bone remodelling induced by the prosthetic devices, thereby promoting improved success rate of treatments and outcome for patients' healthcare (Figure 11-1).

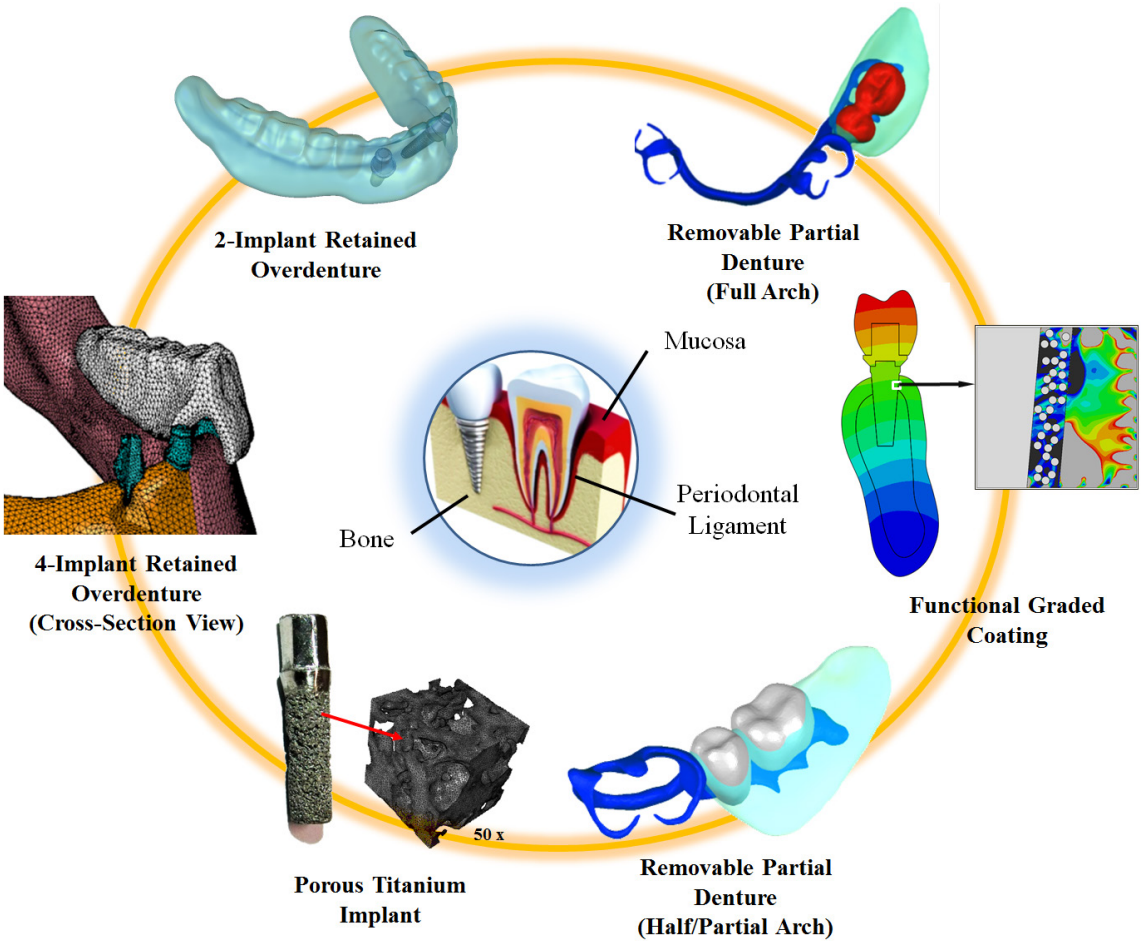

Figure 11-1 Overview of this thesis, which explored dental prosthetic design and optimisation driven by tissue remodelling for improving success rate and outcome of clinical treatment.

The bone remodelling investigated in this thesis can occur directly as a consequence of mechanical stimuli transferred from an implant-bone interface, or indirectly through soft tissue complex, such as periodontal ligament and oral mucosa. The discovery and knowledge learnt in the tissue responses are further applied to design and

optimisation of dental prostheses and treatment planning. Nevertheless, each individual chapter included in this thesis explored distinct aspects of biomedical engineering and their relevance to dentistry, and their outcomes delivered specific contributions to the oral biomechanics and biomaterials. This summary aims to provide a brief conclusion and fundamental interconnection of three clinical areas, thereby providing recommendations for the corresponding future studies which are beyond the scopes and time frame of this PhD candidature.

11.1 Prosthodontics (Chapters 2-7)

The oral mucosa plays an important role in protection, sensation, secretion and thermal regulation of and from the oral environment. Despite these existing understandings, its critical contributions to occlusal loading distribution and residual ridge resorption induced by denture treatments remains understudied, and has recently drawn increasing attention with respect to prosthodontic treatment and assessment. Through several research projects during the course of this candidature, a number of highly relevant outcomes have been discovered in this area.

11.1.1 Key Outcomes

- The mucosa is shown to act like a buffering layer to transfer occlusal forces from the denture to the bony sub-structure beneath, and the stress distribution decreases along the mucosa thickness from the epithelial surface to the mucoperiosteal complex. The complicated anatomy, along with the nonlinear physiological and biomechanical response additionally alters the stress distribution on the same surface significantly. (Chapters 2 & 6)
- Besides the well-studied static response, the time-dependent, volumetric, and interactive responses of the mucosa are also important in understanding the

potential effects induced by the dental prostheses, which remain understudied and the associated material models are preliminary. (Chapter 2)

- Both the mucosal friction coefficient with the denture and its Poisson's ratio depend on the physiological conditions of a subject, and reflect the interactive and volumetric behaviours when loaded. Based on an inverse approach, the friction coefficient was determined as 0.213 and the Poisson's ratio at 0.402 for an elderly patient from her biting force induced *in vivo* contact pressure contour beneath a removable partial denture. (Chapters 2 & 3)
- Introducing dental prosthesis will to a certain extent alter the biomechanical environment of the oral cavity, and the tissue metabolism will be thus changed due to the variation in pathway and stimulation. Positive emission computerized tomography (PET) allows detection of current bone metabolic and remodelling activity rate associated with a functioning denture by the accumulation of 18F-fluoride tracer in a much shorter duration than X-Ray measurement. The PET technique has shown good correlation with mechanical stimulus distributions, such as equivalent stress and strain energy density. (Chapters 2 & 4)
- Hydrostatic pressure, often known as the interstitial fluid pressure, has been found as an effective indicator to residual ridge resorption induced by various types of dentures. The bone volume reduction over 1 year after denture insertion is well correlated with the hydrostatic pressure distribution in the mucosa beneath the denture, while the equivalent stress or strain energy density inside the bone poorly reflected the same pattern. (Chapters 2, 5 & 6)
- In a patient-specific manner, implant-retained overdentures are likely to have more than twice the stress concentration of conventional complete dentures due

to the implant related cantilever effect. On the other hand, the contact area under an implant-retained overdenture is about half that of a complete denture. (Chapters 5 & 6)

- With increased occlusal loading associated with implant-retained overdenture treatments, a greater proportion of the load is transmitted through the implants. However with more implants or their placement further toward the distal end of the dental arch, the cantilever effect can be reduced, but not avoided. Other methods, such as enhancing the denture stiffness by embedding metal wires and beams, are also available to ease this clinical complication. (Chapter 6)
- The contact interface between the denture base and the mucosal surface can be optimised to reduce stress concentration and the consequent bone resorption, based on the contact pressure distribution. This optimisation can be achieved based on a bi-direction evolutionary shape optimisation (BESO) method automatically, from the CT scan of the patient, to the direct material additive fabrication (3D printing). Through this approach, the maximum hydrostatic pressure within the mucosa can be further reduced by 34% from a conventionally moulded denture (the initial denture base), and the uniformity can be improved to nearly 65%, to reduce the cantilever effect at the distal edge. (Chapter 7)

11.1.2 Recommendations for Future Study

1. The existing material constitutive models for the mucosa responses are based on the macroscopic phenomena observed in clinical studies, which barely connect either microscopic or cellular responses, thereby limiting the biomechanical insights of the physiological observations. Consideration of the

heterogeneous and multi-phase (solid and fluid) structure within the mucosa will enhance understanding future studies of this area, and provide more information for both dentistry and biomedical engineering (e.g. biomechanics for other soft tissues).

2. Some fundamental factors, such as morphology and thickness variations, have not yet been investigated for their effects on the mucosal effects. Meanwhile, the maxilla is also very different to the mandible in this respect, and it responses to occlusal loading in a more complex manner for its thinner mucosa with more significant variations.

3. Although hydrostatic pressure has been revealed to be associated with potential residual ridge resorption, no study has clinically simulated this process to provide a numerical guideline, or validated this hypothesis in a time dependent fashion against clinical data acquired at multiple time points.

4. The accumulation of 18F-fluoride tracer through PET is only linked to the static mechanical stimuli at the two time points in this thesis, and it would be interesting to correlate this technique to a time-dependent analysis through bone remodelling.

11.2 Orthodontics (Chapter 8)

Similar to the oral mucosa, the periodontal ligament (PDL) has supportive, sensory, and nutritive functions to the tooth. Its role in the tooth eruption and re-alignment has been gradually recognised. In orthodontic tooth movement (OTM), stresses developed in the PDL leads cells in surrounding bone to respond by apposition and resorption. Specialized cells, such as osteoblasts, cementum and fibroblasts can evolve from undifferentiated ecto-mesenchymal cells upon *in vivo* loading situations. On the other hand, bone and tooth

resorbing cells, such as osteoclasts and odontoclasts, derive from blood-borne macrophages.

11.2.1 Key Outcomes

- The tooth movement speed is dependent on the magnitude of hydrostatic pressure within the PDL, and the direction determined from the displacement vectors in this tissue.
- The higher the PDL hydrostatic pressure, the faster the tooth will move; however, this effect is compromised with increasing orthodontic load, eventually reaching a plateau, at constant speed.

11.2.2 Recommendations for Future Study

1. The orthodontic root resorption (ORR) is one of the critical side effects of orthodontic treatment. The connection between hydrostatic pressure within the PDL and ORR remains unclear. It would be of considerable clinical interest to explore their relationship, and search for an optimal solution to balance the resorption and the treatment timeframe.

11.3 Dental Implantology (Chapters 9-10)

The use of dental implants has revolutionised modern dentistry, and dental implantology serves in multiple areas of dentistry as an effective, sometimes unique, solution. Even though implant research has been ongoing for more than half a century, there are still several challenges ahead, such as stress shielding and osseointegration.

11.3.1 Key Outcomes

- Among the titanium implants with particle sintered surfaces, a functionally graded implant surface morphology by design can lead to a maximum with two

times more osseointegration in the short term and 24% in the long term than a uniform implant surface morphology. (Chapter 9)

- Through an multiobjective optimisation procedure to increase the bone-implant contact (BIC) and reduce the peak Tresca stress (PTS), an optimal solution can be achieved with a balance between these two criteria. (Chapter 9)
- A fully porous titanium surface morphology provides four times more contact surface for the cell attachment than a solid surface, and simultaneously reduces the material property mismatch between the implant and the native bone to avoid stress-shielding. This type of sub-surface morphology can be achieved using injection-moulding manufacture. (Chapters 9 & 10)

11.3.2 Recommendations for Future Study

1. The fully porous titanium remains at the fabrication stage, and limited studies have been performed on the investigation of its osseointegration *in vivo* and *in silico*. By applying the existing knowledge of Wolff's rule in bone remodelling, numerical analysis can provide effective predictions as to tissue ingrowth, and enable further optimising of the structure to the maximum strength with sufficient oxygen diffusion and metabolite removal.